THE UNIVERSITY
of EDINBURGH

Investigating the cell biological mechanisms regulated by the cellular prion protein

Andrew Richard Castle

Doctor of Philosophy

The University of Edinburgh

2017

Declaration

I declare that this thesis has been composed by myself and that no part has been submitted in any previous application for a degree. Experiments were designed by myself or in collaboration with my supervisors. All experiments and data analyses were performed by myself unless otherwise indicated by reference or acknowledgment.

Andrew Castle 

12th May 2017

Abstract

Transmissible spongiform encephalopathies (TSEs) are rare, uniformly fatal neurodegenerative disorders that can affect many mammalian species, including humans. A hallmark of these diseases is the conversion of cellular prion protein (PrP^C) into an abnormally folded form. This misfolded PrP^C is infectious, since it can provide a template for pathogenic conversion of PrP^C in a new host. In addition to any toxicity of the misfolded protein, loss of normal PrP^C function could be involved in the neurodegenerative processes. However, the physiological role of PrP^C is still poorly understood and this project has aimed to address that lack of knowledge. Out of the many putative functions ascribed to PrP^C, the most commonly proposed is that it protects cells from stress. In contrast, I have found that stable transfection of the prion protein gene into SH-SY5Y neuroblastoma cells increases cell death in response to serum removal from the culture medium. Following treatment with several chemical toxins, two out of four stably transfected clones did, generally, display greater viability than untransfected cells that do not express detectable levels of PrP^C. However, knockdown of PrP^C expression by RNA interference had no effect on this stress resistance, indicating that it may not have been mediated directly by PrP^C. Given the lack of robust stress protection afforded by PrP^C transfection, proteomic analyses of the cells were carried out to identify alternative processes that were perturbed as a result of PrP^C expression. The results obtained suggested roles for PrP^C in cytoskeletal organisation and cell cycle regulation. Various proteins involved in cytoskeletal organisation were confirmed by western blotting to be differentially expressed in some or all of the stably transfected clones. Additionally, the expression changes to proteins involved in cell cycle regulation resulted in slower proliferation of the clones compared with untransfected cells, a difference that was reduced following RNA interference-mediated knockdown of PrP^C. Taken together, these data suggested that specific growth factor-activated pathways were differentially regulated in the stably transfected clones. One candidate pathway was nerve growth factor (NGF) signalling, which promotes neuronal survival and differentiation as well as regulating various processes outside of the nervous system. PrP^C-transfection resulted in altered expression of receptors for NGF, suggesting that

the stably transfected clones were, indeed, responding differently to NGF stimulation. However, the molecular mechanism responsible for these expression changes remains to be determined, since co-immunoprecipitation experiments did not identify any physical interactions between PrP^C and the NGF receptors. Nonetheless, a role for PrP^C in modulating NGF signalling has the potential to explain many of the diverse phenotypic observations in PrP^C-null mice and might indicate that loss of PrP^C function is an important part of TSE pathogenesis.

Lay summary

Prion diseases are rare but fatal diseases of the nervous system that can affect humans and other mammals. An important feature of these diseases is the change in shape of a protein – the cellular prion protein (PrP^C) – into an abnormally folded form known as a "prion". When these prions come into contact with the normal form of the protein, it causes this PrP^C to also change shape, resulting in an accumulation of abnormally folded protein. This process appears to be what allows prion diseases to spread from cell to cell and between individuals. Whilst the prions themselves are probably damaging to cells, the change in shape also prevents PrP^C from carrying out its normal function, which may contribute towards the cell death observed in these diseases. Currently though, the normal function of PrP^C is poorly understood, a lack of knowledge that this project has aimed to address. Much of the work was carried out using cultured cells genetically engineered to produce PrP^C, allowing comparison with the original cells that lack the protein. Since previously published research suggests that PrP^C can protect cells from stress, my first experiments were to expose the genetically engineered cells to various forms of stress. In contrast to most previous findings, the PrP^C-positive cells displayed no robust improvement in stress resistance. However, subsequent experiments did find that the presence of PrP^C affected the levels of proteins that maintain the structural integrity of cells and are involved in changing cell shape. Additionally, the PrP^C-positive cells were shown to divide less frequently than cells lacking the protein. One possible explanation for these observations is that PrP^C affects how cells respond to a protein called nerve growth factor (NGF). NGF interacts with receptor proteins on the cell surface, leading to activation of processes within the cell that mainly promote growth and survival. Intriguingly, the levels of the NGF receptors were found to be altered in the PrP^C-positive cells, which suggests that the cells were, indeed, responding differently to NGF. A role for PrP^C in regulating the cellular response to NGF might indicate that a loss of the normal function of PrP^C plays an important role in the nervous system damage that occurs in prion diseases.

Acknowledgements

First and foremost, I would like to thank my primary supervisor Dr Andrew Gill for giving me the opportunity to carry out this PhD project, and for always being available to provide valuable guidance and support throughout. I am grateful to Dr Dominic Kurian for all his help with the project, especially for his role in the proteomic experiments, the data from which forms an integral part of this thesis. I would also like to thank Dr Thomas Wishart for his advice on performing pathway analyses of the proteomic data. Further thanks go to Dr Paula Brunton and Prof. Bruce Whitelaw for their questions and advice at thesis committee meetings. In addition, I would like to acknowledge Paula Stewart for carrying out the sequencing of the *Prnp* vector and Rebecca Hogan for isolating the mouse liver tissues used in the project.

I am particularly grateful to Sonya Agarwal and Fiona Lane for all their help in the lab, especially in the early days of the project. I must also give a huge thank you to all my friends and colleagues within the neurobiology division and in the institute as a whole for making the last four years such a pleasure.

I also need to give a special mention to my colleagues at MedImmune in 2010/11 for making my industrial placement there such a good experience that it convinced me to do a PhD. Finally, I am indebted, as always, to my wonderful parents for supporting me all the way.

Thank you all!

Extra note: Following initial submission of this thesis, material in Chapter 1 was used as the starting point for writing a review article that was published prior to resubmission of this thesis. Reference: Castle, A.R. and Gill, A.C. (2017). Physiological Functions of the Cellular Prion Protein. *Frontiers in Molecular Biosciences* 4:19. doi: 10.3389/fmolb.2017.00019

Table of contents

List of figures

List of tables

Abbreviations

%CV	Percentage coefficient of variation
Aβ	Amyloid beta peptides
ADAM	Disintegrin and metalloproteinase domain-containing protein
Akt	RAC-alpha serine/threonine-protein kinase
APP	Amyloid precursor protein
ATP	Adenosine triphosphate
ATRIP	*Ataxia telangiectasia* and Rad3-related protein (ATR)-interacting protein
BCA	Bicinchoninic acid
BDNF	Brain-derived neurotrophic factor
bp	Base pairs
BSE	Bovine spongiform encephalopathy
cAMP	Cyclic adenosine monophosphate
CDK1	Cyclin-dependent kinase 1
CDS	Coding sequence
CNS	Central nervous system
co-IP	Coimmunoprecipitation
^{Ctm}PrP	Transmembrane form of PrP (C-terminal domain projects into the ER lumen)
DAPI	4',6-diamidino-2-phenylindole
DMEM	Dulbecco's modified Eagle's medium
DMSO	Dimethyl sulphoxide
DRGs	Dorsal root ganglia
EDTA	Ethylenediaminetetraacetic acid
ER	Endoplasmic reticulum
ERK1/2	Extracellular signal-regulated kinases 1 and 2
FASN	Fatty acid synthase
FBS	Foetal bovine serum
GLUD1	Glutamate dehydrogenase 1, mitochondrial

GLUT4	Solute carrier family 2, facilitated glucose transporter member 4
GPI	Glycophosphatidylinositol
HBSS	Hank's Balanced Salt Solution
IPA	Ingenuity Pathway Analysis
kbp	Kilobase pairs
LB	Lysogeny broth
LC-MS/MS	Liquid chromatography-tandem mass spectrometry
LDS	Lithium dodecyl sulphate
LDH	Lactate dehydrogenase
LTP	Long-term potentiation
MAPK	Mitogen-activated protein kinase
MES	2-(N-morpholino)ethanesulfonic acid
MYO1B	Unconventional myosin 1b
NADH	Nicotinamide adenine dinucleotide phosphate
NGF	Nerve growth factor
NMDAR	N-methyl-D-aspartate receptor
NSCs	Neural stem cells
NT-3	Neurotrophin-3
NT-4	Neurotrophin-4
^{Ntm}PrP	Transmembrane form of PrP^{C} (N-terminal domain projects into the ER lumen)
p-Akt	Phosphorylated Akt
p-ERK1/2	Phosphorylated ERK1/2
p-TrkA	Phosphorylated TrkA
$p75^{NTR}$	p75 neurotrophin receptor
p75-CTF	p75 C-terminal fragment
p75-ICD	p75 intracellular domain
PBS	Phosphate-buffered saline
PCK1	Phosphoenolpyruvate carboxykinase, cytosolic
PCR	Polymerase chain reaction
PFA	Paraformaldehyde

PNGase F	Peptide-N-glycosidase F
PNS	Peripheral nervous system
Pro-NGF	Nerve growth factor precursor
PrP^{C}	Prion protein, cellular isoform
PRPF19	Pre-mRNA-processing factor 19
PrP^{Sc}	Prion protein, scrapie (misfolded) isoform
PQ	Paraquat
RhoA	Ras homolog gene family, member A
RNAi	RNA interference
ROCK	Rho-associated protein kinase
ROS	Reactive oxygen species
RPA	Replication protein A
RT	Room temperature
SDA	Sodium deoxycholate
SDS	Sodium dodecyl sulphate
SDS-PAGE	Sodium dodecyl sulphate-polyacrylamide gel electrophoresis
$SH\text{-}SY5Y^{Untr}$	Untransfected control cells for SH-SY5Y cells stably transfected with pCI-neo-MoPrnp
Shadoo	Shadow of prion protein
siRNA	Small interfering RNA
SKP2	S-phase kinase-associated protein 2
SOD	Superoxide dismutase
STAT3	Signal transducer and activator of transcription 3
STI1	Stress-induced-phosphoprotein 1
STS	Staurosporine
SUGT1	Suppressor of G2 allele of S-phase kinase-associated protein 1 (SKP1) homolog
TGFB1	Transforming growth factor beta-1
TM	Tunicamcyin
TrkA	Tropomyosin-related kinase A (a. k. a. high affinity NGF receptor)

TrkB	Tropomyosin-related kinase B (a. k. a. high affinity BDNF/NT-3 receptor)
TSEs	Transmissible spongiform encephalopathies
UBC	Polyubiquitin-C
vCJD	Variant Creutzfeldt-Jakob disease
ZIP	Zrt-, Irt-like

Chapter 1: Introduction

1.1 Transmissible spongiform encephalopathies

Transmissible spongiform encephalopathies (TSEs), also referred to as prion diseases, are disorders characterized by long, pre-clinical incubation periods followed by rapidly progressing neurodegeneration. Although rare, TSEs are uniformly fatal and many mammalian species are susceptible (Fernandez-Borges et al., 2012). Animal TSEs include scrapie in sheep and goats, bovine spongiform encephalopathy (BSE) in cattle and also goats, and chronic wasting disease in deer, whilst sporadic Creutzfeldt-Jakob disease is the most common human TSE (Head, 2013).

As the name indicates, TSEs can be transmitted between individuals, although the degree of transmissibility varies considerably, for instance, chronic wasting disease has spread rapidly through deer populations in North America due largely to the high infectivity of bodily fluids from infected animals (Saunders et al., 2012). Transmission between humans was first recognised in the mid-20th century following studies of the Fore people of Papua New Guinea. This tribe suffered endemically from a TSE called Kuru and the accepted theory is that the disease spread as a consequence of now-outlawed cannibalistic rituals that were practiced when mourning dead relatives. (Collins et al., 2001). In rare circumstances, TSEs can also jump across species, as demonstrated by the emergence of variant Creutzfeldt-Jakob disease (vCJD) in humans. In the mid-1980s, a novel TSE of cattle was identified and this disease, known as BSE, dramatically increased in prevalence over the following years, mainly as a result of the feeding practices used at the time (Nathanson et al., 1997). The first case of vCJD was identified in the UK in 1996 (Will et al., 1996) and later studies indicated that the disease may have been transmitted to humans via the consumption of BSE-infected beef (Ritchie et al., 2009).

Although the threat of a widespread vCJD epidemic has receded, sporadic TSEs, which lack a well-defined cause, and inherited TSEs, such as fatal familial insomnia and Gerstmann-Sträussler-Scheinker syndrome, continue to affect a small number of

people every year. Furthermore, chronic wasting disease represents an emerging threat, since it is growing rapidly in prevalence and has the potential to spread beyond deer to other livestock species and, conceivably, to humans (Saunders et al., 2012). Consequently, there is an unmet need for effective treatments of TSEs. Various therapeutic approaches have been and are being investigated. However, like other neurodegenerative diseases, early diagnosis is a major issue – the preclinical stage of disease can last for years or even decades (Collins et al., 2004) and by the time clinical symptoms do appear the damage may be irreversible, at least using current technologies.

1.1.1 The prion hypothesis

TSEs are unusual infectious diseases, since no bacterium, virus or other living organism seems to be involved in their transmission. The initial evidence for this came from studies of mice experimentally infected with scrapie by intracerebral inoculation of infected brain homogenate. Prior to inoculation, the homogenates were exposed to UV radiation at wavelengths that would irreparably damage the nucleic acid genome of a virus or bacterium and yet the mice still developed disease, indicating that the infectious agent of scrapie does not contain nucleic acid (Alper et al., 1978). The estimated molecular weight of the scrapie agent also seemed to be too small for a virus (Alper et al., 1966; Alper, 1985). Subsequently, a novel protein was isolated from scrapie-infected hamster brain and its concentration appeared to be proportional to infectivity (Prusiner et al., 1982; McKinley et al., 1983). This discovery led to the prion hypothesis, which proposed that this protein was the major component of the infectious agent of all TSEs – the term “prion” derives from *pro*teinaceous *in*fectious particle (Prusiner, 1982). The protein in the scrapie agent was later shown to be a host-encoded protein that can undergo conversion to a partially protease-resistant, misfolded form (McKinley et al., 1983; Prusiner et al., 1985; Horwich and Weissman, 1997). Known as PrP^{Sc} (scrapie isoform of the prion protein), the misfolded protein is thought to act as a template for converting the normally folded form, known as the cellular prion protein (PrP^{C}), into more PrP^{Sc} (Horwich and Weissman, 1997). PrP^{Sc} is prone to aggregation, which results in the

formation of oligomers, proto-fibrils, and the large amyloid plaques commonly (although not always) found in TSE-infected brains (Kitamoto et al., 1986). However, the latest evidence suggests that it is the soluble, oligomeric species rather than the plaques that are the most neurotoxic (Ugalde et al., 2016).

Recently, the prion concept has been extended to encompass other neurodegenerative diseases, including multiple systems atrophy (Prusiner et al., 2015), Alzheimer's disease and Parkinson's disease (Goedert, 2015). These diseases also involve accumulation of misfolded protein within the nervous system and the spread from cell to cell seems to occur in a "prion-like" manner.

Whilst PrP^{Sc} appears to be toxic in its own right, loss of normal PrP^{C} function may also play some role in the progression of TSEs (Mays et al., 2014). Therefore, a great deal of research has focused on investigating the physiological function of PrP^{C}. This research will be summarised later in the chapter; firstly, we must consider the biochemistry/molecular biology of the protein itself.

1.2 The cellular prion protein and its gene

1.2.1 Evolutionary history of prion genes

Homologs of the prion protein gene (*PRNP*) are present in all vertebrate lineages and, certainly among mammalian species, both the amino acid sequence and structure of PrP^{C} are well-conserved; for example, human and sheep PrP^{C} share 95 % sequence identity (Pastore and Zagari, 2007). The variability in sequence and structure that does exist is thought to give rise to the so-called "species barrier" that limits transmissibility of TSEs between species (Hagiwara et al., 2013).

In addition to *PRNP*, the mammalian prion gene family includes *SPRN*, which encodes shadow of prion protein (shadoo), and *PRND*, which codes for a protein known as doppel. In the human genome, *PRNP* and *PRND* are situated directly

adjacent to one another on chromosome 20, whilst *SPRN* is found on chromosome 10. It was proposed relatively recently that *PRNP*, *PRND* and possibly also *SPRN* are evolutionarily descended, at least in part, from the LIV-1 branch of the ZIP (Zrt-, Irt-like) metal ion transporter family (Schmitt-Ulms et al., 2009; Ehsani et al., 2011; Ehsani et al., 2012).

1.2.2 Structure of the *PRNP* gene and its regulation

In humans, the *PRNP* gene consists of a region of 35 kilobase pairs (kbp) on chromosome 20, whilst in mice the gene covers 38 kbp of sequence on chromosome 2 (Sakudo et al., 2010). Figure 1.1 shows the structure of the gene in both species as well as the mature mRNA transcripts that are produced – the numbering comes from NCBI references sequences NM_011170.3 (murine *Prnp*, transcript variant 1) and NM_ 000311.4 (human *PRNP*, transcript variant 1), although other transcript variants with differing 5' or 3' untranslated regions seem to exist in humans and in mice. Murine *Prnp* consists of three exons, the first two of which are short sequences separated by an intron of ~2.2 kbp that both contribute to the 5' untranslated region of the mature mRNA (Kim et al., 2008). A ~24 kbp intron separates exon 2 from exon 3, which contains the protein-coding sequence (CDS) of the gene. Human *PRNP* only has two exons that are separated by an intron of ~13 kbp but again the CDS is contained entirely within the final exon (Kim et al., 2008).

Although *PRNP* has a short GC-rich region immediately upstream of the transcription start site, as well as other features common to housekeeping genes (Puckett et al., 1991; Sakudo et al., 2010), intron 1 and the sequences upstream of the transcription start site also contain evolutionarily conserved, putative binding sites for numerous transcription factors, including Sp1 (Basler et al., 1986), activator proteins 1 and 2 (Mahal et al., 2001), forkhead box protein 03 (Liu et al., 2013), regulatory factor X1, heat shock factor 2, GATA-binding factor 3, thyrotrophic embryonic factor, myocyte enhancer factor 2, ecotropic viral integration site 1, E4 promoter-binding protein 4 and nuclear matrix protein 4/cas-interacting zinc finger protein (Kim et al., 2008). These regulatory sequences enable dynamic control of

PrP^C expression in response to various factors and conditions (Linden et al., 2008). For example, treatment of cultured cells with nerve growth factor (NGF), insulin or insulin-like growth factor induces PrP^C expression (Kuwahara et al., 2000; Zawlik et al., 2006; Liu et al., 2013). Additionally, endoplasmic reticulum (ER) stress, oxidative stress and genotoxic stress are all reported to cause upregulation of expression (Dery et al., 2013; Cichon and Brown, 2014; Bravard et al., 2015).

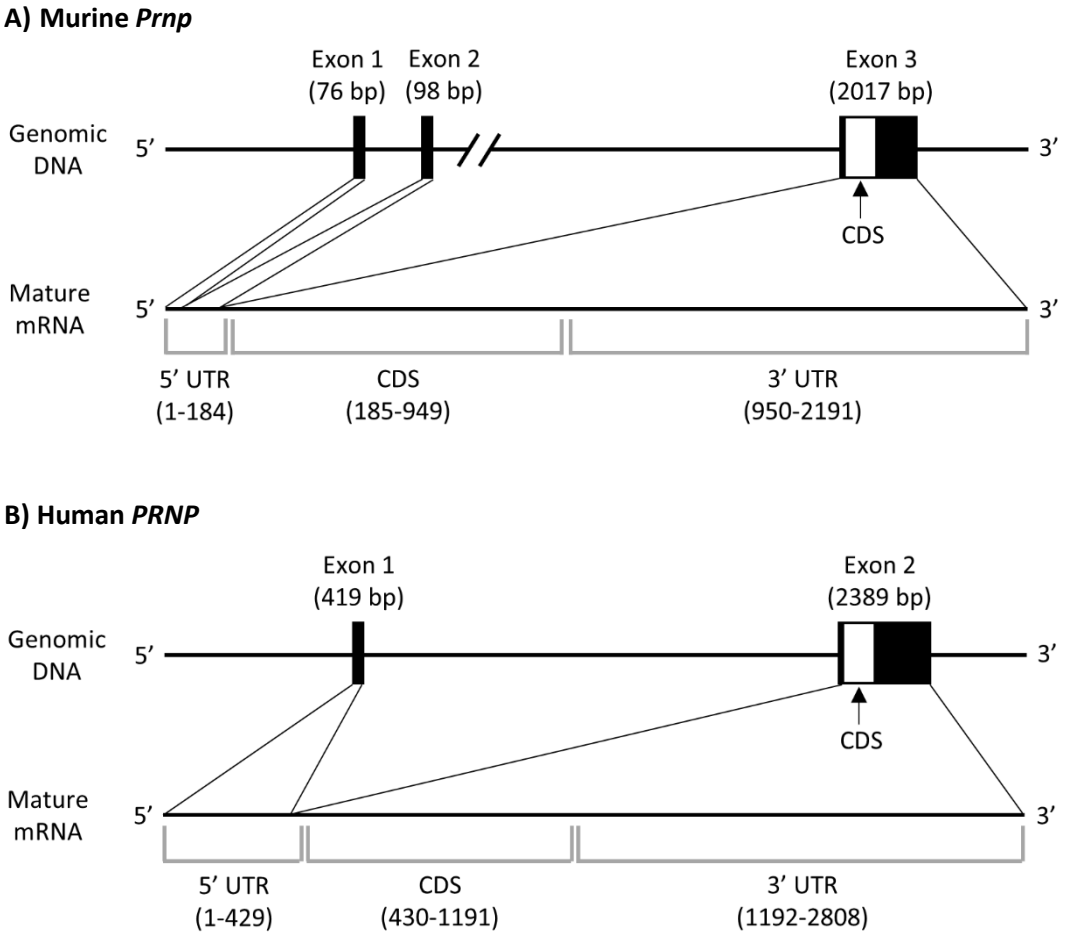

Figure 1.1 – Structure of *PRNP* and its mRNA transcripts

A & B) Schematic representations of the *PRNP* gene in the murine and human genomes in addition to the mature mRNA transcripts produced following removal of introns. The entire coding sequence (CDS) derives from a single exon in both species. The cut lines in image **A** indicate that the intron between exons 2 and 3 is much longer than the intron between exons 1 and 2 in image **B**. UTR = untranslated region.

1.2.3 PrP^C structure

This section focuses on the structure of PrP^C in humans but, as previously mentioned, the main structural features are conserved among mammalian species. Figure 1.2 shows these features in more detail. Briefly, PrP^C is first synthesised as a precursor protein of 253 amino acids. The N-terminal signal sequence (residues 1-22) codes for entry into the endoplasmic reticulum (ER) and the C-terminal signal sequence (residues 231-253) for the later addition of a glycophosphatidylinositol (GPI) anchor. Following cleavage of these signal sequences, the mature protein of 208 amino acids (residues 23-230) is trafficked to the cell surface and attaches to the extracytoplasmic face of the cell membrane via its GPI anchor (Linden et al., 2008). The N-terminal domain of PrP^C lacks stable secondary/tertiary structure; this is known as a "random coil" conformation and it may enable PrP^C to interact with multiple partners (Bakkebo et al., 2015). The N-terminal domain also contains four tandem repeats of a sequence of eight amino acids. One study showed that this octapeptide repeat region was the most well-conserved part of the PrP^C sequence among the 53 species analysed, which suggests it could be a functionally important domain (Kim et al., 2008). A hydrophobic region (residues 112-133) spans the divide between the N- and C-terminal domains and may be involved in PrP^C dimerisation (Rambold et al., 2008; Beland and Roucou, 2013). The C-terminal domain itself has a globular structure, consisting of three alpha-helices, two beta-strands and interconnecting loops (Riek et al., 1996; Haire et al., 2004). Pathogenic conversion of PrP^C to PrP^{Sc} involves a reduction in the amount of alpha-helical structure and an increase in beta-sheet conformation (Pan et al., 1993). Two N-linked glycosylation sites (residues 181 and 197) are also found within the C-terminal domain and the vast majority of PrP^C is generally thought to be di-glycosylated, although this may not be the case for all tissue or cell types (Williams et al., 2004; Lee and Baskakov, 2014).

Whilst doppel and shadoo are considerably smaller than PrP^C, both share some of the structural features of the larger protein. Doppel is similar in structure to the PrP^C C-terminal – it has three alpha helices and two beta sheets as well as two N-glycosylation sites. On the other hand, shadoo is comparable to the PrP^C

N-terminal, since it contains a hydrophobic domain, a positively-charged region of tandem repeats and also appears to exist in a random coil configuration (Watts et al., 2007). Both doppel and shadoo are GPI-anchored, like PrP^C (Silverman et al., 2000; Watts et al., 2007).

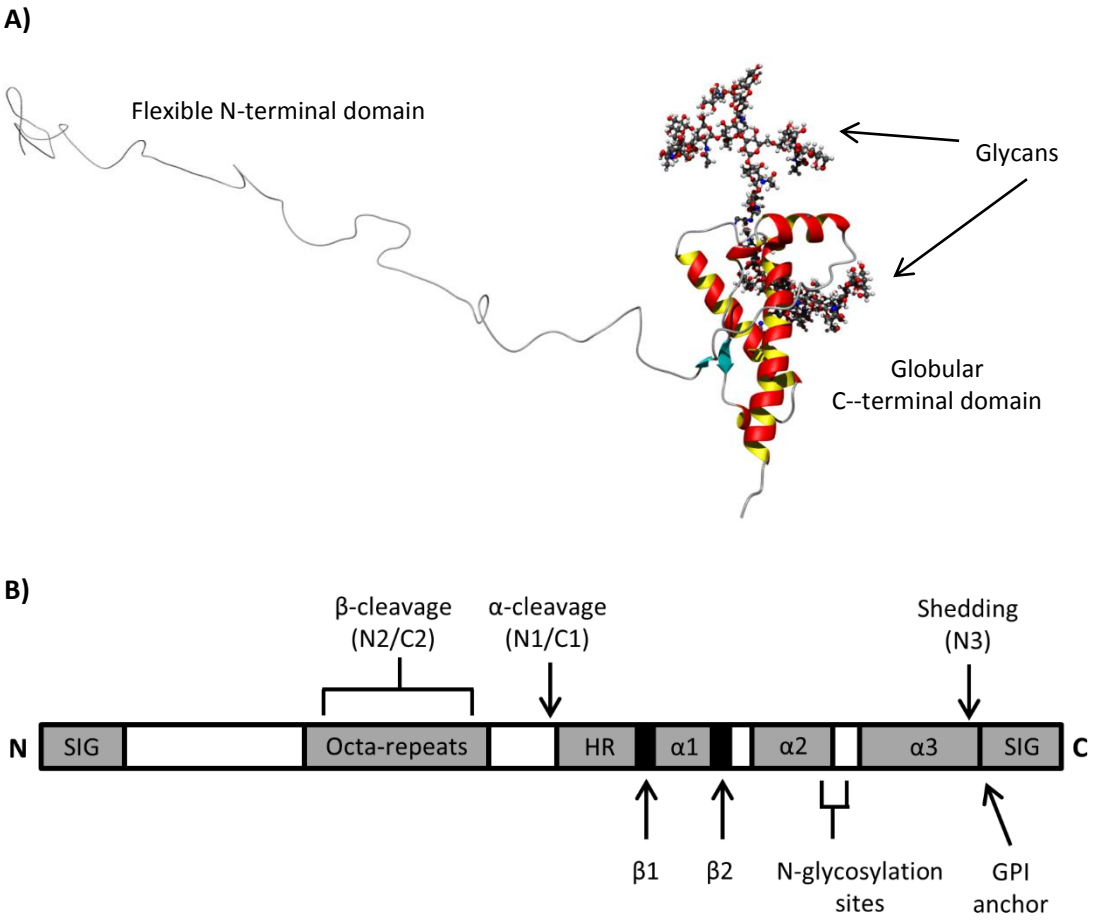

Figure 1.2 – Representations of PrP^C structure

A) Ribbon diagram of the structure of PrP^C. The globular C-terminal domain contains three alpha-helices shown in red and yellow and two beta-sheets shown in turquoise. The N-terminal domain is presented in a random coil configuration. **B)** Schematic representation of PrP^C highlighting its key structural features. SIG = Signal peptide; HR = hydrophobic domain. Sites of proteolytic cleavage events are also marked on the diagram.

1.2.4 Distribution of PrP^C expression

PrP^C expression in the brain seems to increase throughout development, reaching a peak in early life before reducing somewhat in adulthood (Sales et al., 2002; Adle-Biassette et al., 2006). The regions where PrP^C remains particularly abundant in the adult brain, at least in the case of hamsters, appear to be areas with high levels of ongoing neurogenesis, specifically the hippocampus and olfactory bulb (Sales et al., 2002). Interestingly, there is some evidence that neuronal PrP^C expression is high in the vicinity of synapses and low or even undetectable in the cell soma (Sales et al., 1998; Bailly et al., 2004; Adle-Biassette et al., 2006). It is unclear how PrP^C expression in the brain is affected by the ageing process – one study reported increased PrP^C levels in the brains of aged mice (Williams et al., 2004), whilst analysis of post-mortem human brain tissues showed that PrP^C expression in the hippocampus was significantly reduced in older individuals (Whitehouse et al., 2010). The glycan profile of PrP^C also seems to undergo age-related changes, reportedly resulting in the increased abundance of complex oligosaccharides linked to PrP^C (Goh et al., 2007)

Most reports indicate that PrP^C is present in glia, including astrocytes (Lima et al., 2007; Hartmann et al., 2013), oligodendrocytes (Moser et al., 1995; Bribian et al., 2012) and microglia (Adle-Biassette et al., 2006), although one study found PrP^C expression to be inhibited following differentiation of neural precursors into glial cell types (Steele et al., 2006). Non-neural cells of the forebrain also stain for PrP^C, including the endothelial cells in blood vessel walls (Adle-Biassette et al., 2006). Furthermore, at least during development, PrP^C is expressed in the dorsal and ventral root ganglia of the spinal cord (Tremblay et al., 2007; Peralta et al., 2012; Ganley et al., 2015) as well as sensory and motor axons (Manson et al., 1992) and associated Schwann cells (Follet et al., 2002). Outside of the nervous system, PrP^C is found in immune cells, including T lymphocytes, natural killer cells and mast cells (Durig et al., 2000; Haddon et al., 2009). PrP^C expression has also been detected in teeth (Schneider et al., 2007) and in various organs, such as the heart, pancreas, intestine, spleen and kidneys (Peralta and Eyestone, 2009).

Within an individual cell, the majority of PrP^C is GPI-anchored to the extracytoplasmic face of the cell membrane, specifically in microdomains called lipid rafts (Vey et al., 1996). However, presumably to control the cell surface pool of PrP^C, the protein seems to be subject to cycles of internalisation followed by trafficking back to the cell membrane via recycling endosomes (Shyng et al., 1995; Sunyach et al., 2003). Indeed, studies using a GFP reporter system have suggested that PrP^C is expressed in recycling endosomes and also in the Golgi apparatus (Lee et al., 2001a; Magalhaes et al., 2002; Nikles et al., 2008). There are also reports of nuclear and mitochondrial localisation of PrP^C expression, which may be part of the response to stress (Morel et al., 2008; Sorice et al., 2012; Besnier et al., 2015; Bravard et al., 2015).

1.2.5 Proteolytic processing of PrP^C

Mature PrP^C can be proteolytically processed in several ways to produce a number of fragments, many of which appear to be bioactive. The sites within the PrP^C molecule where these cleavage events can take place are indicated in Figure 1.2b. The major (alpha) cleavage is thought to occur within the Golgi apparatus (Walmsley et al., 2009) or in an acidic endosomal compartment (Shyng et al., 1993), and results in the production of N- and C-terminal fragments respectively referred to as N1 and C1. Most N1 is subsequently shed from the cell, whilst C1 reportedly remains anchored to the cell membrane like the full length form (Harris et al., 1993; Vincent et al., 2000; Laffont-Proust et al., 2006). Often, C1 makes up a large proportion of the total, cellular PrP^C pool – around 50 % on average in sheep cerebral cortex, for example (Campbell et al., 2013). Alpha-cleavage occurs just outside of the hydrophobic domain of PrP^C, seemingly at the codon 110/111 peptidyl bond (human numbering) (Chen et al., 1995; Watt et al., 2005), although a recent report suggested that the presence of copper ions can shift the cleavage site by a few amino acid residues (McDonald et al., 2014). The disintegrin and metalloproteinase domain-containing protein (ADAM) family may be responsible for alpha-cleavage, particularly ADAM17. The activity of ADAM17 and, therefore, the rate of alpha-cleavage can be modulated by protein kinase C through its effects on the extracellular signal-related

kinases 1 and 2 (ERK1/2) signalling pathway (Vincent et al., 2000; Cisse et al., 2008; Cisse et al., 2011). ADAMs 8 and 10 may also play a role in alpha-cleavage (Vincent et al., 2001; McDonald et al., 2014), although some more recent studies have found no evidence for any involvement of ADAMs in the process (Beland et al., 2012; Wik et al., 2012).

Beta-cleavage of PrP^C occurs within the octapeptide repeat region, which results in a longer C-terminal fragment called C2 and the shorter N-terminal fragment N2. A recent study suggested that PrP^C can be cleaved between the adjacent His and Gly residues of each repeat (residues 61/62, 69/70, 77/78, 85/86 for human PrP^C), although one of these sites may be favoured over the others *in vivo* (McDonald et al., 2014). The beta form of proteolytic processing seems to take place at the cell surface, leading to release of N2 and retainment of C2 on the cell membrane (Mange et al., 2004; Watt et al., 2005). The discovery that beta-cleavage is mainly driven by reactive oxygen species (ROS) in the presence of copper ions suggested that it could be a response to oxidative stress (McMahon et al., 2001; Mange et al., 2004; Watt et al., 2005; McDonald et al., 2014) but the process may also occur physiologically, since C2 is found in healthy brain tissues of various species, albeit in small amounts (Mange et al., 2004; Campbell et al., 2013). C2 contains the alpha-cleavage site, which raises the possibility that C2 levels are usually low not because beta-cleavage is rare but because C2 is rapidly processed to C1 (Watt et al., 2005), although whether this sequential cleavage actually takes place *in vivo* is debatable (Sunyach et al., 2007; McDonald et al., 2014).

In the third form of processing, PrP^C is cleaved by ADAM10 at the 227/228 peptidyl bond (mouse numbering), which removes the GPI anchor and the three adjacent amino acid residues, resulting in shedding of the remaining, virtually full-length protein, sometimes known as N3, into the extracellular medium (Taylor et al., 2009; McDonald et al., 2014). Although the overall effect seems to be beneficial, shedding has a complex effect on TSE disease progression. On the one hand, it reduces the pool of PrP^C available for pathogenic conversion to PrP^{Sc} within cells; on the other, shedding may contribute to increased extracellular conversion and spreading of

misfolded protein by releasing PrP^{C} and possibly also PrP^{Sc} from the cell surface (Altmeppen et al., 2013; Altmeppen et al., 2015).

In addition to the various fragments produced by the aforementioned cleavage events, there are a few other forms of PrP^{C} that can be found at low levels within cells. Their formation seems to arise from an inefficiency in the ER-targeting signal peptide of PrP^{C}, which results in a small percentage of precursor molecules failing to translocate fully into the ER lumen. Some of this PrP^{C} does not enter the ER at all and is simply retained in the cytoplasm with its signal sequences uncleaved and without a GPI anchor. Interestingly, the levels of this immature, non-translocated PrP seem to be upregulated by ER stress (Orsi et al., 2006). More attention has been focused on the so-called ^{Ctm}PrP, which partially enters the ER – the hydrophobic domain of PrP^{C} acts as a transmembrane domain, leaving the C-terminal domain within the ER lumen and the N-terminal domain in the cytoplasm. Reports suggest that ^{Ctm}PrP is retained either in the ER or the Golgi before eventual degradation by the proteasome (Stewart et al., 2001; Stewart et al., 2005). Although usually produced at very low levels *in vivo*, mutations within the hydrophobic domain that make it more hydrophobic can increase ^{Ctm}PrP levels and, if the increase is sufficiently extreme, this can lead to a neurodegenerative phenotype in mouse models (Hegde et al., 1998; Stewart et al., 2005; Chakrabarti et al., 2009; Beland and Roucou, 2013). Strikingly, several mutations that have this effect are risk factors for Gerstmann-Sträussler-Scheinker syndrome, which implicates ^{Ctm}PrP in its pathogenesis (Mastrianni, 2010; Beland and Roucou, 2013). Another transmembrane form of PrP^{C} called ^{Ntm}PrP can be produced if the molecule inserts into the ER membrane in the opposite orientation to ^{Ctm}PrP i.e. the C-terminal domain rather than the N-terminal domain protrudes into the cytoplasm. However, very little research has focused on ^{Ntm}PrP (Chakrabarti et al., 2009).

1.2.6 Why investigate PrP^{C} function?

It is important to understand the physiological function of PrP^{C} in order to determine whether a loss of its function plays a role in the pathogenesis of TSEs. This is a

possibility given that data from various animal models indicate that PrP^C levels fall as disease progresses (Mays et al., 2014). Interestingly, conversion to PrP^{Sc} seems to have a negligible impact on PrP^C levels and, instead, PrP^C may be downregulated as a protective response to inhibit prion replication, as has been proposed by Mays et al. (2014). In a similar manner, therapeutic interventions to further reduce PrP^C expression or block its ability to interact with PrP^{Sc} (and, potentially, any other proteins) are being investigated; better knowledge of PrP^C function would aid in assessing the safety of these approaches. Additionally, knowing which proteins interact with PrP^C physiologically may be of use for developing other strategies for the treatment of TSEs. Finally, as described in later sections, there are some beneficial functions of PrP^C that could be exploited independently for therapeutic purposes. For these reasons, a significant amount of research effort has gone towards uncovering the physiological role of PrP^C and the knowledge gained from such work will be covered in the following sections.

1.3 PrP^C-knockout animal models

1.3.1 PrP^C knockout mice

Various animal models have been used to investigate PrP^C function. Firstly, in the early 1990s, two lines of PrP^C-knockout mice, referred to as Zurich I (Bueler et al., 1992) and Npu (Manson et al., 1994), were independently generated by gene targeting methods. PrP^C knockout completely prevented scrapie transmission to these mice, which provided strong evidence for the prion hypothesis (Bueler et al., 1993; Prusiner et al., 1993). Additionally, the Zurich I and Npu PrP^C-null mice were useful for generating antibodies against PrP^C and PrP^{Sc} (Prusiner et al., 1993; McCutcheon et al., 2014), since wild type mice would not be expected to mount an effective immune response to a self-antigen. More relevant to this thesis, however, is that the function of PrP^C could also be investigated in the PrP^C-null mice. Initial analyses identified no striking phenotypes of either knockout line, although there were (non-significant) indications of worse performance by the Zurich I mice in certain learning tasks (Bueler et al., 1992; Manson et al., 1994). The lack of clear phenotype

was surprising given the high degree of conservation of PrP^C structure among mammalian species (Pastore and Zagari, 2007), which suggests an important function for the protein. However, more recent studies have identified several phenotypes of these PrP^C-null mice, which will be covered in the following sections.

In the years after the generation of the Zurich I and Npu PrP^C-null mice, several groups independently produced additional lines for various reasons; these are known as Rcm0 (Moore et al., 1995), Ngsk (Sakaguchi et al., 1996), Rikn (Yokoyama et al., 2001) and Zurich II (Rossi et al., 2001). Unlike the Zurich I and Npu knockout mice, all the newer lines were shown to develop a late-onset ataxia due to death of cerebellar Purkinje neurons (Sakaguchi et al., 1996; Moore et al., 1999; Rossi et al., 2001; Yokoyama et al., 2001). The reintroduction of PrP^C into the Ngsk line rescued the ataxic phenotype, which seemed to confirm that it was caused by ablation of PrP^C expression (Nishida et al., 1999). However, the particular gene targeting methods used for production of the Rcm0, Ngsk, Rikn and Zurich II knockouts resulted in the generation of intergenic mRNA transcripts consisting of the undisrupted, non-protein-coding exons of *Prnp* and the exons of the neighbouring *Prnd*. Therefore, doppel was expressed under the control of the *Prnp* regulatory sequences, leading to ectopic doppel expression in the brains of the PrP^C-null mice but not the wild type controls (Moore et al., 1999) – according to the GeneAtlas U133A mouse transcriptome dataset (Su et al., 2004) accessible through the BioGPS gene annotation portal (Wu et al., 2016), doppel is normally expressed at high levels in the testes but at negligible levels in most other tissues, including the brain. The presence of the ataxic phenotype only in knockout mice with ectopic doppel expression in the brain suggested that the cerebellar Purkinje neurons were dying from doppel-mediated neurotoxicity rather than a lack of PrP^C. Further evidence obtained *in vitro* confirmed that doppel was toxic to neuronal cells, but only in the absence of PrP^C expression (Sakudo et al., 2005; Qin et al., 2006). Although the ability of PrP^C to block the neurotoxic effects of doppel may derive from a physical interaction between the proteins (Qin et al., 2006), this is unlikely to be a physiological function of PrP^C in the brain given that doppel is not usually expressed there.

The ectopic doppel expression makes it difficult to interpret the phenotypes of RcmO, Ngsk, Rikn and Zurich II PrP^C knockout mice. Additionally, the mixed genetic background of the Zurich I line (and also the Ngsk, Rikn and Zurich II lines) means that PrP^C-null individuals may differ from their wild type counterparts at genomic sites other than the *Prnp* locus (Steele et al., 2007). Even extensive backcrossing to one of the parental strains or to a different inbred strain may not eliminate this issue completely (Gerlai, 1996; Nuvolone et al., 2013), so some of the phenotypes observed in the Zurich I mice may be due to polymorphisms in *Prnp*-linked genes compared with the wild type control mice rather than a lack of PrP^C expression. Indeed, a specific phenotype associated with Zurich I (and Ngsk) PrP^C-null mice – increased phagocytosis of apoptotic cells by macrophages – was traced to a polymorphism in the nearby gene encoding tyrosine-protein phosphatase non-receptor type substrate 1 (also known as signal-regulatory protein alpha-1) (Nuvolone et al., 2013). The Npu line and a new knockout line called Zurich III, created using transcription activator-like effector nuclease genome editing technology (Nuvolone et al., 2016), are free from the problem of interfering linked genes, since they were generated on pure genetic backgrounds.

1.3.2 Other PrP^C-null animal models

In addition to the mouse models, PrP^C expression has also been knocked out in cattle, a natural host of TSEs. Detailed clinical and histopathological examinations as well as analyses of blood samples and isolated peripheral blood lymphocytes identified no overt abnormalities in these PrP^C-null cattle (Richt et al., 2007). However, these observations were made in relatively young cattle (up to 20 months of age) and the samples sizes were small, so subtle phenotypes would have been difficult to detect.

Recently, the first non-laboratory animals lacking PrP^C expression were identified. Naturally occurring PrP^C-null animals represent a useful resource for studying PrP^C function, since they are free from the confounding factors that can be introduced by genetic manipulation. The animals in question were goats of the Norwegian Dairy Goat breed that were homozygous for a *Prnp* allele with a

premature stop codon at residue 32 i.e. only a few amino acids after the end of the N-terminal signal sequence (Benestad et al., 2012). These PrP^C-null goats appeared to reproduce and behave normally (Benestad et al., 2012), although they may have increased red blood cell and neutrophil counts (Reiten et al., 2015).

1.4 PrP^C function

1.4.1 Stress-protection

The most extensive body of work relating to PrP^C function addresses the putative stress-protective properties of the protein. Initial evidence came from PrP^C protecting neuronal cells from serum withdrawal (Kuwahara et al., 1999) – the loss of growth and survival factors present in serum results in activation of mitochondria-dependent apoptotic signalling driven by a protein called Bax (Deckwerth et al., 1996). Over subsequent years, further studies using primary neurons and neuronal cell lines appeared to confirm that PrP^C expression confers protection against serum deprivation-induced apoptosis (Bounhar et al., 2001; Kim et al., 2004; Roucou et al., 2005; Krebs et al., 2007; Wu et al., 2008). However, the interpretation of the data produced by Kuwahara et al. (1999), Kim et al. (2004) and Wu et al. (2008) is complicated by their use of "HpL" cell lines. Kuwahara et al. (1999) describe the generation of these cells via immortalisation of primary hippocampal neurons derived from Rikn PrP^C-null mouse embryos. As described in section 1.3.1, the Rikn line of knockout mice display ectopic doppel expression in the brain and, consequently, the HpL cell lines also express doppel (Sakudo et al., 2005). Therefore, survival differences in response to serum deprivation between these cells and the control cell lines derived from wild type mice could have been due to the toxic effects of doppel expression. Additionally, the increased resistance to serum withdrawal following reintroduction of PrP^C into the HpL cells (Kim et al., 2004; Wu et al., 2008) may simply have been caused by PrP^C interacting with doppel and inhibiting its neurotoxicity (Moore et al., 1999; Sakudo et al., 2005; Qin et al., 2006), which, as explained in section 1.3, is unlikely to be a physiologically relevant function of PrP^C. After the issue affecting the HpL cell lines was recognised, the

Zurich I PrP^C-null mice that are not afflicted by the ectopic doppel expression were used for the production of additional immortalised hippocampal cell lines. However, there are conflicting reports over whether or not PrP^C expression confers significant protection against serum deprivation in these cells (Nishimura et al., 2007; Oh et al., 2008).

A number of studies have assessed the impact of PrP^C expression on the response to staurosporine (STS) treatment. STS is a potent but relatively non-selective adenosine triphosphate (ATP)-competitive kinase inhibitor (Ruegg and Burgess, 1989; Meggio et al., 1995), which seems to induce mitochondria-independent apoptotic signalling as well as affecting the same apoptotic pathways activated by serum deprivation (Zhang et al., 2004). PrP^C has been reported to protect against STS-mediated cell death in primary hippocampal neurons isolated from Zurich I mice, possibly via interactions with stress-induced-phosphoprotein 1 (STI1) (Lopes et al., 2005; Beraldo et al., 2010; Ostapchenko et al., 2013). STI1 is a secreted protein thought to bind to PrP^C and induce activation of the pro-survival protein kinase A signalling pathway. Interestingly, studies of primary cortical neurons derived from the Zurich I line of knockout mice found that expression of full length PrP^C actually increased susceptibility to STS (Paitel et al., 2004; Guillot-Sestier et al., 2009), although the N1 fragment produced by alpha-cleavage was apparently neuroprotective (Guillot-Sestier et al., 2009). Expression of full length PrP^C in several other cell lines has also been associated with poorer viability following STS treatment (Paitel et al., 2002; Paitel et al., 2003; Sunyach et al., 2007; Guillot-Sestier et al., 2009).

In addition to any direct effects on apoptosis, PrP^C reportedly protects cells from oxidative stress. For example, basal levels of ROS and lipid peroxidation were lower in PrP^C-transfected neuroblastoma and epithelial cell lines compared with untransfected controls (Rachidi et al., 2003; Zeng et al., 2003). Moreover, PrP^C expression by primary neurons, astrocytes and cell lines has been associated with lower levels of damage following exposure to various compounds that induce oxidative stress (Brown et al., 1997b; Brown et al., 2002; Senator et al., 2004; Anantharam et al., 2008; Dupiereux et al., 2008; Bertuchi et al., 2012; Alfaidy et al.,

2013). One potential mechanism is that PrP^C modulates the activities of the antioxidant enzymes that convert ROS into less toxic products – several studies have shown lower superoxide dismutase (SOD) and glutathione peroxidase activities in the absence of PrP^C expression (Brown et al., 1997b; Miele et al., 2002; Rachidi et al., 2003; Sakudo et al., 2003; Paterson et al., 2008). Since ROS appear to induce beta-cleavage of PrP^C in the presence of copper ions (McMahon et al., 2001; Mange et al., 2004; Watt et al., 2005; McDonald et al., 2014), the C2 or N2 fragments could actually be responsible for these putative antioxidant properties of PrP^C. Indeed, it has been reported that N2 lowers ROS production in response to serum deprivation in neuronal cell lines and neural stem cells (NSCs) (Haigh et al., 2015a; Haigh et al., 2015b). As well as potentially increasing the activities of antioxidant enzymes, a recent study proposed that PrP^C translocates to the nucleus in response to oxidative stress-induced DNA damage and directly activates the DNA base excision repair pathway by interacting with AP endonuclease and enhancing its activity (Bravard et al., 2015). Additionally, PrP^C-mediated activation of the tyrosine-protein kinase Fyn may lead to a stress-protective release of calcium ions from stores in the ER (Krebs et al., 2007). Not all the evidence agrees with an antioxidant role for PrP^C though – other studies have found no differences in SOD activity between PrP^C-null and wild type mice in the spinal cord, spleen or brain (Hutter et al., 2003; Steinacker et al., 2010). Additionally, although PrP^C protected neuroblastoma cells from the oxidative toxin 3-morpholinosynonimine hydrochloride via activation of the phosphatidylinositol-4,5-bisphosphate 3-kinase (PI3K)-RAC-alpha serine/threonine-protein kinase (Akt) signalling pathway, PrP^C transfection actually increased susceptibility to hydrogen peroxide treatment (Vassallo et al., 2005). Incidentally, PI3K-Akt signalling can activate the mammalian target of rapamycin pathway, leading to reduced levels of autophagy and perhaps explaining the reported connections between PrP^C and autophagy (Oh et al., 2008; Barbieri et al., 2011; Nah et al., 2013; Shin et al., 2014).

Finally, PrP^C has been implicated in the response to ER stress, which is caused by accumulation of unfolded/misfolded proteins within the ER. A cell responds to ER stress by triggering the unfolded protein response, which consists of the following:

1) upregulated expression of chaperones to improve protein folding; 2) global inhibition of protein synthesis; 3) an increase in ER volume; and 4) activation of the ER-associated protein degradation pathway (Halliday and Mallucci, 2014). Interestingly, ER stress-response elements have been found within the human *PRNP* promoter, explaining why PrP^C expression was induced following treatment of breast carcinoma cells with toxins that induce ER stress. In the same study, knockdown of PrP^C expression in several cancer cell lines resulted in increased cell death in response to these toxins (Dery et al., 2013). Higher PrP^C expression in spite of the global ER-stress-induced reduction of protein synthesis suggests a potential role for PrP^C in the unfolded protein response, although results from other studies argue against a protective role for PrP^C during ER stress (Roucou et al., 2005; Anantharam et al., 2008).

1.4.2 Cellular differentiation

In addition to its reported role in neuroprotection, several studies have shown that PrP^C promotes neurite outgrowth processes, and interactions of PrP^C with STI1 (Lopes et al., 2005), neural cell adhesion molecule 1 (Santuccione et al., 2005), epidermal growth factor receptor (Llorens et al., 2013), integrins (Loubet et al., 2012), laminin (Graner et al., 2000) or metabotropic glutamate receptors (Beraldo et al., 2011) have been put forward as potential explanations. Downstream of these putative interactions appears to be activation of ERK1/2 signalling (Lopes et al., 2005; Caetano et al., 2008), which may promote neurite extension by inhibiting the ras homolog gene family, member A (RhoA)-Rho-associated protein kinase (ROCK) pathway (Loubet et al., 2012; Llorens et al., 2013). RhoA-ROCK signalling stabilises the actin cytoskeleton, thereby inhibiting the development of filopodia – these dynamic protrusions from the neurite growth cone respond to the extracellular environment to guide migration of the developing neurite (O'Connor et al., 1990).

Neurite outgrowth is a feature of neuronal differentiation, which raises the possibility that PrP^C is not just involved in neurite outgrowth but instead plays a wider role in regulating differentiation, and perhaps not only within the nervous system. Indeed, it

has been proposed that PrP^C influences some of the earliest differentiation processes that occur during embryogenesis; for example, indirect modulation of the polysialylation of neuronal cell adhesion molecule 1 by PrP^C may be involved in the regulation of epithelial-to-mesenchymal transition, a process that enables cell migration and is, therefore, vital during development (Mehrabian et al., 2015; Mehrabian et al., 2016). Additionally, knockdown of PrP^C expression in cultured human embryonic stem cells delayed spontaneous differentiation into the three germ layers (Lee and Baskakov, 2013). In a similar manner, PrP^C expression has been shown to promote guided differentiation of human embryonic stem cells and neural precursors into neurons, astrocytes and oligodendrocytes (Steele et al., 2006; Lee and Baskakov, 2014). PrP^C is also implicated in the regulation of T lymphocyte differentiation in the thymus (Aude-Garcia et al., 2011).

Differentiation often involves a change in cell morphology, such as neurite extension, and this will likely require altered expression of cytoskeletal proteins. Several proteomic studies have identified such changes in cell lines in which PrP^C has been knocked down or over-expressed and also in PrP^C-null liver tissues compared with wild type controls (Provansal et al., 2010; Weiss et al., 2010; Arora et al., 2013; Mehrabian et al., 2014). Analyses of brain tissues have been less successful at detecting differential expression of cytoskeletal proteins or, indeed, of any proteins at all (Crecelius et al., 2008; Mehrabian et al., 2016), although this could be the result of the averaging out of cell type-specific effects of PrP^C over an entire tissue. Another common feature of differentiation is a change to cell cycle progression; for instance, neural precursors withdraw from the cell cycle as they differentiate into post-mitotic neurons. PrP^C has been shown to inhibit proliferation of oligodendrocyte precursors (Bribian et al., 2012), neuronal cells (Kim et al., 2005) and cells derived from the intestinal epithelium (Morel et al., 2008). In the case of NSCs, one study found that expression of full length PrP^C promoted proliferation, whilst the cleavage fragments N1 and N2 appeared to be inhibitory (Haigh and Collins, 2014). Signalling mediated by ROS (Le Belle et al., 2011) may be important for regulating proliferation and self-renewal of NSCs as well as their differentiation into neurons, and, interestingly, the effects of the different N-terminal PrP fragments on NSC

proliferation apparently arose from modulation of intracellular ROS levels (Haigh and Collins, 2014). Therefore, the effect of PrP^C on NSC proliferation could be a consequence of its supposed antioxidant properties or, conversely, protection from oxidative stress by PrP^C may result from a role in regulating physiological levels of ROS. Positive regulation of proliferation by PrP^C has also been observed in neuroblastoma cells – the proposed mechanism was PrP^C interacting with EGFR to promote activation of the PI3K-Akt pathway (Llorens et al., 2013). PI3K-Akt-dependent mammalian target of rapamycin activation might also drive the increased protein synthesis required for differentiation processes, such as changes in morphology (Roffe et al., 2010).

1.4.3 Neuronal excitability

As described in the previous section, an interaction between PrP^C and metabotropic glutamate receptors has been linked to the regulation of neurite outgrowth (Beraldo et al., 2011). There are also reports of PrP^C interacting with other neurotransmitter receptors, including α7 nicotinic acetylcholine receptors (Beraldo et al., 2010), kainate receptors (Carulla et al., 2011), α-amino-3-hydroxy-5-methyl-4-isoxazolepropionic acid receptors (Kleene et al., 2007) and N-methyl-D-aspartate receptors (NMDARs) (Khosravani et al., 2008). NMDARs are a subclass of ionotropic glutamate receptors and are particularly implicated in excitotoxic death of neurons; this can occur when overactivation of NMDARs causes dysregulation of intracellular calcium homeostasis, leading to disruption of various physiological processes (Bondy and Lee, 1993). NMDAR-mediated excitotoxicity contributes to neuronal death in TSEs and other neurodegenerative disorders (Muller et al., 1993; Gorman, 2008). Intriguingly, PrP^C has been reported to inhibit NMDAR activity, which suggests that PrP^C may protect neurons from excitotoxic death (Khosravani et al., 2008). There is some evidence for this *in vivo*; for instance, PrP^C knockout mice have been shown to display increased excitotoxicity in the hippocampus following N-methyl-D-aspartate[1] injection or ischaemic insult and in the retina in response to

[1] N-methyl-D-aspartate mimicks the effect of glutamate on NMDARs but does not activate any other type of glutamate receptor.

damaging light intensities (Sakurai-Yamashita et al., 2005; Frigg et al., 2006; Khosravani et al., 2008). Furthermore, knockout in zebrafish of one of its two *Prnp* paralogs affected NMDAR currents in a way that hinted at a greater susceptibility to excitotoxicity, suggesting that this putative function of PrP^C may be conserved over wide evolutionary distance (Fleisch et al., 2013). Aside from affecting neurotransmitter receptor activity by direct interaction it has also been proposed that PrP^C expression by astrocytes promotes glutamate clearance from the synapse (Brown and Mohn, 1999).

If PrP^C can modulate the activities of neurotransmitter receptors then a role in learning and memory also seems plausible. Indeed, Zurich I PrP^C-null mice display abnormal behaviour in nest building and novel environment exploration tasks and their age-related decline in short-term memory is reported to be more pronounced than that of wild type controls (Schmitz et al., 2014). Moreover, the effect of ageing on memory can apparently be blocked by infusing wild type mice with a peptide containing the putative PrP^C binding site of STI1 (Rial et al., 2009). Mice overexpressing PrP^C were similarly protected from age-related memory decline (Rial et al., 2009).

1.4.4 Myelin maintenance

One of the clearest phenotypes of PrP^C knockout mice is a widespread demyelination of the peripheral nervous system (PNS) that begins in early adulthood. This phenotype has been observed in the Zurich I and Npu knockout mice as well as the newly generated Zurich III line (Bremer et al., 2010; Nuvolone et al., 2016). Lack of PrP^C seems to result in defective myelin maintenance, since signs of cycles of demyelination and remyelination can be observed in the mice (Bremer et al., 2010). Interestingly, Bremer et al. (2010) showed that neuron-specific PrP^C expression was sufficient to rescue this phenotype, whilst PrP^C expression purely in Schwann cells was not. Recently, it was reported that an interaction between the PrP^C N-terminal and the G-protein coupled receptor 126 on the surface of Schwann cells could be responsible for the myelin maintenance signalling (Kuffer et al., 2016). In the

original paper by Bremer et al. (2010) there was also some evidence that alpha-cleavage of neuronal PrP^C was required to prevent demyelination, perhaps suggesting that N1 released by the cleavage interacts in some way with Schwann cells to promote myelin maintenance. No myelin-related abnormalities were seen in the central nervous system (CNS) of the knockout mice, although a reduction in spinal cord expression of PrP^C has been found in human patients with multiple sclerosis, a demyelinating disease of the CNS (Scalabrino et al., 2015).

1.4.5 Circadian rhythm

The distinctive clinical feature of the TSE known as fatal familial insomnia is severe disruption of the sleep-wake cycle (Collins et al., 2001). Strikingly, PrP^C-null mice also exhibit disruptions to their sleep structure, including faster cycling through the different stages of sleep and more brief awakenings than wild type mice (Tobler et al., 1996; Tobler et al., 1997; Sanchez-Alavez et al., 2007). The cause of these issues may be impaired production of melatonin, the hormone produced by the pineal gland that regulates sleep timing as well as other processes. Melatonin release is under control of the suprachiasmatic nucleus of the hippocampus, which is the master regulator of the circadian rhythms that drive the sleep-wake cycle. The result is that melatonin levels vary according to a 24 hour cycle – levels are highest in the hours of darkness and, for a nocturnal animal like a mouse, lower levels are required for sleep initiation. One study found that serum melatonin levels of PrP^C-knockout mice were much lower than in wild type mice during the dark phase of the cycle but were higher during the light phase, which probably contributed to the sleep disruption (Brown et al., 2002). A network of proteins called the circadian clock work together to generate circadian rhythms and, strikingly, *Prnp* mRNA levels seem to be subject to circadian oscillations in the suprachiasmatic nucleus in addition to other areas of the rat forebrain (Cagampang et al., 1999). Therefore, PrP^C may be involved in the regulation of the sleep-wake cycle, suggesting that a loss of this function could play a role in the pathogenesis of fatal familial insomnia.

Given that metabolic processes can also be regulated in a circadian manner (Dibner et al., 2010), one might expect PrP^C-null mice to exhibit changes to such processes. It is therefore interesting to note that abnormalities in glucose homeostasis have been detected in these mice (Strom et al., 2011; Brito et al., 2013). Specifically, Strom et al. (2011) demonstrated that blood glucose levels in these mice were slower to return to normal after intraperitoneal injection of glucose, although insulin secretion by the pancreas and tissue sensitivity to insulin were not affected in this particular study. In contrast, Brito et al. (2013) reported that insulin resistance developed more quickly in response to a high fat diet in PrP^C-knockout mice than in their wild type counterparts.

1.4.6 Metal ion homeostasis

A number of early studies of PrP^C function focused on an apparent ability to bind copper ions at the cell membrane via the octapeptide repeat region of the protein (Hornshaw et al., 1995a; Hornshaw et al., 1995b; Brown et al., 1997a). Subsequently, PrP^C interactions with Cu^{2+} have been implicated in the regulation of NMDAR activity (Gasperini et al., 2015), astrocytic glutamate uptake (Brown and Mohn, 1999), protection against oxidative stress (Watt et al., 2007) and maintenance of Cu^{2+} homeostasis in the placenta (Alfaidy et al., 2013). However, whilst it seems certain that PrP^C can bind Cu^{2+}, the relevance of this interaction *in vivo* has been questioned. Firstly, it has been reported that PrP^C-dependent internalisation of Cu^{2+} by cells in culture did not occur when the concentration of Cu^{2+} in the extracellular medium was at a physiological relevant level (Rachidi et al., 2003). Secondly, whilst some studies have demonstrated that PrP^C expression is protective against oxidative stress caused by excessive Cu^{2+} levels (Rachidi et al., 2003; Watt et al., 2007), Cingaram et al. (2015) showed that transfecting PrP^C into the Zpl PrP^C-null hippocampal cell line did not reduce Cu^{2+}-mediated toxicity. Thirdly, binding of Cu^{2+} by PrP^C in the presence of ROS is supposed to promote internalisation of PrP^C followed by its beta-cleavage, possibly as part of the response to oxidative stress (McMahon et al., 2001; Watt et al., 2005; McDonald et al., 2014), and yet other researchers have found no evidence to connect Cu^{2+}-mediated endocytosis of PrP^C

with its antioxidant role (Zeng et al., 2003). Furthermore, one report suggests that Cu^{2+} binding is not involved in PrP^C endocytosis at all (Sunyach et al., 2003),

Studies of neuronal cell lines showed that PrP^C transfection offered no protection against the oxidative DNA damage induced by treatment with high levels of Mn^{2+}, Co^{2+} or Zn^{2+} (Cingaram et al., 2015). However, neuroblastoma cells were protected from the toxic effects of exposure to large amounts of Fe^{2+} (Watt et al., 2007). Interestingly, Zurich I PrP^C-null mice show signs of iron deficiency in the brain, liver, spleen and kidneys (Singh et al., 2009; Haldar et al., 2015), and recent work has proposed that PrP^C could have ferrireductase activity (i.e. it can convert Fe^{3+} to Fe^{2+}) (Singh et al., 2013; Haldar et al., 2015), thereby enhancing iron uptake via divalent-metal transporter 1 and/or ZIP14 (Tripathi et al., 2015). Alternatively, PrP^C may interact with a separate ferrireductase enzyme to modulate its activity (Tripathi et al., 2015). Together, these findings implicate PrP^C in the cellular uptake of iron and any protective effect of PrP^C against Fe^{2+}-induced oxidative stress could be linked to this putative role.

1.4.7 Roles in immune cells

Because TSEs are neurodegenerative disorders, much of the research into PrP^C function has focused on its role in the nervous system. However, PrP^C is also expressed in immune cells, including T-lymphocytes, natural killer cells and mast cells (Durig et al., 2000; Haddon et al., 2009). Mast cells reportedly express high levels of PrP^C, some of which is shed from the cell membrane as the N3 fragment (Haddon et al., 2009). When activated, mast cells release various inflammatory mediators, including histamine, prostaglandins and cytokines (Stempelj and Ferjan, 2005). Interestingly, treatment of cultured mast cells with compounds that induce activation resulted in rapid shedding of a large proportion of the cellular pool of PrP^C, suggesting that the protein could be involved in the inflammatory response (Haddon et al., 2009). Mast cells are also involved in angiogenesis (Cantarella et al., 2011), a process that PrP^C seems to modulate within the placenta, although this function may be more linked to the putative antioxidant properties of PrP^C (Alfaidy

et al., 2013). Moreover, in addition to other pain mediators, mast cells secrete NGF, which sensitises nociceptive neurons to painful stimuli and has long-term effects on neuronal connectivity within the spinal cord, potentially leading to the development of chronic pain (Hefti et al., 2006; Pezet and McMahon, 2006; Gold and Gebhart, 2010; Kuner, 2010; Cantarella et al., 2011). In a similar manner, PrP^C knockout in mice is associated with altered sensitivity to pain, although the reports are inconsistent: one study found that the PrP^C-null mice showed a hypersensitivity to pain (Gadotti and Zamponi, 2011), whilst another showed that PrP^C-null mice were more resistant to pain than their wild type counterparts (Meotti et al., 2007). It is possible that PrP^C expression could modulate pain sensitivity via a role in regulating mast cell function, although Gadotti and Zamponi (2011) reported that loss of PrP^C-dependent NMDAR inhibition was most likely responsible for the hypersensitivity to pain displayed by the PrP^C-null mice in their study.

PrP^C expression by T-lymphocytes may be involved in their differentiation, since knockdown of PrP^C resulted in an increased tendency for T-cells to develop a pro-inflammatory phenotype (Hu et al., 2010). Additionally, in a model of autoimmune encephalomyelitis, PrP^C knockout mice experienced a more severe disease phenotype that was linked to increased T-cell-dependent neuroinflammation (Tsutsui et al., 2008), possibly because PrP^C is involved in the signalling complexes that regulate T-cell activation (Mabbott et al., 1997; Mattei et al., 2004). Contrastingly, another study using the encephalomyelitis model found no evidence that PrP^C knockout drove T-cells towards a more inflammatory phenotype; instead, the increased disease severity appeared to stem from the loss of PrP^C expression within the CNS, not the immune system (Gourdain et al., 2012).

As explained in section 1.3.2, the first non-laboratory animals lacking PrP^C expression were identified recently (Benestad et al., 2012). No overt abnormalities were identified in these PrP^C-null goats (Benestad et al., 2012), although they were reported recently to have increased neutrophil numbers compared with wild type goats (Reiten et al., 2015). Work is still ongoing to characterise fully the phenotypes of these animals.

1.4.8 Mitochondrial homeostasis

Mouse studies have shown that PrP^C knockout has no effect on the membrane potential or baseline respiration rate of mitochondria nor does it alter the activities of the individual complexes of the electron transport chain (Brown et al., 2002; Miele et al., 2002; Lobao-Soares et al., 2005). However, transcriptomic and proteomic analyses of brain tissue and cultured cells have identified specific subunits within each of the five electron transport chain complexes that vary in their expression according to the presence or absence of PrP^C (Miele et al., 2002; Ramljak et al., 2008; Stella et al., 2012). Furthermore, fewer mitochondria were found in the brains and myocardium of Npu PrP^C-null mice than in wild type controls, although the mitochondria that were present were larger and had increased maximal respiratory capacities, presumably to compensate for the reduced numbers (Miele et al., 2002; Paterson et al., 2008). The enhanced maximal respiratory capacity of individual PrP^C-null mitochondria was linked to a higher level of activity of electron transport chain complex I, which was, in turn, associated with an increase in superoxide production (Paterson et al., 2008). Dealing with this extra superoxide could explain why superoxide dismutase 2, which is found within mitochondria and converts superoxide into either hydrogen peroxide or molecular oxygen, is more active in PrP^C-null mice (Brown et al., 1997b; Miele et al., 2002; Paterson et al., 2008). Additionally, it is possible the apparent antioxidant properties of PrP^C could derive from a role in maintaining mitochondrial homeostasis and, consequently, preventing excessive production of ROS.

1.4.9 Roles in regulating levels of amyloid beta and tau

Beta-cleavage of the amyloid precursor protein (APP) by beta-secretase 1 produces a fragment called sAPPβ that is subsequently cleaved by gamma-secretase to produce amyloid beta peptides (Aβ). PrP^C has been reported to inhibit beta-secretase 1 (Parkin et al., 2007; Whitehouse et al., 2013), which suggests that PrP^C expression should protect against the development of Alzheimer's disease – accumulation of misfolded Aβ is a key feature of the disease. A feedback loop has also been proposed

that consists of the APP intracellular domain (the other fragment produced by cleavage of sAPPβ) activating cellular tumour antigen p53, which subsequently upregulates PrP^C, leading to further inhibition of beta-secretase 1 activity (Vincent et al., 2009). However, recent work has questioned whether the APP intracellular domain is able to induce PrP^C expression (Lewis et al., 2012) and one study found that PrP^C expression was actually associated with higher rates of APP beta-cleavage (McHugh et al., 2012).

It has been suggested that PrP^C downregulates transcription of microtubule-associated protein tau, which could also be protective against Alzheimer's disease, since accumulation of neurofibrillary tangles consisting of hyperphosphorylated tau is the other major molecular feature of the disease (Chen et al., 2010). Conversely, oligomeric forms of Aβ are reported to bind to PrP^C at either its extreme N-terminal region (Chen et al., 2010; Dohler et al., 2014) or between residues 92 and 110 (Lauren et al., 2009), which may elicit toxic effects via hyperactivation of the tyrosine-protein kinase Fyn signalling pathway (Vergara et al., 2015). The C1 fragment that is left at the cell membrane following alpha-cleavage of PrP^C lacks both the putative Aβ binding sites. Therefore, the reduced levels of hippocampal PrP^C and the increased rates of alpha-cleavage in the cortex that have been reported in the brains of patients with sporadic Alzheimer's disease could be a protective response (Whitehouse et al., 2010; Beland et al., 2014). On the other hand, one study found that higher levels of PrP^C in serum were correlated with poorer cognitive function in an elderly human population (Breitling et al., 2012), although the increase in serum PrP^C could indicate a loss of PrP^C from neuronal membranes.

1.5 Overall conclusions on the current understanding of PrP^C function

As summarised in the previous sections, PrP^C has been associated with a diverse array of functions. However, the issues described in section 1.3.1 that affect several of the PrP^C knockout mouse lines – ectopic doppel expression in the brain and the impact of polymorphisms in genes flanking the *Prnp* locus – cast doubt upon the

results obtained from studies of these mice or of cells derived from them. This problem particularly affects the data showing that PrP^C protects cells from apoptosis, so the idea that PrP^C is a stress-protective protein is certainly open for debate. Arguably, the evidence that PrP^C protects against oxidative stress is more consistent and convincing, although this putative function, as far as I am aware, has largely been observed *in vitro* or in the Zurich I knockout mice and has not been confirmed in Npu PrP^C-null mice. Furthermore, it has been proposed that the recently identified role for PrP^C in directly protecting cells from genotoxic stress (Bravard et al., 2015) may, instead, be due to polymorphisms between the Zurich I mice and their wild type counterparts in a neighbouring gene that encodes WD repeat-containing protein 76 (Nuvolone et al., 2016).

The deficits in myelin maintenance and control of the sleep-wake cycle are, perhaps, the most reliable phenotypes observed in PrP^C knockout mice – adult-onset demyelination of the PNS has been observed in the Npu, Zurich I and Zurich III lines (Bremer et al., 2010; Nuvolone et al., 2016) and sleep abnormalities have been identified in Zurich I and Npu PrP^C-null mice (Tobler et al., 1996; Sanchez-Alavez et al., 2007). Moreover, the observations that melatonin production is disrupted in PrP^C-knockout mice (Brown et al., 2002) and that *Prnp* mRNA expression oscillates in a circadian manner in the suprachiasmatic nucleus (and other regions) of the rat forebrain (Cagampang et al., 1999) warrant further attention, since they suggest a wider role for PrP^C in the regulation of the sleep-wake cycle.

There have been numerous studies linking PrP^C expression to the induction of neurite outgrowth and PrP^C also appears to modulate the expression of certain cytoskeletal proteins and affect cell proliferation. Together, these data hint at a role for PrP^C in modulating differentiation processes, which will often include changes to cell morphology and to cell cycle regulation. This hypothesis is supported by recent studies that implicate PrP^C in epithelial-to-mesenchymal transition (Mehrabian et al., 2015; Mehrabian et al., 2016), stem cell differentiation (Steele et al., 2006; Lee and Baskakov, 2013; Lee and Baskakov, 2014) and T-lymphocyte differentiation (Aude-Garcia et al., 2011).

Interactions between PrP^C and several different neurotransmitter receptors have been identified, which may be a consequence of the random coil configuration of the PrP^C N-terminal that reportedly enables the protein to bind to multiple partners (Bakkebo et al., 2015). However, there are some conflicts in the literature surrounding the putative role of PrP^C in regulating neuronal excitability via these interactions. For example, the apparent ability of PrP^C to inhibit NMDAR activity (Khosravani et al., 2008) could potentially explain the observed protective effect of PrP^C expression against excitotoxic neuronal death (Sakurai-Yamashita et al., 2005; Frigg et al., 2006; Khosravani et al., 2008) and yet, another study of Zurich I PrP^C-null mice found that the contribution of NMDAR-mediated currents to excitatory postsynaptic potentials in the hippocampus was not affected by the absence of PrP^C expression (Collinge et al., 1994). Collinge et al. (1994) reported instead that PrP^C knockout weakened fast inhibitory postsynaptic potentials generated via gamma-aminobutyric acid receptors but, again, this finding was questioned by other researchers who identified no effects of PrP^C ablation on these inhibitory currents (Lledo et al., 1996).

Most of the effects of PrP^C knockout on mitochondrial homeostasis are restricted to altered expression of a few proteins in the electron transport chain – any overall impairments to mitochondrial function appear to be quite subtle and, as far as I am aware, have only been observed in the Npu line of PrP^C-knockout mice (Miele et al., 2002; Paterson et al., 2008). Similarly, whilst the evidence for PrP^C binding Cu^{2+} is strong (Hornshaw et al., 1995a; Hornshaw et al., 1995b; Brown et al., 1997a), this function may not have much impact in a physiological context (Rachidi et al., 2003; Sunyach et al., 2003; Zeng et al., 2003; Cingaram et al., 2015). The high levels of PrP^C expression by mast cells and the reported shedding of the protein upon activation (Haddon et al., 2009) are certainly intriguing findings but, overall, there has been very little study of the functional consequences of PrP^C expression in immune cells. Finally, the reported connection between PrP^C and APP processing could be very important, given the ever-increasing heath and economic burden of Alzheimer's disease. However, the conflicting nature of the evidence means that it is unclear whether PrP^C expression is protective against the disease or not.

1.6 Project aims

Whilst PrP^C appears to contribute to a wide variety of cellular processes, knowledge of the underlying molecular mechanisms remains rather limited. The main aim of my project was to investigate these mechanisms to improve understanding of the physiological function of PrP^C. A clearer description of PrP^C function would be useful in two ways: firstly, it should aid the development of treatments for TSEs, diseases that currently lack any effective therapies; and secondly, medically useful properties of PrP^C that are independent of its role in TSEs, such as its putative stress-protective function, could also be exploited for therapeutic purposes.

The specific objectives of the project were as follows:

- Stably transfect the *Prnp* protein-coding sequence into the SH-SY5Y neuroblastoma cell line to create a cellular model for investigating PrP^C function, and then characterise the model (Chapter 3)
- Expose the stably transfected cells to various forms of stress in order to clarify the role that PrP^C plays in the response to stress (Chapters 3 and 4)
- Perform proteomic analyses comparing PrP^C-transfected SH-SY5Y cells with untransfected controls to identify the proteins that vary in their expression levels as a result of PrP^C transfection, and then use this information to identify potential pathways and processes regulated by PrP^C (Chapters 4 and 5)
- Follow up the putative functions of PrP^C suggested by the proteomic analyses and, if possible, identify the molecular mechanisms responsible (Chapters 5 and 6)
- Investigate whether putative functions of PrP^C identified from the cellular model can be confirmed *in vivo* by performing molecular analyses using tissues from PrP^C-null and wild type control mice (Chapters 5 and 6)

Chapter 2: Materials and methods

2.1 Generation of vector containing *Prnp* coding sequence

The full coding sequence (CDS) of the murine *Prnp* gene was cloned into the pCI-neo mammalian expression vector as described in the following sections. All reagents were from Promega unless otherwise specified.

2.1.1 Amplification of murine *Prnp* CDS by the polymerase chain reaction

Genomic DNA was obtained from a wild type C3H mouse brain using the Wizard SV Genomic DNA Purification System. The *Prnp*[2] CDS was amplified from genomic DNA by the polymerase chain reaction (PCR). Reactions consisted of template genomic DNA mixed with Platinum PCR SuperMix High Fidelity (Thermo Fisher Scientific) and 400 nM forward and reverse primers (Sigma-Aldrich). The forward primer contained an EcoRI restriction site (sequence: GGAATTCCACC-ATGGCGAACCTTGGCTACTG) and the reverse primer a SalI site (sequence: GCGTCGACTCATCCCACGATCAGGAAGATG). For the forward primer, the "CACC" between the EcoRI site and the start codon provided a "Kozak" consensus sequence to ensure efficient ribosome binding of the mRNA. The PCR program used was as follows: initial denaturation at 95 °C for 3 min; 35 cycles of 30 s denaturation at 95 °C, 30 s primer annealing at 55 °C and 90 s extension time at 68 °C; and a final 5 min extension at 68 °C.

Blue/Orange loading dye was added to PCR products before they were loaded into a 1 % (w/v) agarose gel containing SYBR Safe DNA stain (Thermo Fisher Scientific). The 50-base pairs (bp) DNA step ladder was also loaded for band sizing. The PCR products were separated by electrophoresis at 100 V in tris-acetate-ethylenediaminetetraacetic acid running buffer. DNA was visualised using a UV transilluminator and bands were present around the 800 bp size expected for the *Prnp*

[2] Mouse PrP^C can vary at amino acids 108 and 189, depending on which *Prnp* allele (*Prnp*^{a} or *Prnp*^{b}) is encoded in the genome. The C3H inbred mouse strain carries the *Prnp*^{a} allele.

CDS. These bands were excised and purified using the PureLink Quick Gel Extraction Kit (Thermo Fisher Scientific).

2.1.2 Restriction enzyme digestions

1 µg purified PCR product was digested overnight at 37 °C using 20 units of EcoRI (NEB). Buffer salts were removed by ethanol precipitation and the DNA resuspended in nuclease-free H_2O. The DNA was further digested at 37 °C for 1 h using 10 units of SalI, which was then heat inactivated at 65 °C for 15 min. The digested DNA was electrophoresed as described in the previous section and the bands at ~800 bp were again excised and purified using the PureLink Quick Gel Extraction Kit.

1 µg pCI-neo mammalian expression vector was simultaneously digested for 4 h at 37 °C with 12 units of EcoRI and 10 units of SalI in restriction enzyme buffer D. One unit of thermosensitive alkaline phosphatase was also included in the reaction to dephosphorylate the vector ends. Enzymes were heat activated at 74 °C for 20 min before the digested plasmid DNA was electrophoresed and gel purified as described above.

2.1.3 Insertion of PCR product into pCI-neo vector

The PCR product and vector were ligated using the LigaFast Rapid DNA Ligation System. XL-1 Blue cells (Agilent) were transformed directly with the ligation product according to the manufacturer's protocol. The cells were grown on lysogeny broth (LB) agar plates overnight at 37 °C. Antibiotic selection during this and subsequent steps was with 100 µg/ml ampicillin and 30 µg/ml tetracycline.

Colonies were checked for the presence of the desired insert by colony PCR. Reactions consisted of 1 unit FastStart Taq DNA polymerase and the associated buffer (Roche), 200 µM deoxynucleotides (Thermo Fisher Scientific), nuclease-free H_2O and 200 nM forward and reverse primers (AAGGCTAGAGTACTTAATACGA

and CATTAACCCTCACTAAAGGGA, respectively; Sigma-Aldrich). The primers were designed against vector sequences flanking the inserted DNA to ensure the insert was in the correct orientation. Individual colonies were sampled using pipette tips, which were placed into the reaction tubes. The PCR program used was as follows: initial denaturation at 95 °C for 4 min; 40 cycles of 30 s denaturation at 95 °C, 30 s primer annealing at 50 °C and 90 s extension time at 72 °C; and a final 5 min extension at 72 °C. PCR products were analysed by agarose gel electrophoresis as described previously; the only change was the use of tris-borate-ethylenediaminetetraacetic acid running buffer instead of tris-acetate-ethylenediaminetetraacetic acid to improve resolution of small DNA fragments. TrackIt 1 kb Plus DNA ladder (Thermo Fisher Scientific) was also loaded into the gel for band sizing. Presence of bands at ~850 bp indicated that the vector contained the *Prnp* CDS.

Successfully transformed colonies were expanded overnight in 3 ml liquid LB medium at 37 °C. Glycerol stocks were prepared by mixing equal volumes of each culture with LB medium containing 30 % (v/v) glycerol and snap freezing on dry ice before storage at -80 °C. Plasmid DNA was isolated from the remainder of each culture using the Qiaprep Miniprep Kit (Qiagen).

2.1.4 Sequencing of vectors containing the *Prnp* CDS insert

Sequencing PCRs were set up using the BigDye Terminator v3.1 Cycle Sequencing Kit (Applied Biosystems). Reactions consisted of 1.5-2.5 µg purified plasmid DNA, 10 % (v/v) BigDye Ready Reaction Mix, 15 % (v/v) sequencing buffer, 250 nM primer and nuclease-free H_2O. For each plasmid clone, separate reactions were prepared to enable sequencing in forward and reverse directions. Each of these reactions contained either the forward or reverse primer described in the previous section. The PCR program used was 25 cycles of 10 s denaturation at 96 °C, 15 s primer annealing at 53 °C and 4 min extension time at 60 °C.

PCR products were purified by ethanol/ethylenediaminetetraacetic acid (EDTA) precipitation. Firstly, EDTA was added to a final concentration of 25 mM. Secondly, PCR products were mixed with pure ethanol in a ratio of 1:3 and incubated at room temperature (RT) for 15 min. Precipitated DNA was pelleted by centrifugation at 1300 x g for 30 min at 4 °C. The supernatants were removed and the DNA resuspended in 70 % (v/v) ethanol. Precipitated DNA was again pelleted by centrifugation at 1300 x g, this time for 15 min at 4 °C. After removing the supernatants, the pelleted DNA samples were air dried for 15 min before storage at 4 °C.

Sequencing was carried out in-house by Ms. Paula Stewart, a research assistant who is an experienced user of the sequencing equipment. Paula resuspended the pelleted DNA in Hi-Di Formamide (Applied Biosystems) and analysed the samples using an Applied Biosystems 3130 Genetic Analyser. I manually checked the obtained sequence chromatograms using the DNASTAR Lasergene software suite to ensure that the automated base calling was accurate.

2.1.5 Production of pCI-neo-MoPrnp

Five out of six plasmid clones contained the *Prnp* CDS with no errors. The clone that gave the best quality sequencing data was chosen for further use. The corresponding glycerol stock was streaked onto LB agar and colonies were grown overnight at 37 °C. Antibiotic selection was as described in section 2.1.3. One colony was selected and expanded in liquid LB medium, again at 37 °C. Once the culture had reached an optical density (at 600 nm) of approximately 2.0, plasmid DNA was purified using the PureLink HiPure Plasmid Maxiprep Kit (Thermo Fisher Scientific). Finally, 500 ng of the plasmid clone and 500 ng of empty pCI-neo vector were analysed by agarose gel electrophoresis as described in section 2.1.3. This was to confirm that the purified plasmid clone still contained the *Prnp* CDS, as indicated by slower migration on the gel due to its increased size. In later sections, the plasmid clone is referred to as pCI-neo-MoPrnp.

2.2 Routine culture of SH-SY5Y cells

Human neuroblastoma SH-SY5Y cells were purchased from the European Collection of Cell Cultures. SH-SY5Y cells were routinely maintained as adherent cultures in Dulbecco's modified Eagle's medium (DMEM; formulation containing high glucose, GlutaMAX and pyruvate), supplemented with minimal essential medium non-essential amino acids, 10 % (v/v) foetal bovine serum (FBS) and 1 % (v/v) penicillin-streptomycin solution (final concentrations of 50 units/ml penicillin, 50 µg/ml streptomycin). All reagents were from Thermo Fisher Scientific. The medium described is referred to as "growth medium" and was used for all experiments unless stated otherwise.

Unless stated otherwise, cells were cultured in Nunc tissue culture flasks or plates with the Nunclon Delta surface treatment. Cultures were incubated at 37 °C in 5 % CO_2 and were normally subcultured 1-2 times per week. The growth medium was replaced every 3-5 days.

2.2.1 Subculturing

Cells were rinsed with Hank's Balanced Salt Solution (HBSS) and detached by treatment with 0.05 % (w/v) trypsin/0.02 % (w/v) EDTA in HBSS for 5 min at 37 °C. Trypsin was neutralised by addition of at least an equal volume of growth medium. Cell clumps were dissociated by gently pipetting up and down ~15 times. The cell suspension was further diluted as required for seeding flasks or plates. If the cell suspension needed to be concentrated instead, cells were pelleted by centrifugation at 200-300 x g for 10 min at RT and resuspended in an appropriate volume of growth medium.

If a cell count was required before plating, a sample of cell suspension was mixed in equal parts with 0.4 % (w/v) trypan blue stain (Sigma-Aldrich). A coverslip was affixed to a haemocytometer and one of the chambers filled with the stained cell

suspension sample. The total number of viable cells in the four large corner squares of the chamber was determined. Cells overlapping the top and left hand sides of the squares were included, while those overlapping the bottom and right hand sides were excluded. All blue-stained (dead) cells were excluded. The total count was multiplied by 5000 to give the number of cells per ml in the original suspension.

2.2.2 Cryopreserving cells

Cells were detached from tissue culture flasks as described in the previous section. Cells were centrifuged at 200-300 x g for 10 min at RT. Pelleted cells were resuspended in freeze medium (45 % (v/v) DMEM, 45 % (v/v) FBS, 10 % (v/v) dimethyl sulphoxide (DMSO) and 1 % (v/v) penicillin-streptomycin solution) that had been chilled to 4 °C. Cell clumps were dissociated by gently pipetting up and down ~15 times. Cells were aliquoted into cryovials at a concentration of 1 x 10^6/ml or greater and were slowly cooled overnight to -80 °C inside a Nalgene "Mr. Frosty" freezing container. Frozen cells were transferred to a -150 °C electric freezer for long-term storage.

2.2.3 Reviving frozen cells

Cryovials of frozen cells were transferred on dry ice from -150 °C storage to the laboratory. Cells were thawed rapidly in a 37 °C water bath and clumps were dissociated by gently pipetting up and down ~15 times. Cell suspensions were transferred to 15 ml Falcon tubes and diluted as required with pre-warmed growth medium prior to seeding flasks. If cells were to be cultured initially in small flasks (25 cm^2 surface area) then the cell suspensions were first pelleted by centrifugation at 200-300 x g for 10 min at RT. Pelleted cells were resuspended in growth medium before seeding flasks. These steps were necessary for culturing in smaller flasks as the DMSO concentration in the medium would have been toxic otherwise. Irrespective of the flask size, the growth medium was replaced after 24 h to remove cell debris and residual DMSO. Cells were then cultured as described in the previous sections.

2.3 Generation of PrP^C-expressing SH-SY5Y cells

The following sections describe the stable transfection of SH-SY5Y cells with the pCI-neo-MoPrnp mammalian expression vector (see section 2.1 for details of production) and the subsequent derivation of monoclonal, PrP^C-expressing lines.

2.3.1 Determining appropriate concentration of selection antibiotic

The pCI-neo plasmid carries a neomycin phosphotransferase gene that provides resistance to the antibiotic G-418. Prior to transfection, an appropriate G-418 concentration for selection was determined by seeding a 96-well tissue culture plate with SH-SY5Y cells. The cell suspension was serially diluted so that the densities ranged from 2000 per well down to a single cell. Cells were exposed to G-418 (Geneticin; Thermo Fisher Scientific) concentrations between 100 and 1200 µg/ml over a 12 day period. Growth medium changes (including G-418 at the appropriate concentrations) were carried out at 4, 8 and 10 days post treatment to remove dead cells and to maintain the antibiotic selection. The health of the cells was monitored regularly by observation under a light microscope. The lowest G-418 dose that resulted in zero viable cells after 12 days exposure was identified. A slightly higher dose was chosen for selection of stable transfectants to allow for batch-to-batch variation in G-418 activity. Proliferation from wells containing a single cell was also monitored by microscopic observation. This was to ensure that SH-SY5Y cultures could be grown successfully from just one original cell.

2.3.2 Transfection procedure

SH-SY5Y cells in growth medium were seeded into a 24-well tissue culture plate at two different densities: “high” i.e. ~70 % confluent at transfection; and “low” i.e. ~35 % confluent. After 24 h cells were transfected using Lipofectamine LTx and the associated PLUS Reagent (Thermo Fisher Scientific). The manufacturer’s protocol was followed. A range of Lipofectamine LTx concentrations (1, 1.5, 2 and 2.5 µl per

well) were tested and 1 µg per well pCI-neo-MoPrnp DNA was used. Untreated cells and cells treated with just the transfection reagents (mock-transfected) were included on the same plate. After 6 h, the cells were subcultured into a 12-well tissue culture plate as described in section 2.2.1. pCI-neo-MoPrnp-transfected cells that had been subject to the different transfection conditions described above were pooled into a single cell suspension before plating. Cells were recovered for 72 h to allow transfected cells to start expressing neomycin phosphotransferase. Next, the growth medium was replaced with fresh growth medium containing 500 µg/ml G-418. Stable transfectants were selected for ~3 weeks and the growth medium (still containing 500 µg/ml G-418) was refreshed 3 times per week. Mock-transfected and untransfected cells were monitored over the same period to confirm that cells not transfected with pCI-neo-MoPrnp could not survive the antibiotic selection.

2.3.3 Limiting dilution to generate monoclonal lines

Polyclonal transfected SH-SY5Y cells in growth medium were seeded into a 96-well tissue culture plate. The cell suspension was serially diluted so that some wells should have contained just a single cell. The plate was viewed under a light microscope 4 days after plating. Based on the typical proliferation rate of the cells, those wells containing a single colony of fewer than 8 cells were assumed to have contained just 1 cell at plating. Wells not meeting this criteria were ignored from this point onwards. Clonal cultures were expanded over several weeks with regular growth medium changes (every 2-4 days). Clones were subcultured into plates with larger wells when necessary. Extremely slow growing clones were discarded. The remaining clones were expanded until sufficient numbers were present to cryopreserve stocks for later use (see section 2.2.2).

2.3.4 Culturing transfected SH-SY5Y cells for experiments

Genetic drift can cause phenotypic changes in long-term cell cultures. Therefore, pCI-neo-MoPrnp-transfected cells and untransfected control cells (SH-SY5Y^{Untr}) were cultured for 6 weeks only before restarting from frozen stocks. SH-SY5Y^{Untr}

cells were approximately matched to the stably transfected clones in terms of total weeks in culture.

Transfected clones were routinely maintained in growth medium containing 200 µg/ml G-418 to guard against epigenetic silencing of the *Prnp* transgene. G-418 was removed from these cultures at least 48 h before use in experiments.

2.4 Preparation of protein samples for western blotting

2.4.1 Cell lysis

Lysates were prepared from tissue culture plates or flasks of subconfluent SH-SY5Y cells. After removal of growth medium, the cell monolayers were gently washed twice with ice-cold phosphate-buffered saline (PBS; 10 mM Na_2HPO_4, 150 mM NaCl, pH 7.3-7.5). The subsequent steps were used when preparing cell lysates for the western blotting experiments described in Chapters 3-5. Cells were lysed in ice-cold radioimmunoprecipitation assay lysis buffer (150 mM NaCl, 50 mM tris, 1 % (v/v) Triton X-100, 0.5 % (w/v) sodium deoxycholate (SDA), 0.1 % (w/v) sodium dodecyl sulphate (SDS), pH 7.4) containing protease inhibitors (Roche Complete Mini Protease Inhibitor Cocktail tablets). Phosphatase inhibitors (Roche PhosSTOP Phosphatase Inhibitor Cocktail tablets) were also included when blotting for phosphorylated proteins. Following ~15 min incubation on ice, lysed cells were scraped into one corner of the wells and collected into tubes. Cell lysates were sonicated (on ice) for 5 min to shear DNA, before centrifugation at 16100 x g for 10 min at 4 °C. Supernatants were either processed immediately for protein quantification and/or western blotting, or were snap frozen on dry ice and stored at -80 °C for later use.

When performing western blots to detect a high-molecular weight, cell membrane-associated receptor, I discovered that the aforementioned radioimmunoprecipitation assay lysis buffer was not effective at extracting and solubilising the protein.

Subsequently, the lysis buffer was changed to the following formulation: 150 mM NaCl, 50 mM tris, 1 % (v/v) Triton X-100, 0.25 % (w/v) SDA and 1.5 % (w/v) N-octyl glucopyranoside, pH 7.4. Because this lysis buffer appeared to improve the yield of most proteins, it was used when preparing cell lysates for all the western blot experiments described in Chapter 6. Aside from the altered buffer, the lysis method was the same as detailed above except that the sonication step was omitted.

2.4.2 Brain homogenisation

Frozen mouse brain tissues were available from previous work to investigate proteomic and transcriptomic changes induced by PrP^C knockout. In that study, the entire forebrain was removed, split in two and snap frozen in liquid nitrogen before storage at -80 °C. Age- and sex-matched PrP^C-null (Npu knockout line) and wild type control (129/Ola strain) tissues were isolated from mice of various ages, the oldest being ~700 days of age. Here, tissues from mice ~550 days of age were used.

Forebrain tissues were removed from -80 °C storage and placed in dounce homogenisers. An appropriate volume of ice-cold radioimmunoprecipitation assay lysis buffer (formulation given in the previous section) containing protease inhibitors, and phosphatase inhibitors if necessary, was added to give a 10 % (w/v) homogenate. Tissues were manually homogenized and the lysates transferred to Falcon tubes for 2 h incubation at 4 °C with agitation to allow lysis to complete. Lysates were centrifuged at 16100 x g for 20 min at 4 °C to remove debris. Supernatants were either processed immediately for protein quantification and/or western blotting, or were snap frozen on dry ice and stored at -80 °C for later use.

2.4.3 Liver homogenisation

Four wild type (129/Ola) and four PrP^C-null (Npu) mice aged 14-15 weeks were culled prior to removal of their livers, which were subsequently snap frozen in liquid nitrogen. These steps were carried out by Ms. Rebecca Hogan, who is a senior

animal technician within the Roslin Institute Biological Resource Facility. Subsequently, I homogenised the tissues using the method detailed in the previous section.

2.4.4 Protein quantification by dot blot

Immobilon-P PVDF membranes (Millipore) were rehydrated in methanol for 2 min and equilibrated in PBS for 10 min. Reactivated membranes were secured into a 96-well BioDot microfiltration apparatus (BioRad) according to the manufacturer's instructions. 100 µl per well PBS were added to each well and a vacuum was applied. 100 µl per well of cell or tissue lysate samples, as well as protein standards at a range of suitable concentrations (either bovine serum albumin or recombinant truncated ovine PrP), all diluted in PBS, were added in triplicate. Drainage was by gravity flow to facilitate sample binding to the membrane. The membrane was washed with 100 µl per well PBS, followed by two washes with 200 µl per well PBS containing 0.3 % (v/v) Tween-20. Again drainage was by gravity flow. Once all the wash solution had passed through, the membrane was removed from the apparatus and several washes were performed as follows: two 5 min washes with PBS with agitation; a 30 min wash at 37 °C with PBS/0.3 % Tween-20; three 5 min washes with PBS/0.3 % Tween-20 with agitation; and finally three rinses with Milli-Q H_2O to remove buffer salts. Membranes were incubated for at least 2 h (up to overnight) with ~20 ml Protogold colloidal gold solution (BBI). Stained membranes were rinsed with Milli-Q H_2O, air dried and scanned. ImageQuant TL or ImageJ software packages were used for densitometric analysis. A standard curve was produced in Excel based on the absorbance values from the protein standards and sample concentrations were determined accordingly.

2.4.5 Protein quantification by bicinchoninic assay

Bicinchoninic (BCA) assays were used as an alternative to dot blotting. The Pierce Microplate BCA Protein Assay Kit – Reducing Agent Compatible (Thermo Fisher Scientific) was used. The bovine serum albumin standard provided was serially

diluted in PBS to give concentrations of 125-2000 µg/ml. Cell or tissue lysate samples were also diluted as appropriate in PBS. 13 µl of standards and samples were pipetted in triplicate into wells of a kit-supplied 96-well plate. For samples in 8 M urea buffer, 5 µl samples were loaded instead and 8 µl PBS added on top to reduce the urea concentration to ~ 3 M, the maximum compatible with this assay. The BCA working reagent was prepared by mixing 50 parts BCA reagent A with 1 part BCA reagent B. 260 µl working reagent were added to each well. The plate was sealed, placed on a plate shaker for 1 min and then incubated at 37 °C for 30 min. After 5 min to cool to RT, absorbance at 570 nm was quantified using a Synergy HT plate reader. A standard curve was produced in Excel based on the absorbance values from the protein standards and sample concentrations were determined accordingly.

2.4.6 Peptide-N-glycosidase F-mediated digestion of protein samples

An NEB Peptide-N-glycosidase F (PNGase F) kit was used. Protein samples were diluted in glycoprotein denaturing buffer (final concentrations of 0.5 % (w/v) SDS and 40 mM DTT) and then heated to 95 °C for 5 min. G7 reaction buffer, NP-40 and PNGase F were added to samples to final concentrations of 1X, 1 % (v/v) and 50 units/µl, respectively. The remaining volume was made up with Milli-Q H_2O. Reactions were incubated at 37 °C for 1 h to remove N-linked glycans from proteins. NuPAGE lithium dodecyl sulphate (LDS) sample buffer (Thermo Fisher Scientific) containing 5 % (v/v) β-mercaptoethanol was added to de-glycosylated protein samples at a ratio of 1:3. PNGase F was inactivated by heating the samples to 72 °C for 5 min. Samples were analysed by western blotting as described in the following sections.

2.5 Western Blotting

2.5.1 Sodium dodecyl sulphate-polyacrylamide gel electrophoresis

When necessary, the total protein contents of cell or tissues lysates were quantified as described in sections 2.4.4 and 2.4.5. The data were used to ensure equal sample loading for sodium dodecyl sulphate polyacrylamide gel electrophoresis (SDS-PAGE). However, a prior protein assay was normally omitted if the samples for comparison were known to be of approximately equal concentrations and if the gel loading control method described in the following section was to be used.

SDS-PAGE was performed under reducing and denaturing conditions using the Novex NuPAGE gel system (Thermo Fisher Scientific). Protein samples were diluted as necessary in their original buffer. NuPAGE LDS sample buffer containing 5 % (v/v) β-mercaptoethanol was added to diluted protein samples at a ratio of 1:3. Samples were denatured by heating to 70 °C for 10 min. Pre-cast NuPAGE gels were secured into an XCell SureLock Mini Cell and running buffer was added to both chambers. Gels of varying polyacrylamide concentrations and buffer systems (bis-tris or tris-acetate) were used depending on the molecular weight of the protein of interest. The running buffer also varied for the same reason (either 2-(N-morpholino)ethanesulfonic acid (MES) SDS, 3-(N-morpholino)propanesulfonic acid SDS or tris-acetate SDS).

Protein samples were loaded into the gels alongside appropriate protein standards. SeeBlue Plus2 Pre-Stained Standard was used for monitoring transfer, whilst MagicMark XP Western Protein Standard was used for molecular weight-sizing of bands when imaging blots. HiMark Pre-Stained Protein Standard was used in place of MagicMark for high-molecular weight proteins. Protein samples were separated by electrophoresis at constant voltage until the loading dye reached the bottom of the gel.

2.5.2 Loading control

For each set of samples prepared for quantitative western blotting, a loading control gel was prepared to control for errors either in sample preparation or associated with the initial protein quantification assay (if performed). This is a published method (Eaton et al., 2013) and was preferred over normalisation to standard reference proteins because many such proteins appear to vary in their expression depending upon the presence or absence of PrP^{C}.

Briefly, the loading control gel was secured into the same tank as a gel used for blotting. Following electrophoresis as described in the previous section, loading control gels were incubated in ~20 ml InstantBlue stain (Expedeon) for 1 h. After several washes with Milli-Q H_2O to reduce background, imaging and quantification were performed using the LI-COR Biosciences Odyssey Infrared Imaging System and associated ImageStudio software. A blank lane of the gel was used for setting the background correction. Rectangles were drawn over each sample-containing lane (normally covering bands from 20-180 kDa). The integrated intensity values obtained were used to correct the associated western blot data for loading error.

2.5.3 Semi-dry transfer

Following SDS-PAGE, gels were equilibrated for 10 min in ice-cold transfer buffer (100 mM tris, 190 mM glycine, pH not adjusted). The transfer buffer also contained methanol at concentrations from 5-20 % (v/v) depending upon the molecular weight of the protein of interest (higher concentrations for low-molecular weight proteins). Meanwhile, Immobilon FL PVDF membranes (Millipore) were briefly rehydrated in methanol, rinsed twice with Milli-Q H_2O and equilibrated in transfer buffer for 5 min. Transfer stacks were assembled in a Novex Semi-Dry Blotter (Thermo Fisher Scientific) according to the manufacturer's protocol. Transfer was for 1 h at 140 mA for a single gel or at 280 mA for two gels. Membranes were air dried to optimize retainment of bound protein.

For high-molecular weight proteins that transferred poorly under the above conditions (generally > 100 kDa), the methanol-containing transfer buffer was used for the anode side of the transfer stack only (membrane; bottom filter papers). A transfer buffer of 100 mM Tris, 190 mM glycine and 0.1-0.2 % (w/v) SDS was used for the cathode side (gel; top filter papers) to improve movement of proteins out of the gel.

2.5.4 Blocking and immunostaining

Membranes were rehydrated in methanol, rinsed twice with Milli-Q H_2O and placed in PBS for 2 min. All subsequent steps were carried out at RT and with agitation unless stated. Membranes were incubated in Odyssey Blocking Buffer (LI-COR Biosciences) for 1 h. After a PBS rinse, membranes were incubated overnight at 4 °C with primary antibodies diluted in Odyssey Blocking Buffer containing 0.1 % (v/v) Tween-20 (full details of primary antibodies used are provided in Appendix I). Next, membranes were washed four times for 5 min with PBS containing 0.1 % (v/v) Tween-20. Membranes were protected from light for all subsequent steps. Membranes were incubated for 1 h with either IRDye 680RD goat anti-mouse IgG or IRDye 800CW goat anti-rabbit IgG secondary antibodies (LI-COR Biosciences) diluted 1:10000 in a mixture of Odyssey Blocking Buffer and PBS (1 part to 3 parts, respectively), still with 0.1 % (v/v) Tween-20. Four washes with PBS/0.1 % (v/v) Tween-20 were again performed, followed by two washes with PBS to remove residual Tween-20. Membranes were air-dried again before imaging and quantification (if required) using the LI-COR Biosciences Odyssey Infrared Imaging System and associated ImageStudio software. Rectangles were drawn around each band and a local background correction applied (subtraction of the median intensity of pixels just outside the top and bottom edges of the rectangle). The integrated intensity values obtained were considered to be proportionate to the amount of protein present. To allow data from replicate blots to be combined, integrated intensity values were normalised to a common control sample or group of samples.

2.6 PrP^C co-immunoprecipitation

The buffer used for cell lysis consisted of either 150 mM NaCl, 50 mM tris, 1 % (v/v) Triton X-100, 0.25 % (w/v) SDA and 1.5 % (w/v) N-octyl glucopyranoside (pH 7.4) or of the same components except for the omission of SDA. Cell lysis was performed as described in section 2.4.1. Lysates were kept on ice prior to measurement of total protein concentration by BCA assay as described in section 2.4.5. Subsequently, lysates were diluted to 1 mg/ml using the appropriate lysis buffer i.e. the buffer that was used for cell lysis. Samples of each cell lysate were removed at this point and NuPAGE LDS sample buffer (Thermo Fisher Scientific) containing 5 % (v/v) β-mercaptoethanol was added at a ratio of 1:3. The samples were denatured by heating to 95 °C for 10 min and were then snap frozen until use.

The stock solution of protein G-conjugated magnetic beads (Cell Signalling Technology) was vortexed gently to resuspend the beads. Appropriate volumes of bead slurry were added to microcentrifuge tubes (10 µl beads per 100 µl lysate). To wash the beads, lysis buffer was added at a ratio of 10 parts to 1 part bead slurry. Following gentle vortexing, the beads were pelleted by spinning the tubes in a microcentrifuge at 2000 rpm for 30 s. Next, the tubes were placed in a magnetic separation rack for 1 min to pull the beads to one side. Supernatants were removed and the cell lysates were added to the washed beads. After 1 h incubation at 4 °C with gentle agitation, the beads were separated from the lysates by centrifuging and placing the tubes in a magnetic rack, as described above. The pre-cleared lysates were transferred to fresh tubes and either BC6 anti-PrP antibody (McCutcheon et al., 2014) or mouse IgG_1 isotype control antibody (Cell Signalling Technology #5415) were added to final concentrations of 16 µg/ml. The lysates were incubated with the antibodies overnight at 4 °C with gentle agitation. Further tubes containing pre-washed beads were prepared as described above. The lysate-antibody solutions were added to beads and incubated for 3 h at 4 °C with gentle agitation. The beads and any antibody-antigen complexes bound to them were separated from the solution as described above and these supernatants were then removed. Three washes of ~5 min with the appropriate lysis buffer (using a volume twice that of the original lysate)

were performed to remove non-specifically bound proteins. After the final wash, the antibody-antigen complexes were eluted from the beads by adding undiluted NuPAGE LDS sample buffer containing 5 % (v/v) β-mercaptoethanol, vortexing heavily and heating to 95 °C for 15 min to denature the proteins. Subsequently, the samples were vortexed again and centrifuged at 16100 x g for 2 min. The eluents were transferred to new tubes and either snap frozen or used immediately for further analysis.

The samples obtained from PrP^C co-immunoprecipitation experiments were analysed by western blotting as described in section 2.5 and also by SDS-PAGE followed by silver staining to detect protein bands. Silver staining was performed using the SilverQuest Silver Staining Kit (Thermo Fisher Scientific) and the basic staining protocol provided with the kit was followed. The stained gels were washed with Milli-Q H_2O and imaged using a flatbed scanner.

2.7 Immunofluorescence assays

2.7.1 General protocol

All following steps were carried out at RT unless stated. All wash steps were for 5 min and were carried out with gentle agitation, while all other incubation steps involved no agitation.

SH-SY5Y cells growing in culture were detached from flasks and pelleted as described in section 2.2.1. Pelleted cells were resuspended in growth medium and seeded either into cell culture surface-treated, 96-well, black-walled Nunc plates with a coverglass base (Thermo Scientific), if the cells were to be examined by confocal microscopy, or into optically clear tissue cultures plates, in the case of widefield fluorescence imaging. After 16 or 24 h incubation at 37 °C, cells were fixed by adding 10 % (w/v) paraformaldehyde (PFA) in PBS to the medium already present to give a final PFA concentration of 2 % (w/v). The PFA/medium solution was removed

and replaced with 2 % PFA in PBS for a further 10 min incubation. After three washes with PBS, cells were permeabilised if required (further details are given in the following section). Next, cells were treated with a blocking solution of 5 % (v/v) normal goat serum (Sigma-Aldrich) in PBS for 1 h. Cells were incubated overnight at 4 °C with the appropriate primary antibody diluted in 5 % normal goat serum in PBS. Full details of the primary antibodies used are provided in Appendix I. After three further PBS washes, cells were incubated in the dark for 1 h with goat anti-mouse or goat anti-rabbit IgG Alexa Fluor 555-conjugated secondary antibodies (Thermo Fisher Scientific) diluted 1:500 in 5 % normal goat serum in PBS. Cells were again washed three times with PBS before 5 min incubation with the fluorescent nuclear stain 4',6-diamidino-2-phenylindole (DAPI; Thermo Fisher Scientific) at a concentration of 300 nM in PBS. If actin cytoskeleton staining was required, DAPI solution was replaced with 5 units/ml Alexa Fluor 647 phalloidin (Thermo Fisher Scientific) for a 20 min incubation. After a final PBS wash, cells were left in PBS and the plates were sealed and stored in the dark at 4 °C until imaging.

2.7.2 Permeabilisation treatments

Depending on the staining requirements, one of the following permeabilisation methods was used: 1) incubation in PBS containing 0.1 % (v/v) Triton X-100 for 10 min at RT; 2) incubation for 10 min at -20 °C in methanol that had been pre-chilled to -20 °C; or 3) treatment with 0.1 % (w/v) saponin. For methods 1 and 2, cells were washed once with PBS before blocking. For method 1, 0.01 % (v/v) Triton X-100 was included in the blocking solution. For method 3, no separate permeabilisation step was included; instead, saponin was included in the blocking solution and at all subsequent incubation steps up until the final PBS wash.

2.7.3 Fluorescence microscopy

Confocal images were captured using a Zeiss LSM 710 microscope and the associated Zen Black software. The smart set-up function was used to minimise

crosstalk among the required imaging tracks. The range indicator was used to adjust laser power, master gain and digital offset settings to minimise the number of saturated and zero intensity pixels. The pinhole size was set to 1 airy unit for the imaging track with the longest wavelength (DAPI) and slice thickness in the z-plane was maintained across the other imaging tracks. All images were taken with a scan speed of 8 and bit depth of 12. The image resolution was either 1024 x 1024 or 2048 x 2048 pixels. Image processing was performed using the Zen Black software and brightness settings were adjusted digitally if required.

Widefield fluorescence images were taken using a Zeiss Axiovert inverted microscope using a triple pass filter (excitation at 407/494/576 nm; emission at 457/530/628 nm). The Scion VisiCapture software was used for imaging. Exposure time was set manually according to the preview image and multiframe averaging (4 frames) was used to minimise background noise. Images from the different fluorescence channels were assembled using ImageJ.

2.8 Morphological analysis of cells by phase contrast microscopy

SH-SY5Y cells growing in culture were detached from flasks and pelleted as described in section 2.2.1. Pelleted cells were resuspended in growth medium and seeded onto optically clear tissue culture plates. After 24 h incubation at 37 °C, cells were fixed with PFA as described in section 2.7.1. After three PBS washes, cells were left in PBS and the plates were sealed and stored at 4 °C until imaging. Phase contrast images were taken using a Zeiss Axiovert inverted microscope. Image capture was the same as described above for widefield fluorescence imaging.

2.9 RNA interference-mediated knockdown of PrP^C expression

Silencer Select small interfering RNAs (siRNAs) were purchased from Thermo Fisher Scientific. Sequences of sense strands for the PrP-specific siRNAs were CGUGAAAACAUGUACCGCUTT (referred to as s72188) and GCAGGCCCAUG-AUCCAUUUTT (referred to as s72190). Negative control siRNA 1, which has "no significant sequence similarity to mouse, rat or human gene sequences" (Thermo Fisher Scientific, [n.d.]-b) and cyanine dye 3-labelled glyceraldehyde 3-phosphate dehydrogenase positive control siRNA were also purchased. The sequences for the control siRNAs are not publicly available.

2.9.1 Initial assessment of siRNA transfection efficiency

As an initial test of transfection efficiency, the cyanine dye 3-labelled glyceraldehyde 3-phosphate dehydrogenase siRNA was reverse transfected into SH-SY5Y cells as follows. Firstly, the lyophilised siRNA was resuspended in nuclease-free H_2O to make a 30 μM stock. This stock and Lipofectamine RNAi Max (Thermo Fisher Scientific) were both diluted in a modified form of Eagle's minimal essential medium known as OptiMEM[3] (Thermo Fisher Scientific) by factors of 1:17 and 1:50, respectively. Equal parts of these solutions were mixed and incubated for 5 min at RT to form siRNA-lipid complexes at 10X the desired final concentrations. A mock transfection control, consisting of Lipofectamine RNAi Max incubated only with OptiMEM, was also prepared. 96-well, black-walled, clear-bottomed, tissue culture-treated Costar plates were pre-treated in duplicate with the complexes. SH-SY5Y cells growing in culture were detached from flasks and pelleted as described in section 2.2.1. Pelleted cells were resuspended in growth medium lacking antibiotics and were added to the plates, on top of the siRNA-lipid complexes, at a density of 30000 per well. After 16-18 h incubation the growth medium was removed

[3] In addition to standard cell culture medium constituents, OptiMEM contains insulin, transferrin, thymidine and the purine derivative hypoxanthine (Thermo Fisher Scientific, [n.d.]-a). The exact concentrations of these components are not publicly available.

and, following a wash with HBSS, was replaced with serum-free medium (same constituents as growth medium, except for the addition of N-2 supplement (Thermo Fisher Scientific) and the lack of serum). Either immediately afterwards or 24 h later, Hoescht 33342 dye was added to the culture medium to give a final concentration of 2.5 μg/ml. Following the method described in section 2.7.3, widefield fluorescence images were captured at both time points in order to visualise siRNA uptake.

2.9.2 Optimisation of siRNA transfection

PrP-specific and negative control siRNAs were resuspended in nuclease-free H_2O to make 10 μM stocks. SH-SY5Y cells were reverse transfected with these siRNAs in duplicate as described in the previous section, except for the following changes: 1) Lipofectamine RNAi Max was initially diluted 1:25 rather than 1:17; 2) the siRNAs were tested at final concentrations of 2.5, 5 and 10 nM; and 3) in addition to 96-well plates, reverse transfections were also performed in 24-well tissue culture plates (120 000 cells per well). After 16-18 h incubation the growth medium was removed and, following a wash with HBSS, was replaced with serum-free medium (formulated as described in section 2.9.1). 24 h after serum deprivation, cell viability was assessed for the 96-well plates as described in section 2.10.5. The only change was that cells not treated with Lipofectamine RNAi Max and/or siRNAs were used as controls for 100 % viability. At the same time point, cells growing in 24-well plates were lysed as described in section 2.4.1. PrP^C expression levels in the lysates were determined by quantitative western blotting as described in section 2.5. The lowest siRNA dose to give an acceptable level of PrP^C knockdown was chosen for future use.

2.9.3 Quantification of RNA interference-mediated PrP^C knockdown

To obtain reliable data on the typical PrP^C knockdown achieved using 5 nM siRNA concentrations, five independent experiments were performed. The method was similar to that described in the previous section, except for the following changes: 1) for the “untreated” controls, wells were pre-treated with OptiMEM only; 2) a

mock transfection condition was also included (see section 2.9.1); 3) cells were seeded at a density of 100 000 per well into 24-well tissue culture plates; and 4) cells were lysed at 44 and 68 h post transfection. PrP^C levels in the treated samples were expressed as percentages of the "untreated" control level. To investigate the duration of PrP^C knockdown when using 15 nM siRNA concentrations, a further experiment was performed. The method was the same as described above, except that cells were initially seeded at a density of 16000 per well into standard growth medium, prepared as described in section 2.2, and mock-transfected or siRNA s72190-transfected cells were not included in the experiment. Cells were lysed at 4, 5, 6 or 7 days post transfection. At each time point, PrP^C expression in the siRNA s72188-transfected cells was expressed as a percentage of the expression level in negative control siRNA-transfected cells.

2.9.4 Assessing the impact of PrP^C knockdown on expression of other proteins

Negative control siRNA 1 and PrP siRNA s72188 stocks were diluted to 300 nM with OptiMEM medium. Lipofectamine RNAi Max was diluted 1:25, also in OptiMEM. Equal parts of these solutions were mixed and incubated for 5 min at RT to form siRNA-lipid complexes at 10X the desired final concentrations. T25 tissue culture flasks were pre-treated with the complexes. Additional flasks were pre-treated with the same volume of pure OptiMEM in order to provide "untreated" controls. SH-SY5Y cells growing in culture were detached from flasks and pelleted as described in section 2.2.1. Pelleted cells were resuspended in growth medium lacking antibiotics and were added to the flasks, on top of the siRNA-lipid complexes, at a density of 400 000 cells per flask. The medium was removed after 16 h incubation and fresh growth medium was added. 72 h post transfection, cells were subcultured into 6-well tissue culture plates by following the method described in section 2.2.1 – this step was required to equalise the culture densities when cell lines with different proliferation rates were being compared. Cells were lysed 24 h later as described in section 2.4.1 and the lysates obtained were analysed by quantitative western blotting as described in section 2.5.

2.10 Stress treatment assays

2.10.1 General protocol

SH-SY5Y cells growing in culture were detached from flasks and pelleted as described in section 2.2.1. Pelleted cells were resuspended in growth medium and seeded onto 96-well, black-walled, clear-bottomed, tissue culture-treated Costar plates at a density of 30000 per well. After 16-18 h incubation, the growth medium was removed and, following a wash with HBSS, was replaced with serum-free medium (formulated as described in section 2.9.1) that contained toxins prepared as described in the following section. After 24 h incubation at 37 °C, cell viability and either cytotoxicity or morphological changes were assessed by the methods detailed in later sections.

2.10.2 Information on stress treatments

Toxins were serially diluted initially using the same diluents as the stock solutions. The diluted toxins were then added to serum-free medium before treating cells. This was to ensure potentially cytotoxic buffers were at the same concentrations in the culture medium irrespective of toxin dose. Toxin buffer-only treated cells were also included in each assay to control for any toxicity of the buffer. Paraquat dichloride hydrate (PQ; Sigma-Aldrich) dilutions were prepared in HBSS, yielding a final HBSS concentration in the culture medium of 3.3 % (v/v). Cells were exposed in duplicate to 500, 1000, 1500, 2000 or 10000 μM PQ. Staurosporine (STS) and tunicamycin (TM), both from Streptomyces spp. (Sigma-Aldrich), were diluted in DMSO, yielding a final concentration of DMSO in the culture medium of 0.5 % (v/v). Cells were exposed in duplicate to 25, 50, 75, 100 or 600 nM STS, or 1, 5, 10 or 15 μg/ml TM.

For serum deprivation assays, cells were incubated for 7 days in serum-free medium containing no toxins and also no N-2 supplement since this promotes cell survival.

Cell viability and morphological changes were assessed in duplicate by the methods detailed in the following sections at 2 h or 1, 2, 4, 6 or 7 days after serum removal.

2.10.3 Stress treatments incorporating siRNA transfection

96-well, black-walled, clear-bottomed, tissue culture-treated Costar plates were pre-treated in duplicate with siRNA-lipid complexes that had been prepared as described in section 2.9.4, except that the final siRNA concentration was 5 nM not 15 nM. Some wells were pre-treated with the same volume of pure OptiMEM to provide an "untreated" control. SH-SY5Y cells growing in culture were detached from flasks and pelleted as described in section 2.2.1. Pelleted cells were resuspended in growth medium lacking antibiotics and were added to the plates, on top of the siRNA-lipid complexes, at a density of 30000 per well. After 16-18 h incubation the growth medium was removed and, following a wash with HBSS, was replaced with 100 µl per well serum-free medium. 44 h after initially seeding the plates, 25 µl per well of serum-free medium containing PQ or STS were added on top of the medium already present. Final PQ and STS concentrations were 1000 µM and 50 nM, respectively. Concentrations of the original toxin buffers were as described in section 2.10.2. After 24 h incubation at 37 °C, cell viability and cytotoxicity were assessed by the methods detailed in the following sections.

2.10.4 Lactate dehydrogenase cytotoxicity assays

Lactate dehydrogenase (LDH) assays were carried out following PQ and STS treatments only. The LDH cytotoxicity kit II from Abcam was used. After 24 h toxin incubation the plate was shaken gently to ensure even distribution of LDH in the culture medium. The plate was centrifuged at 600 x g for 10 min to precipitate any floating cells on the well bottoms. Meanwhile, the kit-supplied substrate mix containing water-soluble tetrazolium salt 1 was reconstituted at 135 mg/ml in Milli-Q H_2O. The LDH reaction mix was prepared by adding 50 parts LDH assay buffer to 1 part water-soluble tetrazolium salt 1 substrate mix. 10 µl culture medium from each well was added to 100 µl LDH reaction mix. Reactions were prepared in an optically

clear 96-well plate. After mixing on a plate shaker, the plates were incubated at RT. Absorbance values were measured using a Wallac 1420 plate reader. The reference background absorbance at 620 nm was subtracted from the absorbance at 450 nm. The incubation time depended upon the reaction speed – absorbance values were measured periodically until either the 100 % cytotoxicity control samples had reached an absorbance at 450 nm of ~2.0 or the incubation time had exceeded 90 min. The 100 % cytotoxicity controls were medium samples from cells treated with either 10000 µM PQ or 600 nM STS, depending on the assay. These toxin concentrations had been shown previously to result in 0 % viability as measured by the assay described in the following section. Cells treated only with the buffer were considered to be 0 % cytotoxicity controls. Percentage cytotoxicity values following toxin treatment were determined using these controls.

2.10.5 Cell viability assays using PrestoBlue

PrestoBlue viability assays were carried out after all four stress treatments. 1 part PrestoBlue (Thermo Fisher Scientific) was added to 10 parts culture medium for all cell-containing wells and serum-free medium-only control wells. Plates were placed on a shaker for 30 s to mix before incubation at 37 °C for 1 h. If fluorescence measurements could not be made immediately then reactions were stopped by adding SDS to 3 % (w/v) final concentration and the plates were stored in the dark at 4 °C until ready. Fluorescence readings were taken using a Fluostar Optima plate reader (BMG Labtech) with 550/10 nm excitation and 580/10 nm emission filters. The mean signal from serum-free medium was subtracted from the signals from the other wells. For toxin treatment assays, cells treated with only the toxin buffer were considered 100 % viable. Percentage viability values following toxin exposure were determined using these controls. For serum deprivation assays, background-corrected signals from the 1, 2, 4, 6 and 7 day time points were divided through by the 2 h time point signals. This was to correct for any small differences among the cell lines tested in terms of cell densities after serum deprivation and/or their efficiency at reducing PrestoBlue. At each time point from day 1 onwards, the mean corrected

signal from wells containing SH-SY5Y^{Untr} was set to 100 and the corrected data for the other cell lines were normalised accordingly.

2.10.6 Capturing phase contrast images of cells after stress treatment

For tunicamycin treatment and serum deprivation, phase contrast images of the cells were taken in place of the LDH assay. Cell plating and stress treatments were as described in section 2.10.1, except for the following changes: 1) cells were plated at a density of 100 000 cells per well into 24-well tissue culture plates; and 2) media were prepared using a DMEM formulation lacking phenol red (Thermo Fisher Scientific). Phase contrast images were taken using a Zeiss Axiovert inverted microscope at the same time points as for the viability assays. Cells were imaged live in their culture medium. Image capture was the same as described in section 2.7.3 for widefield fluorescence imaging.

2.11 Proliferation assays

2.11.1 Monitoring proliferation using PrestoBlue

SH-SY5Y cells growing in culture were detached from flasks and pelleted as described in section 2.2.1. Pelleted cells were resuspended in growth medium and seeded into 96-well, black-walled, clear-bottomed, tissue culture-treated Costar plates at a density of 2500 per well. Over the following 7 days, cell numbers were assessed in duplicate at 24 h intervals using the PrestoBlue viability reagent. The method was as described in section 2.10.5. At each time point, the mean fluorescence signal from medium-only wells was subtracted from the signals from the cell-containing wells. The mean signal from the wells containing the slowest growing cell line (PrP^{C}-transfected clone 1G3) was set to 100 and signals from other wells were normalised accordingly.

2.11.2 Monitoring proliferation using nuclear staining and counting

SH-SY5Y cells growing in culture were detached from flasks and pelleted as described in section 2.2.1. Pelleted cells were resuspended in growth medium lacking phenol red and seeded in duplicate onto 12-well tissue culture plates at a density of 27000 per well. At 16 h or 4 days after plating, phenol red-negative growth medium containing 12.5 µg/ml Hoescht 33342 nuclear stain (Thermo Fisher Scientific) was added to cell-containing wells, giving a final concentration of 2.5 µg/ml. Cells were incubated in the dark at 37 °C for 20 min. Widefield fluorescence imaging was performed immediately afterwards according to the method described in section 2.7.3. Three images per well were taken using the 5X objective. To control for the tendency of SH-SY5Y cells to congregate towards the well centre, images were always taken one field of view in from the well wall. Image files were converted to 8-bit TIFFs within ImageJ and nuclei were distinguished from background using the "adjust threshold" function. A plug-in macro was used to count the number of nuclei present and measure their size. Since SH-SY5Y cells are prone to clumping, one image was examined manually and ~10 clumps of cells were matched to the corresponding "objects" identified by the macro. An average cell size was calculated from these clumps, allowing automated estimation of the number of cells in different-sized clumps. For both time points, the mean cell number per image for the slowest growing cell line (PrP^C-transfected clone 1G3) was set to 100 and cell numbers for the other cell lines were normalised accordingly.

2.11.3 Proliferation assays incorporating siRNA transfection

The assay format described in the previous section was modified as follows to investigate how PrP^C knockdown affected proliferation: 1) plates were pre-treated with siRNA-lipid complexes prepared as described in section 2.9.4; and 2) cells were cultured in growth medium lacking antibiotics. The mean fluorescence signal from the negative control siRNA-transfected cells was set to 100. The data from PrP siRNA s72188-transfected cells were normalised accordingly.

2.12 Nerve growth factor stimulation of SH-SY5Y cells

SH-SY5Y cells growing in culture were detached from flasks and pelleted as described in section 2.2.1. Pelleted cells were resuspended in growth medium and seeded onto 6-well tissue culture plates at a density of 500 000 cells/ml. After 24 h incubation the growth medium was removed and, following a wash with HBSS, was replaced with serum-free medium (formulated as described in section 2.9.1). Cells were incubated in the serum-free medium for 3.5 h to allow growth factor-activated pathways to return to baseline activity levels. NGF was serially diluted in serum-free medium from a 100 µg/ml stock to give solutions containing 5X the desired final concentrations of 3, 10, 30 and 100 ng/ml. Subsequently, the NGF solutions were added to the appropriate wells in duplicate. Following 5 min stimulations, cells were lysed as described in section 2.4.1 and the lysates obtained were analysed by quantitative western blotting as described in section 2.5.

2.13 Proteomic analyses of SH-SY5Y cell lysates

2.13.1 Cell lysis for proteomic analysis

Instead of lysing directly in the flasks, cells were detached and pelleted before lysis to allow samples with higher total protein concentrations to be prepared. Cells were detached and pelleted as described in section 2.2.1, except that soybean tryspin inhibitor (Sigma-Aldrich) was used for trypsin neutralisation if the cells had been cultured in serum-free medium i.e. during toxin exposure. The pelleted cells were gently resuspended in HBSS before further centrifugation at 200-300 x g for 10 min at RT. The supernatant was removed and cells were gently resuspended in 1 ml HBSS before transfer to low protein-binding microcentrifuge tubes (used for all subsequent steps). After a further spin at 200-300 x g for 10 min at RT, the supernatant was again removed. Cells were resuspended in freshly prepared urea lysis buffer (8 M urea, 0.1 % (w/v) SDS, 50 mM HEPES in HPLC quality H_2O, pH 8.0) at a ratio of 7 volumes of buffer to 1 volume of cell pellet. Lysates were

vortexed and pipetted up and down vigorously to ensure total cell lysis prior to incubation at RT for 15 min. Lysates were subjected to multiple ~40 s pulses of sonication (on ice) until they were no longer viscous and were then centrifuged at 16100 x g for 15 min at RT. The supernatants were removed and the total protein concentrations were determined by BCA assay as described in section 2.4.5. The cell lysates were then snap frozen and stored at -80 °C for later processing.

2.13.2 Protein digestion, dimethyl-labelling and liquid chromatography-tandem mass spectrometry

All steps in this section were carried out by staff at the Proteomics and Metabolomics Facility in Roslin, specifically Dr Dominic Kurian. Firstly, 100 µg of each sample were digested with Lys-C protease and subsequently by trypsin following standard methods of in-solution digestion. Stable isotopic reductive dimethylation of the resulting peptides was performed using Sep-Pak columns (Waters Corporation) by following standard methods (Boersema et al., 2009). The peptides were acidified by addition of trifluoroacetic acid to 0.1 % (v/v) concentration before loading onto conditioned Sep-Pak columns. Peptides from SH-SY5Y^{Untr} and stably transfected clones were labelled with 'light' and 'heavy' labelling reagents, respectively. The 'light' buffer consisted of 0.8 % (w/v) formaldehyde and 0.12 M sodium cyanoborohydride carrying hydrogens in their natural isotopic distributions in MES buffer. The 'heavy' buffer consisted of 0.8 % (w/v) deuterated formaldehyde and 0.12 M sodium cyanoborohydride in MES buffer. The loaded peptides were labelled by passing the respective labelling reagents through the columns five times. The peptides were washed and eluted with 0.1 % (v/v) trifluoroacetic acid in 70 % (v/v) acetonitrile. The eluted peptides were concentrated using a speed vacuum concentrator. The labelled 'light' and 'heavy' peptides were mixed together before fractionation by strong cation exchange chromatography on a Polysulphoethyl A column (PolyLC Inc USA). Fractions were desalted on Stage-Tip columns (Rappsilber et al., 2007). Each fraction of peptides was loaded onto an Acclaim PepMap100, C18, 3 µm, 100 Å, 75 µm (internal diameter) × 50 cm column (Thermo Fisher Scientific) using an UltiMate RSLCnano LC System (Dionex). Peptides eluted

by reverse phase chromatography were analysed by a micrOTOF-Q II mass spectrometer (Bruker) that was operated in data-dependent mode, automatically switching between MS and MS2 mode. The m/z values of tryptic peptides were measured using a MS scan (300-2000 m/z), followed by MS/MS scans of the six most intense peaks. Rolling collision energy for fragmentation was selected based on the precursor ion mass and a dynamic exclusion was applied for 60 s.

2.13.3 Processing of raw mass spectral data

Dr Dominic Kurian processed the raw spectral data using DataAnalysis software (Bruker) and the resulting peaklists were searched using the Mascot 2.4 server (Matrix Science) against the Uniprot human protein sequence database, which contained 89,796 entries at that time. Mass tolerance on peptide precursor ions was fixed at 25 ppm and on fragment ions at 0.1 Da. The peptide charge states were set as 2+ and 3+. Carbamidomethylation of cystein was used as a fixed modification and oxidation of methionine and light and heavy dimethylation of N-terminus and lysine were chosen as variable modifications. The false discovery rate for peptide IDs was limited to < 1 % after searching decoy databases. Dimethyl quantification was performed using the WARP-LC 1.3 plug-in to the ProteinScape 3.1 software (Bruker) to integrate the extracted chromatograms of every precursor ion. Peptide ratios were normalised by setting the overall median of the peptide ratios to one, thereby correcting for unequal protein sampling. For each identified protein, ProteinScape calculated its overall expression ratio by converting the associated individual peptide ratios into the log scale and then determining the antilog of the median of those values. The software also calculated percentage coefficients of variation (%CV) based on these log-transformed peptide ratios.

2.14 Analyses of publically available microarray data

The GeneAtlas GNF1M and U133a microarray datasets, both originally reported by Su et al. (2004), were accessed using the BioGPS gene annotation portal (Wu et al.,

2016) on 20-Nov-2015. The datasets contained baseline gene expression data from 61 young adult mouse tissues (2-3 months of age) and 79 human tissues, respectively. The BioGPS correlation tool was used to select genes with similar expression patterns to *PRNP* (Pearson correlation coefficient > 0.75). The filtered datasets were analysed using Qiagen's Ingenuity Pathway Analysis (IPA) software, as described below.

2.15 Overall summary of data analysis and statistics

For proteomic experiments, data output from the ProteinScape software was filtered to exclude proteins with expression ratios determined from < 3 unique peptides, since these ratios were considered unreliable. Next, fold change thresholds were applied to select proteins with high confidence of differential expression between the samples. The criteria used for these filtering processes are explained in detail in Chapter 4. Pathway analyses of the proteomic datasets were performed using the IPA core analysis suite. The software was set to use all available data sources and to consider only experimentally confirmed interactions between proteins, both direct and indirect. The network analysis settings were 35 molecules per network and 10 networks per analysis (if possible), with endogenous chemicals not included within the networks. The same settings were applied when analysing the filtered microarray datasets using IPA.

For all other quantitative experiments (western blotting, viability assays, cytotoxicity assays and proliferation assays), summary graphs showing the arithmetic mean values (+/- standard error of the mean) from multiple independent experiments or multiple biologically independent samples were prepared using Microsoft Excel. Statistical analyses of such data were also performed in Excel. Differences between groups were tested for significance ($p < 0.05$) using one- or two-sample t-tests as appropriate. In all cases the unpaired form of the two-sample t-test (not assuming equal variances) was used.

Chapter 3: Production and characterisation of stable, PrP^C-expressing, monoclonal SH-SY5Y cell lines

3.1 Introduction

The aim of my project has been to investigate the molecular mechanisms regulated by PrP^C to improve understanding of its physiological role. Initial studies of PrP^C function focused on PrP^C-knockout mice, which were produced independently by several laboratories. No clear developmental or behavioural alterations were identified at first (Bueler et al., 1992; Manson et al., 1994) but more recent work has identified various abnormalities in these mice (Tobler et al., 1996; Miele et al., 2002; Sakurai-Yamashita et al., 2005; Bremer et al., 2010; Strom et al., 2011; Rial et al., 2014). Analysing PrP^C function by studying knockout mice is useful for identifying the downstream consequences of a lack of PrP^C expression but the underlying molecular mechanisms are more easily investigated *in vitro*. Given that PrP^C is highly expressed in the nervous system (Sales et al., 2002; Adle-Biassette et al., 2006), one option for investigating PrP^C function *in vitro* is to isolate primary neurons from embryonic mice. Since primary neurons retain many of their *in vivo* characteristics, they can be considered more physiologically relevant than cell lines, which either have a cancerous origin or were artificially immortalised after isolation. However, there are a number of caveats associated with the use of primary cells. Firstly, each time primary cells are isolated, the resulting cultures will differ slightly, whereas cell lines can be cryopreserved, allowing repeated study of cells at similar passage numbers. Secondly, compensatory mechanisms active during the development of PrP^C-null mice might complicate analysis of PrP^C function in primary neurons. As an alternative, genetic manipulations such as PrP^C overexpression, knockout or knockdown can be performed in culture instead but primary cells are relatively difficult to transfect using standard methods (Karra and Dahm, 2010). Finally, culturing of mammalian primary neurons can be problematic due to their sensitivity to "physical stress, alterations in temperature, pH shifts, or changes in osmolarity" (Karra and Dahm, 2010). For the above reasons, we decided to use a well-characterised cell line called SH-SY5Y for investigating PrP^C function *in vitro* – background information on these cells is provided in the following section. My first steps using the SH-SY5Y cells were to generate monoclonal lines that stably expressed PrP^C. Although polyclonal cultures can be obtained more quickly, their

behaviour can change over time as rapidly proliferating cells outgrow those that proliferate slower. Monoclonal lines, on the other hand, should remain stable, at least in the short term. Having isolated several stably transfected clones, initial characterisation work consisted of assessing the level and localisation of PrP^C expression and determining whether PrP^C transfection had any impact on cell morphology.

3.1.1 Background on SH-SY5Y neuroblastoma cells

The parental cell line of SH-SY5Y is SK-N-SH, which was itself derived in 1970 from a bone marrow biopsy taken from a 4-year-old female patient with metastatic neuroblastoma (Biedler et al., 1973) – this rare form of cancer arises from an element of the sympathetic nervous system and mainly affects young children (Cheung and Dyer, 2013). SK-N-SH cultures reportedly consist of two distinct, co-existing types of cell with either neuroblast-like or epithelial-like morphologies (Biedler et al., 1973). Subcloning of SK-N-SH led to the creation of the SH-SY5Y cell line, which was originally reported to consist entirely of neuroblast-like cells that extend short, neurite-like processes (Biedler et al., 1978; Encinas et al., 2000). More recently, however, it has been recognised that SH-SY5Y cultures also contain a low proportion of "S-type" cells in addition to the neuroblast-like cells that are known as "N-type" (Encinas et al., 2000). The S-type cells are so-named due to their increased substrate-adherence; therefore, these cells are selected against when subculturing because they tend to remain attached to the previous culture vessel (Encinas et al., 2000).

SH-SY5Y cells in standard culture are reported to show characteristics of immature catecholaminergic neurons (Kovalevich and Langford, 2013) – catecholamines include the neurotransmitters dopamine and noradrenalin. This feature of the SH-SY5Y cell line has led to its widespread adoption as a model for Parkinson's disease (Xicoy et al., 2017), which is characterised by loss of dopaminergic neurons within the substantia nigra of the brain. SH-SY5Y cells can be further differentiated towards a mature dopaminergic phenotype by treating first with retinoic acid and then with the phorbol ester 12-O-tetradecanoyl phorbol-13 actetate (Xicoy et al.,

2017). Researchers have also developed other differentiation protocols that drive the cells towards alternative mature neuronal phenotypes; for instance, exposure solely to 12-O-tetradecanoyl phorbol-13 actetate seems to promote differentiation into a noradrenergic/adrenergic neuronal population (Pahlman et al., 1981), whilst treatment purely with retinoic acid appears to induce a cholinergic phenotype (Presgraves et al., 2004). Furthermore, sequentially exposing SH-SY5Y cells to retinoic acid and then brain-derived neurotrophic factor may prevent the S-type cells overgrowing the neuronal cells, a problem that seems affect cultures differentiated with retinoic acid alone (Encinas et al., 2000). Other, more advanced cell culture approaches have also been taken, such as growing the cells in an extracellular matrix gel and inducing differentiation by treating with a cocktail of growth factors consisting of brain-derived neurotrophic factor, neuregulin, nerve growth factor and vitamin D_3 (Agholme et al., 2010).

As will always be the case for tumour-derived cell lines, SH-SY5Y cells display several chromosomal abnormalities, including chromosome 7 trisomy and duplication of the short arm of chromosome 1 (Yusuf et al., 2013). In addition to the main karyotype, there appears to be a sideline karyotype that becomes more prevalent with increasing passage number (Yusuf et al., 2013) – this could reflect accumulation of the rarer S-type cells and suggests that the phenotype of the cell line may not remain stable over prolonged periods in culture.

Unlike most neuron-like cells, SH-SY5Y cells lack detectable PrP^C expression (Perera and Hooper, 1999), which means that the effects of introducing PrP^C into the cells can be studied without any meaningful interference from endogenously expressed PrP^C. As a consequence, this cell line has been used extensively to investigate PrP^C function (Watt et al., 2005; Parkin et al., 2007; Watt et al., 2007; Dupiereux et al., 2008; Rambold et al., 2008; Wang et al., 2009; Weiss et al., 2010; Bravard et al., 2015). All of these cited studies solely used the undifferentiated form of the cell line in their reported experiments.

3.2 Production of stable, PrP^C-expressing, monoclonal SH-SY5Y cell lines

The entire murine *Prnp* coding sequence (CDS) (NCBI ref: NM_011170.3; $Prnp^a$ allele) was amplified by polymerase chain reaction (PCR) from genomic DNA before being inserted into the pCI-neo mammalian expression vector between the EcoRI and SalI sites of its multiple cloning region. This vector contains a cytomegalovirus immediate-early enhancer/promoter element that drives constitutive expression of inserted transgenes in most cell types (Promega, 2009). Figure 3.1a shows this and other features of the vector in diagrammatic form, whilst Figure 3.1b & c show the sequence of the multiple cloning region before and after insertion of the *Prnp* CDS. The "CACC" between the EcoRI site and the start codon in the final construct provided a "Kozak" consensus sequence to ensure efficient ribosome binding of the mRNA.

Agarose gel electrophoresis of the expression construct confirmed that it contained extra DNA, since it migrated more slowly than the empty vector (Figure 3.2a). After transformation with the recombinant vector, XL-1 Blue *E.coli* were cultured overnight and eight of the resulting colonies were tested for presence of the transgene by colony PCR. Primers designed to bind to vector sequences flanking the inserted DNA were used to ensure the *Prnp* CDS was correctly orientated. Figure 3.2b confirms that DNA fragments matching the expected length of ~840 base pairs (bp) could be amplified by PCR from six of the eight colonies. Plasmid DNA containing the transgene was isolated from the six colonies for sequencing, which was performed in both directions to improve accuracy. Although the inserted DNA exactly matched the murine *Prnp* CDS for five of the six clones, the best quality sequencing data was obtained from clone 4. Therefore, this clone, hereafter referred to as pCI-neo-MoPrnp, was chosen for transfection into the SH-SY5Y cells.

A) pCI-neo vector

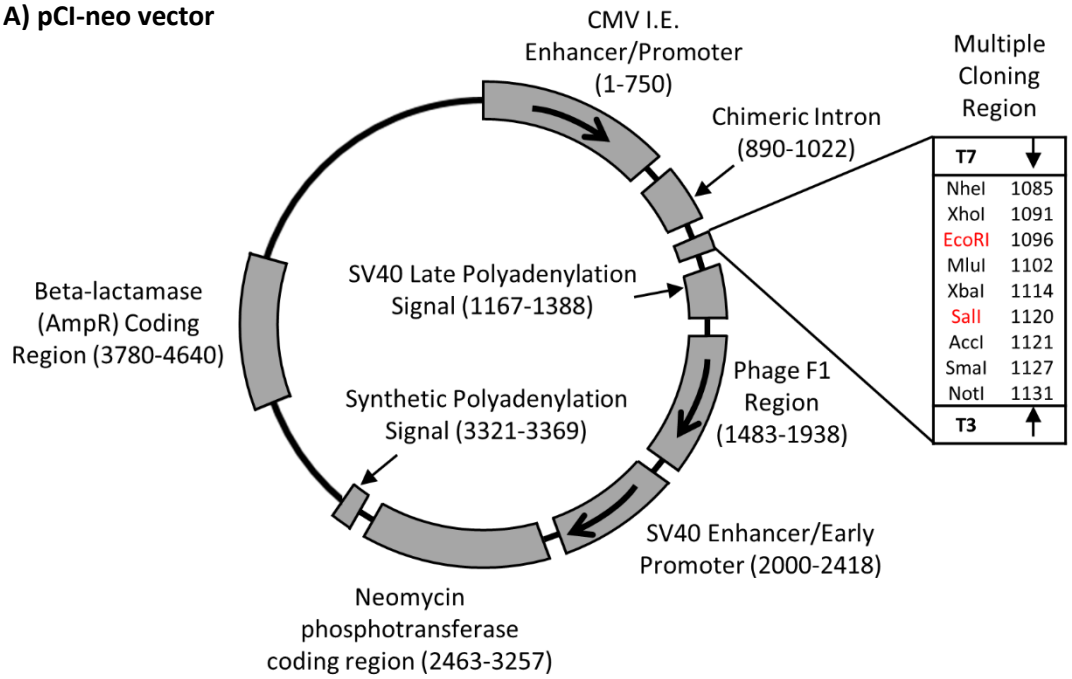

B) Multiple cloning region of empty vector

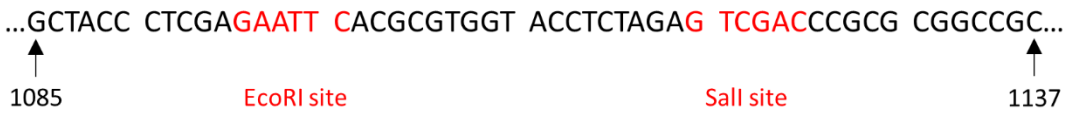

C) Multiple cloning region after insertion of *Prnp* CDS

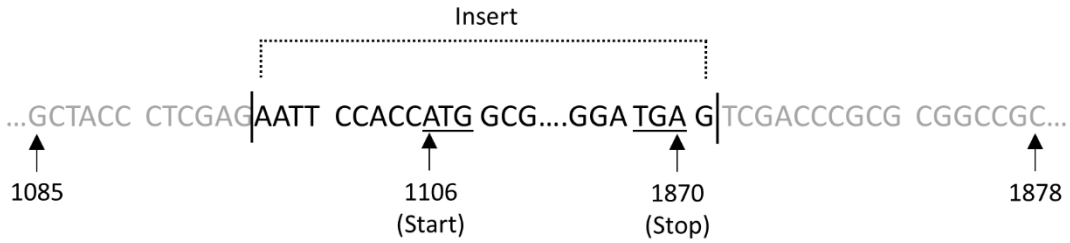

Figure 3.1 – Generating the pCI-neo-MoPrnp expression construct

A) Diagram showing the various features of the pCI-neo vector (base pair-numbering shown in brackets). Expression of sequences inserted into the multiple coding region is driven by a cytomegalovirus (CMV) immediate-early (I.E) enhancer/promoter. **B)** The multiple cloning region sequence of pCI-neo highlighting the EcoRI and SalI sites used for insertion of the

Prnp CDS. **C)** The multiple cloning region sequence after insertion of the *Prnp* CDS. Vector sequence is coloured in grey; the insert is in black. The *Prnp* CDS covered bases 1106-1870 of the sense strand of the pCI-neo-MoPrnp construct and the start and stop codons are underlined in the diagram.

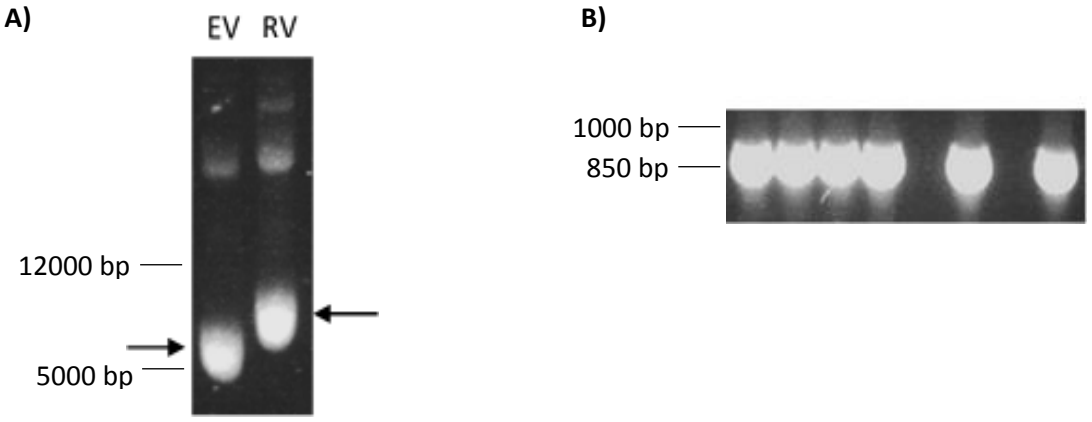

Figure 3.2 – Successful insertion of *Prnp* coding sequence into pCI-neo vector

A) Agarose gel electrophoresis of the pCI-neo vector before and after insertion of the *Prnp* CDS. The recombinant vector (RV) band migrated slower than the empty vector (EV) band due to the inserted DNA fragment. Because the vectors are supercoiled, whereas the ladder consists of linear DNA fragments, the bp sizes given should not be taken as exact. **B)** Agarose gel electrophoresis of PCRs to confirm that the *E.coli* colonies obtained after transformation with the recombinant vector contained the *Prnp* CDS. DNA fragments of the expected size (around 840 bp) were amplified from six out of the eight colonies tested. The other colonies may have been transformed with empty vector that had re-ligated after restriction enzyme digestion.

pCI-neo carries a resistance gene against the antibiotic G-418, which enabled selection for cells that had stably integrated the vector into their genome. Firstly though, I needed to determine the optimum G-418 dose for selection. Therefore,

cultured SH-SY5Y cells were exposed to G-418 concentrations between 100 and 1200 µg/ml over a 12-day period. Cell viability was monitored by observation under a light microscope. 400 µg/ml G-418 was the lowest dose to cause total cell death within the assay time period but, in order to control for batch-to-batch variation in G-418 activity, a slightly higher dose of 500 µg/ml was chosen for selection of stable transfectants.

pCI-neo-MoPrnp was transfected into SH-SY5Y cells using Lipofectamine LTx. Several transfection reactions were set up using dilutions of Lipofectamine LTx stock between 1:200 and 1:500. After 6 hours, the transfected cells were pooled and allowed to recover for a further 72 hours before addition of G-418. Significant cell death was observed over the next few days due to loss of the vector. However, after a week of G-418 selection, colonies of stably transfected cells were visible and this polyclonal culture was maintained until 3 weeks post transfection. At this point, PrP^C expression was assessed by immunofluorescence microscopy using the 6H4 anti-PrP primary antibody from Thermo Fisher Scientific. PrP^C staining of varying intensity was visible in most cells in the transfected culture (Figure 3.3a) and the staining was often punctate, which may have been caused by PrP^C aggregation due to overexpression or, alternatively, may have been an artefact of permeabilising the cells with Triton X-100. As expected, no PrP^C expression could be detected in untransfected SH-SY5Y cells that had been cultured alongside the transfected cells (Figure 3.3b).

Polyclonal, PrP^C-transfected SH-SY5Y cells were serially diluted in a 96-well tissue culture plate so that some wells contained just a single cell. 4 days later, wells containing a single colony of fewer than eight cells were assumed to have contained a single cell at plating. Monoclonal lines were derived from these wells and were cultured over the next few weeks until they had expanded sufficiently for frozen stocks to be prepared. This was achieved for nine clones; several others were discarded due to extremely slow rates of proliferation. Subsequently, six clones were assayed for PrP^C expression by seeding the cells into tissue culture plates, lysing 24 hours later and then analysing by western blotting using the BC6 anti-PrP^C primary

antibody (McCutcheon et al., 2014). Based on a single replicate, quantification of PrP^C immunostaining appeared to separate the clones into a group of four high-expressors and a group of two low-expressors (Figure 3.4). I decided to select two clones with high expression (1G3 and 1F3) and two with lower expression (2E3 and 1B5) for further use.

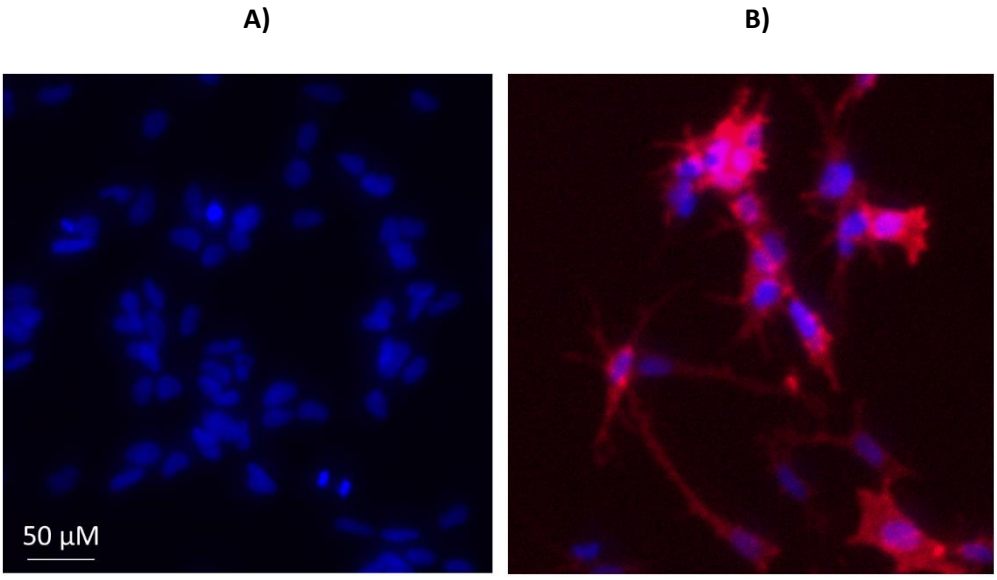

Figure 3.3 – Polyclonal, transfected SH-SY5Y cells express PrP^C

Widefield fluorescence images of fixed, Triton-permeabilised, untransfected **(A)** or PrP^C-transfected **(B)** SH-SY5Y cells taken using a x10 objective. Nuclei were stained with DAPI and are shown in blue. PrP^C was detected by use of the 6H4 anti-PrP^C primary antibody (Thermo Fisher Scientific #7500996) and is shown in red. The scale bar shown applies to both panels. Camera exposure settings were the same for both images. PrP^C staining was absent in untransfected cells but was detectable in most transfected cells. Staining intensity varied among the transfected cells, suggesting that different cells expressed different amounts of PrP^C.

Frozen stocks were also prepared from the untransfected cells that had been cultured alongside the transfected cells. These cells, subsequently referred to as $SH\text{-}SY5Y^{Untr}$, were used in all experiments involving the transfected cells to provide a control

population approximately matched in terms of weeks in culture. Since SH-SY5Y^{Untr} could not be cultured in the presence of G-418, the selection antibiotic was removed from transfected cultures at least 48 h before an experiment.

A)

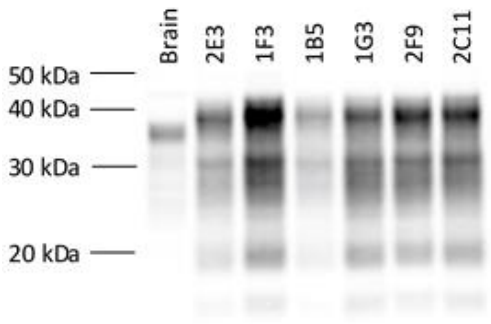

B)

Sample	Normalised PrP^C expression
Mouse brain	1.00
Clone 2E3	2.76
Clone 1F3	7.21
Clone 1B5	2.94
Clone 1G3	6.07
Clone 2F9	5.98
Clone 2C11	6.61

Figure 3.4 - Initial assessment of PrP^C expression in stably transfected clones

A) Fluorescent western blot image showing PrP^C immunostaining in a mouse brain homogenate and in cell lysates from stably transfected clones. PrP^C was detected by use of the BC6 anti-PrP^C primary antibody (McCutcheon et al., 2014). **B)** Table summarising quantification data from the western blot. For each lane, the entire band pattern shown was included when calculating staining intensity. After correcting for loading errors, signals were normalised to the signal from the brain homogenate.

3.3 Characterisation of stably transfected SH-SY5Y clones

3.3.1 Similar level of PrP^C expression among clones analysed

Before using the stably transfected clones to investigate PrP^C function, I needed to specifically determine the magnitude and localisation of their PrP^C expression. The levels of PrP^C in clones 2E3, 1B5, 1G3 and 1F3 had previously been estimated by western blotting of a single set of cell lysates (Figure 3.4); however, to improve the accuracies of these estimates, three more sets of cell lysates were prepared and analysed by western blotting. The experimental format was the same as before – the stably transfected clones were seeded into tissue culture plates and lysed 24 hours later. The results from these experiments[4] showed that, on average, all four clones expressed similar amounts of PrP^C (Figure 3.5), whilst the mean expression level among the clones was around four times that of mouse forebrain (C3H strain). Given that brain tissue contains multiple cell types and that neurons reportedly express more PrP^C than glial cells (Witusik et al., 2007), PrP^C expression by the stably transfected clones was probably at a physiologically relevant level for a neuronal cell. These results conflict with those shown in Figure 3.4, which suggested that clones 1G3 and 1F3 expressed more PrP^C than 2E3 and 1B5. One explanation is that the Figure 3.4 data derived from a single biological replicate and is, therefore, less reliable. However, the data shown in Figure 3.4 was an early assessment of PrP^C expression, whereas the Figure 3.5 data includes analyses of cells that had spent several more weeks in culture. Therefore, it may be that there was an initial period of instability in PrP^C expression followed by normalisation to a level of expression that was similar in all clones.

Figure 3.5a demonstrates in diagrammatic form the PrP^C immunostaining pattern that would be expected from brain tissue: a strong band corresponding to di-glycosylated, full length PrP^C at ~33 kDa; fainter bands at ~29 and ~26 kDa for mono- and

[4] Note that Figure 3.5c summarises data from all four independently prepared sets of cell lysates i.e. including the single set that was used to obtain the data for Figure 3.4.

un-glycosylated, full length PrP^C, respectively; and, potentially, further faint bands at ~23, 19 and 16 kDa representing the different glycoforms of the C1 fragment.

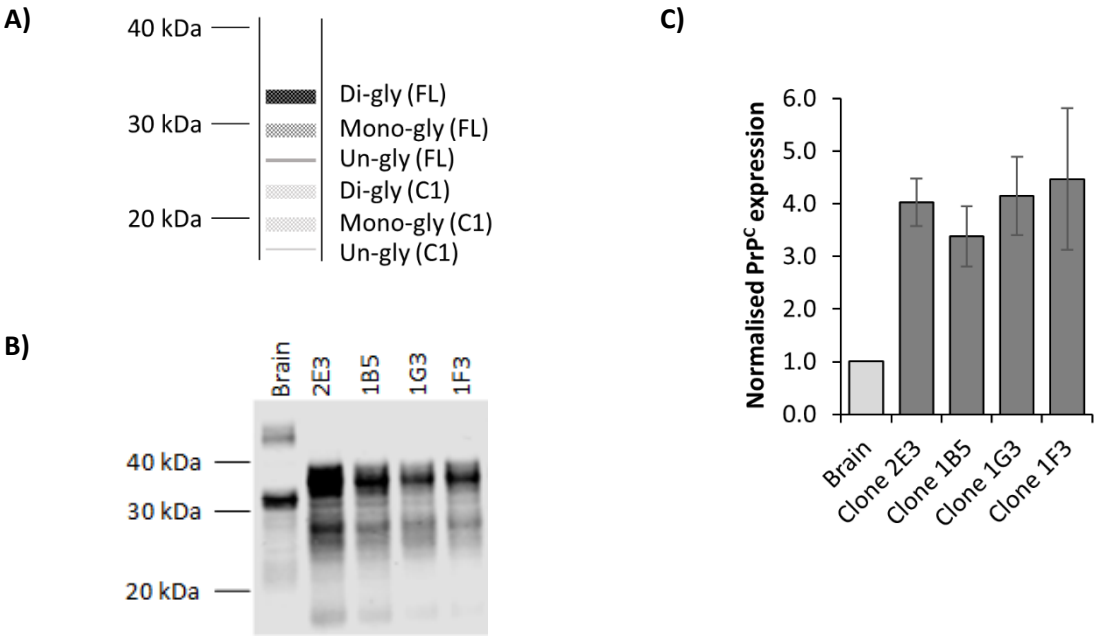

Figure 3.5 – Stably transfected clones expressed similar levels of PrP^C

A) Diagrammatic representation of the typical PrP^C immunostaining pattern obtained from brain tissue, showing the approximate molecular weights of the di-, mono- and un-glycosylated forms of full length (FL) PrP^C and the C1 fragment. **B)** PrP^C expression was assessed by western blotting of four independently prepared sets of cell lysates. A representative blot image is shown. PrP^C was detected by use of the BC6 anti-PrP^C primary antibody (McCutcheon et al., 2014). "Brain" = mouse forebrain homogenate; "Untr" = SH-SY5Y^{Untr}. For each lane, staining intensity was calculated from the entire band pattern shown except for the band at around 50 kDa in the mouse brain lane, which was thought to be non-specific. **C)** Bar chart summarising PrP^C quantification data from the western blotting experiments. For each membrane, after correction for loading errors, signals from the clones were normalised to the brain homogenate signal. The mean normalised expression values (+/- standard error of the mean) are displayed in the bar chart.

Figure 3.5b shows that, whilst the mouse forebrain homogenate approximately displayed this expected band pattern, the bands obtained from the lysates of the stably transfected clones were shifted to higher apparent molecular weights. One hypothesis for this was altered glycosylation, which was investigated by digesting a clone 2E3 cell lysate with peptide-N-glycosidase F (PNGase F), an enzyme that removes N-linked glycans from glycoproteins (Gates et al., 2004). Both oligosaccharides linked to the PrP^C C-terminal domain are susceptible to this enzyme, although the GPI anchor is not removed. Following PNGase F treatment, western blotting for PrP^C revealed two strong bands at ~17 and 26 kDa in the brain homogenate and cell lysate lanes (Figure 3.6). These bands correspond to the un-glycosylated forms of C1 and full length PrP^C, respectively, whilst the very faint bands in between may be due to incomplete PNGase F digestion. In conclusion, these results confirmed that the abnormal SDS-PAGE migration of the transgenic PrP^C must have been due to glycosylation differences.

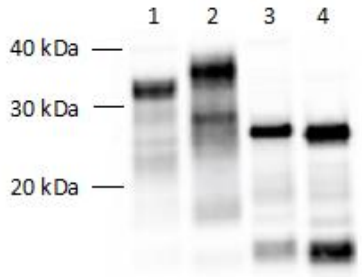

Figure 3.6 – Differential PrP^C glycosylation explains altered SDS-PAGE migration

Fluorescent western blot image comparing PrP^C immunostaining patterns obtained from PNGase F-treated and mock-treated cell and tissue lysates. PrP^C was detected by use of the BC6 anti-PrP^C primary antibody (McCutcheon et al., 2014). Labels are as follows: 1 = mouse brain homogenate, mock treatment; 2 = SH-SY5Y clone 2E3, mock treatment; 3 = mouse brain homogenate, PNGase treatment; 4 = clone 2E3, PNGase treatment. For mock treatments, buffer components were the same but PNGase F was not included. PrP^C band patterns from brain and clone 2E3 samples were virtually identical after PNGase F digestion of N-glycans.

Glycan intermediates are generated in the ER before being attached to newly-synthesised proteins. Subsequent modifications of these glycans occur partly in the ER but mainly in the Golgi (Gates et al., 2004). Therefore, altered expression compared to brain of the transferases that carry out these modifications could explain the increased size of the glycans on the transgenic PrP^C. Such alterations to glycosylation are reported to occur frequently in cell lines but are thought to have few biological consequences (Varki and Lowe, 2009). Aside from the differences in glycan size, the majority of PrP^C expressed by the stably transfected clones was di-glycosylated as was the case in mouse forebrain.

The glycans attached to forebrain PrP^C increased its apparent molecular weight by ~7 kDa, whilst those on the transgenic PrP^C expressed by clone 2E3 added 10-11 kDa. Interestingly, a band that could have been mono-glycosylated C1 was observed at the expected apparent molecular weight of ~19 kDa in the clone 2E3 lysate that had not been digested with PNGase F (Figure 3.6, lane 2). Assuming that the relatively strong band at 28/29 kDa, also in lane 2, corresponds to di-glycosylated C1 then it is possible that only one of the glycans was larger than normal.

As mentioned above, PNGase F digestion confirmed that the C1 fragment was present in clone 2E3. Furthermore, the PrP^C band patterns obtained by western blotting were virtually identical among the clones analysed (Figures 3.4 and 3.5), which indicates that alpha-cleavage of PrP^C occurred in all of them. Quantification of the bands in Figure 3.6 revealed that C1 made up 40 % of total PrP^C expressed by clone 2E3 compared with 28 % for the forebrain homogenate. Whilst these figures may not be exact since the primary antibody affinities for full length PrP^C and C1 may differ, the data certainly suggest that more PrP^C was subject to alpha-cleavage in the transfected cells than in mouse forebrain.

3.3.2 Similar PrP^C localisation patterns among clones analysed

After analysing PrP^C expression by the stably transfected clones by western blotting, the subcellular distribution of PrP^C staining was assessed by immunofluorescence…

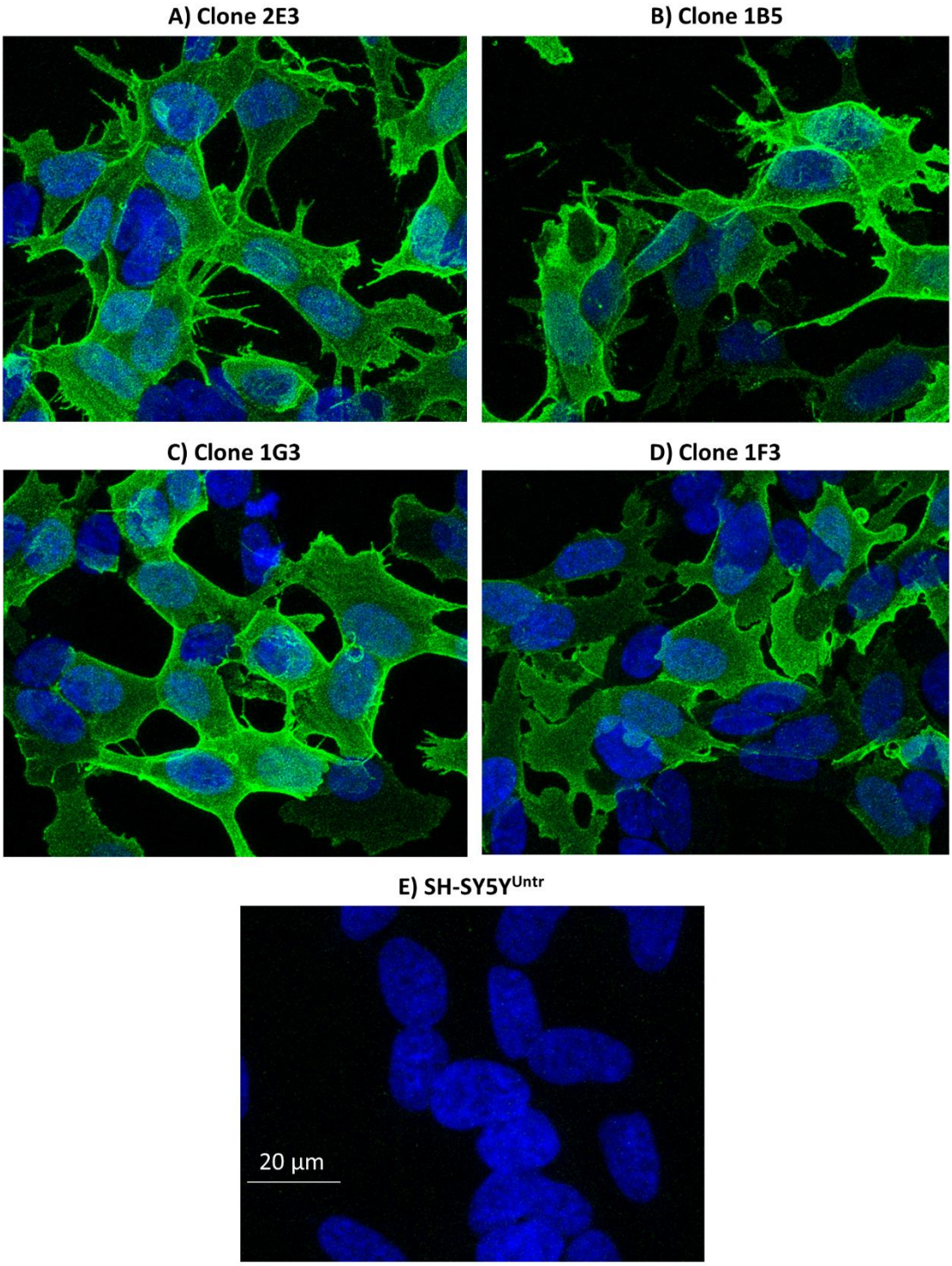

Figure 3.7 – Stably transfected clones expressed PrP^{C} on the cell surface

A-E) Confocal images of fixed, non-permeabilised SH-SY5Y cells taken using a x40 objective. Images are maximum intensity projections from z-stacks. Nuclei were stained with DAPI and are shown in blue. PrP^{C} was detected by use of the 6H4 anti-PrP^{C} primary antibody (Thermo

Fisher Scientific #7500996) and is shown in green. The scale bar shown applies to all panels. Cell surface-associated PrP^C staining is visible for all the transfected clones **(A-D)**, whilst no PrP^C expression was detected in SH-SY5Y^{Untr} cultures **(E)**. Microscope settings were adjusted when capturing images **A-D** to best reveal the distribution of PrP^C expression. Therefore, variation in staining intensity between images does not necessarily represent variation in PrP^C expression levels.

…microscopy to check that the protein was expressed in a physiologically relevant location. The cells were seeded into tissue culture plates and fixed 24 hours later. No permeabilisation step was included prior to staining to ensure that only cell surface-associated PrP^C could be detected. Following PrP^C immunostaining and nuclear counterstaining, images were captured using a confocal microscope. These images again confirmed the lack of PrP^C expression by SH-SY5Y^{Untr} (Figure 3.7e), whereas the clones were shown to express PrP^C on the cell surface as expected (Figure 3.7a-d) – generally, PrP^C is GPI-anchored to the extracytoplasmic face of the cell membrane and is concentrated in lipid rafts microdomains (Vey et al., 1996). A few individual cells, particularly from clone 1F3, displayed no detectable PrP^C expression (Figure 3.7d). This is unlikely to have been due to cells clumping on top of each other since the images shown in Figure 3.7 are maximum intensity projections from z-stacks – some PrP^C staining would be expected at some of the z-coordinates even if cells were in different planes. Therefore, it is possible that "clone" 1F3 was not entirely clonal i.e. some cells within the culture were expressing a very low level of PrP^C, which was undetectable under the imaging settings used.

After confirming that the stably transfected clones expressed PrP^C at the cell surface, I assessed whether any intracellular PrP^C was expressed. The experimental format was the same except that cells were methanol-permeablised after fixation to enable detection of intracellular epitopes by the antibody. Again, confocal z-stack images were acquired. High-magnification, single z-slice images hinted at the presence of cytoplasmic staining, although the cell-surface staining intensity was considerably more intense for all four clones (Figure 3.8a-d).

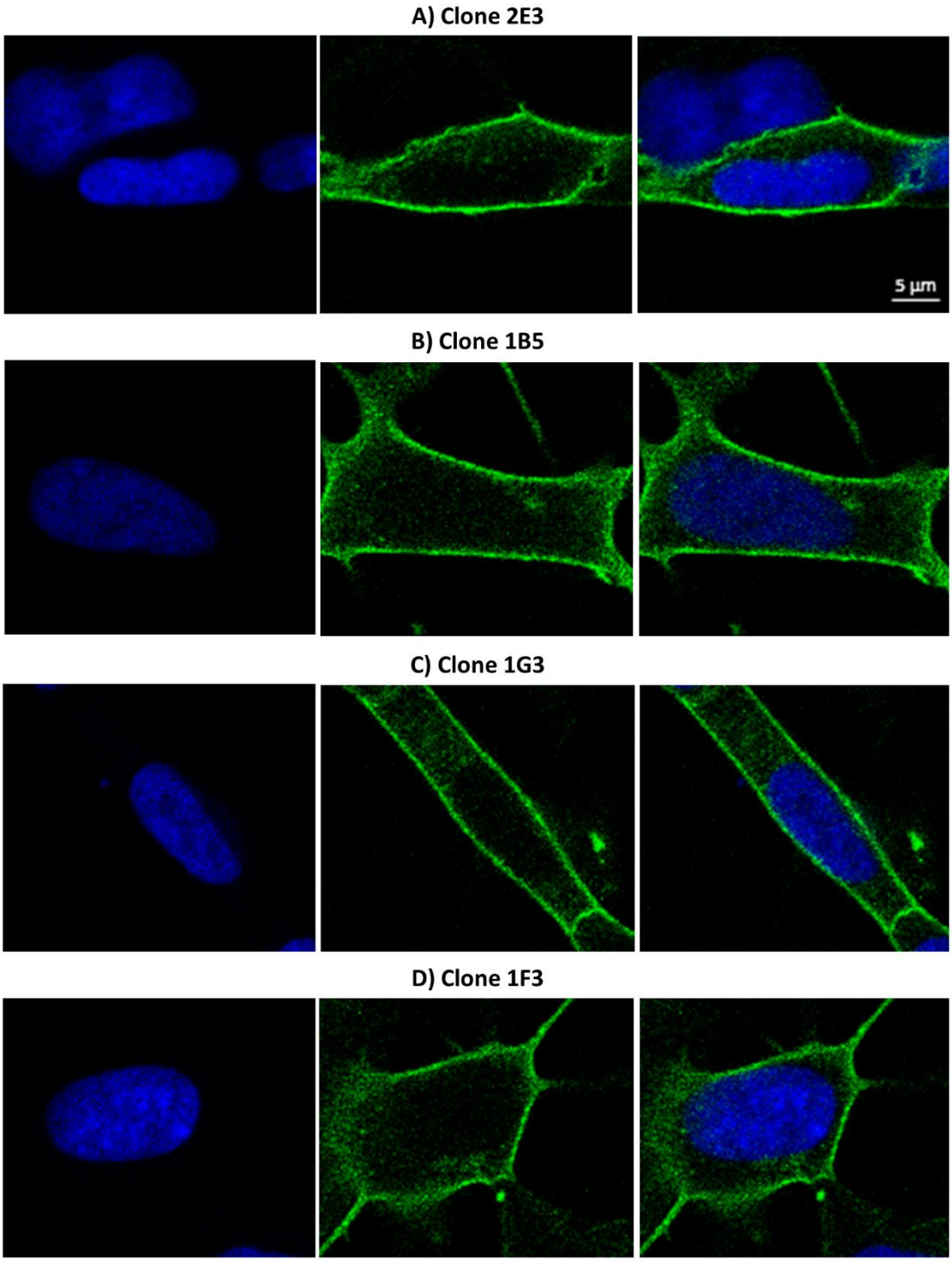

Figure 3.8 – Low levels of intracellular PrP^C staining in stably transfected clones

A-D) Confocal images of fixed, methanol-permeabilised SH-SY5Y cells taken using a x40 objective. Nuclei were stained with DAPI and are shown in blue. PrP^C was detected by use of

the 6H4 anti-PrP^C primary antibody (Thermo Fisher Scientific #7500996) and is shown in green. The images show slices through the middle of the cells in the z-plane and single-channel and merged versions are provided in each case. The scale bar shown applies to all panels. Microscope settings were adjusted when capturing each image to best reveal the distribution of PrP^C expression. Therefore, staining intensity is not necessarily representative of PrP^C expression level. For all clones, the highest-intensity PrP^C immunostaining is at the cell surface but some intracellular staining is also visible.

Some of the intracellular staining may have been newly synthesised PrP^C in the process of being trafficked to the cell membrane. Another explanation is that PrP^C is reported to undergo cycles of internalisation followed by trafficking back to the cell membrane via recycling endosomes (Shyng et al., 1995; Sunyach et al., 2003), which presumably is a mechanism to enable rapid control of the level of PrP^C at the cell surface.

3.3.3 Morphological differences between stably transfected clones and untransfected SH-SY5Y cells

Having obtained confirmation that the majority of PrP^C expressed by the stably transfected clones was trafficked to the cell surface as expected, I further characterised the PrP^C-transfected cells by analysing their morphology. Once again, the cells were seeded into tissue culture plates and fixed 24 hours later before images were captured using a phase contrast microscope. These images showed that the morphologies of clones 2E3 and 1B5 were very similar to SH-SY5Y^{Untr} – the cells had the same stellate morphology with short, occasionally branching, neurite-like protrusions (Figure 3.9a-c). This morphology is very similar to images of SH-SY5Y cells that have been published in other studies (Prince and Oreland, 1997; Weiss et al., 2010). However, clone 1G3 was rather different in appearance to SH-SY5Y^{Untr} and clones 2E3 and 1B5 – adjacent cells appeared to be joined together by their somas and almost none of the fine, neurite-like protrusions were evident in the culture (Figure 3.9d).

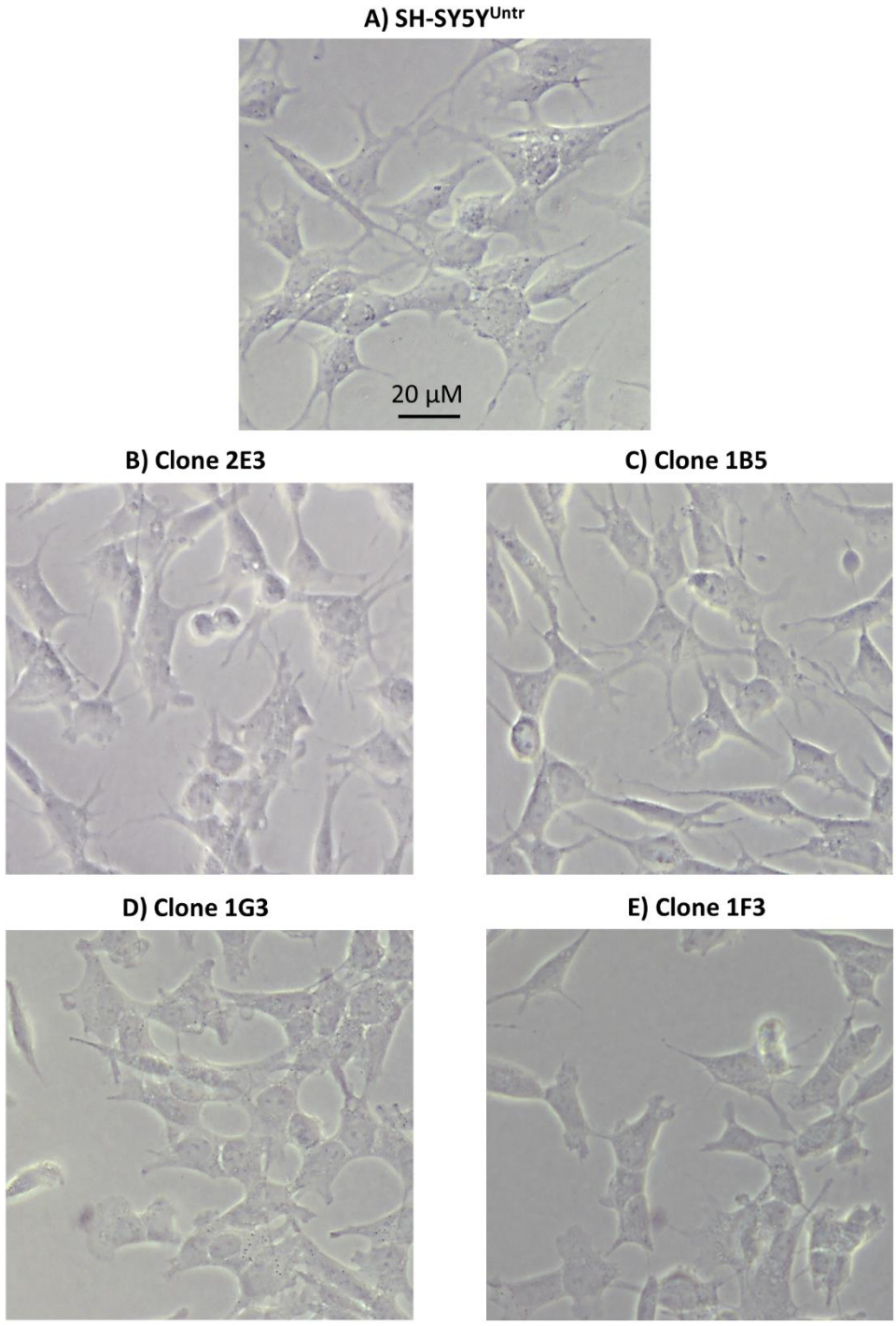

Figure 3.9 – Clone-specific morphological alterations identified among the stably transfected clones

A-E) Phase contrast images of fixed SH-SY5Y cells taken using a x40 objective. The scale bar shown applies to all panels. Clone 1G3 displayed an altered morphology compared with SH-SY5Y^{Untr} – the cell bodies were shaped differently and clone 1G3 cells produced almost

no neurite-like protrusions. Clone 1F3 exhibited some morphological changes that similar to clone 1G3, whereas clones 2E3 and 1B5 seemed almost identical to SH-SY5Y^{Untr}.

Clone 1F3 also displayed similar morphological alterations (Figure 3.9e), although the changes were arguably less dramatic than those exhibited by clone 1G3. The variations in morphology were surprising given that the levels and localisation patterns of PrP^C expression were similar among the clones. Consequently, it seemed that some factor other than PrP^C was responsible and Chapter 4 covers work that was carried out to address this possibility.

3.4 Alterations to stress responses in the stably transfected clones

The previous sections reported on experiments to characterise four SH-SY5Y clones that stably expressed PrP^C. The results showed that the clones expressed similar levels of PrP^C and that the exogenous PrP^C was mainly expressed at the cell surface, although some limited cytoplasmic staining was detected – this subcellular distribution of PrP^C expression was consistent with results from other studies (Vey et al., 1996; Lee et al., 2001a; Nikles et al., 2008). Additionally, phase contrast imaging of the cells identified some as yet unexplained clone-specific morphological alterations compared with $SH\text{-}SY5Y^{Untr}$.

The first experiments I performed using the stably transfected SH-SY5Y clones were to investigate the role played by PrP^C in the response to stress. Arguably, stress-protection is the function most commonly ascribed to PrP^C; this is because a large number of studies have found that PrP^C expression enhances the survival of cultured cells in response to toxins and other treatments that induce apoptosis (Kuwahara et al., 1999; Lopes et al., 2005; Roucou et al., 2005; Beraldo et al., 2010). PrP^C expression also reportedly protects cells from damage caused by various agents that induce oxidative stress (Brown et al., 2002; Senator et al., 2004; Anantharam et al., 2008; Bertuchi et al., 2012; Bravard et al., 2015). However, there are conflicting reports of a lack of stress protection by PrP^C and some studies have even found that PrP^C expression enhances cell death in response to stress (Paitel et al., 2004; Vassallo et al., 2005; Sunyach et al., 2007; Steinacker et al., 2010). Furthermore, the issues described in section 1.3 that affect several of the PrP^C-knockout mouse lines – ectopic doppel expression in the brain and the problems caused by creating the lines on mixed genetic backgrounds – cast doubt upon the results obtained from studies of these mice or of cells derived from them. Consequently, the putative involvement of PrP^C in cellular stress-protection required clarification. To achieve this, I exposed the stably transfected SH-SY5Y clones to a range of different stresses that broadly covered the spectrum of previously reported stress-protective functions of PrP^C. Firstly, the cells were treated with the oxidative toxin paraquat dichloride (PQ).

Within a cell, various enzymes convert PQ into a reduced intermediate that, in turn, causes the production of ROS (Senator et al., 2004). The toxin treatment protocol reported by Dupiereux et al. (2008) was followed – this study found that PrP^C transfection into SH-SY5Y cells was protective against exposure to PQ. Briefly, cells were seeded into plates in serum-containing medium and allowed to recover for 16-18 hours. Next, the medium was exchanged for serum-free medium containing the neuronal supplement N-2 and the toxin. Serum deprivation should inactivate receptors that are constitutively activated by growth factors present in serum, thereby removing potential confounding elements from an experiment. The N-2 supplement promotes survival of neuroblastoma cells and was included to mitigate against the stress caused by serum deprivation itself. Otherwise, it would have been difficult to separate out the impact of serum removal from that of the toxin treatment. Unlike serum, N-2 is chemically defined, consisting of transferrin, insulin, progesterone, putrescine and selenite (Thermo Fisher Scientific, [n.d.]-c). Typically, serum would be removed a few hours before carrying out a treatment to allow growth factor signalling pathways to return to baseline. However, Dupiereux et al. (2008) did not do this. Since we were initially attempting to replicate their results for PQ treatment of PrP^C-expressing SH-SY5Y cells, we decided to follow their method exactly. In order to be consistent, the same method was also used for treatment with the other toxins. Following a 24-hour incubation with the toxin, cell survival in response to PQ was assessed by use of the PrestoBlue cell viability reagent. PrestoBlue contains the weakly fluorescent dye resazurin, which is converted in the reducing environment of the cytoplasm to the highly fluorescent resorufin (Invitrogen, 2012). This reaction does not take place in dead cells. Therefore, fluorescence intensity should be directly proportional to the number of viable cells.

SH-SY5Y cells were exposed to PQ concentrations between 500 and 2000 μM as well as a higher dose of 10000 μM. The results from five independent experiments showed that clone 1F3 was significantly more resistant to 500 and 1000 μM PQ than $SH\text{-}SY5Y^{Untr}$ ($p < 0.001$ in both cases; Figure 3.10a). This difference in viability was most marked at 500 μM (96 % viability for clone 1F3 vs 54 % for $SH\text{-}SY5Y^{Untr}$). Clone 1G3 displayed improved viability compared with $SH\text{-}SY5Y^{Untr}$ following

treatment with 500 μM PQ ($p < 0.001$) but was slightly more sensitive than SH-SY5Y^{Untr} at 1500 μM ($p = 0.016$). Clones 2E3 and 1B5 responded similarly to SH-SY5Y^{Untr}, although clone 1B5 did show slightly reduced viability at 500 and 1500 μM doses of PQ ($p = 0.036$ and $p = 0.047$, respectively). However, PQ has been shown previously to interfere with mitochondrial function in SH-SY5Y cells, probably before causing cell death (Dupiereux et al., 2008). Since nicotinamide adenine dinucleotide phosphate (NADH) produced by mitochondria is the main compound responsible for resazurin reduction, impaired mitochondrial function can result in lower fluorescence signals independent of any reduction in viable cell number. Therefore, to confirm the results obtained from the viability assays, PQ-mediated cytotoxicity was assessed by measuring lactate dehydrogenase (LDH) release. Damage to the cell membrane causes LDH to leak out into the culture medium. Consequently, the amount of LDH activity in a sample of medium should be proportional the number of dead or damaged cells (Abcam, 2012). Treatment with 10000 μM PQ resulted in approximately 0 % viability, as measured using the PrestoBlue reagent, for all clones and SH-SY5Y^{Untr}. This dose was used as the 100 % cytotoxicity control for the LDH assays. The results from four independent experiments showed that the differences between the stably transfected clones in terms of their responses to PQ exposure were generally more extreme according to the LDH assay than they were when assessing viability (Figure 3.10b). At all PQ doses tested, clones 1G3 and 1F3 displayed significantly lower levels of cytotoxicity than SH-SY5Y^{Untr}, whilst clones 2E3 and 1B5 did not. For example, at 2000 μM PQ, cytotoxicity was ~100 % for SH-SY5Y^{Untr} (and clones 2E3 and 1B5) but just 20 % for clone 1F3. Overall, the viability and cytotoxicity measurements obtained after PQ treatment were highly consistent – both assay formats ranked the transfected clones similarly in terms of their resistance to the toxin and percentage survival and percentage cytotoxicity at a particular dose of PQ generally added up to ~100 %. Interestingly though, cytotoxicity remained low for clones 1G3 and 1F3 even at PQ doses that reduced viability, as measured using the PrestoBlue reagent, to very low levels.

A)

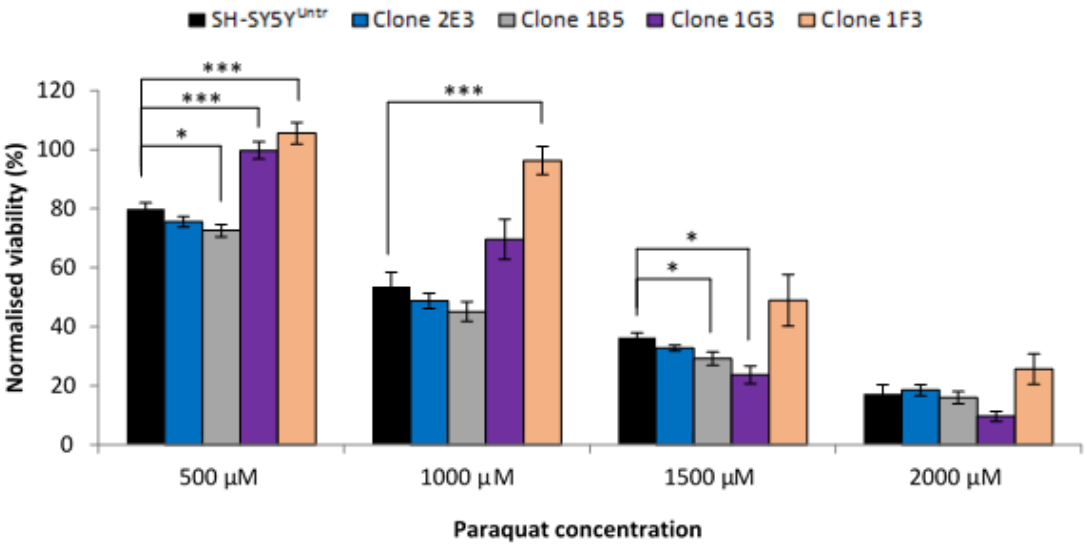

B)

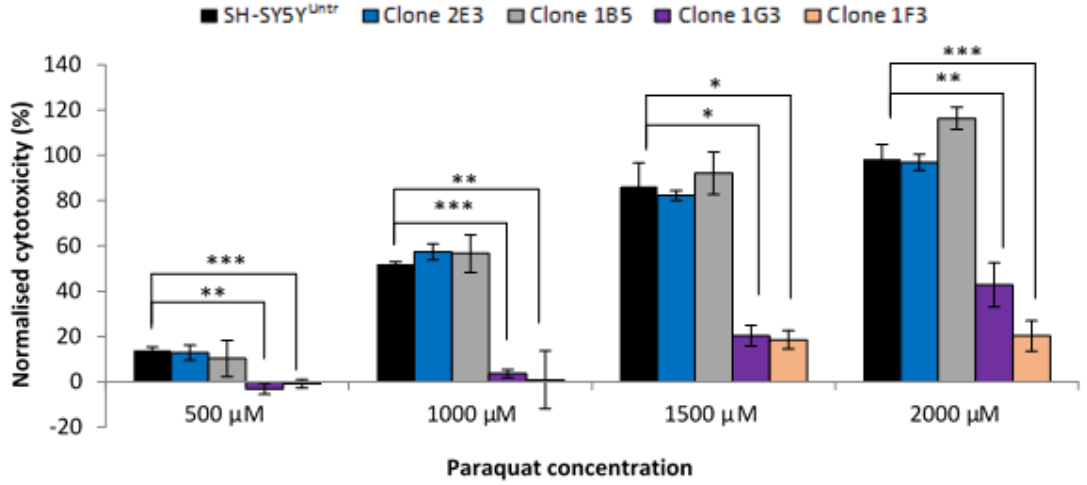

Figure 3.10 – Clone-specific resistance of stably transfected cells to paraquat treatment

Bar charts showing viability **(A)** and cytotoxicity **(B)** of SH-SY5Y cells after 24 h exposure to a range of PQ concentrations. The mean values (+/- standard error of the mean) from five **(A)** or four **(B)** independent experiments are displayed in the bar charts. Differences between SH-SY5Y^{Untr} and each transfected clone were tested for significance ($p < 0.05$) using unpaired, two-sample t-tests. Key: * for $p < 0.05$; ** for $p < 0.01$; and *** for $p < 0.001$.

During routine culturing of the SH-SY5Y cells, I observed that cultures of the stably transfected clones seemed to have more non-adherent cells than SH-SY5Y^{Untr} cultures and it was difficult to determine whether these floating cells were alive or not. Interestingly, the American Type Culture Collection (ATCC) advise treating SH-SY5Y cells supplied by them as semi-adherent i.e. the monolayer and cells in suspension should be taken forward together when subculturing (ATCC, [n.d.]). The cells I used were purchased from the European Collection of Cell Cultures, which instead recommends subculture of purely the monolayer cells – I cultured the cells according to this method. However, when optimising conditions for PQ treatment, I performed an assay using cells that had been processed for plating as if they were semi-adherent. Although only SH-SY5Y^{Untr} and clone 2E3 cells were included in this experiment, the viability data were very similar to those obtained with cells harvested purely from the monolayer (data not shown). This suggests that excluding non-adherent cells from the cultures prior to stress-exposure had little impact on the results obtained.

Having assessed the responses of the SH-SY5Y cell lines to PQ treatment, the effect of exposing the cells to the ATP-competitive protein kinase inhibitor staurosporine (STS) was investigated. STS binds to many kinases with high affinity but low selectivity (Ruegg and Burgess, 1989; Meggio et al., 1995) and is thought to induce both mitochondria-dependent and mitochondria-independent apoptotic signalling processes (Zhang et al., 2004). Since STS is solubilised in dimethyl sulphoxide (DMSO), I first confirmed that presence of relatively low DMSO concentrations of up to 1 % (v/v) in the culture medium had no discernible impact on cell viability over a 24-hour period, as measured using the PrestoBlue reagent (data not shown). Subsequently, toxicity caused by STS concentrations between 50 and 200 nM as well as a higher dose of 600 nM was assessed in the same way as for PQ. Six independent experiments were performed and data from PrestoBlue viability assays reported in Figure 3.11a & b show that clones 1G3 and 1F3 were more viable than SH-SY5Y^{Untr} in response to 25 nM ($p = 0.028$ and $p = 0.016$, respectively) and 50 nM doses of STS ($p = 0.020$ and $p = 0.044$, respectively). Clone 1G3 also displayed significantly greater viability than SH-SY5Y^{Untr} when exposed to 100 nM STS ($p = 0.049$).

A)

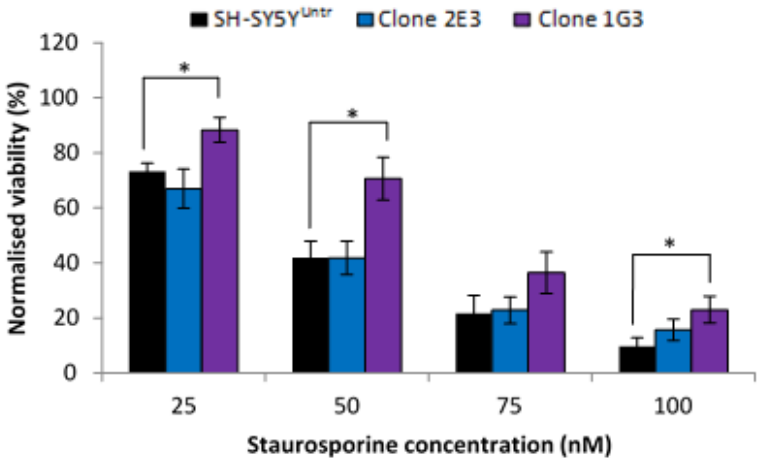

B)

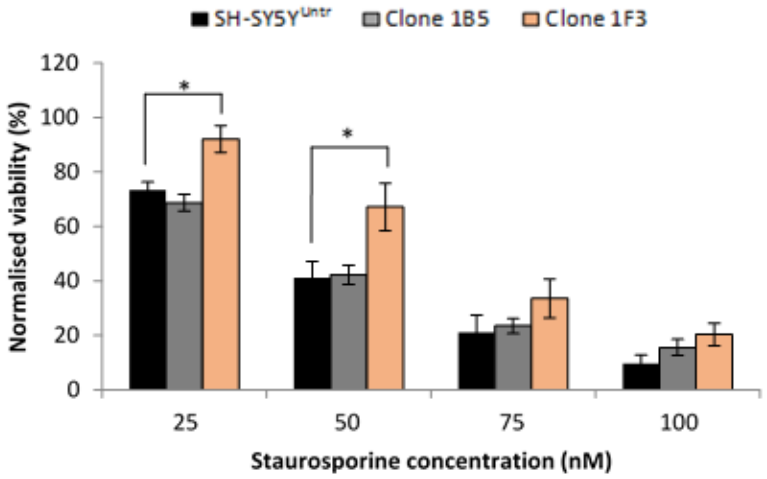

C)

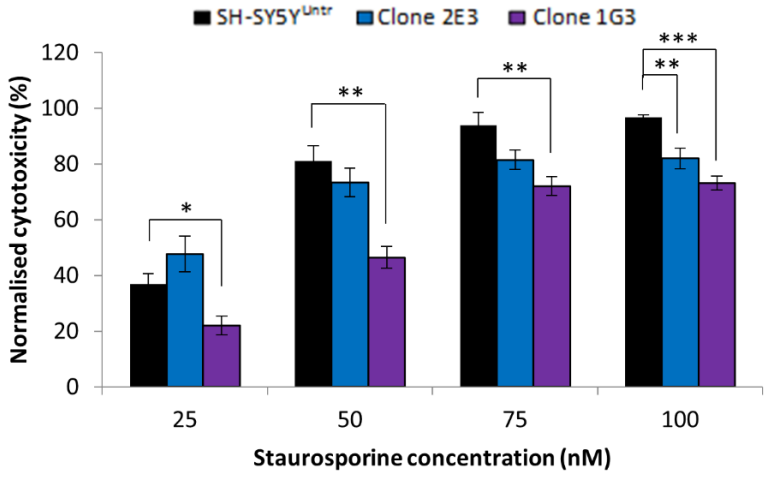

Figure 3.11 – Clone-specific resistance of stably transfected cells to staurosporine treatment

See following page for legend…

D)

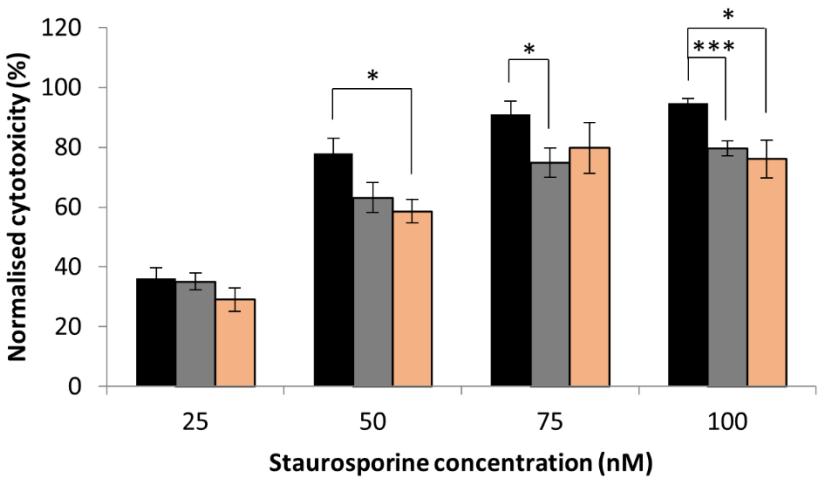

Figure 3.11 – Clone-specific resistance of stably transfected cells to staurosporine treatment

Bar charts showing viability **(A & B)** and cytotoxicity **(C & D)** of SH-SY5Y cells after 24 h exposure to a range of STS concentrations. The mean values (+/- standard error of the mean) from at least five independent experiments are displayed in the bar charts. Differences between SH-SY5Y^{Untr} and each transfected clone were tested for significance ($p < 0.05$) using unpaired, two-sample t-tests. Key: * for $p < 0.05$; ** for $p < 0.01$; and *** for $p < 0.001$. The first biological replicate for clones 2E3 and 1G3 was performed separately to the first replicate for clones 1B5 and 1F3. Therefore, the charts had to be split up to accommodate this data.

The largest difference between PrP^{C}-transfected and untransfected cells was observed following treatment of clone 1G3 with 50 nM STS (71 % viability vs 42 % for SH-SY5Y^{Untr}). In a similar manner to the PQ treatments, clones 2E3 and 1B5 as well as SH-SY5Y^{Untr} were all comparable in terms of their viability in response to STS. To confirm these results, measurements of cytotoxicity were again obtained by LDH assay. Since cell viability was ~0 % for all clones and SH-SY5Y^{Untr} following 600 nM STS treatment, this dose was used as the 100 % cytotoxicity control for these experiments. Figure 3.11c & d show the data from six independent experiments, which indicate that percentage cytotoxicity was significantly lower for clone 1G3 than for SH-SY5Y^{Untr} at all STS doses tested. Any reduction in

cytotoxicity was less convincing for clone 1F3, although it was statistically significant at 50 nM ($p = 0.017$) and at 100 nM ($p = 0.030$). Small but statistically significant reductions compared with SH-SY5Y^{Untr} were also observed for clone 2E3 and 1B5 at some doses but not all.

The third toxin that the SH-SY5Y cells were exposed to was tunicamycin (TM), which inhibits protein N-glycosylation within the ER (Sigma-Aldrich, [n.d.]), thereby inducing ER stress. TM was included in these experiments due to a recent finding that PrP^{C} expression is induced by ER stress (Dery et al., 2013), although the importance of PrP^{C} in the response to this form of stress is unclear. I assessed cell viability of the SH-SY5Y cell lines following treatment with TM concentrations of 1-15 µg/ml and, once again, the PrestoBlue reagent was used. The results from four independent experiments showed that clones 1G3 and 1F3 were more viable than SH-YS5Y^{Untr} in response to TM (Figure 3.12a), although these differences were…

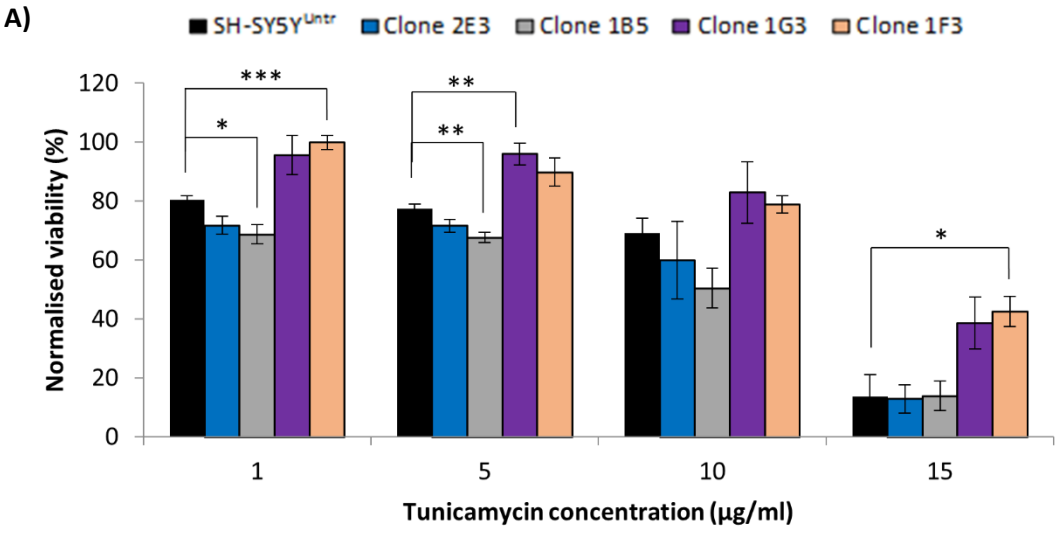

Figure 3.12 – Clone-specific resistance of stably transfected cells to tunicamycin treatment

See following page for legend…

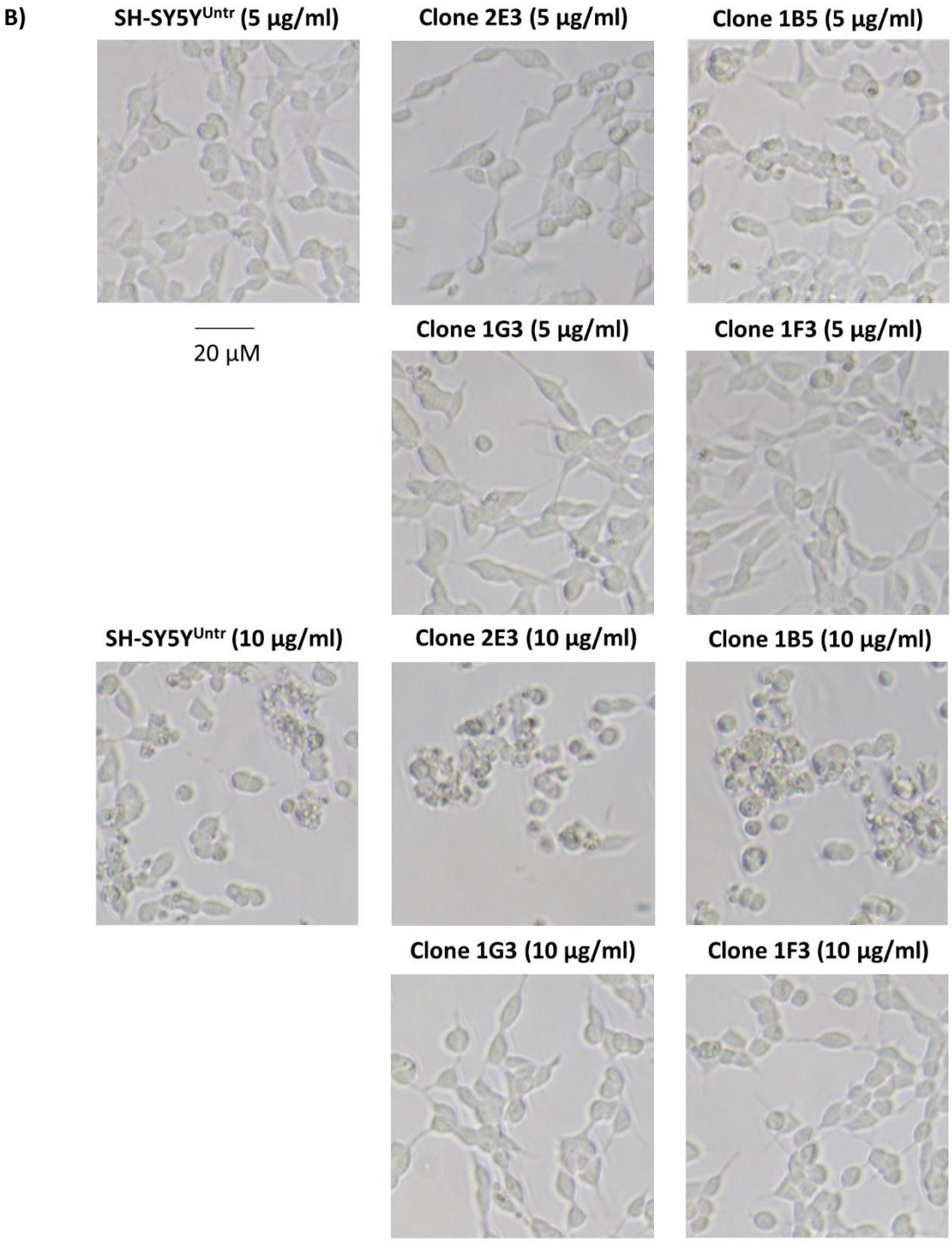

Figure 3.12 – Clone-specific resistance of stably transfected cells to tunicamycin treatment

A) Bar chart showing viability of SH-SY5Y cells after 24 h exposure to a range of TM concentrations. The mean values (+/- standard error of the mean) from four independent experiments are displayed in the bar chart. Differences between SH-SY5Y^{Untr} and each

transfected clone were tested for significance ($p < 0.05$) using unpaired, two-sample t-tests. Key: * for $p < 0.05$; ** for $p < 0.01$; and *** for $p < 0.001$. **B)** Phase contrast images of live SH-SY5Y cells taken using a x10 objective following 24 h exposure to 5 or 10 µg/ml TM. The scale bar shown applies to all panels.

…statistically significant only at the 5 µg/ml concentration for clone 1G3 ($p = 0.009$) and at 1 and 15 µg/ml for clone 1F3 ($p < 0.001$ and $p = 0.037$, respectively). Clone 1B5 was slightly but significantly less viable than SH-SY5Y^{Untr} at 1 and 5 µg/ml ($p = 0.030$ and $p = 0.005$, respectively). For all the cell lines, percentage viability changed little between 1 and 10 µg/ml TM but a 15 µg/ml dose was much more toxic. Interestingly, when considering all four clones together, the mean viability measurements for PrP^{C}-transfected cells were almost the same as for SH-SY5Y^{Untr} over the 1-10 µg/ml dose range.

I was unable to assess TM-mediated cytotoxicity by measuring LDH release, because TM could not be prepared at a high enough concentration to kill all cells for the 100 % cytotoxicity control. Such a concentration would have exposed the cells to so much DMSO that it would have been hard to separate out its effect from that of the toxin. Another option for a 100 % cytotoxicity control was to treat cells with a lysis buffer but this gave unreliable results (data not shown). As a further alternative, I tried to optimise a viability assay based on nuclear staining using the Hoescht 33342 dye. This method allows discrimination of viable and dead cells based on the shape and/or size of their nuclei. Unfortunately, SH-SY5Y cells are prone to clumping, especially when stressed, which meant that individual cells were hard to identify, thereby affecting the accuracy of the analysis. Instead, I decided to capture and analyse phase contrast images of the cells after they had been cultured in the presence of TM for 24 hours. It was difficult to discern visual signs of toxicity after treatment with 1 or 5 µg/ml TM (Figure 3.12b shows the images for 5 µg/ml TM). This is in spite of the reduction in viability at this dose for some of the cell lines (Figure 3.12a). However, when treated with 10 µg/ml TM, clone 2E3 and 1B5 cultures consisted almost entirely of clumped, floating cells that were presumably

either dead or dying (Figure 3.12b). At the same concentration of TM, there were still some healthy-looking SH-SY5Y^{Untr} that remained attached to the plate, although many had detached, whilst clones 1G3 and 1F3 appeared entirely unaffected. The images for 15 μg/ml TM treatment were very similar to those from 10 μg/ml, except that clone 1F3 cells were also starting to clump and float (data not shown).

Finally, I assessed how the stably transfected clones survived in response to serum deprivation – this activates mitochondria-dependent apoptosis driven by a protein called Bax (Deckwerth et al., 1996) and also mimics the neuronal death in response to trophic factor deprivation that plays a key role in the development of the nervous system. As per the toxin treatments, cells were plated in serum-containing medium and allowed to recover for 16-18 hours. This time though, when the medium was changed to serum-free, the N2 supplement was not included as this would have promoted survival. Again using the PrestoBlue reagent, cell viability was quantified at several time points over a week of serum deprivation. Comparing resorufin fluorescence signals across different time points is not particularly accurate since day-to-day environmental variations can affect fluorescence values when the plate is scanned. Therefore, for each time point, signals were normalised against those obtained from SH-SY5Y^{Untr}. For this reason, viability is not reported as a percentage of the viability at the point of serum depriving. Four independent experiments were performed and Figure 3.13a shows that, in contrast to the toxin treatments, the stably transfected clones were more susceptibility to serum deprivation than SH-SY5Y^{Untr}. Reduced viability compared with SH-SY5Y^{Untr} was statistically significant from day 1 onwards for clone 1G3, from day 2 for clone 1F3 and from day 6 for clones 2E3 and 1B5. Clone 1G3 appeared to be most affected by serum withdrawal – by day 7, the mean resorufin fluorescence signal from wells containing clone 1G3 was only 12 % of that from wells containing SH-SY5Y^{Untr}. As was the case for TM treatment, phase contrast images of the cells were analysed to corroborate the results from the viability assays. Figure 3.13b shows that the toxic effects of serum deprivation were visually evident by day 4 for clone 1G3 – the monolayer was quite sparse and there were many rounded-up, floating cells – and, by day 6, clone 1G3 cells were mainly dead. The other cultures, with the possible exception of clone 1F3,

appeared healthy after 4 days serum deprivation but, by day 6, quite a few floating cells were visible for all the clones, less so for SH-SY5Y^{Untr}. Images taken at day 7 (not shown) were very similar to those from day 6. Overall, these results were highly consistent with the viability data shown in Figure 3.13a.

In conclusion, the only difference between clone 2E3 and SH-SY5Y^{Untr} in terms of their responses to the three toxins was a slight but significant reduction in cytotoxicity following exposure to 100 nM STS for clone 2E3. Apart from significant reductions in cytotoxicity when treated with 75 or 100 nM doses of STS, clone 1B5 was also no more resistant than SH-SY5Y^{Untr}; in fact, the viability of clone 1B5 was significantly lower than SH-SY5Y^{Untr} in response to 500 or 1500 µM PQ and 1 or 5 µg/ml TM. In contrast, clones 1G3 and 1F3 generally displayed enhanced viability and reduced cytotoxicity compared with SH-SY5Y^{Untr} following exposure to the toxins. All four clones were significantly more susceptible to serum deprivation than SH-SY5Y^{Untr} cells and, interestingly, the reductions in viability seemed to be more pronounced for clones 1G3 and 1F3 than for clones 2E3 and 1B5.

A)

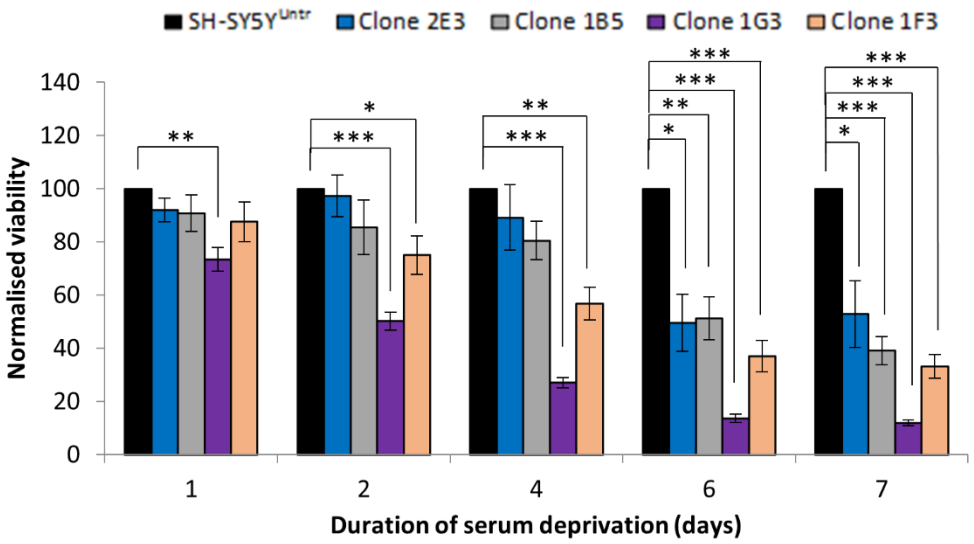

Figure 3.13 – PrP^C transfection increased susceptibility to serum deprivation

See following page for legend…

B)

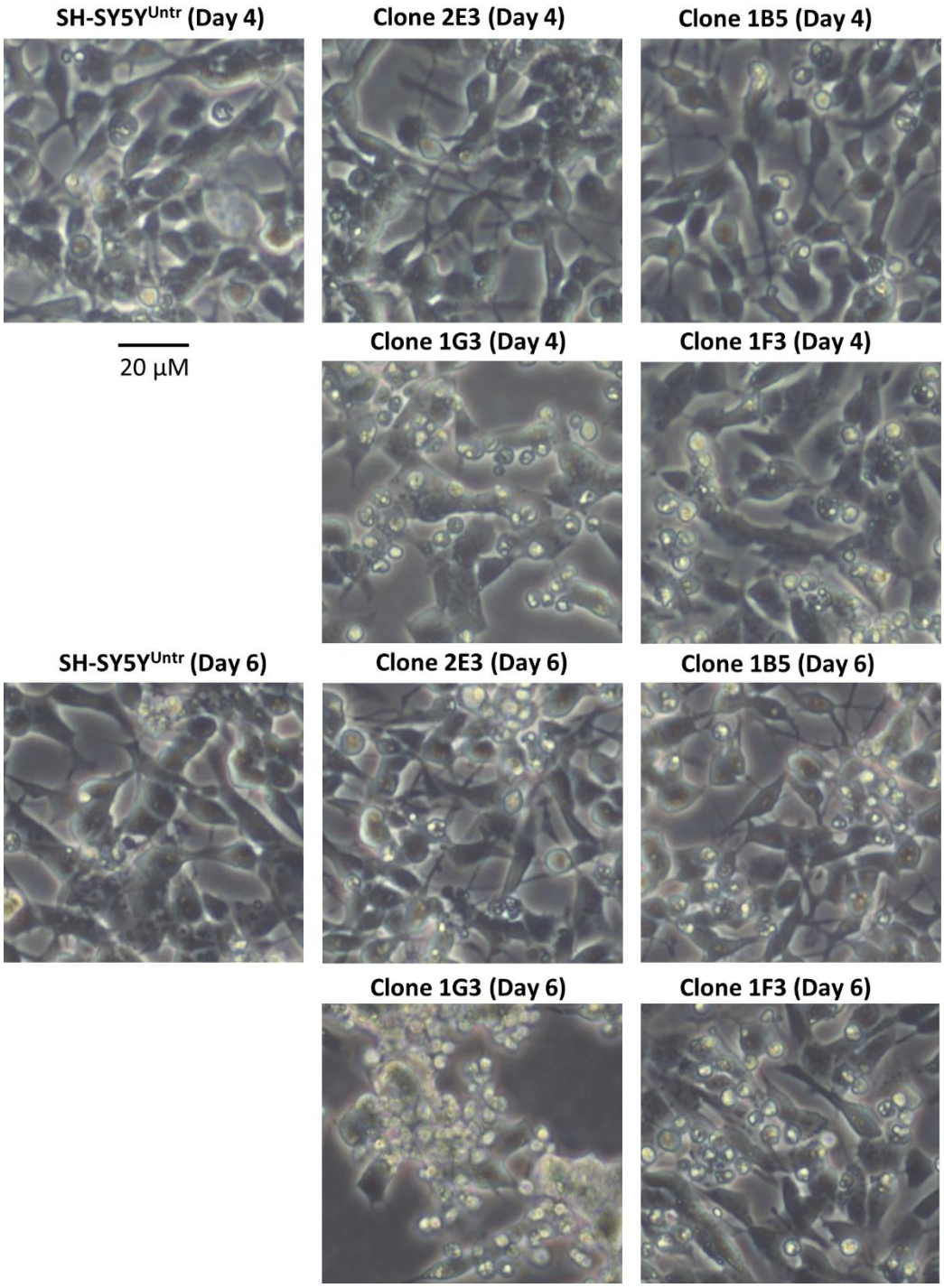

Figure 3.13 – PrP^{C} transfection increased susceptibility to serum deprivation

A) Bar chart showing viability of SH-SY5Y cells in response to serum deprivation. The mean values (+/- standard error of the mean) from five independent experiments are displayed in

the bar chart. Differences between SH-SY5Y^{Untr} and each transfected clone were tested for significance ($p < 0.05$) using unpaired, two-sample t-tests. Key: * for $p < 0.05$; ** for $p < 0.01$; and *** for $p < 0.001$. **B)** Phase contrast images of live SH-SY5Y cells taken using a x10 objective after 4 or 6 days serum deprivation. The scale bar shown applies to all panels.

3.4.1 Discussion

Although a large number of studies have found that PrP^{C} expression protects cells from stress, there is some controversy in the literature relating to this putative function. Consequently, I attempted to clarify whether or not PrP^{C} was stress-protective by exposing the stably transfected clones to several different forms of stress. Two clones, 1G3 and 1F3, displayed improved survival compared with SH-SY5Y^{Untr} in response to treatment with the oxidative toxin PQ, whereas two other clones showed no such improvement; in fact, the viability of clone 1B5 was significantly reduced compared with the control line when treated with 500 or 1500 μM PQ. Interestingly, the magnitude of the enhanced resistance of clones 1G3 and 1F3 to PQ exposure appeared to be greater when measuring cytotoxicity based on LDH release compared to using reduction of resazurin, the active component of the PrestoBlue reagent, as a measure of cell viability. Since resazurin is mainly reduced by NADH produced by mitochondria, this finding might indicate that clones 1G3 and 1F3 could tolerate more mitochondrial dysfunction caused by PQ-induced oxidative stress than SH-SY5Y^{Untr} (and the other clones) before cell death started to occur, at which point LDH would be released.

Stable transfection of PrP^{C} into SH-SY5Y cells had a similar clone-specific effect on resistance to the protein kinase inhibitor STS, which is thought to induce apoptosis through both mitochondria-dependent and mitochondria-independent pathways (Zhang et al., 2004). Again, survival of clones 1G3 and 1F3 was enhanced compared with SH-SY5Y^{Untr}, whilst clones 2E3 and 1B5 were generally as susceptible to STS as the control line, although cytotoxicity measurements were slightly but

significantly lower for these clones at specific doses of STS. Largely the same pattern was observed when exposing the SH-SY5Y cells to the N-glycosylation inhibitor TM – clones 1G3 and 1F3 showed significantly improved viability compared with SH-SY5Y^{Untr}, at least at some doses of TM, whereas no such effect was observed for clones 2E3 and 1B5. Intriguingly, in spite of apparent reductions in viability for some of the cell lines following treatment with 1 μg/ml TM, percentage viability measurements were similar at 5 and 10 μg/ml concentrations. However, increasing the dose to 15 μg/ml TM resulted in greatly reduced viability for all the lines. One interpretation of these results is that there are two phases of TM-mediated toxicity: induction of ER stress at relatively low concentrations of the toxin and cell death at higher doses. This suggests that the reductions in "viability" of SH-SY5Y^{Untr} and clones 2E3 and 1B5 that were observed at 1 and 5 μg/ml doses of TM may not have been due to cell death. Further evidence for this is that dead, floating cells were absent from images of the cell lines that were captured following exposure to 5 μg/ml TM. Therefore, the observed reductions in fluorescence signals in the viability assay at the lower doses of TM may have been caused by an impairment of mitochondrial function resulting from inhibition of protein synthesis, which is part of the unfolded protein response that is triggered by ER stress. Reduced mitochondrial activity and, consequently, a lower level of NADH production would result in less resazurin reduction even if no cell death had occurred. Therefore, the fact that reductions in fluorescence signals in the viability assays following treatment with 1 or 5 μg/ml TM were not observed for clones 1G3 and 1F3 might indicate that these clones were more resistant than SH-SY5Y^{Untr} (and the other clones) to mitochondrial impairment caused by ER stress.

Various studies have identified a protective role for PrP^{C} in the response to oxidative stress (Brown et al., 2002; Anantharam et al., 2008; Bertuchi et al., 2012; Bravard et al., 2015), including when this form of stress was induced by treating cells with PQ (Senator et al., 2004; Dupiereux et al., 2008). However, other reports suggest that PrP^{C} does not protect cells from oxidative damage (Hutter et al., 2003; Steinacker et al., 2010). Again, there is mixed evidence of a beneficial effect of PrP^{C} expression when cells are exposed to STS – some studies find that PrP^{C} expression confers

protection (Lopes et al., 2005; Beraldo et al., 2010; Ostapchenko et al., 2013), others report that it enhances toxicity (Sunyach et al., 2007; Guillot-Sestier et al., 2009). Finally, a recent study found that PrP^C expression appears to be induced under ER stress, whilst knockdown of PrP^C levels resulted in increased death in response to toxins that induce ER stress, such as TM (Dery et al., 2013). Once again though, other published data suggests that PrP^C expression is not associated with protection from ER stress (Roucou et al., 2005; Anantharam et al., 2008). Taken together, the results presented in this chapter partially support a protective role for PrP^C in the cellular responses to these forms of stress, although the clone-specific nature of this putative stress-protection requires further investigation, especially since PrP^C expression levels and subcellular localisation patterns were similar among the clones. One possible explanation for the variability in stress responses among the clones is that small differences in the levels and/or localisation patterns of PrP^C expression were present but were not detected in the characterisation experiments that were reported on in section 3.3. However, it seems unlikely that small differences in PrP^C expression would cause any great variability in stress responses given that PrP^C levels in all four clones were higher than the overall expression level in mouse forebrain. A second possibility is that PrP^C expression was initially higher in clones 1G3 and 1F3 than in the other clones, as was suggested by the results of a single western blot experiment that was carried out prior to preparing frozen stocks of each clone (Figure 3.4). Later, PrP^C expression may have normalised to a stable level that was relatively consistent among the clones. If this were the case then it is conceivable that PrP^C expression in clones 1G3 and 1F3 initially exceeded some kind of threshold that resulted in a permanent change to the cells i.e. a change that persisted even after a subsequent reduction in PrP^C expression. The lack of stress-resistance observed for clones 2E3 and 1B5 could be because the PrP^C expression levels of these clones never reached this hypothetical threshold. Thirdly, stable transfection requires integration of the expression vector into the host cell genome, and insertion within a gene or regulatory region can result in phenotypic changes that are independent of expression of the transgene. However, to explain the variability in stress responses, disruptive insertion events would have needed to have occurred in two of the four clones, which seems highly unlikely. A related possibility

is that the process of isolating clones was responsible for the differences between them. This is because in addition to the neuroblast-like cells with their short, neurite-like processes, SH-SY5Y cultures reportedly contain some cells that are known as "S-type" due to their greater substrate adherence (Encinas et al., 2000). Since the clones were theoretically derived from single cells, it may be that clones 2E3 and 1B5 originated from N-type cells, whilst clones 2E3 and 1B5 were from S-type cells – this would be consistent with morphologies of the clones. However, I did not observe these two distinct phenotypes in the SH-SY5Y cultures before transfection; all the cells appeared to fit the "N-type" description.

In addition to the three toxins, the SH-SY5Y cells were also subjected to serum deprivation, which reportedly induces mitochondria-dependent apoptosis (Deckwerth et al., 1996). In contrast to the results obtained with the toxins, all four stably transfected clones displayed significantly poorer viability in response to serum withdrawal than SH-SY5Y^{Untr}. Although these data seemingly contradict an extensive body of research suggesting that PrP^{C} expression is protective against serum deprivation (Bounhar et al., 2001; Kim et al., 2004; Roucou et al., 2005; Krebs et al., 2007; Wu et al., 2008), the results from several of these studies (Kuwahara et al., 1999; Kim et al., 2004; Wu et al., 2008) are questionable due to the expression of doppel by the hippocampal neuronal cell line used in the experiments. PrP^{C} appears to be able to interact with doppel to suppress its reported neurotoxic properties (Moore et al., 1999; Sakudo et al., 2005; Qin et al., 2006). Therefore, the stress-protective effect of PrP^{C} expression in the hippocampal cell line may have been due to this interaction, which is of limited physiological relevance considering that doppel is not normally expressed in neuronal cells (GeneAtlas U133A dataset (Su et al., 2004) accessed through BioGPS (Wu et al., 2016)).

The results in this chapter provide good evidence that PrP^{C} expression was responsible, either directly or indirectly, for increasing SH-SY5Y cell death in response to serum deprivation. However, the clone-specific nature of the altered responses to toxin treatment meant that some artefact of the transfection and/or clone isolation process could have caused the enhanced resistance of clones 1G3 and 1F3.

This issue was addressed by transiently knocking down PrP^C expression in the stably transfected clones – partial rescue of the increased resistance to toxin treatment of clones 1G3 and 1F3 would support the involvement of PrP^C in the altered stress responses displayed by these clones. Results from these experiments are reported in the following chapter, as are data from proteomic analyses of the molecular changes caused by stable transfection of PrP^C into SH-SY5Y cells. The dual aims of these proteomic experiments were to identify processes regulated by PrP^C and to determine why the clones differed in their responses to stress. These differences among the clones were further probed by comparing the proteomic changes that were induced by STS treatment in SH-$SY5Y^{Untr}$ and clone 2E3 with those identified in clone 1G3.

Chapter 4: Investigating the reasons for the variable stress responses of the stably transfected clones

4.1 Assessing whether PrP^C expression was responsible for the enhanced resistance to toxin treatment of clones 1G3 and 1F3

The previous chapter covered the production and characterisation of stably transfected, PrP^C-expressing SH-SY5Y clones. When serum was withdrawn from the culture medium, all four clones were more susceptible to apoptosis than $SH\text{-}SY5Y^{Untr}$, providing good evidence that PrP^C expression enhances the sensitivity of SH-SY5Y cells to serum deprivation. In contrast, following exposure to three chemical toxins that induce different forms of cellular stress, two of four clones (1G3 and 1F3) displayed enhanced survival compared with $SH\text{-}SY5Y^{Untr}$, whilst the other two clones (2E3 and 1B5) generally did not. Clones 1G3 and 1F3 were also morphologically different from the others. The clone-specific nature of these changes in the absence of any detectable variations among the clones in the levels and localisation patterns of PrP^C expression cast doubt upon whether the resistance to toxin treatment of clones 1G3 and 1F3 was a result of PrP^C expression or simply an artefact of the transfection and/or clone isolation process. To test this, I examined the effect of PrP^C knockdown on the resistance to stress of the stably transfected clones. For practical reasons, these experiments and most others covered in this chapter were restricted to just two stably transfected clones: one clone that exhibited the morphological changes and enhanced resistance to toxin treatment (1G3) and one that did not (2E3).

After reviewing several options for knocking down protein expression, I decided to use a small interfering RNA (siRNA). This method is arguably the easiest and the quickest to optimise, although use of a suitable negative control siRNA is essential to control for confounding effects, including off-target activity of the siRNA and potential activation of the anti-viral interferon response[5]. Previous studies had shown that SH-SY5Y cells could be transfected successfully with siRNAs using cationic

[5] Since the siRNA duplexes used in these experiments were less than 30 bp in length, the interferon response should not have been activated (Kleinschmidt et al., 1968 cited by Whitehead et al., 2011).

lipid reagents (Van Kolen et al., 2013; Zhang et al., 2013). Additionally, PrP^C expression had previously been knocked down using this method in a similar mouse neuroblastoma cell line (Daude et al., 2003; Parkin et al., 2007).

4.1.1 Optimisation of PrP^C knockdown by RNA interference

Before attempting to knock down PrP^C expression in the stably transfected SH-SY5Y clones, the efficiency of siRNA transfection needed to be optimised. I chose a reverse transfection method i.e. wells were treated with the siRNA-transfection reagent complexes and the cell suspensions (in this case clone 1G3) were added on top. 16-18 hours after reverse transfection with a positive control siRNA labelled with a fluorescent dye (cyanine dye 3), the medium was exchanged for serum-free medium containing the N-2 supplement in order to match the format of the toxin treatment assays. Widefield fluorescence images were captured immediately and 24 hours later to assess transfection efficiency. Figure 4.1 demonstrates that, ~40 hours post transfection, most cells contained the fluorescent siRNA molecules. The data from ~16 hours post transfection was very similar (not shown). After this successful initial experiment, two PrP-specific siRNAs were tested for their ability to knock down PrP^C expression. SiRNA s72188 targets *PRNP* mRNA codons 152-159 while s72190 targets 137-143. Since purchasing these siRNAs, s72188 has been shown to knock down PrP^C successfully in an epithelial cell line (Mehrabian et al., 2015). I tested 2.5, 5 and 10 nM doses of the siRNAs using the same method described above, except that PrP^C expression levels were analysed by western blotting at the two time points. Neither siRNA was effective at knocking down PrP^C expression at the early time point (data not shown). However, by ~40 hours post transfection, PrP^C levels were greatly reduced (Figure 4.2a & b). At all concentrations, s72188 appeared to be more effective than s72190 at knocking down PrP^C expression and transfection with 5 or 10 nM s72188 reduced PrP^C levels by similar amounts (Figure 4.2a & b). PrestoBlue viability assays also showed that transfection with either siRNA at 2.5 or 5 nM concentrations had no detectable effect on cell viability (Figure 4.2c). Transfection with 10 nM s72190 may have reduced viability slightly, although this could have been an artefact since the data were from a single experiment only.

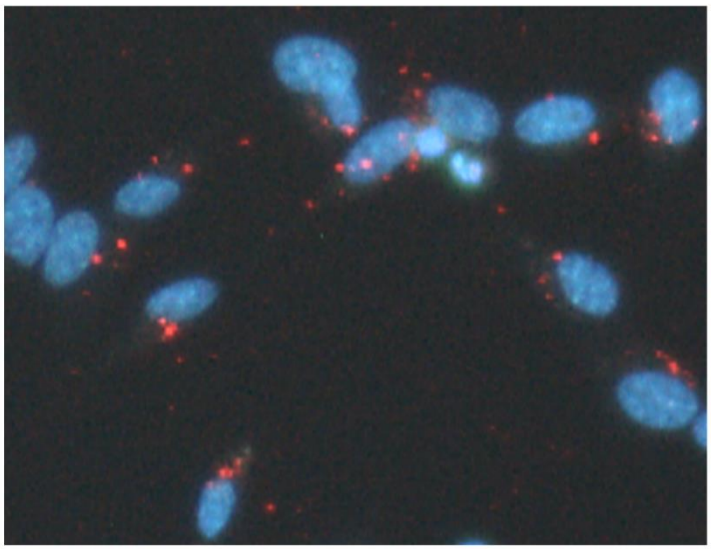

Figure 4.1 – Successful transfection of SH-SY5Y cells with a control siRNA

Widefield fluorescence image of live clone 1G3 cells taken 40 h after transient transfection with cyanine dye 3-labelled positive control siRNA. The image was taken using a x20 objective. Nuclei were stained with DAPI and are shown in blue. Fluorescent siRNA molecules appear red. Red staining was visible in most cells, indicating that they had taken up some siRNA molecules.

For future experiments, I decided to use a 5 nM concentration of siRNA to ensure sufficient PrP^C knockdown, whilst minimising the effects of off-target binding. Oddly, a negative control siRNA reported to have "no significant sequence similarity to mouse, rat, or human gene sequences" (Thermo Fisher Scientific, [n.d.]-b) also seemed to affect PrP^C expression in this initial experiment (Figure 4.2a & b) but no such effect was observed subsequently. Given that PrP^C appeared to be effectively knocked down by siRNA s72188 by ~40 hours post transfection, the plan was to expose the cells to toxins for 24 hours from this point onwards. In order to make the timings work from a practical point of view, the toxin treatments were actually performed ~44 hours after transfecting the cells. Five independent experiments confirmed that siRNA s72188 significantly reduced PrP^C expression at…

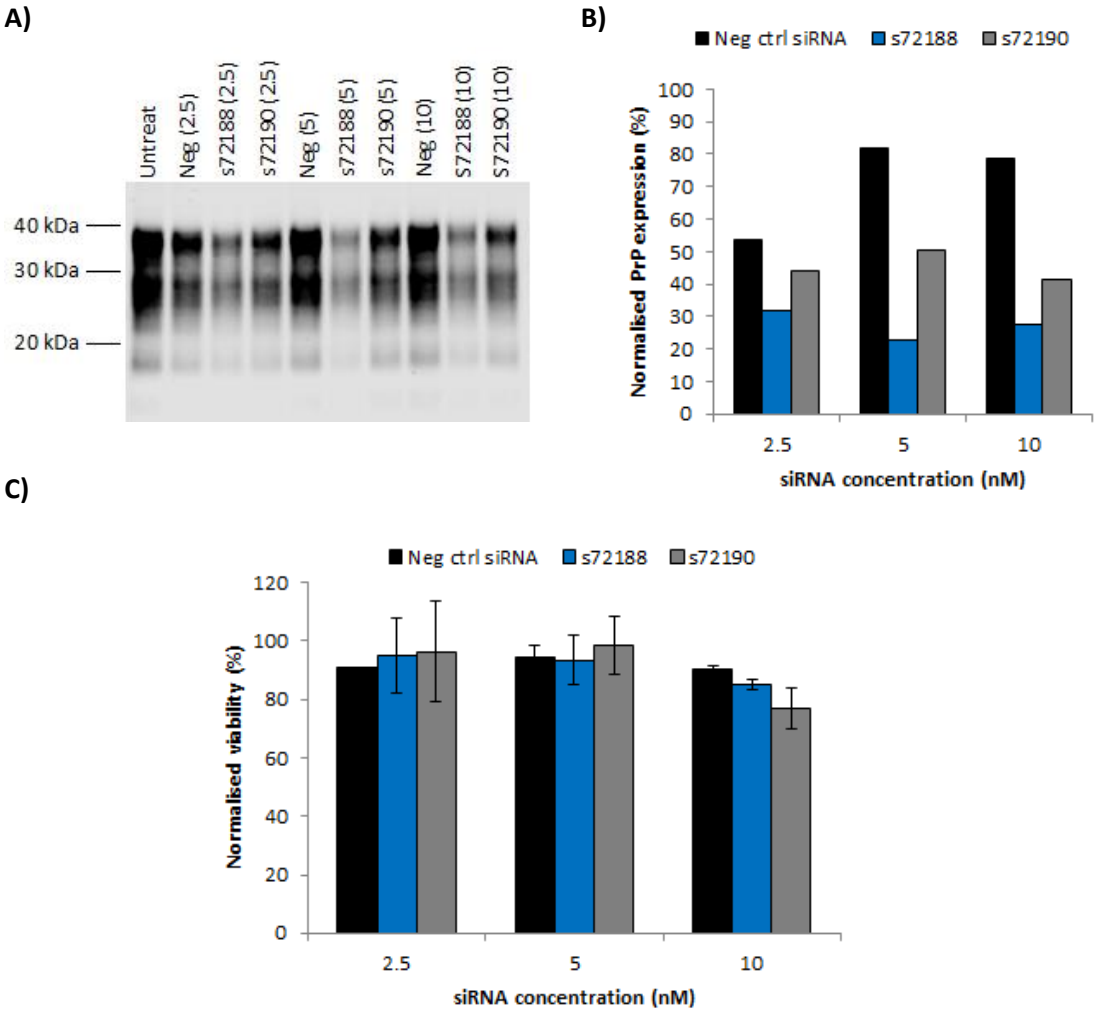

Figure 4.2 – Optimisation of siRNA concentration for transfection

A) Fluorescent western blot image showing PrP^C immunostaining in clone 1F3 lysates prepared 40 h after transient transfection with a negative control siRNA (neg ctrl) or PrP siRNAs s72188 or s72190. PrP^C was detected by use of the BC6 anti-PrP^C primary antibody (McCutcheon et al., 2014). "Untreat" = no siRNA transfection. siRNA concentrations (nM) are given in brackets. **B)** Bar chart summarising PrP^C quantification data from the western blot. After correcting for loading errors, data were normalised to the signal from the cells not transfected with any siRNA. **C)** Bar chart showing viability of clone 1F3 40 h after transient transfection with a range of concentrations of the siRNAs described above. The mean values (+/- standard deviation) from two technical replicates are displayed in the bar chart.

A) Clone 2E3 (44 h)

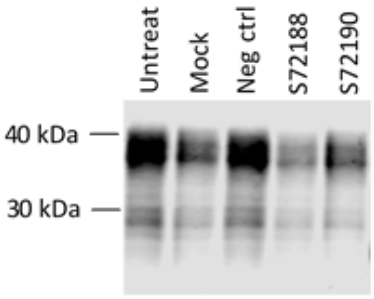

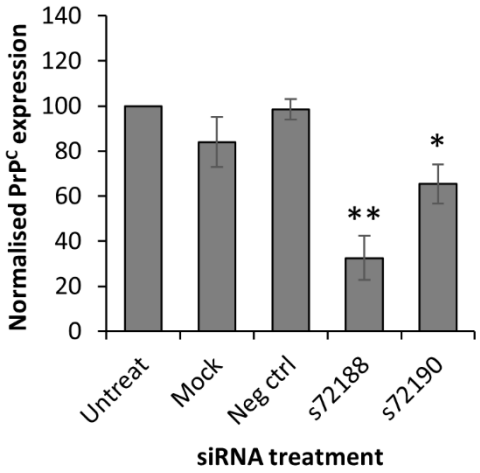

B) Clone 2E3 (68 h)

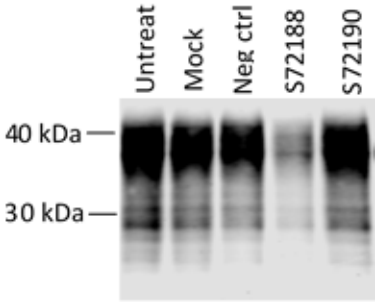

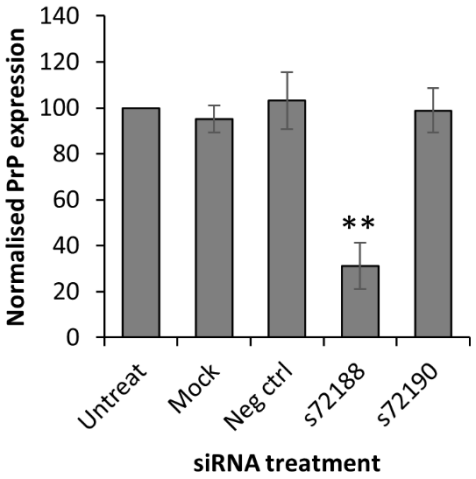

C) Clone 1G3 (44 h)

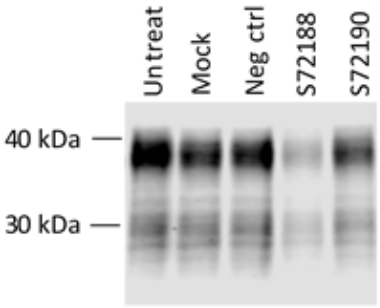

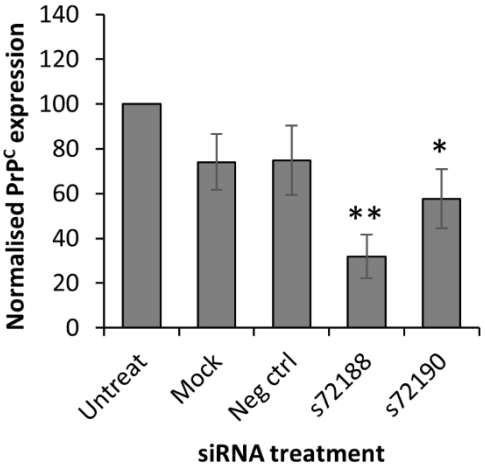

Figure 4.3 – SiRNA s72188 efficiently knocked down PrP^C expression in clones 2E3 and 1G3

See following page for legend…

D) Clone 1G3 (68 h)

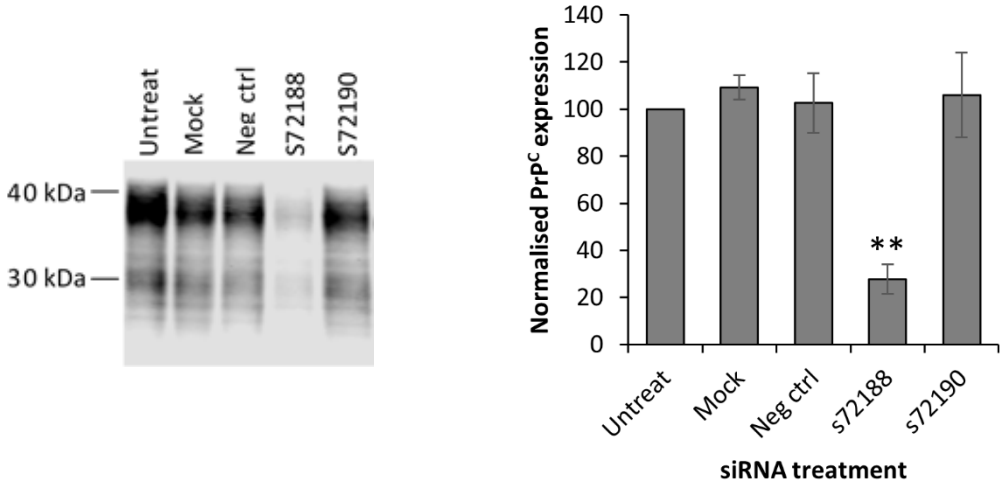

Figure 4.3 – SiRNA s72188 efficiently knocked down PrP^C expression in clones 2E3 and 1G3

A-D) Representative western blot images and bar charts summarising quantification of PrP^C immunostaining from at least four independent experiments. PrP^C was detected by use of the BC6 anti-PrP^C primary antibody (McCutcheon et al., 2014). Data are shown for clones 2E3 and 1G3 at both 44 and 68 h after mock-transfection or transient transfection with a negative control siRNA (neg ctrl) or PrP siRNAs s72188 or s72190. For each membrane, after correction for loading errors, data were normalised to the signal from the cells not transfected with any siRNA ("untreat"). The mean normalised expression values (+/- standard error of the mean) are displayed in the bar charts. Differences between "untreated" and mock- or siRNA-transfected cells were tested for significance ($p< 0.05$) using one-sample t-tests. Key: * for $p < 0.05$; ** for $p < 0.01$.

…around 44 and 68 hours post transfection in clones 2E3 and 1G3 compared with controls (Figure 4.3a-d). The degree of knockdown was 67-72 %, which is comparable to other studies that employed siRNA-mediated knockdown of PrP^C (Parkin et al., 2007; Silber et al., 2014). Furthermore, PrP^C expression was not significantly altered in my experiments by mock transfection or transfection with the negative control siRNA. SiRNA s72190 significantly reduced PrP^C expression by clone 2E3 at the 44 hour time point but the expression level had returned to normal

by the later time point. Therefore, I chose siRNA s72188 for use in future experiments.

4.1.2 Lack of effect of PrP^C knockdown on the resistance to stress of the stably transfected clones

Having optimised knockdown of PrP^C expression using siRNA s72188, I assessed whether this would affect the resistance of clone 1G3 to PQ treatment. Clone 2E3 and SH-SY5Y^{Untr} were also included in the experiments. Cells were reverse transfected as described previously and, 16 hours later, the medium was exchanged for serum-free medium containing the N-2 supplement. Around 44 hours post transfection, cells were treated with 1000 μM PQ – this dose was chosen because it had resulted in the largest differences between cell lines in the earlier experiments in terms of viability and cytotoxicity measurements (Figure 3.10). Following a 24-hour exposure to the toxin, PrestoBlue viability and LDH cytotoxicity assays were performed. The results of three independent experiments showed that, when not transfected with siRNAs, SH-SY5Y^{Untr} and clone 2E3 cultures had similar levels of viability (36 and 35 %, respectively), as expected, whereas viability of clone 1G3 was maintained around 85 % (Figure 4.4a). Similarly, percentage cytotoxicity for clone 1G3 was much lower than for the other cell lines (Figure 4.4b). However, for all the cell lines, there were no significant differences in viability or cytotoxicity following transfection with the negative control siRNA compared with the PrP siRNA. Indeed, the non-significant trend towards increased viability of clone 1G3 following transfection with the PrP siRNA was in the opposite direction to what would have been expected if PrP^C expression had been responsible for the increased resistance to PQ treatment of that clone.

The effect of PrP^C knockdown on cell survival in response to STS exposure was investigated using the same assay format as per treatment with PQ. Cells were treated with 50 nM STS since this was the concentration that had produced the greatest differences in survival among the cell lines (Figure 3.10). Again, three independent experiments were performed. In contrast to the data shown in…

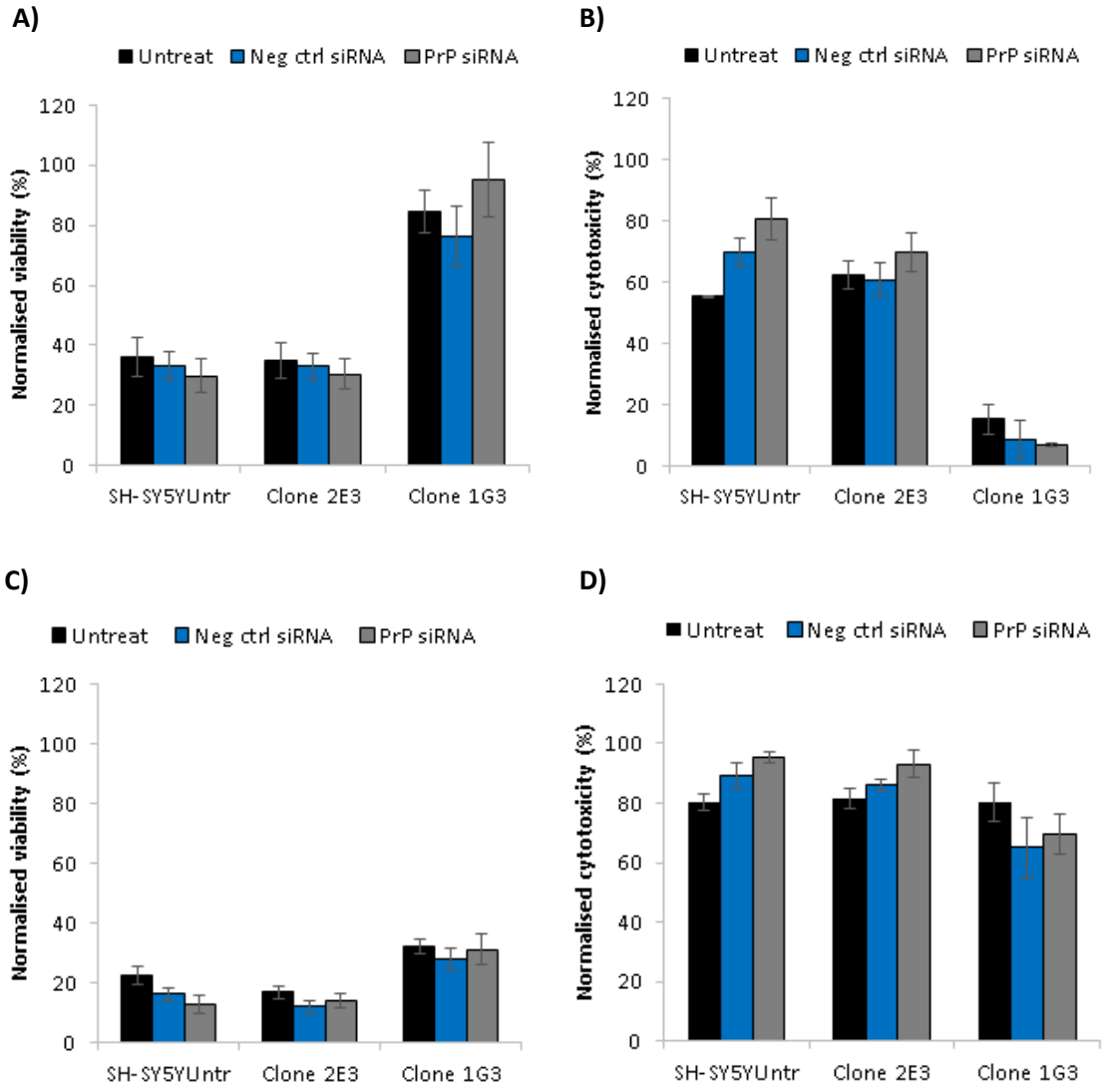

Figure 4.4 – Knockdown of PrP^C expression did not rescue the enhanced survival of clone 1G3 in response to paraquat or staurosporine treatment

Bar charts showing viability **(A & C)** and cytotoxicity **(B & D)** values for SH-SY5Y cultures after 24 h exposure to 1000 µM PQ **(A & B)** or 50 nM STS **(C & D)**. 44 h before PQ or STS treatment, cells had been transiently transfected with negative control siRNA or PrP siRNA (s72188) or had not been transfected with any siRNA ("untreat"). The mean normalised values (+/- standard error of the mean) from three independent experiments are displayed in the bar charts. For each cell type, differences in viability or cytotoxicity between negative control- and PrP siRNA-transfected cells were tested for significance ($p < 0.05$) using unpaired, two-sample t-tests. No comparisons met the significance threshold.

...Chapter 3, when not transfected with either siRNA, viability and cytotoxicity measurements from clone 1G3 cultures were not greatly different from cultures the other cell lines (Figure 4.4c & d). The poorer survival of clone 1G3 in these experiments could have been due to the extended period spent in serum-free medium compared with the previous experiments, since clone 1G3 was particularly sensitive to serum deprivation (Figure 3.13). However, the survival-promoting N-2 supplement present in the serum-free medium should have prevented any cell death resulting from serum deprivation. As was the case for PQ treatment, transfection with the PrP siRNA did not alter viability or cytotoxicity compared with negative control siRNA transfection for any of the cell lines, although the fact that clone 1G3 did not exhibit any enhanced resistance to STS treatment in these particular experiments means that any effect of the PrP siRNA might have been difficult to detect.

Taken together, the above results suggest that PrP^{C} expression was not directly responsible for the enhanced resistance to treatment with PQ or STS that was displayed by clones 1G3 and 1F3 in comparison with SH-SY5Y^{Untr}. This lack of PrP^{C}-mediated protection from the oxidative damage induced by PQ is in contrast with a number of previous studies that report a protective role for PrP^{C} against oxidative stress (Brown et al., 2002; Senator et al., 2004; Anantharam et al., 2008; Dupiereux et al., 2008; Bertuchi et al., 2012; Bravard et al., 2015). Having said this, potential mechanisms put forward to explain this putative protective effect include modulation of antioxidant enzyme activity (Brown et al., 1997b; Miele et al., 2002; Rachidi et al., 2003; Sakudo et al., 2003; Paterson et al., 2008) and direct enhancement of DNA repair processes by PrP^{C} (Bravard et al., 2015), both of which have been questioned by other studies (Hutter et al., 2003; Zanetti et al., 2014; Nuvolone et al., 2016). The reports of how PrP^{C} expression affects the cellular response to STS exposure are quite mixed: it has been suggested that PrP^{C} expression is protective against STS-induced apoptosis (Lopes et al., 2005; Beraldo et al., 2010; Ostapchenko et al., 2013) and yet other studies have found that it enhances vulnerability to the toxin (Sunyach et al., 2007; Guillot-Sestier et al., 2009). My results seem to fit between these two opposing sides, since they suggest no positive

or negative effect of PrP^C expression on susceptibility to the toxicity resulting from STS treatment.

One caveat associated with these knockdown experiments is that reducing PrP^C levels by ~70 % for a short period may not have been sufficient to reverse the effects of stable transfection, especially given that ~30 % of the normal PrP^C expression level of the clones is roughly equivalent to the overall PrP^C expression level in mouse forebrain (based on data shown in Figure 3.5). Therefore, whilst the enhanced resistance to toxin treatment of clones 1G3 and 1F3 may have been the result of an artefact of the transfection and/or clone isolation process, it cannot be ruled out that PrP^C was involved in some way. For example, western blot analysis of PrP^C expression by the clones suggested that clones 1G3 and 1F3 might initially have expressed higher levels of the protein than clones 2E3 and 1B5 (see Figure 3.4). This could have resulted in changes to the phenotypes of clones 1G3 and 1F3 that did not occur in the other clones and were not reversible by knocking down PrP^C expression.

Data presented in Chapter 3 shows that clones 1G3 and 1F3 were more resistant to TM than SH-SY5Y^{Untr}, as was the case for the other toxins. However, mainly due to time constraints, no experiments were performed to assess the effects of PrP^C knockdown on susceptibility to TM treatment. The other reason was that evidence from the initial experiments of a protective role for PrP^C against TM exposure was less convincing than for PQ and STS – when considering all four clones together, the mean viability measurements for the PrP^C-transfected cells were almost the same as for SH-SY5Y^{Untr} at most of the TM doses. However, experiments were carried out to assess whether knocking down PrP^C expression affected the responses of the SH-SY5Y cell lines to serum deprivation. The method consisted of reverse transfecting the cells with the siRNAs and serum depriving 72 hours later to ensure that PrP^C levels had reduced sufficiently by the time of inducing stress. Viability measurements were subsequently made at 2 and 4 days post serum deprivation. Unexpectedly, extremely poor viability was observed for all the cell lines – large numbers of dead, floating cells were present by day 4 even in the wells containing

SH-SY5Y^{Untr} (data not shown), which contrasts with the healthy appearance of the untransfected cultures at this time point in the initial experiments (Figure 3.13b). The consequence of the enhanced toxicity of serum deprivation in the experiments incorporating PrP^{C} knockdown was that viability of clone 1G3 was so low at the point of measurement that the results were not reliable. Unfortunately, I did not have time to solve these issues to enable the acquisition of meaningful data. Nevertheless, the original data reported in Chapter 3 provides good evidence that PrP^{C} expression was responsible for increasing the sensitivity of SH-SY5Y cells to serum deprivation; this is because, in spite of some variability among the stably transfected clones, all four clones displayed significantly reduced viability compared with SH-SY5Y^{Untr}. This finding contradicts several studies that found that PrP^{C} expression protected cells from serum withdrawal (Bounhar et al., 2001; Kim et al., 2004; Roucou et al., 2005; Krebs et al., 2007; Wu et al., 2008) but, as discussed in the previous chapter, there are issues surrounding the reliability of several of those studies (Kuwahara et al., 1999; Kim et al., 2004; Wu et al., 2008).

The results reported in this section suggest that the clone-specific increase in resistance to toxin treatment that resulted from PrP^{C} transfection may have been independent of PrP^{C} expression. However, there was still no explanation of what might have been responsible for the variability in stress responses among the clones. Global proteomic analyses of the cells were carried out in an attempt to answer this question and others.

4.2 Proteomic changes in stably transfected clones 2E3 and 1G3 compared with untransfected cells

The results described in the previous section suggested that PrP^C expression may not have been directly responsible for the enhanced resistance to toxin treatment of clones 1G3 and 1F3 compared with SH-SY5Y^{Untr}. Consequently, proteomic analyses of the SH-SY5Y cells were carried out with the dual aims of identifying processes regulated by PrP^C (covered in Chapter 5) and to investigate in more detail the reasons for the variability in stress responses among the clones. Proteomic studies enable the expression levels of thousands of proteins to be quantified simultaneously and the focus on proteins gives this approach a distinct advantage over other methods of analysing global gene expression patterns, such as microarrays or RNAseq, which quantify mRNA levels instead; mRNA abundance can often be a poor predictor of protein expression level (Gygi et al., 1999; Schwanhausser et al., 2011) and it is proteins not mRNAs that are the "active agents of the cell" (Steen and Mann, 2004).

At the time of starting our experiments, most published proteomic investigations of PrP^C function had used traditional two-dimensional gel-based protein separation methods (Ramljak et al., 2008; Weiss et al., 2010). Membrane-associated and low-abundance proteins are poorly detected by this approach and there are issues with reproducibility (Abdallah et al., 2012). In contrast, modern "shotgun" proteomic methods, as used here, are faster and offer much improved proteome coverage compared with 2-D gel electrophoresis, although specific proteins isoforms are harder to identify since peptide fragments are detected rather than intact proteins (Steen and Mann, 2004). In our experiments, separate comparisons between SH-SY5Y^{Untr} and clone 2E3 and between SH-SY5Y^{Untr} and clone 1G3 were performed. This format enabled comparison of the proteomic changes present in a clone (1G3) that exhibited the altered morphology and enhanced resistance to toxin treatment with the proteomic changes identified in a clone that did not display these phenotypes (2E3). A triplex experiment to simultaneously compare all three lines was theoretically possible but the required methods had not yet been optimised. For each comparison, two independently prepared sets of lysates were analysed

separately. Following enzymatic digestion of the proteins in the lysates, the resulting peptides from the SH-SY5Y^{Untr} sample were labelled with a "light" dimethyl label and the peptides from the clone 2E3 or clone 1G3 sample were labelled with the "heavy" version. Next, the samples were mixed together and fractionated by liquid chromatography methods. The eluted peptides were subsequently analysed by liquid chromatography-tandem mass spectrometry (LC-MS/MS). The raw spectral data obtained were analysed using computer software to identify peptides and the small mass difference imparted by the label enabled discrimination of which sample the peptides were from and, consequently, the calculation of expression ratios. The peptides were searched against the Uniprot human protein sequence database to determine the proteins present in the original samples. Protein expression ratios were calculated by the ProteinScape 3.1 software by averaging the abundance ratios for all the peptides associated with a particular protein. Percentage coefficients of variation (%CV) for the expression ratios were also calculated. The lists of proteins were then filtered according to several criteria to identify those differentially expressed between the samples. Firstly, only proteins identified from more than two quantified unique peptides in both replicate datasets were included to ensure that the expression ratios could be relied upon. Secondly, various fold change thresholds were assessed to judge at what point the "noise" in the data, caused by technical and biological variability, became unacceptable. For the datasets comparing SH-SY5Y^{Untr} with clone 2E3, applying fold change cut-offs of (+/-) 1.2, 1.3 or 1.4 resulted in 138, 59 or 23 differentially-expressed proteins[6], respectively. Of these proteins, ~80 % were differentially expressed in the same direction in both biological replicates for the (+/-) 1.2 or 1.3 cut-offs, whereas this proportion rose to 91 % for a (+/-) 1.4 cut-off (Figure 4.5). These results suggested that, for the less stringent cut-offs, a sizeable proportion of proteins could have been identified as upregulated or downregulated in both biological replicates simply due to technical or biological variability rather…

[6] These figures are underestimates since the initial identification of proteins common to both experimental replicates was carried out using an Excel macro that missed a small number of proteins that should have been included – these were identified manually and later added into the final list.

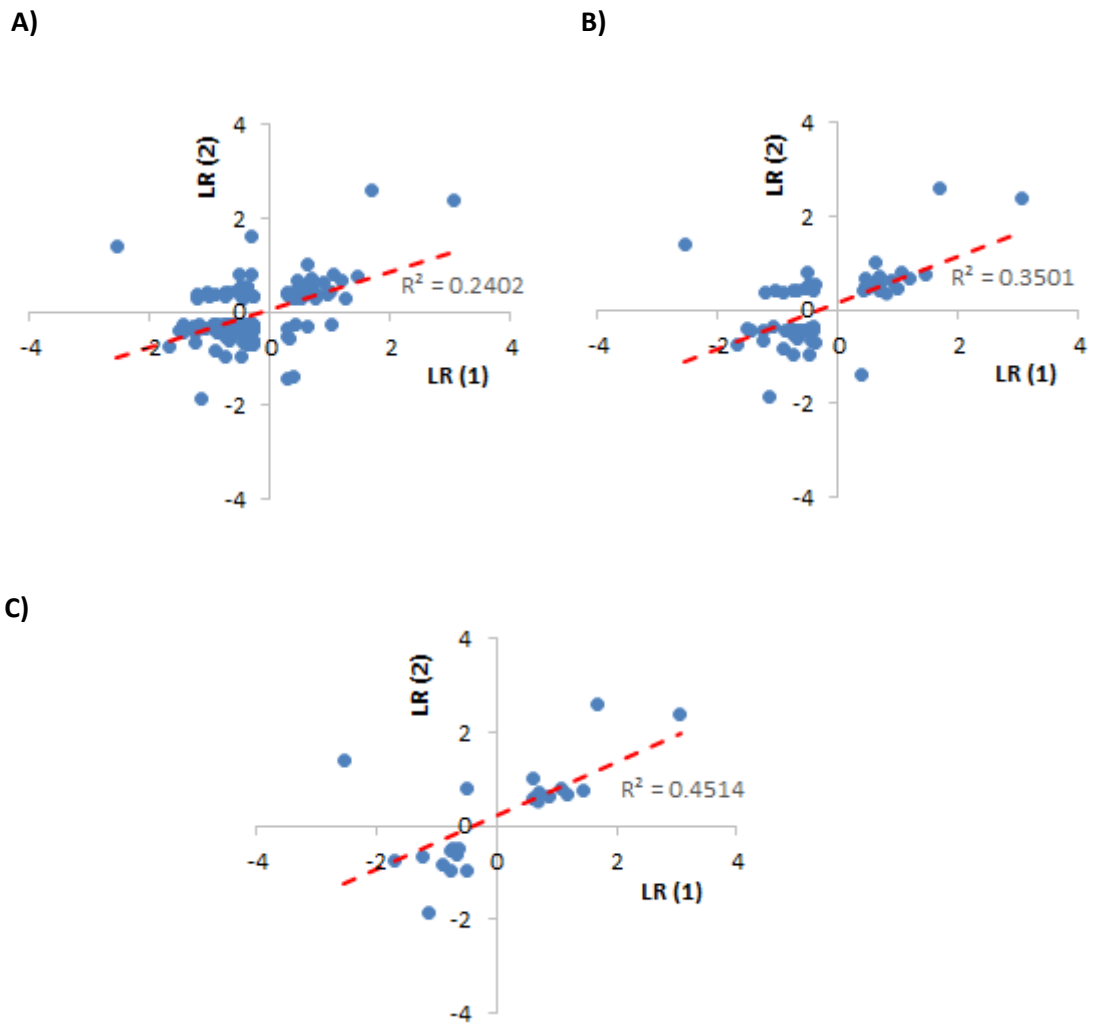

Figure 4.5 – Selection of appropriate fold change cut-off for proteomic data

Scatter plots of protein expression ratios obtained from the two replicate proteomic experiments comparing SH-SY5Y^{Untr} with clone 2E3. Only proteins with expression ratios calculated from more than two unique peptides were included. Fold change cut-offs of (+/-) 1.2 **(A)**, 1.3 **(B)** or 1.4 **(C)** were then applied. Expression ratios were converted to log ratios (LR; base 2) for the plots to enable better visualisation of negative fold changes. If a data point appears in either the top right or bottom left corner squares this indicates that the expression level of that protein was altered in the same direction for both biological replicates. Linear trendlines fitted by Excel are shown on the graphs as are the associated R-squared values.

…than a true, consistent difference in expression. Therefore, the stricter (+/-) 1.4 fold change cut-off was chosen to reduce the number of false positives. The same cut-off was also used for the SH-SY5Y^{Untr} vs clone 1G3 proteomic experiments to make it easier to compare between the analyses. The third filtering step was to check the individual peptide abundance ratios for the few proteins with %CVs greater than 100, since such a high %CV suggested that the expression ratio was not particularly reliable. In the absence of an objective statistical test, I was cautious not to arbitrarily exclude proteins; at the same time, it was important not to falsely identify proteins as differentially expressed if their expression ratios were plainly inaccurate. Consequently, three proteins were removed from the final, filtered list of proteomic differences between SH-SY5Y^{Untr} and clone 2E3 due to outlying peptide abundance ratios skewing the overall expression ratio for the protein[7]. The numbers of proteins remaining after each of the filtering steps are shown in Table 4.1.

After carrying out the aforementioned filtering steps, there were 346 proteins differentially expressed between SH-SY5Y^{Untr} and clone 1G3, consisting of 131 upregulated and 215 downregulated proteins. Only 22 proteins were differentially expressed between SH-SY5Y^{Untr} and clone 2E3, 12 upregulated and 10 downregulated. This disparity may be because clone 2E3 was more similar to SH-SY5Y^{Untr} in terms of its morphology and stress responses than was the case for clone 1G3. All the differentially expressed proteins in clone 2E3 are reported in Table 4.2, whilst Table 4.3 contains a subset of the proteomic changes observed in clone 1G3 (the 12 most upregulated and 12 most downregulated proteins). The full list of 346 differentially expressed proteins is provided in Appendix II. Prior to any subsequent analysis, the proteomic data were validated as described in the following section.

[7] All three proteins excluded were reported to be differentially expressed by < 2 fold and yet, in each case, an expression ratio of > 10 or < 0.1 was reported for one of the peptides. Removal of these clearly anomalous peptides from the quantification resulted in protein expression ratios of close to 1.00, therefore suggesting that these proteins were not differentially expressed.

	Number of identified proteins	
	SH-SY5Y^{Untr} vs clone 2E3	SH-SY5Y^{Untr} vs clone 1G3
Total (expt 1, expt 2)	2349, 2886	3224, 3018
Total (in both expts)	1677*	2438*
# quant. peptides > 2	840*	1203*
Expr. ratio >= 1.4 or <= 0.83	25	346
Final list after error checking	22	346
Final list (upreg., downreg.)	12, 10	131, 215

Table 4.1 – Filtering of proteomic datasets to generate lists of differentially expressed proteins

The table shows the numbers of remaining proteins from the proteomic datasets after cumulatively applying the described filtering criteria – these had to be met for both experimental replicates. "# quant. peptides > 2" means that only proteins with expression ratios calculated from more than two associated unique peptides were included. "error checking" means checking protein expression ratios with %CVs > 100. *these figures are underestimates for the reasons explained in footnote 6.

		Experiment 1			Experiment 2			Combined
Uniprot ID	Protein	Mascot Score	# quant. peptides	%CV	Mascot Score	# quant. peptides	%CV	Mean fold change
O15240	Neurosecretory protein VGF	707	8	60	1007	8	18	+6.79
P80723	Brain acid soluble protein 1	173	4	22	209	3	8	+4.62
P08670	Vimentin	8099	60	67	7223	56	26	+2.20
Q96CN7	Isochorismatase domain-containing protein 1	1535	11	83	1716	12	37	+1.93
P17677	Neuromodulin	745	7	60	674	7	16	+1.79
Q96FC7	Phytanoyl-CoA hydroxylase-interacting protein-like	111	3	20	163	4	24	+1.71
P63104	14-3-3 protein zeta/delta	3478	24	116	2496	16	58	+1.69
O14531	Dihydropyrimidinase-related protein 4	454	6	72	427	6	62	+1.64
Q9BWM7	Sideroflexin-3	462	6	28	480	7	6	+1.52
P68363	Tubulin alpha-1B chain	6267	35	86	4006	31	63	+1.52
Q71U36	Tubulin alpha-1A chain	6004	35	86	3839	32	60	+1.51
P07355	Annexin A2	1819	10	119	2156	19	18	+1.51
P09543	2',3'-cyclic-nucleotide 3'-phosphodiesterase	160	3	34	228	4	185	-2.74

Table 4.2 – List of proteins differentially expressed in clone 2E3 compared with untransfected SH-SY5Y cells

See following page for legend…

		Experiment 1			Experiment 2			Combined
Uniprot ID	Protein	Mascot Score	# quant. peptides	%CV	Mascot Score	# quant. peptides	%CV	Mean fold change
P52306	Rap1 GTPase-GDP dissociation stimulator 1	147	3	339	312	4	56	-2.47
Q9Y263	Phospholipase A-2-activating protein	302	3	29	142	3	8	-2.20
P23921	Ribonucleoside-diphosphate reductase large subunit	931	8	77	334	6	13	-1.89
Q9GZL7	Ribosome biogenesis protein WDR12	370	3	55	335	3	82	-1.83
P08240	Signal recognition particle receptor subunit alpha	305	4	79	260	3	14	-1.56
P38117	Electron transfer flavoprotein subunit beta	481	6	50	256	4	17	-1.55
O75223	Gamma-glutamylcyclotransferase	820	6	86	399	3	12	-1.53
Q92621	Nuclear pore complex protein Nup205	400	4	33	787	8	57	-1.47
Q92823	Neuronal cell adhesion molecule	920	10	77	883	12	33	-1.42

Table 4.2 – List of proteins differentially expressed in clone 2E3 compared with untransfected SH-SY5Y cells

This table shows all the proteins from the SH-SY5Y^{Untr} vs clone 2E3 proteomic experiments that were identified from > 2 quantified unique peptides (# quant. peptides) and met the (+/-) 1.4 fold change cut-off in both replicate datasets. For each protein, the mean expression ratio from the two replicates was calculated and converted to fold change.

		Experiment 1			Experiment 2			Combined
Uniprot ID	Protein	Mascot Score	# quant. peptides	%CV	Mascot Score	# quant. peptides	%CV	Mean fold change
Q96CX2	BTB/POZ domain-containing protein KCTD12	1087	10	33	926	7	58	9.57
P21291	Cysteine and glycine-rich protein 1	1288	9	16	1648	11	29	9.02
A0A075B730	Epiplakin	606	9	33	667	9	124	7.40
P17301	Integrin alpha-2	1180	13	27	1283	8	31	7.40
Q86W92	Liprin-beta-1	662	6	16	950	7	16	4.93
O00151	PDZ and LIM domain protein 1	645	16	32	864	17	38	4.67
P08670	Vimentin	11289	3	8	12934	4	21	4.30
Q13642	Four and a half LIM domains protein 1	2080	8	15	2785	7	16	4.06
P56730	Neurotrypsin	413	68	39	648	74	79	3.91
Q15942	Zyxin	1321	12	8	1779	10	9	3.88
B7Z385	Adenylyl cyclase-associated protein	230	7	10	401	6	16	3.81
P20020	Plasma membrane calcium-transporting ATPase 1	910	11	22	962	13	18	3.77
Q9BPU6	Dihydropyrimidinase-related protein 5	641	4	104	486	5	1196	-7.69
P09172	Dopamine beta-hydroxylase	580	6	27	540	3	34	-6.67

Table 4.3 – Subset of proteins differentially expressed in clone 1G3 compared with untransfected SH-SY5Y cells

See following page for legend…

		Experiment 1			Experiment 2			Combined
Uniprot ID	Protein	Mascot Score	# quant. peptides	%CV	Mascot Score	# quant. peptides	%CV	Mean fold change
P07948	Tyrosine-protein kinase Lyn	490	5	25	492	4	42	-5.41
F8WCN3	Creatine kinase U-type, mitochondrial	331	6	51	239	3	94	-5.00
E7EMV2	Neurofilament medium polypeptide	528	4	25	572	3	58	-4.76
P14854	Cytochrome c oxidase subunit 6B1	442	4	21	598	4	51	-3.57
A6NKG5	Retrotransposon-like protein 1	1057	3	23	898	3	21	-3.45
Q9UGI8	Testin	952	5	21	1058	4	214	-3.28
P35520	Cystathionine beta-synthase	431	6	23	485	6	29	-3.28
H3BRM5	Cytochrome c oxidase subunit 5A, mitochondrial	264	4	10	96	3	5	-3.03
Q9Y617	Phosphoserine aminotransferase	422	7	14	663	7	12	-3.03
P13073	Cytochrome c oxidase subunit 4 isoform 1, mitochondrial	336	15	44	238	9	18	-2.74

Table 4.3 – Subset of proteins differentially expressed in clone 1G3 compared with untransfected SH-SY5Y cells

This table shows all the proteins from the SH-SY5Y^{Untr} vs clone 2E3 proteomic experiments that were identified from > 2 quantified unique peptides (# quant. peptides) and met the (+/-) 1.4 fold change cut-off in both replicate datasets. The 12 most upregulated and 12 most downregulated proteins are shown here and the remaining proteins are listed in **Appendix II**. For each protein, the mean expression ratio from the two replicates was calculated and converted to fold change.

4.2.1 Successful validation of proteomic data by western blotting of cell lysates

The accuracy of the proteomic data described in the previous section was validated by quantitative western blotting for a subset of the targets. To make this process more efficient, I aimed to select targets that were differentially expressed in clones 2E3 *and* 1G3 compared with SH-SY5Y^{Untr} based on the proteomic data – this enabled simultaneous validation of the accuracy of both datasets. Clone 1B5 and 1F3 lysates were also included in these western blotting experiments for completeness. As in previous experiments, cells were seeded into tissue culture plates and lysed 24 hours later. Expression levels of the selected proteins (11 in total) were assessed in at least four independently prepared sets of cell lysates by quantitative western blotting. Figure 4.6 shows a representative western blot for each protein as well as bar charts providing the mean relative expression levels in each clone compared with SH-SY5Y^{Untr}. These data indicate that three of the 11 targets – annexin A2 (Figure 4.6a), neuromodulin (Figure 4.6b) and zyxin (Figure 4.6c) – were expressed at higher levels in all four stably transfected clones compared with SH-SY5Y^{Untr}. Neurosecretory protein VGF (Figure 4.6d) and vimentin (Figure 4.6e) were both significantly upregulated in clones 2E3, 1G3 and 1F3 compared with SH-SY5Y^{Untr} and displayed non-significant trends towards upregulation in clone 1B5 (one-sample t-tests: $p = 0.096$ and $p = 0.058$, respectively). Caldesmon (Figure 4.6f) was significantly more abundant in clones 2E3 and 1F3 than in the control cells and, again, non-significant trends towards upregulation were evident in the other clones (one-sample t-tests: $p = 0.059$ and $p = 0.065$ for clones 1B5 and 1G3, respectively). In general, the magnitudes of the expression changes were greater for clone 1G3 and 1F3 than the other clones, although in the case of neurosecretory protein VGF this trend was reversed. The biological significance of the altered expression levels of these six proteins is explored in Chapter 5. Contrastingly, ribonucleoside-diphosphate reductase large subunit (Figure 4.6g) was significantly downregulated in clones 1B5, 1G3 and 1F3 compared with SH-SY5Y^{Untr} and a non-significant trend towards downregulation was also observed in clone 2E3 (one-sample t-test: $p = 0.077$).

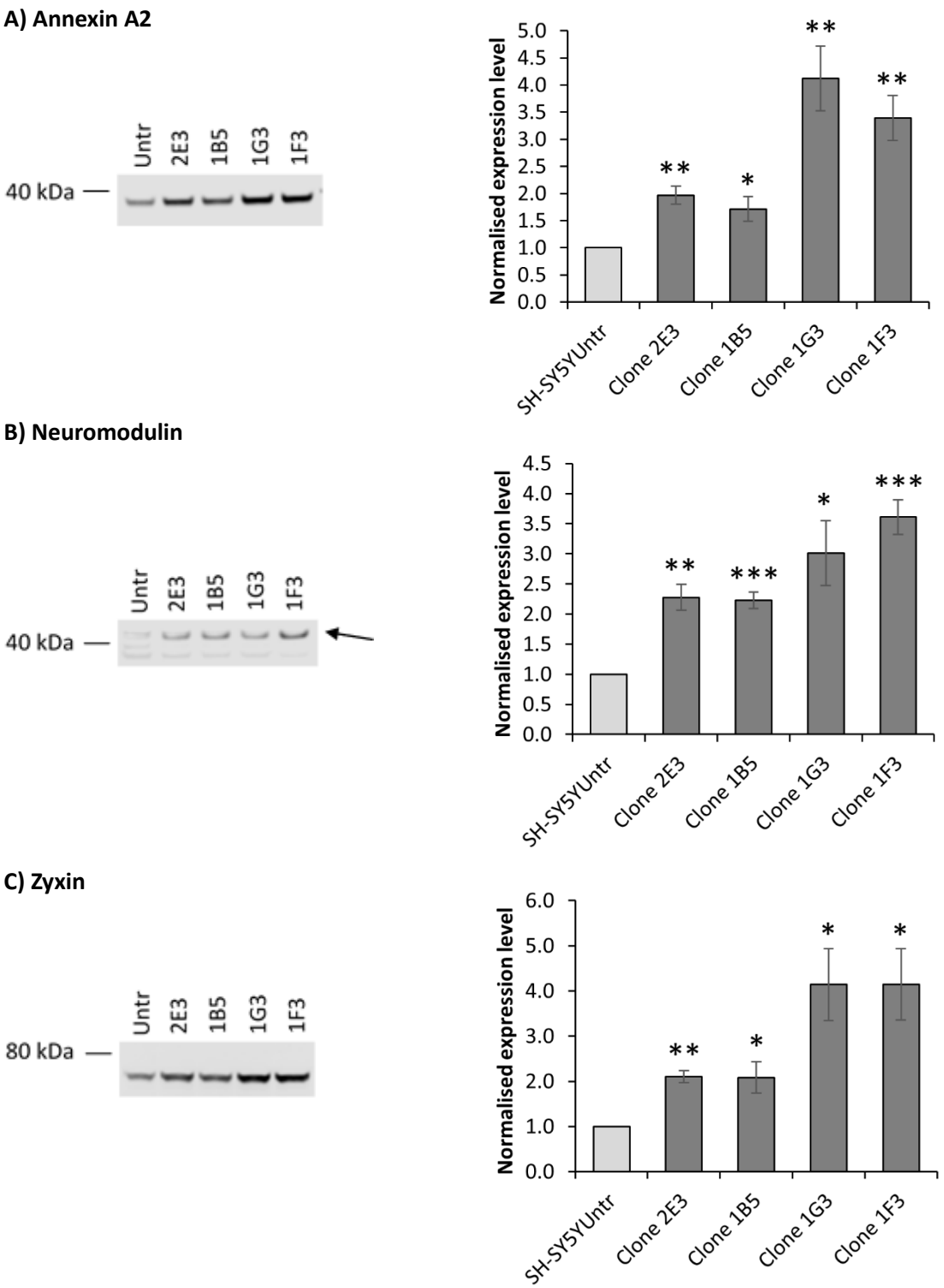

Figure 4.6 – Successful validation of proteomic data by western blotting

See p. 128 for legend…

D) Neurosecretory protein VGF

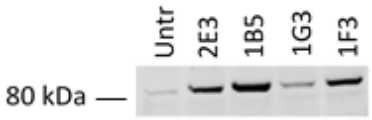

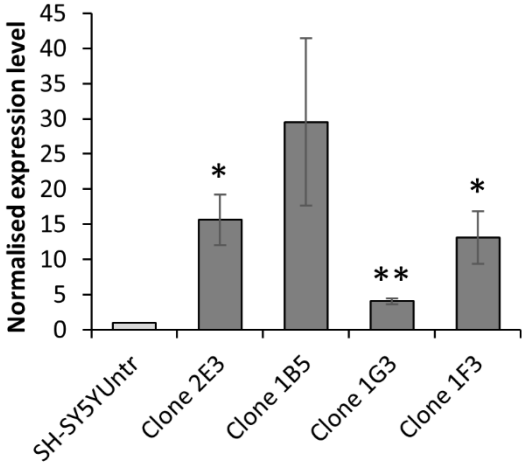

E) Vimentin

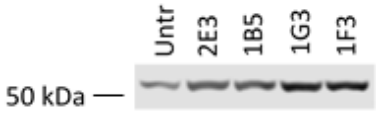

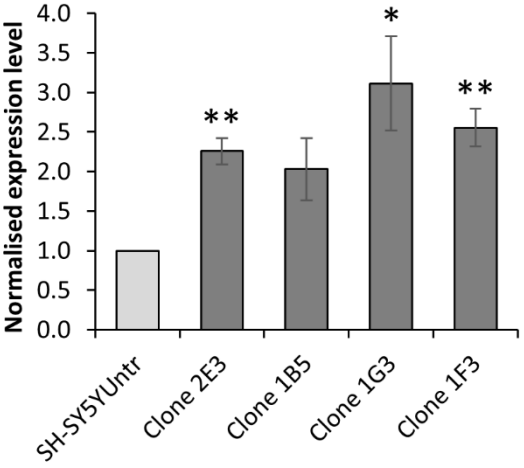

F) Caldesmon

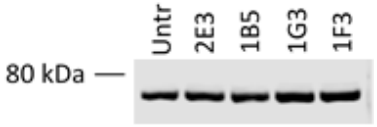

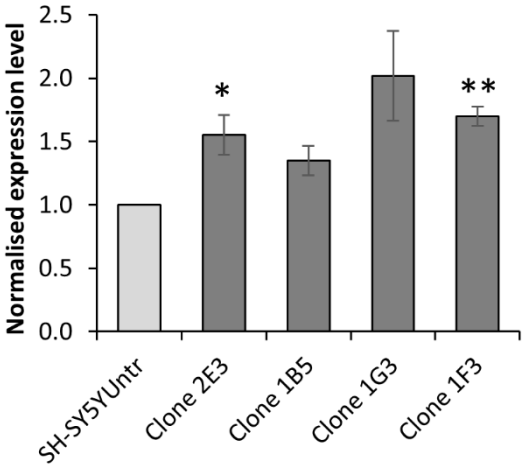

Figure 4.6 – Successful validation of proteomic data by western blotting

See p. 128 for legend…

G) Ribonucleoside-diphosphate reductase large subunit (RRM1)

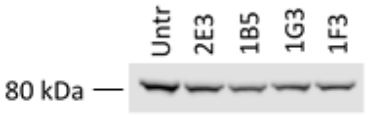

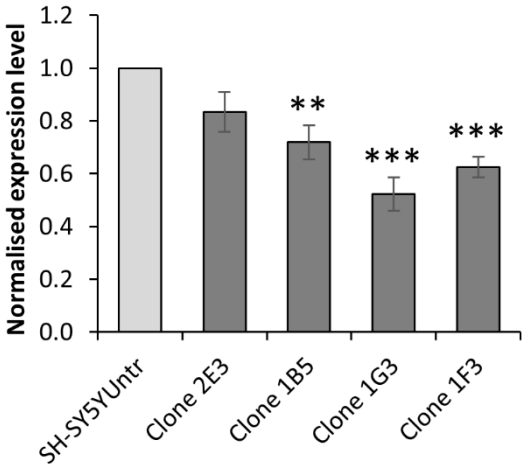

H) E3 ubiquitin-protein ligase BRE1A

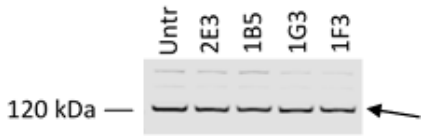

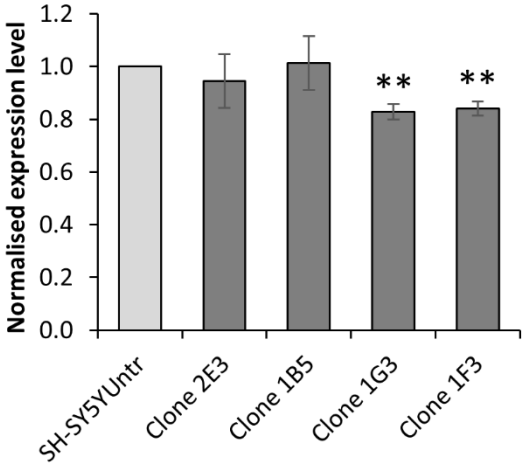

I) Eukaryotic translation initiation factor 1 (eIF1)

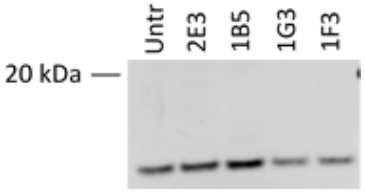

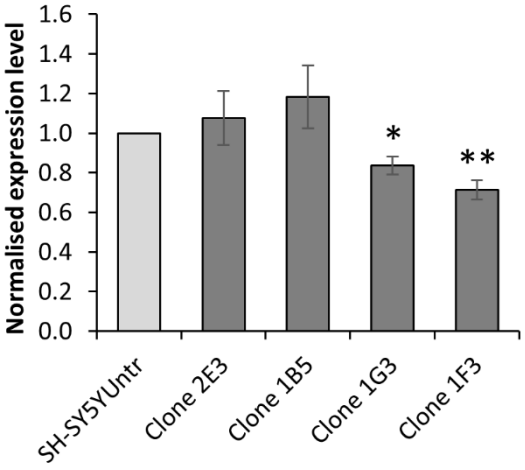

Figure 4.6 – Successful validation of proteomic data by western blotting

See p. 128 for legend…

J) Proliferating cell nuclear antigen (PCNA)

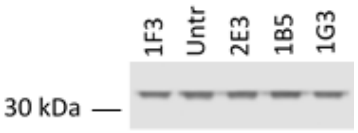

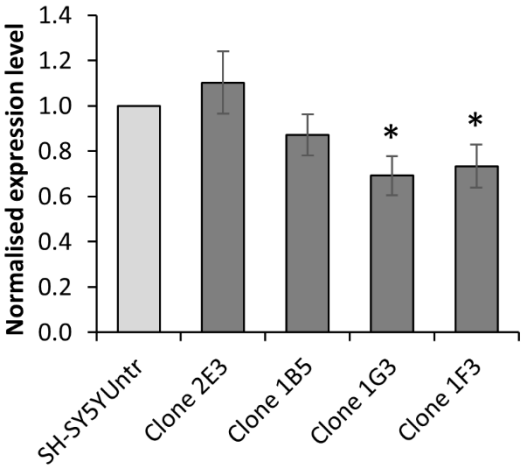

K) Protein kinase C alpha type (PRKCA)

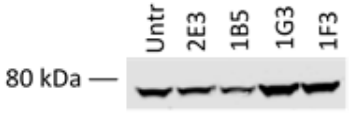

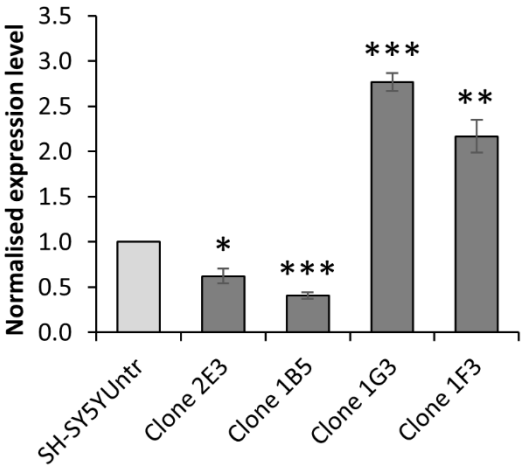

Figure 4.6 – Successful validation of proteomic data by western blotting

A-K) Representative images of western blots for various protein targets and bar charts summarising quantification of immunostaining from at least four independently prepared sets of cell lysates. For each membrane, after correction for loading errors, data were normalised to the signal from the SH-SY5Y^{Untr} lane. The mean normalised expression values (+/- standard error of the mean) are displayed in the bar charts. Expression differences between SH-SY5Y^{Untr} and each clone were tested for significance ($p < 0.05$) using one-sample t-tests. Key: * for $p < 0.05$; ** for $p < 0.01$; and *** for $p < 0.001$. Primary antibodies for all targets except VGF were from Cell Signalling Technology – catalogue numbers were: #8235 **(A)**, #5307 **(B)**, #3553 **(C)**, #5741 **(E)**, #12503 **(F)**, #8637 **(G)**, #11974 **(H)**, #12496 **(I)**, #13110 **(J)**, #2056 **(K)**. Anti-VGF antibody was from Abcam (#ab74140).

	Expression fold change vs SH-SY5Y^{Untr}			
	Clone 1G3		Clone 2E3	
Protein target	Proteomic data	Western data	Proteomic data	Western data
Annexin A2	+3.50	+4.12	+1.51	+1.97
Caldesmon	+2.29	+2.02 (n.s.)	(+1.34)	+1.55
Neuromodulin	+3.48	+3.01	+1.79	+2.28
VGF	+2.46	+4.05	+6.79	+15.61
Vimentin	+4.30	+3.12	+2.20	+2.26
Zyxin	+3.88	+4.14	N/A	+2.10
RRM1	-2.20	-1.92	-1.89	-1.20 (n.s.)
BRE1A	-1.69	-1.21	N/A	-1.06 (n.s.)
eIF1	-1.83	-1.19	(-1.16)	+1.08 (n.s.)
PCNA	-2.09	-1.45	(-1.18)	+1.10 (n.s.)
PRKCA	+1.89	+2.77	(-1.62)	-1.61

Table 4.4 – Proteomic analyses and western blotting produced similar measures of fold change

This table summarises proteomic and western blot data for 11 protein targets. Shown are the mean fold changes in expression between SH-SY5Y^{Untr} and clone 1G3 or clone 2E3 determined from proteomic data (see **Tables 4.2 & 4.3**) and also from western blotting (see **Figure 4.6**). All of the proteins were identified as differentially expressed in the proteomic data unless: 1) the fold change value is shown in brackets, in which case the (+/-) 1.4 fold change cut-off was not met in at least one of the replicate datasets; or 2) the fold change is shown as "N/A", in which case the protein was identified from fewer than three quantified unique peptides in at least one of the replicate datasets, thereby potential making the fold change estimate unreliable. For the western blotting data, all fold changes were statistically significant unless described as "n.s.". Full protein names are given in **Figure 4.6**.

E3 ubiquitin-protein ligase BRE1A (Figure 4.6h), eukaryotic translation initiation factor 1 (Figure 4.6i) and proliferating cell nuclear antigen (Figure 4.6j) were also significantly downregulated in clones 1G3 and 1F3 but displayed no trends towards

differential expression in the other clones compared with the control line, whereas protein kinase C alpha type (Figure 4.6k) was upregulated in clones 1G3 and 1F3 but downregulated in 2E3 and 1B5. In keeping with the results described in Chapter 3, clone 1F3 was similar to 1G3 and clone 1B5 similar to 2E3 in terms of their expression profiles for these 11 proteins.

Importantly, 10 out of 11 targets differentially expressed between SH-SY5Y^{Untr} and clone 1G3 according to the proteomic data were similarly altered when analysed by western blotting. Although the remaining target, caldesmon, was not significantly affected in its expression ($p = 0.065$) as measured by western blotting, the fold change estimate of +2.02 was very close to that obtained by proteomic analysis (+2.29). Six of the 11 targets were also altered in their expression in clone 2E3 compared with SH-SY5Y^{Untr} according on the proteomic data, and western blotting confirmed differential expression for five of the six. The only one not confirmed was ribonucleoside-diphosphate reductase large subunit, which was downregulated according to the proteomic data (-1.89) and was not significantly altered when analysing expression by western blotting (fold change of -1.20; $p = 0.077$). Overall though, the western blotting data suggested that the expression ratios obtained from the proteomic analyses were accurate. Indeed, as shown in Table 4.4, the expression ratios determined by the different methods were relatively consistent in terms of magnitude, including when proteins showed no clear expression change between the samples.

4.2.2 Insights from the proteomic data into the differences among the clones in their responses to stress

One of the reasons for performing the aforementioned proteomic experiments was to investigate the reasons for the variability in stress responses among the clones. When applying the same filtering criteria to both datasets, 346 proteins were differentially expressed in clone 1G3 compared with SH-SY5Y^{Untr} but only 22 were altered in their expression in clone 2E3 compared with the control line. This disparity is probably a result of the molecular changes specific to clone 1G3 that were responsible for the

altered morphology and enhanced resistance to toxin treatment of that clone. An initial assessment of the pathways and processes overrepresented among these differentially expressed proteins was performed using the Ingenuity Pathway Analysis (IPA) software. However, the dataset from the clone 2E3 vs SH-SY5Y^{Untr} experiments was too small (only 22 proteins) to generate meaningful results (data not shown). Nonetheless, some insights into the differences between clones 1G3 and 2E3 can be obtained from the proteomic data. For example, one interesting finding was that neuroblast differentiation-associated protein AHNAK was upregulated by 2.82 fold[8] in clone 1G3 compared with SH-SY5Y^{Untr} and yet largely unchanged in clone 2E3 (fold change of -1.14). Additionally, the neurotransmitter neuropeptide Y was approximately 7 fold more abundant in clone 1G3 compared with SH-SY5Y^{Untr}. This fold change estimate may be unreliable since it is based upon quantification of a single peptide, although the detection of just one peptide in the proteomic analyses may have been because neuropeptide Y is only 36 amino acids in length. In any case, these data raised the possibility that clone 1G3 was more differentiated towards a mature neuronal phenotype than clone 2E3. Interestingly, a previous study found that various agents, including the phorbol ester 12-O-tetradecanoyl phorbol-13 acetate, induced differentiation of SH-SY5Y cells into a mature sympathetic noradrenergic phenotype, and this resulted in increased expression of neuropeptide Y and the axonal growth cone protein neuromodulin (Prince and Oreland, 1997). My western blotting data showed that neuromodulin was also upregulated in clone 1G3 compared with SH-SY5Y^{Untr}, although the same was admittedly true for clone 2E3 (Figure 4.6b). Protein kinase C may also be involved in SH-SY5Y differentiation (Bjelfman et al., 1990) and protein kinase C alpha type expression was upregulated in clones 1G3 and 1F3 compared with the control line but downregulated in clones 2E3 and 1B5 (Figure 4.6k). Reduced expression of proliferating cell nuclear antigen, an immature neuronal marker, in clones 1G3 and 1F3 provides further evidence of neuronal differentiation (Figure 4.6j). However, it is important to state that not all the data fits this hypothesis. Firstly, dopamine beta-hydroxylase, which catalyses an intermediate step in noradrenalin synthesis from dopamine, was actually strongly

[8] Mean expression ratios from the two replicate proteomic experiments were calculated and then converted to fold change. This was the case for all such fold change values given in Chapter 4.

downregulated (-6.67 fold) in clone 1G3 compared with SH-SY5Y^{Untr}. This could suggest differentiation into a non-noradrenergic phenotype but there were no clear signs of this in the proteomic data. Secondly, the immature neuronal marker nestin was upregulated in clone 1G3 (+1.75 fold) but seemingly unchanged (+1.14 fold) in clone 2E3. Thirdly, imaging data presented in Chapter 3 showed that clones 1G3 and 1F3 produced fewer neurite-like protrusions than the others clones. Given that neuritogenesis is part of neuronal differentiation, this finding suggests that clones 2E3 and 1B5 were the more differentiated.

Overall, these proteomic analyses identified some molecular differences between the clones but did not result in a conclusive explanation for the variability in stress responses. Therefore, further proteomic experiments were performed to identify the proteins differentially expressed following STS treatment in SH-SY5Y^{Untr}, clone 2E3 and clone 1G3. It was hoped that subsequent comparisons between the cell lines would identify the molecular changes underlying the differences in stress response.

4.3 Proteomic analyses of staurosporine-treated SH-SY5Y cells

4.3.1 Optimisation of staurosporine treatment conditions

As previously explained, the fact that the level and subcellular localisation of PrP^C expression appeared to vary little among the stably transfected clones (Figures 3.5, 3.7 and 3.8) suggested that the differences among the clones in terms of morphology and stress response may have been an artefact of the transfection and/or clone isolation process. Further evidence was provided by the lack of effect of PrP^C knockdown on survival of the stably transfected clones in response to toxin treatment (Figure 4.4). However, the data shown in Figure 3.4 suggests that clones 1G3 and 1F3 might, initially, have expressed higher levels of the PrP^C than clones 2E3 and 1B5. This could have resulted in changes to the phenotypes of clones 1G3 and 1F3 that did not occur in the other clones and were not affected by subsequent normalisation of PrP^C levels among the clones or by siRNA-mediated knockdown of expression. Whatever the reasons underlying the differences between the clones, the proteomic analyses described in the previous section did not shed much light on the downstream molecular changes that could have been mediating the variable responses to stress. To investigate this further, proteomic experiments comparing stressed and unstressed cells were carried out. Again, SH-SY5Y^{Untr} and clones 2E3 and 1G3 were analysed in these experiments, which allowed additional comparisons with the datasets of baseline proteomic alterations. Cells were stressed by exposure to 50 nM STS, which was chosen because the enhanced survival of clone 1G3 compared with SH-SY5Y^{Untr} was greatest in response to this toxin and at this dose (see Figures 3.10-3.12). However, in these experiments, the key was to detect the initial molecular changes induced by STS treatment, since these would define the cellular response to stress; proteomic alterations caused by cell death processes were of less interest. Because 24-hour exposure to 50 nM STS reduced viability of SH-SY5Y^{Untr} by almost 60 % (Figure 3.11), the time interval of STS treatment needed to be shortened so that cell death did not occur. In order to optimise this time interval, SH-SY5Y^{Untr} cells were seeded into a tissue culture plate and allowed to

recover for ~18 hours. Subsequently, the growth medium was exchanged for serum-free medium containing the N-2 supplement and 50 nM STS. The PrestoBlue viability assay was used to quantify survival after cells had been exposed to STS for 4, 6, 8 or 24 hours. Figure 4.7 shows that 24-hour STS treatment resulted in a ~60 % reduction in cell viability, as expected. Some cell death also seemed to have occurred after 8 hours and possibly after just 6 hours. Consequently, the 4-hour time interval was chosen. Next, phase contrast images of the cell lines were captured following 4-hour exposure to STS in order to determine whether visual signs of a response to the toxin were evident. Figure 4.8 indicates that the cells were responding to STS, as demonstrated by morphological changes to their networks of neurite-like protrusions, changes that seemed less obvious for clone 1G3 than the other cell lines. Taken together, these results suggested that treating the cells with STS for 4 hours would enable detection of the proteomic changes that were part of the initial stress response.

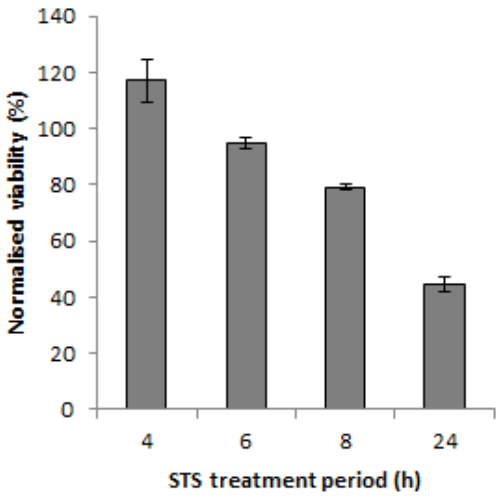

Figure 4.7 – Optimisation of staurosporine treatment duration

Bar chart showing viability of SH-SY5Y^{Untr} after several different time periods of exposure to 50 nM STS. The mean values (+/- standard deviation) from two technical replicates are displayed in the chart. A trend towards reduced viability was evident from 8 h onwards.

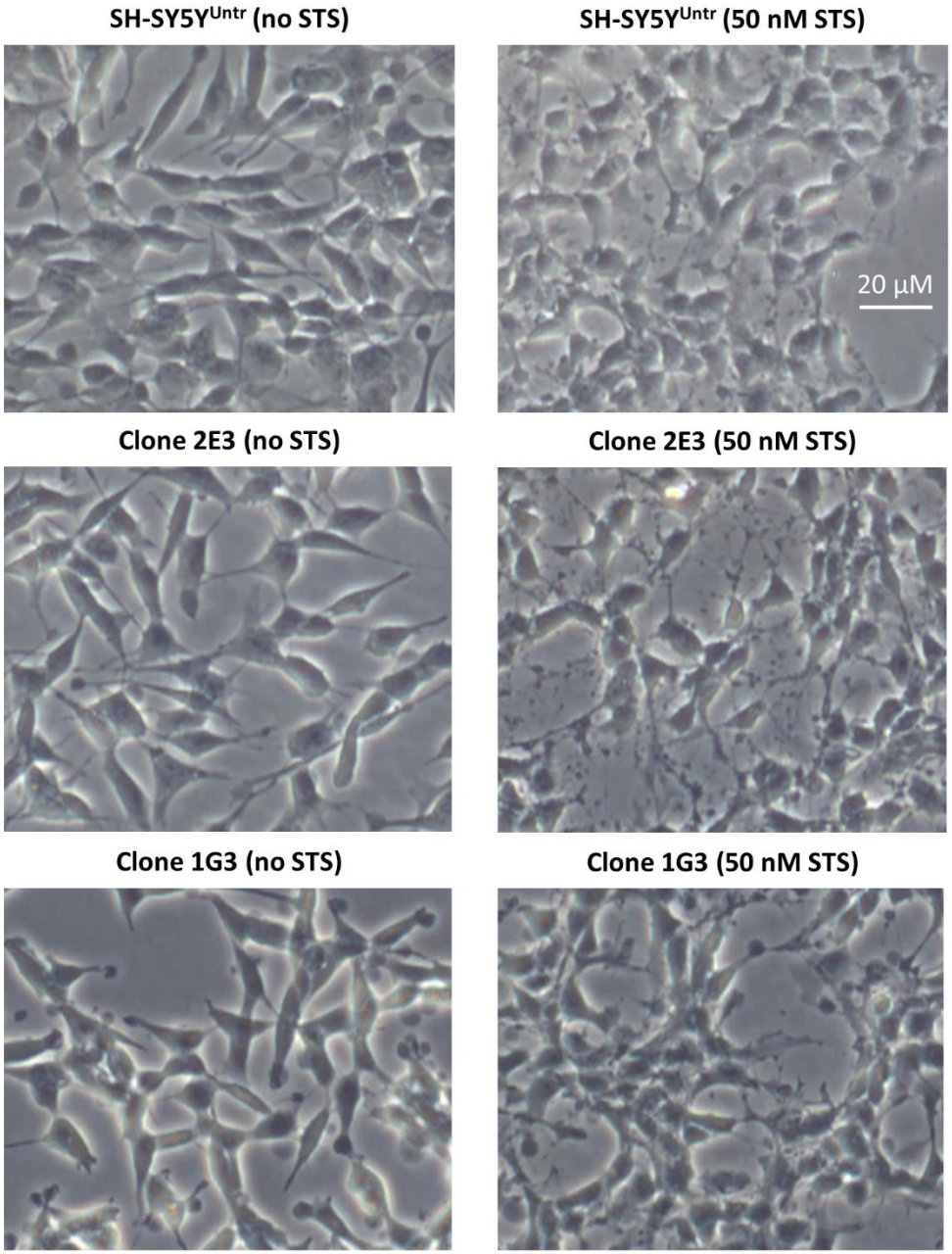

Figure 4.8 – Morphological changes to SH-SY5Y cells induced by staurosporine exposure

Phase contrast images of cells fixed after 4 h treatment with 50 nM STS were taken using a x10 objective. The scale bar shown applies to all panels. For all the cell lines, morphological changes were evident following STS treatment, specifically in terms of alterations to their neurite-like protrusions. These changes seemed to be least pronounced for clone 1G3.

4.3.2 Stress-induced proteomic changes in untransfected and stably transfected SH-SY5Y cells

The experimental format consisted of separate, two-way comparisons between stressed and unstressed cells from each cell line. For each experiment, cells were exposed for 4 hours either to 50 nM STS or to the toxin buffer alone (in this case DMSO). Subsequently, cells were lysed and the protein samples obtained were digested by proteases, labelled either with heavy or light dimethyl labels and analysed by LC-MS/MS, as described in section 4.2. To ensure that the proteomic changes induced by stress could be accurately compared among the cell lines, care was taken to ensure that the time intervals of toxin exposure and the time taken to perform the cell lysis steps were absolutely identical across the individual experiments. Due to time and resource constraints, only one set of cell lysates were analysed for each comparison. As before, the raw spectral data obtained from LC-MS/MS were analysed using computer software to identify peptides and, subsequently, proteins and to calculate expression ratios and the associated %CV values. Subsequently, the lists of proteins were filtered according to several criteria to identify those differentially expressed between the samples. Firstly, only proteins identified from more than two quantified unique peptides in both replicate datasets were included. Secondly, proteins with a %CV for their expression ratio of 50 or more were excluded to minimise the inclusion of false positives resulting from the lack of biological replication. Next, the datasets were uploaded to the Ingenuity Pathway Analysis (IPA) software and a fold change threshold was chosen. The plan was to carry out pathway analyses of the individual datasets and then perform a further comparison analysis using IPA (see the following section for more details) to identify the differences between the cell lines in terms of their responses to STS treatment. For the comparison analysis to work effectively, the datasets of differentially expressed proteins could not be too small. Therefore, the (+/-) 1.4 fold change cut-off used previously was not used again for these experiments, since the number of proteins meeting this threshold in clone 1G3 was only 29. Instead, the cut-off was lowered to (+/-) 1.3, which was still considered sufficiently stringent because applying the %CV cut-off removed a large number of proteins with potentially

unreliable expression ratios that would otherwise have been classed as differentially expressed. The numbers of proteins remaining after each of the filtering steps are shown in Table 4.5. After the final fold change cut-off was applied, SH-SY5Y^{Untr} had the most differentially-expressed proteins (187) after STS treatment, followed by clone 2E3 (110) and clone 1G3 (65). Many more proteins were downregulated than upregulated for all the cell lines – the proportions of differentially-expressed proteins upregulated were 20 %, 31 % and 18 % for SH-SY5Y^{Untr}, clone 2E3 and clone 1G3, respectively (Table 4.5). Tables 4.6-4.8 show the proteins with the largest expression changes in each dataset, whilst the full lists are provided in Appendix II. Since this method of proteomic analysis had already been validated successfully by western blotting (see section 4.2.1), this process was not repeated for the datasets reported here. The results of the pathway analyses are explored in the following section.

	Number of identified proteins		
	SH-SY5Y^{Untr}	Clone 2E3	Clone 1G3
Total	3093	3328	3164
# quant. peptides > 2	1516	1608	1467
%CV < 50	1363	1518	1370
Data entered into Ingenuity Pathway Analysis			
Mapped	1353	1510	1364
Expr. ratio >= 1.3 or <= 0.76	187	110	65
Final list (upreg., downreg.)	38, 149	34, 76	12, 53

Table 4.5 – Filtering of proteomic datasets for pathway analysis

This table shows the numbers of remaining proteins in the proteomic datasets from the STS-treatment experiments after cumulatively applying the described filtering criteria. "# quant. peptides > 2" means that only proteins with expression ratios calculated from > 2 quantified unique peptides were included. A few proteins were not "mapped" by the IPA software and were therefore not included in subsequent analyses; this was either because the accession numbers were not recognised or because of duplicate entries in the datasets (only one of which would be mapped).

Uniprot ID	Protein	Mascot Score	# quant. peptides	%CV	Fold change
Q5TB53	Transmembrane 9 superfamily member 3	184	3	25	+1.74
Q96ST3	Paired amphipathic helix protein Sin3a	451	3	38	+1.70
O43852	Calumenin	1393	15	45	+1.65
O14813	Paired mesoderm homeobox protein 2A	690	3	33	+1.65
Q9BY67	Cell adhesion molecule 1	162	3	20	+1.63
O95218	Zinc finger Ran-binding domain-containing protein 2	530	5	34	+1.62
O00139	Kinesin-like protein KIF2A	304	4	31	+1.61
P11388	DNA topoisomerase 2-alpha	888	11	42	+1.60
P40763	Signal transducer and activator of transcription 3	331	4	49	-2.22
P13693	Translationally-controlled tumor protein	692	7	46	-2.17
Q9Y4G6	Talin-2	338	3	46	-2.08
B1AJY7	26S proteasome non-ATPase regulatory subunit 10	337	3	13	-2.08
E7EM64	COP9 signalosome complex subunit 6	278	3	35	-2.00
Q96H79	Zinc finger CCCH-type antiviral protein 1-like	121	3	11	-2.00
Q9BUT1	3-hydroxybutyrate dehydrogenase type 2	139	3	31	-1.89
C9J2P0	Ubiquitin-conjugating enzyme E2 E1	147	3	48	-1.82
Q04837	Single-stranded DNA-binding protein, mitochondrial	407	6	40	-1.75
P61081	NEDD8-conjugating enzyme Ubc12	302	3	31	-1.75

Table 4.6 – Subset of proteins differentially expressed in SH-SY5Y^{Untr} following staurosporine treatment

See following page for legend…

Uniprot ID	Protein	Mascot Score	# quant. peptides	%CV	Fold change
C9J5D1	N-alpha-acetyltransferase 50	237	3	44	-1.72
P50479	PDZ and LIM domain protein 4	204	3	22	-1.72
Q9Y2Z0	Suppressor of G2 allele of SKP1 homolog	568	3	18	-1.67
Q9H3K6	BolA-like protein 2	451	3	13	-1.67
K7EM13	cAMP-dependent protein kinase type I-alpha regulatory subunit	104	3	1	-1.67
Q9UBG0	C-type mannose receptor 2	575	4	11	-1.64

Table 4.6 – Subset of proteins differentially expressed in SH-SY5Y^{Untr} following staurosporine treatment

This table shows a subset of the proteins that underwent an expression change in SH-SY5Y^{Untr} following exposure to 50 nM STS for 4 h. To be defined as differentially expressed, proteins had to meet the following criteria: 1) > 2 quantified unique peptides (# quant. peptides); 2) fold change >=1.3 or <=0.76; and 3) %CV < 50. The 8 most upregulated and 16 most downregulated proteins are shown here and the remaining proteins are listed in **Appendix II**.

Uniprot ID	Protein	Mascot Score	# quant. peptides	%CV	Fold change
P67870	Casein kinase II subunit beta	287	3	45	+1.72
Q9Y5Q9	General transcription factor 3C polypeptide 3	197	3	31	+1.67
O75525	KH domain-containing, RNA-binding, signal transduction-associated protein 3	197	3	25	+1.64
Q07666	KH domain-containing, RNA-binding, signal transduction-associated protein 1	556	6	17	+1.57
O14813	Paired mesoderm homeobox protein 2A	571	4	32	+1.49
O75691	Small subunit processome component 20 homolog	138	3	37	+1.49
O95881	Thioredoxin domain-containing protein 12	209	3	36	+1.48
Q9UKX7	Nuclear pore complex protein Nup50	280	4	33	+1.45
P40763	Signal transducer and activator of transcription 3	277	3	14	-1.92
Q04837	Single-stranded DNA-binding protein, mitochondrial	525	7	30	-1.79
Q9BRP8	Partner of Y14 and mago	229	3	28	-1.79
P10644	cAMP-dependent protein kinase type I-alpha regulatory subunit	151	3	18	-1.75
Q9BRA2	Thioredoxin domain-containing protein 17	259	3	38	-1.69
Q15113	Procollagen C-endopeptidase enhancer 1	235	3	16	-1.69
P42345	Serine/threonine-protein kinase mTOR	321	3	27	-1.67

Table 4.7 – Subset of proteins differentially expressed in clone 2E3 following staurosporine treatment

See following page for legend…

Uniprot ID	Protein	Mascot Score	# quant. peptides	%CV	Fold change
P29762	Cellular retinoic acid-binding protein 1	207	4	25	-1.61
P31689	DnaJ homolog subfamily A member 1	614	6	32	-1.56
Q9NRX4	14 kDa phosphohistidine phosphatase	250	3	7	-1.56
Q9NUQ9	Protein FAM49B	543	3	42	-1.54
P10645	Chromogranin-A	527	4	19	-1.54
Q96FC7	Phytanoyl-CoA hydroxylase-interacting protein-like	414	6	50	-1.54
D6RDM7	Ubiquitin-conjugating enzyme E2 K	294	4	37	-1.54
Q8WXD2	Secretogranin-3	155	3	5	-1.54
P23381	Tryptophan--tRNA ligase, cytoplasmic	1659	11	38	-1.52

Table 4.7 – Subset of proteins differentially expressed in clone 2E3 following staurosporine treatment

This table shows a subset of the proteins that underwent an expression change in clone 2E3 following exposure to 50 nM STS for 4 h. To be defined as differentially expressed, proteins had to meet the following criteria: 1) > 2 quantified unique peptides (# quant. peptides); 2) fold change >=1.3 or <=0.76; and 3) %CV < 50. The 8 most upregulated and 16 most downregulated proteins are shown here and the remaining proteins are listed in **Appendix II**.

Uniprot ID	Protein	Mascot Score	# quant. peptides	%CV	Fold change
O14787	Transportin-2	215	4	48	+2.04
O43719	HIV Tat-specific factor 1	183	3	47	+1.76
P36915	Guanine nucleotide-binding protein-like 1	417	5	43	+1.46
P24534	Elongation factor 1-beta	600	7	35	+1.45
P10253	Lysosomal alpha-glucosidase	480	3	23	+1.44
Q9BTW9	Tubulin-specific chaperone D	266	4	38	+1.40
Q96ST3	Paired amphipathic helix protein Sin3a	248	3	19	+1.37
Q9NVP1	ATP-dependent RNA helicase DDX18	138	3	15	+1.36
P62937	Peptidyl-prolyl cis-trans isomerase A	1104	7	32	-1.89
E9PL69	Ribonucleoside-diphosphate reductase large subunit	431	4	30	-1.79
Q96A49	Synapse-associated protein 1	402	3	9	-1.64
Q9Y570	Protein phosphatase methylesterase 1	384	5	46	-1.61
Q9BUT1	3-hydroxybutyrate dehydrogenase type 2	222	3	30	-1.59
P29762	Cellular retinoic acid-binding protein 1	416	5	17	-1.56
P47813	Eukaryotic translation initiation factor 1A, X-chromosomal	317	4	48	-1.54
Q9BRP8	Partner of Y14 and mago	305	4	22	-1.54

Table 4.8 – Subset of proteins differentially expressed in clone 1G3 following staurosporine treatment

See following page for legend…

Uniprot ID	Protein	Mascot Score	# quant. peptides	%CV	Fold change
Q96FC7	Phytanoyl-CoA hydroxylase-interacting protein-like	283	6	29	-1.54
Q7LBC6	Lysine-specific demethylase 3B	243	3	47	-1.54
P10643	Complement component C7	939	9	40	-1.52
D6RE99	Histidine triad nucleotide-binding protein 1	204	4	44	-1.52
P48307	Tissue factor pathway inhibitor 2	625	5	17	-1.49
E5RJR5	S-phase kinase-associated protein 1	508	6	46	-1.47
K7EN45	Peptidyl-prolyl cis-trans isomerase NIMA-interacting 1	409	4	34	-1.47
Q99436	Proteasome subunit beta type-7	339	3	43	-1.45

Table 4.8 – Subset of proteins differentially expressed in clone 1G3 following staurosporine treatment

This table shows a subset of the proteins that underwent an expression change in clone 1G3 following exposure to 50 nM STS for 4 h. To be defined as differentially expressed, proteins had to meet the following criteria: 1) > 2 quantified unique peptides (# quant. peptides); 2) fold change >=1.3 or <=0.76; and 3) %CV < 50. The 8 most upregulated and 16 most downregulated proteins are shown here and the remaining proteins are listed in **Appendix II**.

4.3.3 Pathway analysis of stress-induced proteomic changes

After uploading the proteomic data to IPA and filtering for fold change as described in the previous section, core analyses were run for each dataset. The IPA core analysis suite has a number of features, including those that identify the canonical pathways and disease/biofunction categories that are most overrepresented among the proteins/genes in the uploaded dataset. Canonical pathways are standard, well-characterised signalling pathways, whereas disease/biofunction categories are groupings of genes with similar functions according to the database used by the software (known as the Ingenuity Knowledge Base). Another feature of the software is that it can generate *de novo* protein-protein interaction networks. This is achieved by use of an algorithm, which is explained in detail in a whitepaper from Ingenuity Systems (2005). Briefly, proteins are sorted into networks based on information about experimentally confirmed direct and indirect interactions that is recorded in the Ingenuity Knowledge Base. A direct interaction could be transcription factor X inducing expression of protein Y by binding to its promoter, while protein X upregulating protein Y via one or more intermediate proteins would be an indirect interaction.

Once each proteomic dataset had been analysed by IPA individually, a comparison analysis was performed within the software to identify differences among the cell lines in terms of the molecular response to STS treatment. This approach enabled side-by-side viewing of the STS-induced changes to individual biofunctions, canonical pathways and networks etc. that were observed in the different cell lines. Table 4.9 shows the disease/biofunction categories that showed the most overlap with the datasets of differentially expressed proteins, as determined by the right-tailed Fisher exact test. When possible, activation state z-scores are also provided for each category. These z-scores are calculated based upon information from the Ingenuity Knowledge Base about how the expression changes to individual proteins should affect the activity of the entire disease process or biofunction. IPA adds together these predictions to generate an overall z-score, which represents the degree of confidence that the disease process or biofunction is activated (positive

value) or inhibited (negative value). Z-scores > 2 or < -2 are generally considered statistically significant (Ingenuity Systems, [n.d.]), although lower values may still be informative, especially when the analysed datasets are small.

	Activation state z-score after STS treatment		
Diseases and biofunctions	**SHSY5Y^{Untr}**	**Clone 2E3**	**Clone 1G3**
Proliferation of cells	-2.55	-1.99	-2.42
Migration of cells	-3.53	-0.94	-0.79
Cell movement of leukaemia cell lines	-2.43	-2.22	0.00
Invasion of cells	-2.47	-1.00	-1.15
Invasion of breast cancer cell lines	-2.62	-1.73	0.00
Cell movement	-2.84	-0.65	-0.80
Viral infection	-2.47	0.00	-1.63
Proliferation of tumour cell lines	-2.03	0.00	-2.04
Cell death	+2.49	+0.68	-0.79
Apoptosis	+2.60	+0.85	-0.51
Invasion of tumour cell lines	-2.04	-1.38	0.00
Cell viability of breast cancer cell lines	-1.41	-1.94	0.00
Migration of fibroblasts	-1.22	-1.99	0.00
Necrosis	1.78	0.00	-1.16
Proliferation of muscle cells	-2.93	0.00	0.00

Table 4.9 – Key downstream processes altered by staurosporine treatment

This table displays the disease/biofunction categories that had the greatest overlap, according to IPA, with the datasets of STS-induced proteomic changes. The categories are ranked according to the moduli of the means of the activation state z-scores (see main text for more details about z-scores) from the three cell lines. A z-score of 0 is reported either if the overlap p-value (calculated by IPA using the right-tailed Fisher exact test) was not statistically significant or if it was significant ($p < 0.05$) but the Ingenuity Knowledge Base did not contain information on whether the associated proteins were activators or inhibitors of the particular disease process or biofunction.

The “proliferation of cells” biofunction is top of the list in Table 4.9 and had a similarly negative z-score in all the datasets. Inhibition of proliferation by the protein kinase inhibitor STS is not surprising given that long-term treatment with the toxin is known to induce growth arrest of SH-SY5Y cells (Prince and Oreland, 1997), presumably by inactivating the protein kinases involved in driving proliferation. Probably for similar reasons, cell movement/migration of SH-SY5Y^{Untr} was also reduced by exposure to STS. In general, this effect of STS treatment was less dramatic in clones 2E3 and 1G3, although the lack of difference between the clones in this regard means that variable responses to STS in terms of changes to cell movement cannot obviously be linked to the differing responses to stress among the clones. Additionally, the data in Table 4.9 clearly show that apoptotic/necrotic pathways were induced in SH-SY5Y^{Untr}, although the relevant proteomic changes probably represent the initial stages of cell death, since cell viability was not reduced by the STS treatment regime used for these experiments (Figure 4.7). Activation of apoptosis/necrosis was less evident for clone 2E3, whilst these processes were actually predicted to be less active in clone 1G3 following STS exposure, albeit with low confidence. These results approximately matched the viability and cytotoxicity data for STS treatment (Figure 3.11a & c), which showed that clone 1G3 was considerably more resistant than SH-SY5Y^{Untr} and that clone 2E3 was, perhaps, marginally more resistant.

The conclusion from the diseases and biofunctions analysis was that clone 1G3 displayed no obvious protective molecular response to STS treatment but, nevertheless, did seem to be less negatively affected by the toxin than the other cell lines. Further emphasising this point is that protein-protein interaction networks, generated *de novo* by IPA from the proteomic datasets, tended to overlap with each other in a manner that appeared to be largely independent of cell line (Figure 4.9). However, the canonical pathway most convincingly affected by STS treatment provided more interesting insights; this was the extracellular signal-regulated kinase (ERK)/mitogen-activated protein kinase (MAPK) pathway, which is generally pro-survival, although not always (Mebratu and Tesfaigzi, 2009). Table 4.10 shows the proteins in this pathway that were differentially expressed upon STS treatment…

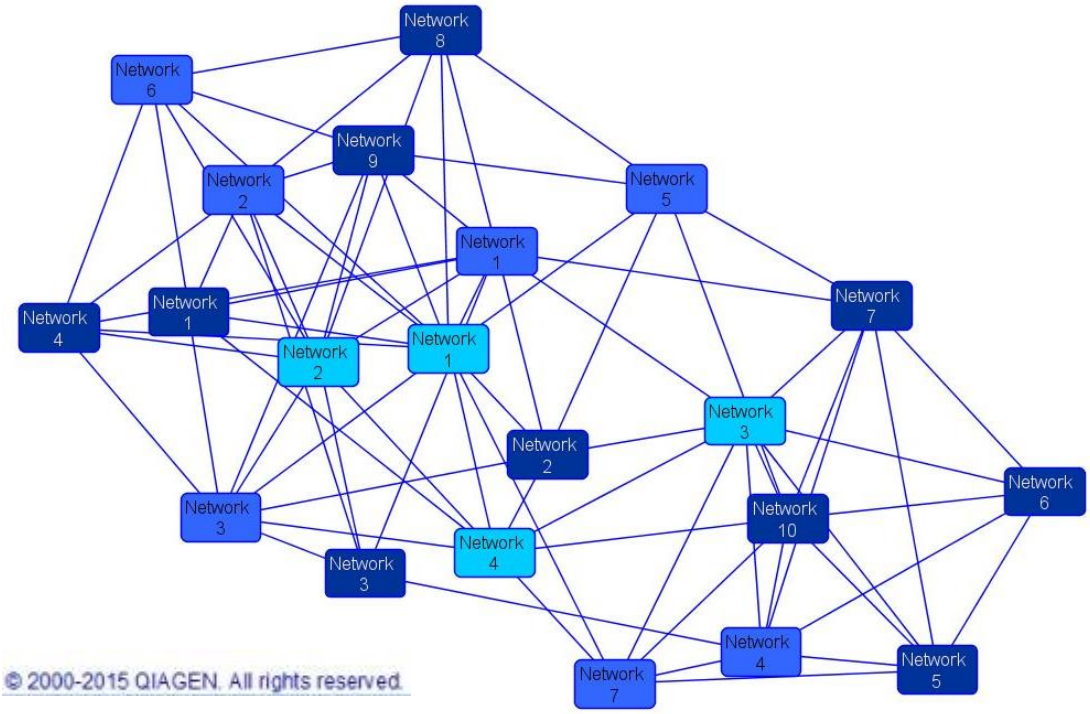

Figure 4.9 – Interrelatedness of networks generated by IPA from the datasets of staurosporine-induced proteomic changes

This diagram highlights that networks, generated *de novo* by IPA from the proteomic changes caused by STS treatment, do not cluster into cell line-specific groups. This suggests that the proteomic changes induced by STS were similar among the cell lines. Connecting lines indicate that those networks share at least one common protein. Networks for SH-SY5Y^{Untr} are coloured dark blue, those for clone 2E3 are a lighter blue and those for clone 1G3 are the lightest coloured.

…in at least one of the cell lines. The activation state z-scores suggested inhibition of ERK/MAPK signalling in SH-SY5Y^{Untr} and clone 2E3, which would be expected due to inhibition of protein kinases in the pathway by STS. However, the components of the ERK/MAPK pathway were not significantly overrepresented (right-tailed Fisher exact test; $p = 0.119$) among the differentially expressed proteins for clone 1G3. Interestingly, one of the terminal transcription factors directly…

	Fold expression change		
Protein	SH-SY5Y^{Untr}	Clone 2E3	Clone 1G3
V-crk avian sarcoma virus CT10 oncogene homolog-like	-1.41	-1.14	-1.22
Phospholipase C, gamma 1	-1.37	-1.32	-1.16
Protein phosphatase 1, catalytic subunit, beta isozyme	-1.49	-1.01	-1.12
Protein phosphatase 2, regulatory subunit B, alpha	-1.37	-1.09	-1.12
Protein kinase, cAMP-dependent, regulatory, type I, alpha	-1.67	-1.75	-1.47
Ras-related C3 botulinum toxin substrate 1	-1.39	-1.33	-1.19
Signal transducer and activator of transcription 3	-2.22	-1.92	-1.11
Talin 2	-2.08	-1.27	-1.30
Overlap p-value for the canonical pathway	0.00283	0.0172	0.119 (n.s.)
Activation state z-score	-1.414	-2.000	N/A

Table 4.10 – Effects of staurosporine treatment on ERK/MAPK pathway

The table shows proteins in the ERK/MAPK canonical pathway, as defined by IPA, that were differentially expressed upon STS treatment in at least one of the cell lines. Fold change values are reported for each protein and those shown in black met the (+/-) 1.3 fold change threshold, whilst those in grey did not. Overlap p-values for the pathway were calculated by IPA using the right-tailed Fisher exact test. The activation state z-scores (see main text for more details about z-scores) suggest that the pathway may have been inhibited in SH-SY5Y^{Untr} and clone 2E3. No z-score was calculated for the pathway in clone 1G3, since the overlap p-value was non-significant (n.s.).

… activated by ERK1/2, signal transducer and activator of transcription 3 (STAT3), was downregulated by around two fold in SH-SY5^{Untr} and clone 2E3 as a result of STS treatment but was virtually unchanged in its expression in clone 1G3. STAT3 is thought to act in a pro-survival manner (Megison et al., 2013), and the proteomic data described in section 4.2 suggested that the baseline level of STAT3 expression

might have been higher in clone 1G3 (mean fold change of +1.690) than SH-SY5Y^{Untr}, although clone 2E3 might also have expressed slightly higher levels of the protein than the control line (fold change of +1.265). As a consequence of higher STAT3 expression levels, STAT3 activity might have been greater in clone 1G3 than the other cell lines prior to STS treatment, resulting in a reduced inhibitory effect of the toxin and improved survival. It should be pointed out though that the baseline expression level estimates may not have been that reliable, because STAT3 did not meet the criteria of more than two quantified unique peptides in either of the proteomic datasets reported in section 4.2.

As previously described, the apparently similar levels and subcellular localisation patterns of PrP^C expression among the stably transfected clones suggested that the differences in their responses to toxin treatment may have been artefacts of the transfection and/or clone isolation process. Further evidence was provided by the lack of effect of PrP^C knockdown on survival of the stably transfected clones in response to PQ or STS treatment. Nonetheless, there had to be some molecular changes that were responsible for the variability in stress responses among the clones and increased activity of the ERK/MAPK pathway in clones 1G3 (and, presumably, also clone 1F3) under normal growth conditions is one potential explanation. An obvious caveat is that these proteomic experiments involved exposure to STS, whereas PQ and TM are not protein kinase inhibitors and so may affect the ERK/MAPK pathway in quite different ways. However, increased ERK/MAPK signalling would be expected to be protective under most circumstances.

Aside from investigating the differences between the clones, the proteomic analyses described in section 4.2 were also carried out with the aim of identifying functions of PrP^C not directly related to stress-protection. The hypothesis was that the proteomic changes common to clones 2E3 and 1G3 were most likely to have resulted from PrP^C expression and Chapter 5 begins by reporting on pathway analysis of this data.

Chapter 5: Elucidating the downstream processes regulated by PrP^C in SH-SY5Y cells

5.1 Identification of molecular changes compared with untransfected cells that were common to clones 2E3 and 1G3

A large number of studies have found that PrP^C expression protects cells from stress, although there is considerable controversy in the literature relating to this putative function. Accordingly, the first experiments performed using the PrP^C-transfected SH-SY5Y cells were to assess their responses to stress. Results showed that the stably transfected clones were less viable than SH-SY5Y^{Untr} following serum deprivation, although clone-specific protection against three chemical toxins was observed. However, knocking down PrP^C did not affect the resistance to toxin treatment of the clones, suggesting that this property was independent of PrP^C expression. Therefore, the results reported in this thesis are not consistent with a direct role for PrP^C in stress protection. This is not the only function that has been linked to PrP^C though; others include neurite outgrowth (Graner et al., 2000; Loubet et al., 2012), circadian rhythm generation (Tobler et al., 1996; Sanchez-Alavez et al., 2007) and myelin maintenance (Bremer et al., 2010; Nuvolone et al., 2016). Consequently, stable transfection of the *Prnp* CDS into the SH-SY5Y cells could have affected other processes; to investigate what these were, the proteomic data reported in section 4.2 were re-analysed. We hypothesised that the expression changes common to both clones were most likely to have resulted from PrP^C expression, so I combined the datasets to identify the proteins that were differentially expressed in clones 2E3 *and* 1G3 compared with SH-SY5Y^{Untr}. The criteria were: 1) identification from more than two quantified unique peptides in all replicate datasets; and 2) fold change of >= 1.2 or <= -1.2 in all replicate datasets. Since the combined proteomic dataset effectively consisted of four biological replicates (two comparing SH-SY5Y^{Untr} and clone 2E3, and two comparing SH-SY5Y^{Untr} and clone 1G3), the fold change cut-off of (+/-) 1.2 was considered sufficiently stringent. Table 5.1 shows the 60 proteins that met these criteria, 11 of which were upregulated and 49 downregulated.

		Fold change compared with untransfected				
		Clone 2E3		Clone 1G3		Combined
Uniprot ID	Protein	Expt 1	Expt 2	Expt 1	Expt 2	Mean fold change
O15240	Neurosecretory protein VGF	+8.33	+5.24	+2.57	+2.35	+4.62
P08670	Vimentin	+2.71	+1.69	+3.52	+5.08	+3.25
P17677	Neuromodulin	+1.52	+2.05	+3.18	+3.78	+2.63
P07355	Annexin A2	+1.53	+1.49	+3.02	+3.98	+2.51
Q05682-5	Caldesmon	+1.34	+1.33	+2.12	+2.46	+1.81
Q96CN7	Isochorismatase domain-containing protein 1	+2.28	+1.58	+1.80	+1.37	+1.76
P10253	Lysosomal alpha-glucosidase	+2.40	+1.22	+1.84	+1.53	+1.75
Q9BWM7	Sideroflexin-3	+1.60	+1.44	+1.95	+1.87	+1.72
Q96FC7	Phytanoyl-CoA hydroxylase-interacting protein-like	+1.74	+1.67	+1.95	+1.36	+1.68
Q9UMS6	Synaptopodin-2	+1.57	+1.30	+1.54	+1.56	+1.49
Q99829	Copine-1	+1.26	+1.28	+1.40	+1.39	+1.33
P23921	Ribonucleoside-diphosphate reductase large subunit	-2.38	-1.56	-1.92	-2.56	-2.03
P35520	Cystathionine beta-synthase	-1.39	-1.41	-2.94	-3.70	-1.96
P52306	Rap1 GTPase-GDP dissociation stimulator 1	-4.55	-1.69	-1.25	-1.49	-1.75
O75223	Gamma-glutamylcyclotransferase	-1.67	-1.41	-1.79	-2.17	-1.72

Table 5.1 – List of proteins differentially expressed in both clones 2E3 and 1G3 compared with untransfected SH-SY5Y cells

Table continues on the following pages – legend displayed on the final page of the table.

		Fold change compared with untransfected				
		Clone 2E3		Clone 1G3		Combined
Uniprot ID	Protein	Expt 1	Expt 2	Expt 1	Expt 2	Mean fold change
O43795-2	Unconventional myosin-Ib	-1.69	-1.20	-1.82	-2.63	-1.70
Q15181	Inorganic pyrophosphatase	-1.85	1.35	-1.45	-2.56	-1.69
Q15021	Condensin complex subunit 1	-2.44	-1.23	-1.61	-1.82	-1.67
O14737	Programmed cell death protein 5	-1.72	-1.32	-1.67	-2.13	-1.66
P18754	Regulator of chromosome condensation	-1.52	-1.35	-1.72	-2.27	-1.65
Q14566	DNA replication licensing factor MCM6	-1.52	-1.27	-1.89	-1.96	-1.61
P11171	Protein 4.1	-1.28	-1.47	-1.54	-2.50	-1.59
P06493	Cyclin-dependent kinase 1	-1.30	-1.49	-1.96	-1.79	-1.59
P22234	Multifunctional protein ADE2	-1.61	-1.20	-1.49	-2.27	-1.56
P38117	Electron transfer flavoprotein subunit beta	-1.69	-1.43	-1.45	-1.72	-1.56
P62913	60S ribosomal protein L11	-1.69	-1.92	-1.30	-1.45	-1.56
Q96GQ7	Probable ATP-dependent RNA helicase DDX27	-1.20	-1.64	-1.64	-1.89	-1.55
Q9Y2Z0	Suppressor of G2 allele of SKP1 homolog	-1.45	-1.35	-1.69	-1.72	-1.54
P45973	Chromobox protein homolog 5	-1.22	-1.52	-1.67	-1.82	-1.52
O95347	Structural maintenance of chromosomes protein 2	-1.49	-1.30	-1.82	-1.56	-1.52
F5GWX5	Chromodomain-helicase-DNA-binding protein 4	-1.52	-1.20	-1.49	-2.08	-1.52

Table 5.1 – List of proteins differentially expressed in both clones 2E3 and 1G3 compared with untransfected SH-SY5Y cells

Table continues on the following pages – legend displayed on the final page of the table.

		Fold change compared with untransfected				
		Clone 2E3		Clone 1G3		Combined
Uniprot ID	Protein	Expt 1	Expt 2	Expt 1	Expt 2	Mean fold change
O60841	Eukaryotic translation initiation factor 5B	-1.89	-1.20	-1.33	-1.85	-1.51
P48634	Protein PRRC2A	-1.75	-1.27	-1.47	-1.61	-1.50
O00410	Importin-5	-1.69	-1.22	-1.67	-1.49	-1.49
Q9BY44	Eukaryotic translation initiation factor 2A	-2.27	-1.20	-1.32	-1.54	-1.49
P43246	DNA mismatch repair protein Msh2	-1.37	-1.35	-1.59	-1.69	-1.49
P11586	C-1-tetrahydrofolate synthase, cytoplasmic	-1.59	-1.35	-1.41	-1.64	-1.49
Q06830	Peroxiredoxin-1	-1.64	-1.20	-1.39	-1.85	-1.48
F5H669	Cleavage and polyadenylation-specificity factor subunit 7	-1.25	-1.20	-1.43	-1.72	-1.47
K7EMT0	Splicing factor 3A subunit 2	-1.92	-1.22	-1.33	-1.59	-1.47
Q2NL82	Pre-rRNA-processing protein TSR1 homolog	-1.27	-1.43	-1.39	-1.92	-1.47
Q92823	Neuronal cell adhesion molecule	-1.43	-1.41	-1.20	-2.00	-1.46
Q92621	Nuclear pore complex protein Nup205	-1.54	-1.41	-1.25	-1.69	-1.45
P22392	Nucleoside diphosphate kinase B	-1.43	-1.28	-1.32	-1.92	-1.45
Q92973	Transportin-1	-1.45	-1.27	-1.35	-1.82	-1.44
Q9UMS4	Pre-mRNA-processing factor 19	-1.23	-1.22	-1.47	-2.13	-1.44
P27694	Replication protein A 70 kDa DNA-binding subunit	-1.39	-1.33	-1.32	-1.79	-1.43

Table 5.1 – List of proteins differentially expressed in both clones 2E3 and 1G3 compared with untransfected SH-SY5Y cells

See following page for legend…

		Fold change compared with untransfected				
		Clone 2E3		Clone 1G3		Combined
Uniprot ID	Protein	Expt 1	Expt 2	Expt 1	Expt 2	Mean fold change
Q9UQ80	Proliferation-associated protein 2G4	-1.22	-1.23	-1.47	-2.04	-1.43
Q9NSD9	Phenylalanine--tRNA ligase beta subunit	-1.56	-1.28	-1.30	-1.61	-1.42
E7EPN9	Protein PRRC2C	-1.49	-1.20	-1.52	-1.49	-1.41
P40227	T-complex protein 1 subunit zeta	-1.25	-1.25	-1.54	-1.69	-1.41
F5GWF6	T-complex protein 1 subunit beta	-1.25	-1.20	-1.37	-1.92	-1.39
P15531	Nucleoside diphosphate kinase A	-1.32	-1.22	-1.33	-1.75	-1.38
G5E9W3	Cleavage and polyadenylation specific factor 3, 73kDa, isoform CRA_b	-1.25	-1.20	-1.43	-1.72	-1.37
P50990	T-complex protein 1 subunit theta	-1.20	-1.20	-1.45	-1.67	-1.36
E9PC52	Histone-binding protein RBBP7	-1.32	-1.27	-1.27	-1.64	-1.36
P61221	ATP-binding cassette sub-family E member 1	-1.20	-1.22	-1.37	-1.72	-1.35
Q99598	Translin-associated protein X	-1.33	-1.37	-1.23	-1.33	-1.32
O43172	U4/U6 small nuclear ribonucleoprotein Prp4	-1.27	-1.22	-1.22	-1.56	-1.30
P62140	Serine/threonine-protein phosphatase PP1-beta catalytic subunit	-1.20	-1.25	-1.37	-1.20	-1.25

Table 5.1 – List of proteins differentially expressed in both clones 2E3 and 1G3 compared with untransfected SH-SY5Y cells

The table shows all proteins from the $SH\text{-}SY5Y^{Untr}$ vs clone 2E3 and $SH\text{-}SY5Y^{Untr}$ vs clone 1G3 proteomic experiments that were identified from > 2 quantified unique peptides (# quant. peptides) and met the (+/-) 1.2 fold change cut-off in all datasets. For each protein, the mean expression ratio over the four experiments was calculated and converted to fold change.

Importantly, this list contained more than half (12 out of 22) of the proteins showing altered expression in clone 2E3 compared with SH-SY5Y^{Untr} according to the (+/-) 1.4 fold change cut-off used for the initial analysis (see Table 4.2). This suggested that many of the proteomic changes observed in clone 2E3 were shared by clone 1G3. As described in section 4.2.1, the accuracy of the proteomic data had already been validated by western blotting for a subset of targets. Subsequently, pathway analysis of the dataset shown in Table 5.1 was carried out using the IPA core analysis suite, as described previously.

5.1.1 Cell cycle regulation

IPA biofunction categories are groupings of genes known to have similar functions based upon the data contained with the software database (Ingenuity Knowledge Base). Summary data from the pathway analysis, shown in Table 5.2, indicates that the cell cycle biofunction was the fourth most overrepresented among the proteins differentially expressed between the stably transfected clones and SH-SY5Y^{Untr}. "Cell cycle" was also one of the biofunction categories making up the highest-confidence protein-protein interaction network generated by IPA – this feature of the software groups together proteins from the dataset that are known to interact with each other either directly or indirectly. Each biofunction consists of multiple subfunctions and Table 5.3 details the 12 differentially expressed proteins that were part of the cell cycle progression subfunction (overlap p-value[9] = 0.000538). One of these proteins was cyclin-dependent kinase 1 (CDK1), which was downregulated in clones 2E3 (expression fold change[10] of -1.39) and 1G3 (-1.85 fold) compared with SH-SY5Y^{Untr}. CDK1 plays a key role in the cell cycle; in fact CDK1 appears capable of driving the mammalian cell cycle in the absence of any other CDKs (Santamaria et al., 2007). Therefore, CDK1 downregulation by the…

[9] IPA uses the right-tailed Fisher exact test to calculate p-values for overrepresentation of biofunctions and pathways in the analysed dataset.
[10] Mean expression ratios for the two replicate proteomic experiments were calculated and converted to fold change. This was the case for all fold change values derived from the proteomic data that are reported in Chapter 5.

Top molecular and cellular functions	p-values	# proteins	Proportion of dataset
DNA replication, recombination and repair	3.77E-02 – 8.57E-06	16	27 %
Cellular assembly and organisation	3.77E-02 – 2.57E-05	21	35 %
Cell death and survival	3.66E-02 – 5.42E-05	27	45 %
Cell cycle	3.49E-02 – 5.44E-05	17	28 %
Cell morphology	3.77E-02 – 1.06E-04	15	25 %
Top networks			**p-score**
Cellular assembly and organisation; DNA replication, recombination and repair; cell cycle			58
Cellular assembly and organisation; DNA replication, recombination and repair; cell-to-cell signalling and interaction			37
Developmental disorder; hereditary disorder; metabolic disease			35

Table 5.2 – Summary of pathway analysis of proteomic changes induced by PrP^C transfection

This table shows the top five most overrepresented molecular and cellular functions identified by IPA from the dataset of proteomic changes induced by PrP^C transfection. The ranking is by p-value (right-tailed Fisher exact test) and ranges are given because IPA calculates p-values for each subfunction within the overall functional category. Also shown are networks generated *de novo* by IPA from the same data. Network p-scores are the negative logarithms (base 10) of the p-values, again determined using the right-tailed Fisher exact test.

…stably transfected clones suggested that PrP^C transfection had slowed down cell cycle progression in the SH-SY5Y cells. Indeed, IPA calculated the activation state z-score[11] for cell cycle progression to be -0.958, which suggests inhibition of the biofunction.

Protein	Mean expression fold change compared with $SH\text{-}SY5Y^{Untr}$	Predicted effect on function
Caldesmon	+1.81	Affected
U4/U6 small nuclear ribonucleoprotein Prp4	-1.30	Increased
Nucleoside diphosphate kinase A	-1.38	Decreased
Proliferation-associated protein 2G4	-1.43	Affected
Replication protein A 70 kDa DNA-binding subunit	+1.43	Decreased
Peroxiredoxin-1	-1.48	Affected
DNA mismatch repair protein Msh2	-1.49	Affected
Suppressor of G2 allele of SKP1 homolog	-1.54	Affected
60S ribosomal protein L11	-1.56	Affected
Cyclin-dependent kinase 1	-1.59	Decreased
Regulator of chromosome condensation	-1.65	Affected
Ribonucleoside-diphosphate reductase large subunit	-2.03	Affected

Table 5.3 – Proteins involved in cell cycle progression showed altered expression upon PrP^C transfection

This table shows the 12 proteins in the cell cycle progression biofunction, as defined by IPA, that were differentially expressed in stably transfected clones 2E3 and 1G3 compared with $SH\text{-}SY5Y^{Untr}$. For each protein, the predicted effect on cell cycle progression of the expression change is reported. "Affected" indicates that IPA could not determine the direction of the effect from the data contained in the Ingenuity Knowledge Base.

[11] These z-scores represent the degree of confidence that a biofunction is activated (positive value) or inhibited (negative value). Z-scores > 2 or < -2 are generally considered statistically significant (Ingenuity Systems, [n.d.]), although lower values may still be informative, especially when the analysed datasets are quite small.

In addition to biofunctions and networks, IPA identifies the canonical pathways displaying the greatest overlap with the dataset being analysed. The top canonical pathway identified from the proteins differentially expressed as a result of PrP^C transfection was ras-related nuclear protein signalling (overlap p-value = 0.0000162), which the Ingenuity Knowledge Base reports as vital for nucleocytoplasmic transport of macromolecules through the nuclear pore complex. Interestingly, altered ras-related nuclear protein signalling could be a consequence of CDK1 downregulation, since CDK1 is known to phosphorylate the nuclear pore complex to promote its disassembly during mitosis (Onischenko et al., 2005). Therefore, any change to the activity of the ras-related nuclear protein signalling pathway could have resulted from the altered cell cycle regulation of the stably transfected clones. The same could be true for the apparent alterations to DNA replication, recombination and repair – this was the top biofunction identified from the proteomic data (Table 5.2) and the canonical pathway with the second-highest overlap p-value (0.0000362) was pyrimidine deoxyribonucleotide *de novo* biosynthesis I, which converts ribonucleotides to deoxyribonucleotides, an important step in DNA synthesis. Interestingly, ribonucleoside-diphosphate reductase large subunit is a key protein in the pyrimidine deoxyribonucleotide *de novo* biosynthesis I pathway and was shown by western blotting to be significantly downregulated in three out of four stably transfected clones compared with $SH\text{-}SY5Y^{Untr}$ (Figure 4.6g). The proteomic data also showed that clones 2E3 and 1G3 expressed lower levels of condensin complex subunit 1 and structural maintenance of chromosomes protein 2, which are components of the condensin complex that reorganises chromatin prior to cell division and is required for effective segregation of sister chromatids (Hagstrom and Meyer, 2003). Reduced expression of these proteins and of ribonucleoside-diphosphate reductase large subunit could be explained by slower cell cycle progression, since the need for DNA synthesis would be reduced and a smaller proportion of cells would be in mitosis at any one time.

5.1.2 Cytoskeletal organisation

Cellular assembly and organisation was the second most overrepresented biofunction and was also strongly represented in the two highest-confidence protein-protein interaction networks generated by IPA (Table 5.2). Table 5.4 specifically highlights the 11 proteins from the dataset of differentially expressed proteins that were in the organisation of cytoplasm subfunction (overlap p-value = 0.0357). This subfunction had a positive activation state z-score of +1.524 and includes many proteins involved in cytoskeletal organisation. Furthermore, three of the top five most upregulated proteins in the proteomic dataset were part of the organisation of cytoplasm subfunction: neuromodulin, vimentin and caldesmon. The accuracies of these expression changes were largely confirmed by western blotting (Figure 4.6b, e & f), although the increased caldesmon expression by clone 1G3 was not statistically significant according to this method of analysis (one-sample t-test: p = 0.065). Vimentin is a class-III intermediate filament protein and is, therefore, an integral part of the cytoskeleton. Changes to vimentin expression can also affect cell shape (Mendez et al., 2010), which is of note given the morphological alterations displayed by clones 1G3 and 1F3 (Figure 3.9d & e). Furthermore, Table 5.2 shows that the cell morphology biofunction was overrepresented among the proteins that were differentially expressed as a result of PrP^{C} transfection. This might indicate that clone 2E3 and, by extension, clone 1B5 may also have differed morphologically from $SH\text{-}SY5Y^{Untr}$ in ways that could not be picked up visually.

Change in expression of the actin-binding protein caldesmon is known to cause dramatic reorganisations of the actin cytoskeleton (Grosheva et al., 2006) and caldesmon can also modulate how cells interact with each other and the extracellular environment. For example, caldesmon binds to myosin to inhibit the formation of focal adhesions, which are connections between cells and the extracellular matrix (Helfman et al., 1999). Additionally, caldesmon overexpression can induce broad lamellipodial protrusions (Grosheva et al., 2006), which bear some similarities to the broad connections between cells that were observed in cultures of clones 1G3 and 1F3 (Figure 3.9d & e).

Protein	Mean expression fold change compared with SH-SY5Y^{Untr}	Predicted effect on function
Caldesmon	+1.81	Affected
Cyclin-dependent kinase 1	-1.59	Affected
Protein 4.1	-1.59	Increased
Lysosomal alpha-glucosidase	+2.75	Affected
Neuromodulin	+2.63	Increased
Unconventional myosin-Ib	-1.70	Affected
Nucleoside diphosphate kinase A	-1.38	Increased
Neuronal cell adhesion molecule	-1.46	Decreased
Regulator of chromosome condensation	-1.65	Affected
Neurosecretory protein VGF	+4.62	Increased
Vimentin	+3.25	Affected

Table 5.4 – Proteins involved in organisation of the cytoplasm showed altered expression upon PrP^{C} transfection

This table shows the 11 proteins in the organisation of the cytoplasm biofunction, as defined by IPA, that were differentially expressed in stably transfected clones 2E3 and 1G3 compared with SH-SY5Y^{Untr}. For each protein, the predicted effect on cytoplasmic organisation of the expression change is reported. "Affected" indicates that IPA could not determine the direction of the effect from the data contained in the Ingenuity Knowledge Base.

Although not appearing in the list of differentially expressed proteins from the proteomic experiments due to not meeting the requirement for the number of quantified unique peptides in one of the replicates, a protein called zyxin was confirmed by western blotting as upregulated in all four clones compared with SH-SY5Y^{Untr} (Figure 4.6c). Like caldesmon, zyxin can be localised to actin bundles, seemingly for repair processes (Smith et al., 2010). Zyxin is also present in focal adhesions and adherens junctions that connect neighbouring cells (Hirata et al., 2008). Altered expression of neuronal cell adhesion molecule in the stably transfected clones provides further evidence suggesting that PrP^{C} can modulate

cell-cell interactions. Furthermore, zyxin appears to have a role in maintaining the integrity of neuritic branches that interact with other cells (Luo et al., 2014). In addition to neurite maintenance, the stably transfected clones exhibited altered expression of proteins involved in neurite outgrowth, a process requiring considerable cytoskeletal remodelling. For example, western blotting analyses showed that neuromodulin, a vital part of the axon growth cone, was upregulated in all four clones compared with SH-SY5Y^{Untr} (Figure 4.6b) and neurosecretory protein VGF, which is also thought to be involved in neuritogenesis (Sakamoto et al., 2015), was the most upregulated protein identified by the proteomic analysis. Indeed, western blotting showed that neurosecretory protein VGF was upregulated by an average of ~15 fold in the stably transfected clones. On the other hand, the pathway analysis suggested that the growth of neurites was largely unchanged by PrP^{C} transfection (5 proteins from the proteomic dataset; overlap p-value = 0.0299; activation state z-score of +0.372) and, as reported previously, clones 1G3 and 1F3 seemed to produce fewer neurite-like protrusions than SH-SY5Y^{Untr} (Figure 3.9d & e). It is unclear why PrP^{C} transfection resulted in proteomic changes associated with increased neurite outgrowth, whilst the actual production of neurite-like protrusions was inhibited.

5.1.3 Ubiquitination

Whilst many of the proteomic changes induced by PrP^{C} transfection can be explained by alterations to cell cycle regulation and cytoskeletal organisation, the third highest-confidence protein-protein interaction network generated by IPA should also be mentioned. Figure 5.1 shows this network, which is centred on polyubiquitin C (UBC) and contains 17 of the proteins that were differentially expressed between the stably transfected clones and SH-SY5Y^{Untr}. UBC is involved in ubiquitination, a post-translational modification that usually targets proteins for degradation. Aside from general degradation of unrequired or damaged proteins, ubiquitination is involved in DNA repair processes and also plays a key role in regulating the expression levels of the cyclins and cyclin-dependent kinases that control the cell cycle (Komander and Rape, 2012). A trivial explanation for generation of this…

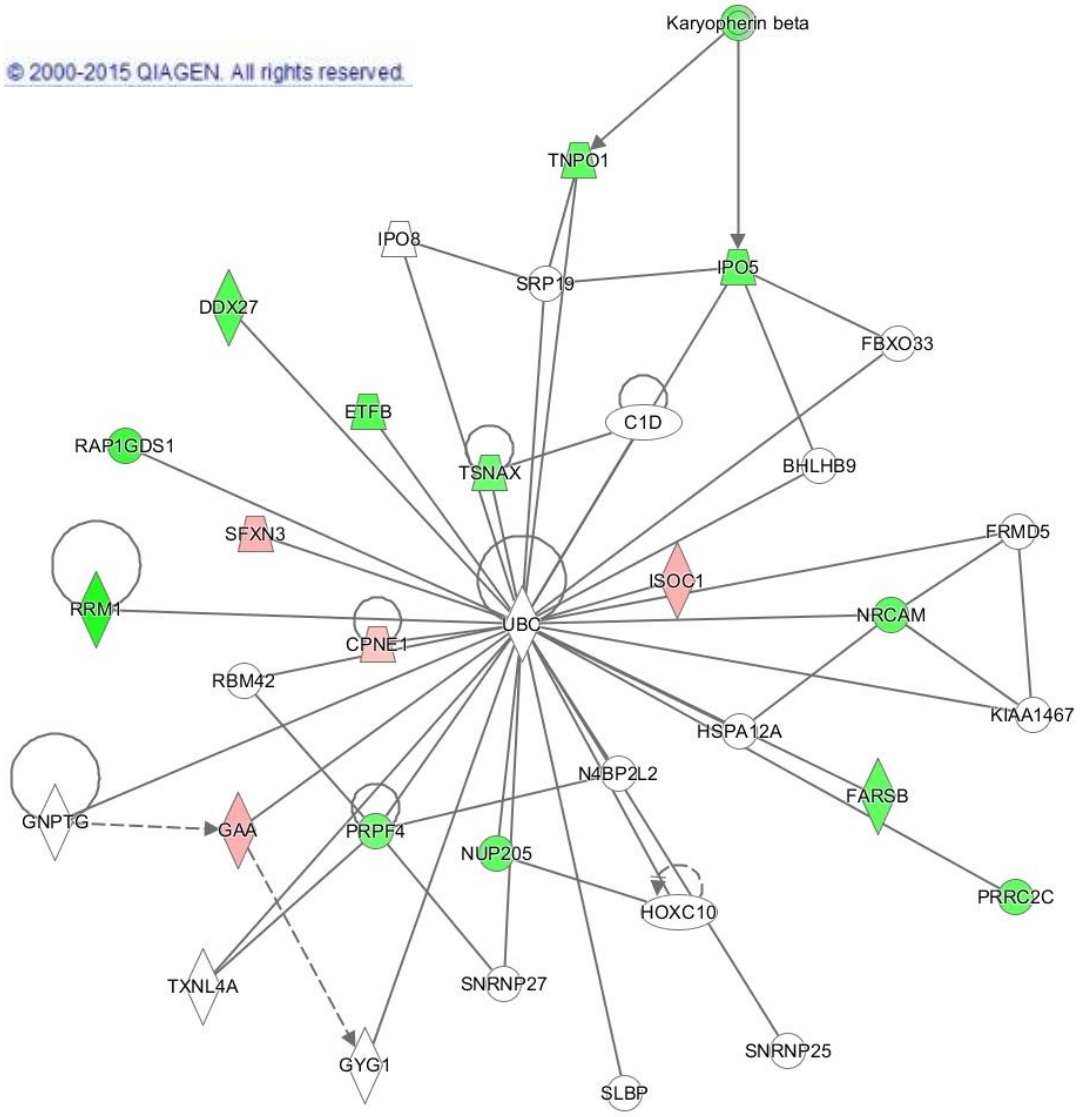

Figure 5.1 – Network generated from the differentially expressed proteins with polyubiquitin C at the centre

This figure shows one of the protein-protein interaction networks generated by IPA from the dataset of proteins that were differentially expressed in the clones 2E3 and 1G3 compared with SH-SY5Y^{Untr}. Experimentally confirmed direct interactions are given by solid lines, indirect interactions by dotted lines. Arrows indicate the direction of regulation i.e. GNPTG upregulates GAA through an indirect interaction. Red-highlighted proteins are those upregulated in the stably transfected clones, green-highlighted proteins were downregulated. An absence of highlighting indicates proteins that were not differentially expressed but were nevertheless highly connected to other proteins in the network.

…network is that IPA simply connected together lots of proteins that can be ubiquitinated and PrP^C is not involved in this process. Nevertheless, given the relatively high network p-score[12] of 35, it seemed possible that PrP^C could modulate overall levels of protein ubiquitination and this is further explored in section 5.4. Another possibility was that any changes to ubiquitination were linked specifically to the apparently altered cell cycle regulation of the stably transfected clones. For example, the nuclear pore complex protein Nup205 is part of the network shown in Figure 5.1, as are three proteins - transportin-1 (TNPO1), importin-5 (IPO5) and karyopherin beta – that are involved in the transport of cargo through the nuclear membrane. Since the nuclear pore complex is disassembled during mitosis, changes to cell cycle progression might affect expression levels of proteins within the complex. These expression changes might have been mediated, at least in part, by differential regulation of ubiquitination of the nuclear pore complex proteins (Hayakawa et al., 2012).

Although not part of the network shown in Figure 5.1, several E3 ubiquitin protein ligases, which are required for transferring ubiquitin to protein substrates, were differentially expressed in the stably transfected clones. For example, pre-mRNA-processing factor 19 (PRPF19) and suppressor of G2 allele of S-phase kinase-associated protein 1 homolog (SUGT1) were both downregulated in clones 2E3 and 1G3 according to the proteomic analyses. Additionally, the expression of E3 ubiquitin-protein ligase BRE1A was assessed by western blotting (see Figure 4.6h) and was shown to be reduced by small but significant amounts in clones 1G3 and 1F3 compared with $SH\text{-}SY5Y^{Untr}$. However, no such downregulation was observed in clones 2E3 and 1B5, suggesting that any expression changes to BRE1A may have been independent of PrP^C expression.

[12] P-scores are the negative logarithms of p-values determined by the right-tailed Fisher exact test.

5.1.4 Cell death and survival

The third most overrepresented biofunction identified by the pathway analysis was cell death and survival. Within the overall category, 11 proteins from the dataset of differentially expressed proteins were part of the cell survival subfunction (overlap p-value = 0.0187), which had an activation z-score of -1.382. Moreover, 25 proteins from the dataset were included in the cell death subfunction (overlap p-value = 0.000862), which had a positive activation z-score (+1.376). These results suggest that the stably transfected clones were less viable than SH-SY5Y^{Untr} under normal culture conditions, which is consistent with the increased sensitivity to serum deprivation that resulted from PrP^{C} transfection (Figure 3.13) and provides further evidence that PrP^{C} expression is not stress-protective in SH-SY5Y cells.

The role of PrP^{C} in the response to stress had already been investigated in detail, as described in Chapters 3 and 4. Therefore, follow-up experiments concentrated on exploring the putative roles of PrP^{C} in cell cycle regulation (section 5.2), cytoskeletal organisation (section 5.3) and protein ubiquitination (section 5.4).

5.2 PrP^C expression inhibits proliferation of SH-SY5Y cells

The altered expression of proteins involved in cell cycle regulation, combined with my own observations from culturing the cells, strongly suggested that PrP^C transfection reduced the proliferation rate of the SH-SY5Y cells. To obtain confirmation that this was the case, the different cell lines were seeded into tissue culture plates at equal densities and allowed to proliferate in standard medium containing foetal bovine serum. Cell counts were performed by staining nuclei with Hoescht 33342, capturing fluorescence images and then using a macro plug-in to the imaging software ImageJ to identify the nuclei and quantify the number of cells in each image. Initial counting was performed ~16 h after seeding to allow cells to adhere to the surface – the presence of floating, non-adherent cells would have disrupted the counting. At this 16 h time point, SH-SY5Y^{Untr} cells were present in slightly greater numbers than the stably transfected clones, although this difference was not significant (Figure 5.2a). However, four days after seeding, the differences in relative cell numbers between SH-SY5Y^{Untr} and the stably transfected clones were much greater and were statistically significant (Figure 5.2b). This confirmed that SH-SY5Y^{Untr} proliferated faster than clones 2E3 and 1G3 and, perhaps, suggests that any differences at 16 h could have been due to some proliferation having already occurred by this point. Additionally, there was no significant difference between the clones in terms of relative cell numbers at Day 4 (one-sample t-test: $p = 0.0673$).

Whilst the results described above seemed clear, a potential confounding factor was the tendency for SH-SY5Y cells to move towards the middle of the well before adhering; this occurred even if the cells were evenly spread over the well surface upon seeding. This was partially controlled for by taking three images per well in exactly the same positions each time. However, to get further confirmation of slower proliferation by the stably transfected clones, an alternative method was employed. This consisted of using the PrestoBlue viability reagent (see Chapter 3 for further information) to quantify the total metabolic activity in each well, which should be proportional to the number of cells present. As before, the cell lines were seeded into plates at equal densities but, this time, cell numbers were measured daily for 6 days.

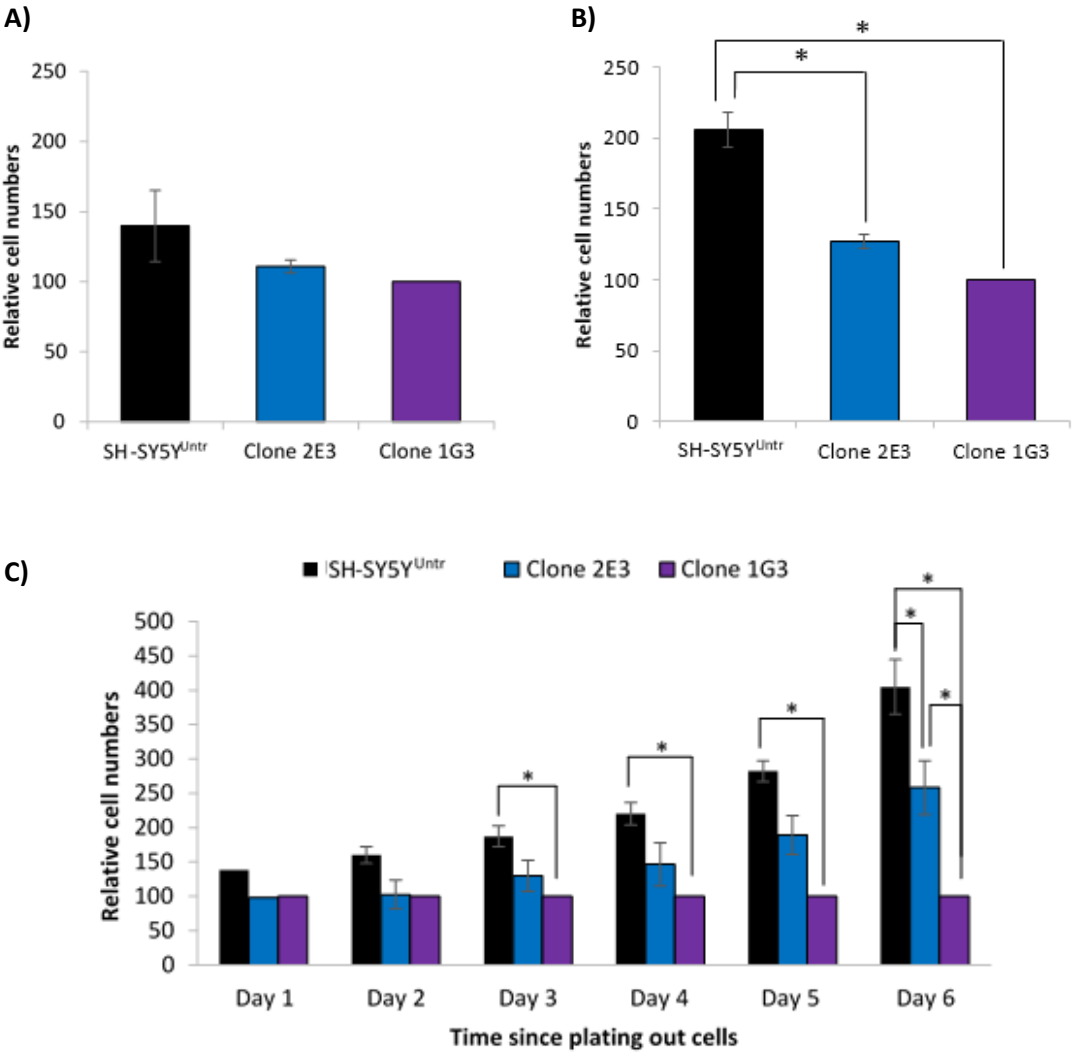

Figure 5.2 – Stably transfected clones proliferated slower than untransfected cells

Bar charts **A** and **B** show relative cell numbers for the different cell lines at 16 h **(A)** and 4 days **(B)** after seeding at equal densities. Nuclear staining followed by automated cell counting from microscope images using ImageJ gave absolute numbers for each cell line, which were then normalised to the slowest-growing line (clone 1G3). Bar chart **C** shows relative cell numbers determined at daily intervals using the PrestoBlue viability reagent instead. The mean normalised values (+/- standard error of the mean) from three **(A & C)** or four **(B)** independent experiments are displayed in the bar charts. Differences in relative cell numbers were tested for significance ($p < 0.05$; indicated with *) using unpaired, two-sample t-tests or one-sample t-tests as appropriate.

Each time point was considered separately, since fluorescence signals obtained on different days could not be accurately compared. The data show that there were significantly more cells in the SH-SY5Y^{Untr} wells than in the clone 1G3 wells from day 3 onwards and this disparity consistently increased over subsequent days (Figure 5.2c). Clone 2E3 proliferated faster than clone 1G3, as shown by a significant difference in relative cell number at day 6. Nonetheless, SH-SY5Y^{Untr} cells were present in significantly greater numbers than both clones at day 6.

Given the potentially PrP^{C}-independent differences in stress responses and morphology between SH-SY5Y^{Untr} and at least some of the stably transfected clones, it was important to confirm that the effect on proliferation was dependent upon PrP^{C}. This was assessed by reverse transfecting the cells either with a negative control siRNA or with the PrP siRNA s72188 – this was performed as described in section 4.1, except that the siRNA dose was increased to 15 nM (from 5 nM) to ensure more effective reduction of PrP^{C} expression. Subsequently, total well metabolic activity was quantified daily over the course of one week using the PrestoBlue viability reagent. Initial findings showed that the transfection procedure was rather toxic to the cells (data not shown), most likely because cells were transfected at low densities (to allow space for proliferation) and sparse cultures are more sensitive to this process. The toxicity manifested in lower total well metabolic activity at Day 1 compared with cells not exposed to the transfection reagent. However, this was not considered an issue, since data from later time points indicated no long-lasting effect on proliferation/viability and, in any case, PrP siRNA-transfected cells could be compared directly with negative control siRNA-transfected cells. Indeed, as would be predicted based on an anti-proliferative role for PrP^{C}, these comparisons showed that PrP^{C} knockdown increased proliferation of clone 1G3 - differences in relative cell numbers compared with negative control siRNA-transfected cultures were significant at 4, 6 and 7 days after seeding at equal densities and the magnitude of the differences increased with time (Figure 5.3c). For clone 2E3, PrP siRNA transfection led to significantly greater cell numbers at day 3, whilst a similar (non-significant) trend could be observed at most other time points (Figure 5.3b), a trend not evident

in the data for SH-SY5Y^{Untr} (Figure 5.3a). These results, therefore, provide reasonable proof that PrP^{C} is a negative regulator of proliferation in SH-SY5Y cells.

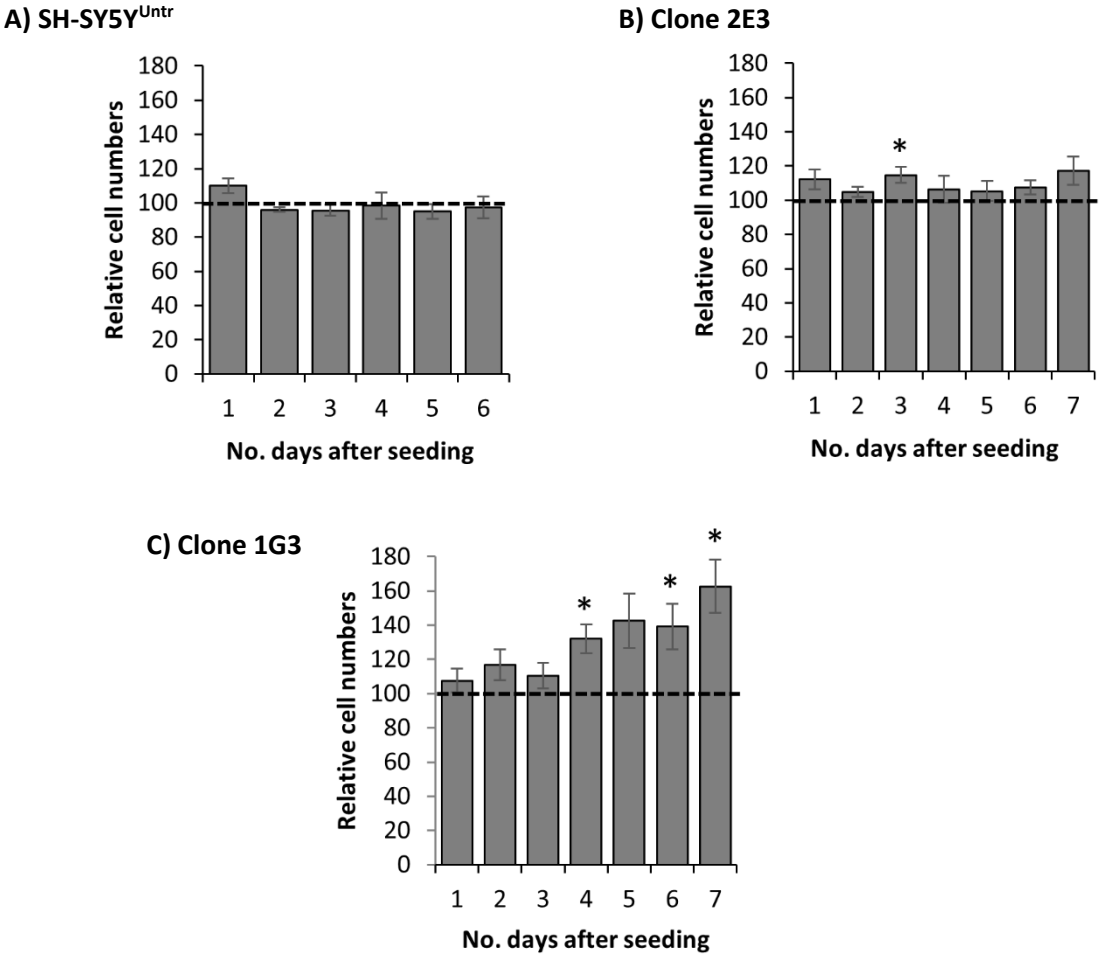

Figure 5.3 – SiRNA-mediated PrP^{C} knockdown enhanced proliferation of clones 2E3 and 1G3

Bar charts showing the cell numbers of PrP siRNA (s72188)-transfected cultures relative to those of negative control siRNA-transfected cultures (marked with dotted line) for the different cell lines at daily intervals after seeding plates at equal densities. Cells were transiently transfected with siRNAs at Day 0 and relative cell numbers were determined using the PrestoBlue viability reagent. The mean normalised values (+/- standard error of the mean) from five independent experiments are displayed in the bar charts. Differences in relative cell numbers were tested for significance ($p < 0.05$; indicated with *) using one-sample t-tests.

One question raised by the proliferation data is why the PrP siRNA was less effective at increasing the proliferation rate of clone 2E3 than that of clone 1G3. Firstly, in the absence of any siRNA transfection, clone 2E3 proliferated faster than clone 1G3 and, therefore, at a rate closer to that of SH-SY5Y^{Untr}, which meant there was less of a difference that could be rescued by knocking down PrP^{C}. Secondly, siRNA-mediated knockdown of expression loses effectiveness over time due to reduction in the siRNA concentration as the cells divide. The degree of PrP^{C} knockdown had been shown previously to be similar for both clones up to 68 h after transfection (Figure 4.3). However, it seemed likely that the faster proliferation rate of clone 2E3 would have caused PrP^{C} expression to begin increasing again earlier than for clone 1G3. To test this, PrP^{C} expression levels in PrP siRNA- and negative control siRNA-transfected cells were compared by western blotting at days 4, 5, 6 and 7 post transfection. Albeit from a single experiment, the data showed that PrP^{C} knockdown was at ~85 % in both clones at Day 4 and PrP^{C} expression began to recover from then onwards (Figure 5.4). Furthermore, at all time points, the percentage knockdown of PrP^{C} expression appeared to be greater for clone 2E3 than clone 1G3, a difference that was most marked at Day 7. This may have contributed towards the relatively limited effect of the PrP siRNA on proliferation of clone 2E3.

The results reported in this section confirm that PrP^{C} acts as a negative regulator of proliferation in SH-SY5Y cells. This is in line with published data from oligodendrocyte precursor cells (Bribian et al., 2012), neuronal cell lines derived from Zurich I PrP^{C}-null mice (Kim et al., 2005) and cells derived from the intestinal epithelium (Morel et al., 2008). Contrastingly, Steele et al. (2006) describe a role for PrP^{C} in promoting proliferation of neural precursors in mouse brain regions that exhibit adult neurogenesis and one study that used a mouse neuroblastoma cell line (N2a) found that PrP^{C} transfection enhanced proliferation (Llorens et al., 2013). This cell type-specificity could be explained by PrP^{C} modulating the cellular response to specific growth factors that different cell types have differing sensitivities to. Intriguingly, Llorens et al. (2013) did identify a potential interaction in N2a cells between PrP^{C} and the epidermal growth factor receptor, and expression of PrP^{C} itself can be induced by other growth factors, including nerve growth factor (NGF)

(Kuwahara et al., 2000; Zawlik et al., 2006) and insulin-like growth factor 1 (Liu et al., 2013). Potential links between PrP^C and growth factor signalling are explored further in Chapter 6.

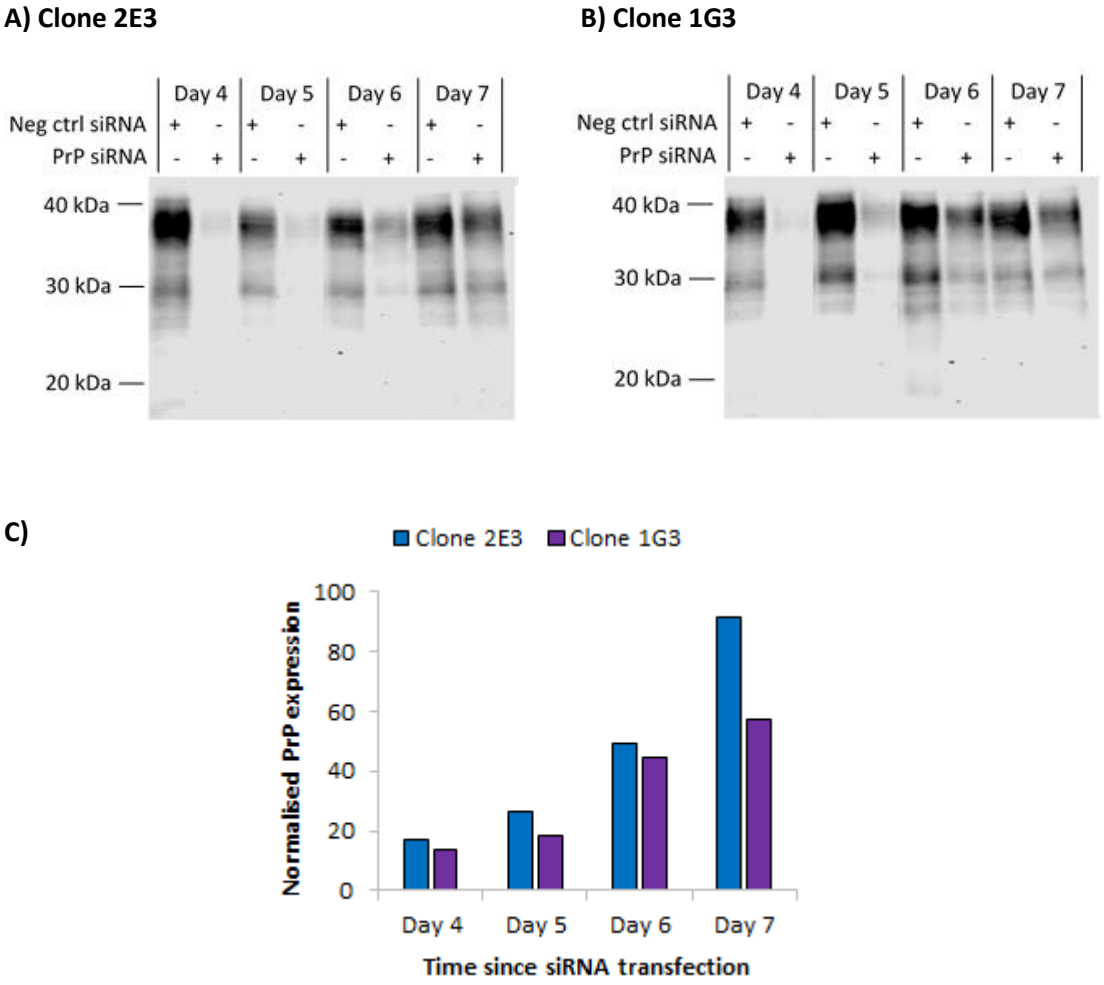

Figure 5.4 – SiRNA-mediated PrP^C knockdown may have lasted for a longer period in clone 1G3 cells compared with clone 2E3

Western blot images and bar chart summarising quantification of PrP^C immunostaining from a single experiment. PrP^C was detected by use of the BC6 anti-PrP^C primary antibody (McCutcheon et al., 2014). Data is shown for clone 2E3 and clone 1G3 lysates that were prepared 4, 5, 6 or 7 days after transient transfection with a negative control siRNA or the PrP siRNA (s72188). After correction for loading errors, data were normalised to the signal from the negative control siRNA-transfected lysate for that time point.

5.3 Further investigating the links between PrP^C and cytoskeletal organisation

5.3.1 Proteins involved in cytoskeletal organisation displayed no significant expression changes in the mouse forebrain as a result of PrP^C knockout

A number of proteins involved in cytoskeletal organisation were differentially expressed in some or all the stably transfected clones compared with SH-SY5Y^{Untr} and, in several cases, the fold changes were large. To investigate the physiological relevance of these data, expression levels of six of these targets – zyxin, vimentin, caldesmon, neuromodulin, annexin A2 and neurosecretory protein VGF - were assessed in PrP^C-null mouse forebrain tissues. The tissues were available from an earlier study carried out by my research group that investigated proteomic and transcriptomic changes induced by PrP^C knockout in mice. These mice are on the 129/Ola background and were originally produced by gene targeting methods in Edinburgh in the early 1990s (Manson et al., 1994) – the knockout line is referred to as "Npu". Age- and sex-matched wild type (129/Ola) and PrP^C-null tissues were available from adult mice of various ages. However, for reasons explained in section 5.5, tissues from mice culled at ~550 days of age were used in this analysis. In the original study, the forebrains were removed and the two hemispheres split apart before freezing in separate tubes. I homogenised 10 half-forebrains of each genotype (five male, five female) and confirmed by western blotting that PrP^C expression was absent in the PrP^C-null tissues (Figure 5.5a). Zyxin was undetectable, which is consistent with previous data from adult mouse brain (Fujita et al., 2009), and, although vimentin could be detected, expression was at an insufficient level for accurate quantification. Caldesmon and neuromodulin were quantifiable but, as shown in Figure 5.5, there was no significant effect of genotype on their expression levels (unpaired, two-sample t-tests: $p = 0.46$ and $p = 0.54$, respectively).

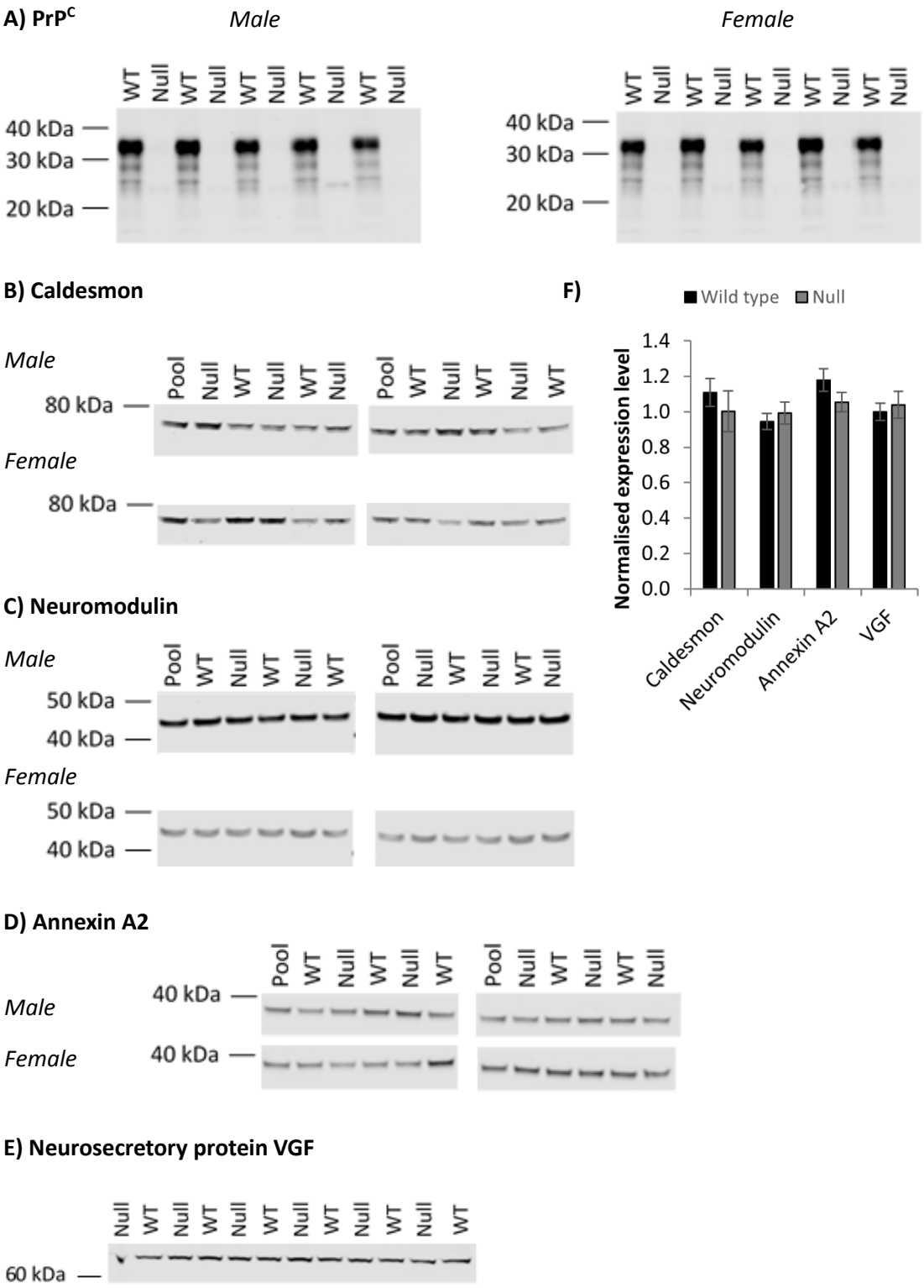

Figure 5.5 – PrP^C knockout did not affect overall mouse forebrain expression of several proteins linked to cytoskeletal organisation

A) Western blot images confirming that PrP^C was detectable in 10 wild type (WT) but not in

10 PrP^C-null mouse forebrain homogenates (5 of each sex for both genotypes). PrP^C was detected by use of the BC6 anti-PrP^C primary antibody (McCutcheon et al., 2014). **B-E)** Representative images of western blots for caldesmon, neuromodulin, annexin A2 and VGF using the same brain homogenates as in **A** (only 6 of each genotype were used when blotting for VGF). Anti-VGF primary antibody was from Abcam (#ab74140); the others were from Cell Signalling Technology and had the following catalogue numbers: #12503 **(B)**, #5307 **(C)** and #8235 **(D)**. **F)** Bar chart summarising quantification of immunostaining for the various protein targets. After correction for loading errors, signals on each blot for caldesmon, neuromodulin or annexin A2 were normalised to a fixed reference sample – a "pool" consisting of equal amounts of all 20 brain homogenates. For each tissue, the mean normalised expression values from at least three technical replicates were calculated. For VGF, the data were normalised to the mean signal from the WT tissues. The far left band in image **E** was not included in quantification due to obvious issues with transfer and/or immunostaining. For all protein targets, overall mean normalised expression values for each genotype were calculated and these are indicated in the bar charts (+/- standard error of the mean). Expression differences between genotypes were tested for significance ($p < 0.05$) using unpaired, two-sample t-tests but no comparisons met the threshold.

Whilst the function of annexin A2 is still poorly understood, it has been implicated in cytoskeletal reorganisation (Singh et al., 2004; Falsey et al., 2006) and was shown by western blotting to be highly upregulated in all four stably transfected clones compared with SH-SY5Y^{Untr} (Figure 4.6a). However, as per the other targets, mouse forebrain expression of annexin A2 was not significantly affected by PrP^C knockout ($p = 0.16$; Figure 5.5). Similarly, neurosecretory protein VGF expression level did not vary with genotype ($p = 0.64$), although these data were obtained from only six wild type and six PrP^C-null tissues due to time constraints.

Whilst these negative results might indicate that PrP^C does not influence cytoskeletal organisation *in vivo*, there are other potential explanations. Firstly, PrP^C expression may have distinct effects depending on the cell type, which could result in changes arising from PrP^C knockout being averaged out over an entire tissue (Mehrabian et al., 2014; Mehrabian et al., 2016). Secondly, the tissues used in these experiments

were from relatively old, adult mice, whereas SH-SY5Y cells are thought to be similar to immature catecholaminergic neurons in terms of phenotype (Kovalevich and Langford, 2013). Therefore, the expression changes seen in SH-SY5Y cells might be replicated only in embryonic or neonatal mouse brains and not in the adult. Thirdly, other studies have identified connections between PrP^C and cytoskeletal organisation before. For example, PrP^C has been proposed to interact directly with annexin A2 (Morel et al., 2008) and vimentin (Zafar et al., 2014; Lappas Gimenez et al., 2015), whilst proteomic analyses of an epithelial cell line showed that PrP^C knockout or knockdown affected expression of annexins as well as cytoskeletal keratins, which are another family of intermediate filament proteins (Mehrabian et al., 2014). Interestingly, induction of PrP^C overexpression in a mouse neuroblastoma cell line downregulated expression of vimentin, as well as other cytoskeletal proteins (Provansal et al., 2010), whereas my experiments showed that vimentin was greatly upregulated in human neuroblastoma cells stably expressing PrP^C.

5.3.2 Alterations to cytoskeletal organisation in clone 1G3 but not in clone 2E3 compared with untransfected SH-SY5Y cells

Whilst several previous studies have identified PrP^C-induced expression changes to proteins involved in cytoskeletal organisation, there has been limited assessment of whether these molecular changes translate into an actual reorganisation of the cytoskeleton. Therefore, I decided to compare the cytoskeletal architectures of $SH\text{-}SY5Y^{Untr}$ and stably transfected clones 2E3 and 1G3 by immunofluorescence staining. Briefly, cells were cultured in optically-clear 96-well plates and fixed 24 hours later. Intermediate filaments and microfilaments were detected using a vimentin antibody and the filamentous actin-binding toxin phalloidin, respectively. After immunostaining, high-magnification z-stack images of the cells were taken using a confocal microscope and maximum intensity projections from these images are shown in Figure 5.6. Overall, the vimentin staining pattern was similar in all cases, although there were subtle differences between clone 1G3 and the other cell lines; specifically, intermediate filaments were visible in the cytoplasm above the…

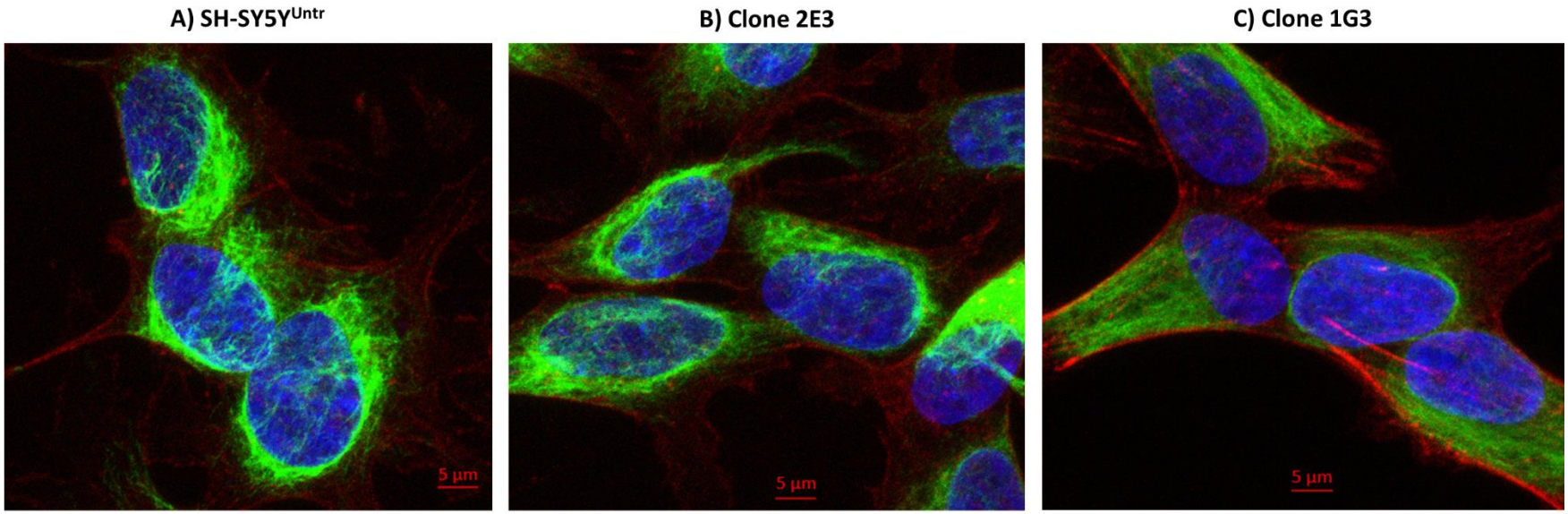

Figure 5.6 – Alterations to actin cytoskeleton in clone 1G3 compared with clone 2E3 and untransfected SH-SY5Y cells

A-C) Confocal images of fixed, saponin-permeabilised SH-SY5Y cells taken using a x63 objective. Nuclei stained with DAPI are shown in blue, vimentin immunostaining in green and phalloidin-stained actin microfilaments in red. The anti-vimentin primary antibody was from Cell Signalling Technology (#5741). Images are maximum intensity projections from z-stacks and microscope settings were adjusted when capturing each image to best reveal the staining. Therefore, variations in signal intensities between images does not necessarily indicate variations in protein expression levels. $SH\text{-}SY5Y^{Untr}$ and clone 2E3 showed similar actin and vimentin staining patterns, whilst the actin microfilaments of clone 1G3 seemed to be organised into thicker bundles.

…nucleus (in the z-plane) for SH-SY5Y^{Untr} and clone 2E3 but not clone 1G3. These data might indicate that the clone 1G3 cells were flatter but, equally, the observable differences may have been an artefact of the imaging process itself. However, whilst SH-SY5Y^{Untr} and clone 2E3 also had similarly organised actin cytoskeletons, clone 1G3 appeared quite different – the broad strands of intense red colour in Figure 5.6c suggested organisation of actin microfilaments into large stress fibres, which are contractile structures required to power processes like cell migration, cell division and neurite outgrowth (Tojkander et al., 2012). These cytoskeletal changes can be explained at the molecular level by downregulation of unconventional myosin-1b (MYO1B; -2.15 fold in proteomic data) and upregulation of non-muscle myosins (+3.25 fold for myosin-9 and +1.68 fold for myosin-10) in clone 1G3 compared with SH-SY5Y^{Untr}. Myosins 9 and 10 are myosin class II proteins, which polymerise into filaments that form stress fibres in conjunction with actin (Tojkander et al., 2012), whilst knockdown of MYO1B reportedly increases the abundance of stress fibres (Makowska et al., 2015). Thick stress fibres, like those found in clone 1G3, are thought to inhibit both cell motility and the ability to undergo shape changes (Tojkander et al., 2012). Indeed, neurite outgrowth seems to require disassembly of stress fibres (Troller and Larsson, 2006), potentially explaining why clone 1G3 produced fewer neurites than the other cell lines (Figure 3.8). Intriguingly, one study found that control, PrP^{C}-expressing 1C11 neuroepithelial progenitor cells displayed reduced actin microfilament stability and enhanced neurite outgrowth compared with cells in which PrP^{C} expression was stably knocked down (Loubet et al., 2012). The authors proposed that PrP^{C} negatively regulates integrin beta-1 signalling, leading to inhibition of the ras homolog gene family, member A (RhoA)/Rho-associated protein kinase (ROCK) pathway that represses neurite outgrowth. Given that integrin beta-1 expression was increased by 2.33 fold in clone 1G3 according to the proteomic data but largely unchanged (+1.21 fold upregulation) in clone 2E3 compared with SH-SY5Y^{Untr}, it may be that enhanced integrin signalling in clone 1G3 led to the formation of thicker, less dynamic stress fibres and reduced levels of neurite outgrowth. Whether this process could have been driven by PrP^{C} expression is unclear given that PrP^{C} inhibited integrin signalling in 1C11 cells (Loubet et al., 2012) and several other studies have also found that PrP^{C} can promote neurite

outgrowth (Lopes et al., 2005; Llorens et al., 2013). However, Loubet et al. (2012) discovered that 1C11 cells overexpressing PrP^C did not extend neurites, which suggests that PrP^C expression may need to be within a certain range for neurite outgrowth to occur. This could explain why clone 2E3 could produce neurite-like protrusions but clone 1G3 could not, since clone 1G3 might have initially expressed more PrP^C than clone 2E3 (see Figure 3.4). Furthermore, in spite of the lack of visual differences between the actin cytoskeletons of clone 2E3 and $SH\text{-}SY5Y^{Untr}$ (Figure 5.6a & b), expression levels of actin-binding proteins zyxin and caldesmon were upregulated in clone 2E3 as they were in clone 1G3 (Figure 4.6c & f), whilst MYO1B was also downregulated in both clones 2E3 and 1G3. The only difference between the clones was that the expression changes were generally of lower magnitude in clone 2E3. Therefore, it is possible that clone 2E3 would have contained thicker stress fibres and produced fewer neurite-like protrusions had the relevant molecular changes been more extreme.

5.4 Further investigating the potential links between PrP^C and ubiquitination

5.4.1 Overall levels of protein ubiquitination in SH-SY5Y cells were unaffected by PrP^C transfection

Pathway analysis of the proteomic changes induced by PrP^C transfection suggested that protein ubiquitination might have been altered in some way in the stably transfected clones. Whilst no clear link between PrP^C and ubiquitination can be made from the literature, deficits in ubiquitination have been shown to precede the neuronal loss and subsequent behavioural changes that occur in TSEs (McKinnon et al., 2016) as well as other neurodegenerative disorders (Figueiredo-Pereira et al., 2015; Opattova et al., 2015). Therefore, protein ubiquitination by the SH-SY5Y cell lines was assessed. As in previous experiments, cells were seeded into tissue culture plates and lysed 24 hours later. Two independently prepared sets of lysates were analysed by western blotting, making use of an antibody that binds to ubiquitin conjugated to proteins as well as the unconjugated form. Figure 5.7a shows the staining pattern obtained – a band at ~8.5 kDa corresponding to monomeric, unconjugated ubiquitin (known as monoubiquitin) and a smear at higher molecular weights indicating detection of ubiquitinated proteins. Although the gaps between lanes for the monoubiquitin bands were difficult to define by eye, the ImageStudio software used for quantification can automatically detect the lane edges based on where the signal intensity drops; therefore, the quantification should have been accurate. Neither the total amount of conjugated ubiquitin nor the abundance of monoubiquitin varied noticeably among clones 2E3, 1B5 and SH-SY5Y^{Untr} (Figure 5.7b & c). By both these measures, ubiquitination appeared slightly reduced in clones 1G3 and 1F3 but there was a great deal of variability between the two replicate sets of cell lysates. In any case, the levels of conjugated ubiquitin and monoubiquitin did not vary significantly between SH-SY5Y^{Untr} and the group of stably transfected clones as a whole (one-sample t-tests; $n = 4$; $p = 0.56$ and $p = 0.18$, respectively).

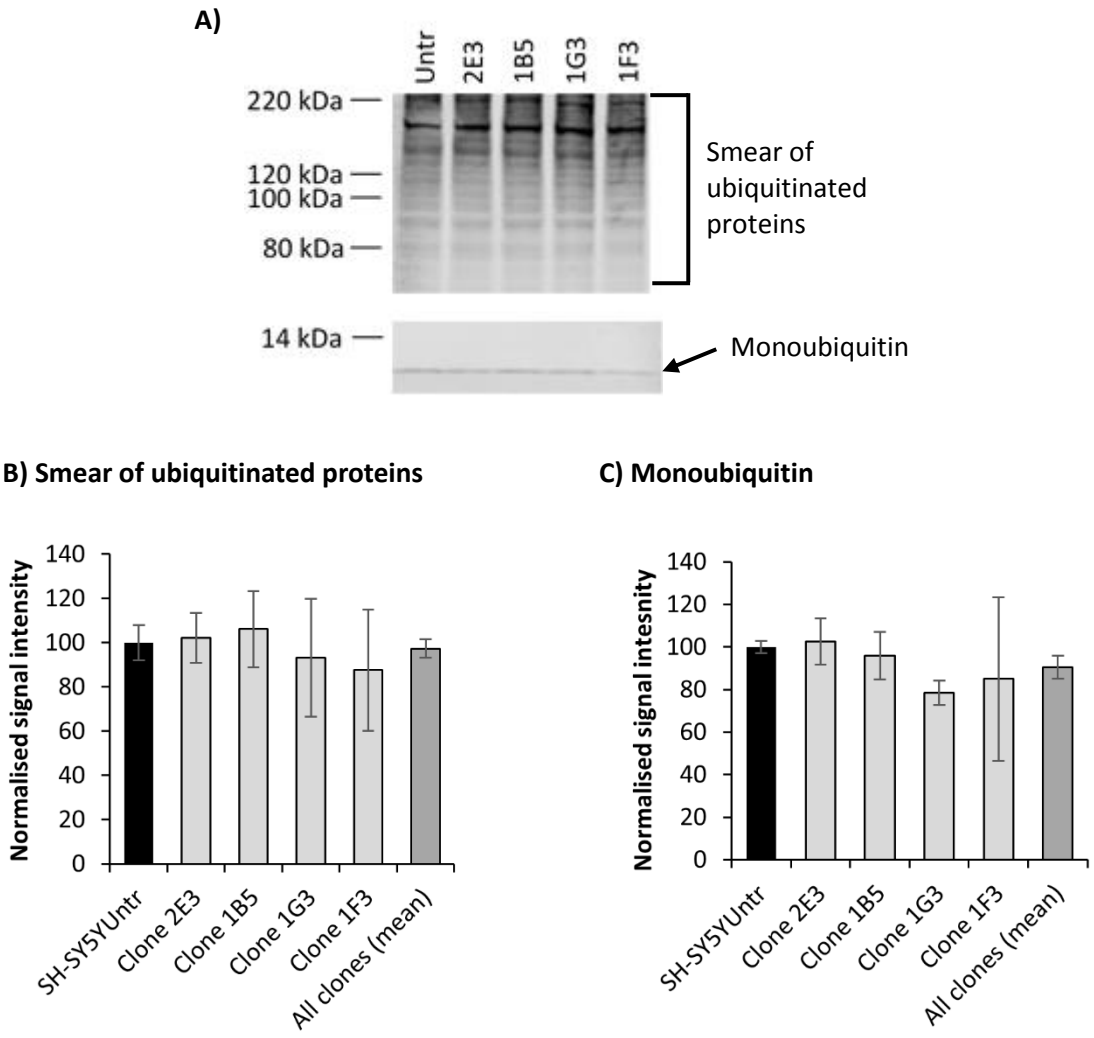

Figure 5.7 – No significant differences in overall protein ubiquitination between untransfected SH-SY5Y cells and stably transfected clones

A) Representative western blot images showing immunostaining of SH-SY5Y cell lysates produced by use of an anti-ubiquitin primary antibody (Millipore #MAB1510). **B & C)** Bar charts summarising quantification of the smear of ubiquitinated proteins (**B**; only quantified staining from 80-200 kDa since bands were extremely faint below 80 kDa) and also monoubiquitin **(C)** from two independently prepared sets of cell lysates. After correction for loading errors, the data were normalised to the signal from the SH-SY5Y^{Untr} lysate. The mean normalised expression values (+/- standard error of the mean) are indicated in the bar charts. There were no clear effects of PrP^{C} transfection on overall protein ubiquitination or levels of free monoubiquitin.

5.4.2 Evidence for regulation of specific ubiquitin ligases by PrP^C

Although it appeared that PrP^C was not regulating protein ubiquitination at a gross level, a more targeted effect was conceivable. One possibility was that PrP^C might regulate ubiquitination of proteins involved in cell cycle progression. Indeed, the aforementioned proteomic analyses showed that E3 ubiquitin-protein ligase SUGT1 was downregulated by 1.39 fold in clone 2E3 and 1.69 fold in clone 1G3 compared with SH-$SY5Y^{Untr}$. SUGT1 is part of the SCF ubiquitin ligase complex, which targets specific cyclins and CDK-regulating proteins for degradation (Kitagawa et al., 1999). Loss of SUGT1 in yeast prevents the G_1/S and G_2/M cell cycle phase transitions (Kitagawa et al., 1999), whilst SUGT1 overexpression is associated with cancer (Iwatsuki et al., 2010). Therefore, reduced SUGT1 expression may have been a consequence of the slower proliferation of the stably transfected clones.

PRPF19 is another E3 ubiquitin-protein ligase that was downregulated in the stably transfected clones (-1.22 fold in clone 2E3 and -1.72 fold in clone 1G3). As a member of the Nineteen complex, PRPF19 is associated with the spliceosome, a large molecular machine that carries out alternative splicing of pre-mRNAs. Splicing factors, such as U4/U6 small nuclear ribonucleoprotein Prp3 are ubiquitinated by PRPF19 in order to modify spliceosome function (Chanarat and Strasser, 2013). Two other proteins involved in pre-mRNA splicing, the U4/U6 small nuclear ribonucleoprotein Prp4 and splicing factor 3A subunit 2, were also downregulated in clones 2E3 and 1G3. However, in addition to its role at the spliceosome, PRPF19 is thought to mediate repair of DNA damage via its interaction with replication protein A (RPA). RPA binds exposed, single-stranded DNA and can recruit ATR-interacting protein (ATRIP), leading to activation of the serine/threonine-protein kinase ATR, which, in turn, initiates various DNA damage response pathways; ubiquitination of the 32 kDa RPA subunit by PRPF19 in response to DNA damage appears to enhance the RPA-ATRIP interaction (Marechal et al., 2014). RPA consists of 70, 32 and 14 kDa subunits, all of which were downregulated in clone 2E3 (-1.35, -1.40

and -1.87 fold, respectively) and clone 1G3 (-1.52, -1.90 and -1.50, respectively[13]) compared with SH-SY5Y^{Untr}. Furthermore, the DNA mismatch repair protein Msh2 was also downregulated in the stably transfected clones (-1.35 fold in clone 2E3 and -1.64 fold in clone 1G3). Overall, it seems likely that the stably transfected clones had reduced spliceosome activity and less active DNA repair processes. Whether these changes were directly controlled by PrP^{C} is unclear; it is conceivable that they were indirect consequences of slower cell cycle progression, for example. One unanswered question is whether less active DNA repair processes led to greater basal levels of DNA damage in the stably transfected clones or, conversely, whether the repair process were downregulated because of reduced damage. The latter argument is supported by previous reports of a role for PrP^{C} in protecting against DNA damage (Senator et al., 2004; Watt et al., 2007; Bravard et al., 2015).

The results presented in this chapter so far have shown that PrP^{C} is a negative regulator of proliferation in SH-SY5Y cells and that PrP^{C} transfection results in altered expression of various proteins involved in cytoskeletal organisation. In one of two clones tested, these molecular changes resulted in modifications to the actin cytoskeleton; specifically, the actin microfilaments of clone 1G3 cells seemed to be organised into fibres that were thicker and, presumably, less dynamic than those of the SH-SY5Y^{Untr} cytoskeleton. Specific E3 ubiquitin-protein ligases involved in pre-mRNA splicing, DNA repair and in modulating the expression of elements of the cell cycle regulatory machinery were also differentially expressed in the stably transfected clones. However, all of these data were obtained from *in vitro* experiments. In contrast, the following section reports on validation of an earlier study to investigate PrP^{C} function that identified protein/gene expression changes resulting from PrP^{C} knockout in mice.

[13] Some of these expression ratios were determined from only two quantified unique peptides and, therefore, may not be particularly reliable.

5.5 Validating proteomic and transcriptomic changes induced by PrP^C knockout in mice

The previous sections of this chapter focused on investigations of PrP^C function in the SH-SY5Y neuroblastoma cell line. To complement the data from the cell model, I returned to an earlier study carried out by my research group that identified proteomic and transcriptomic changes that occurred in the forebrain as a result of PrP^C ablation in mice. The original hypothesis of this study was that the proposed stress-protective role of PrP^C might become more important with age, since oxidative damage and other forms of cellular stress would be expected to build up over time. Therefore, the experiments were designed to examine the molecular changes found in older mice, specifically those culled at either 400 or 700 days old. The proteomic and transcriptomic datasets were combined to generate a list of proteins/genes that were differentially expressed at either or both time points and a subset of these targets was chosen for validation by western blotting. At the time, we were interested in proteins involved in mitochondrial function, neuronal excitability, oxidative stress responses or anti-apoptotic processes, since these were some of the functions most commonly associated with PrP^C in the literature. Antibodies against 17 such proteins were purchased and 11 successfully detected their targets in homogenised forebrain tissues. These were the same homogenates used for quantifying expression of proteins involved in cytoskeletal organisation (see section 5.3.1). However, for the experiments described here, only four wild type and four PrP^C-null forebrain homogenates were analysed (two of each sex for each genotype). Given that the proteomic/transcriptomic data were obtained from mice either 400 or 700 days old, we decided to use forebrain tissues from mice culled in between these time points (~550 days) for initial validation. Data for each of the 11 targets are shown in Figure 5.8 and a summary is provided in Table 5.5. Only two of the 11 targets were confirmed as differentially expressed between wild type and PrP^C-null forebrains; these proteins were connexin-43 and glutamate dehydrogenase 1 (GLUD1), both of which were upregulated as a result of PrP^C knockout (+1.26 and +1.14 fold, respectively). The expression change for connexin-43 was in the same direction as determined by transcriptomic analysis, although the magnitude was much smaller

(4.2 fold upregulation at the mRNA level). For GLUD1, the proteomic analyses gave two opposing fold change estimates (+1.5 and -2.4 in the PrP^C-null tissues). Of the remaining nine targets, only peroxiredoxin-6 and solute carrier family 25 member 36 showed any hints of differential expression by western blotting but these putative changes were not close to significance (unpaired, two-sample t-tests: $p = 0.47$ and $p = 0.34$, respectively).

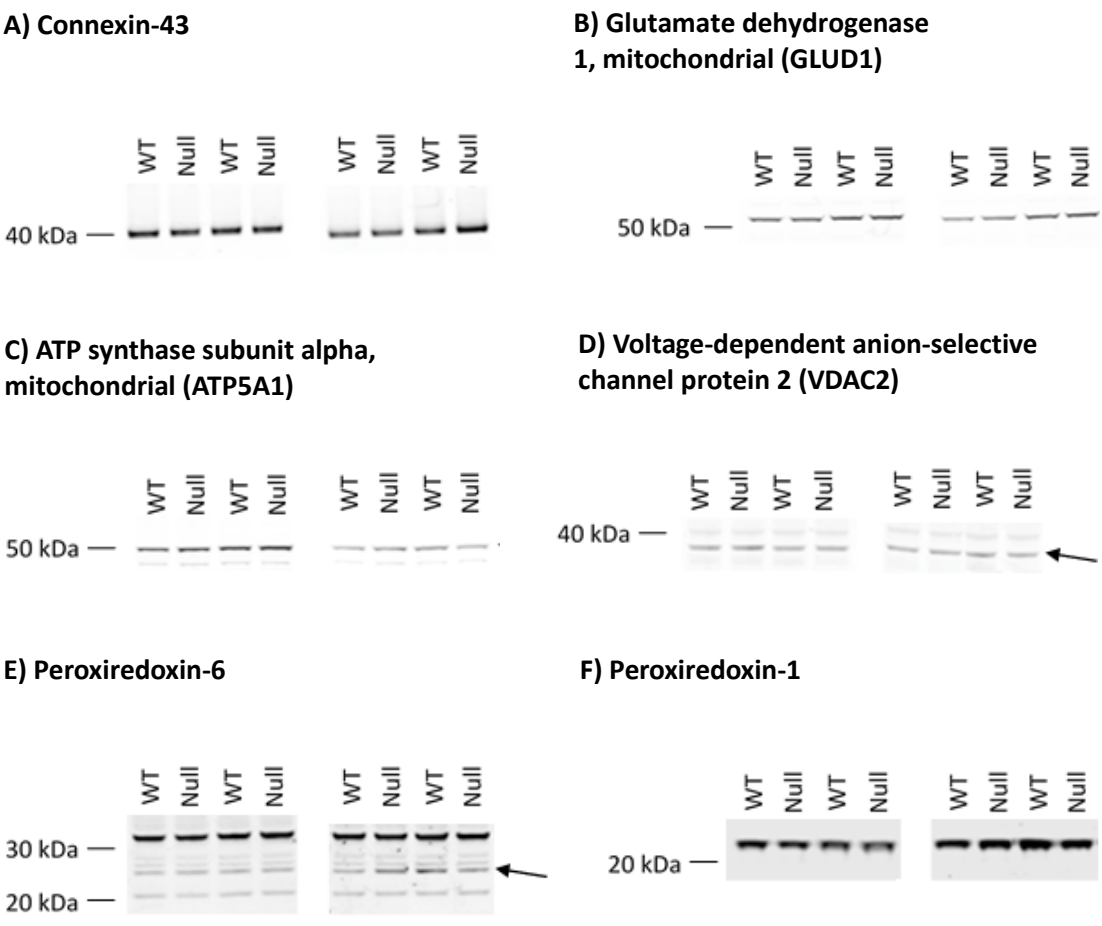

Figure 5.8 – Connexin-43 and glutamate dehydrogenase 1 confirmed as differentially expressed in PrP^C-null mouse forebrains compared with wild type

See following page for legend…

G) Microsomal glutathione S-transferase 3 (MGST3)

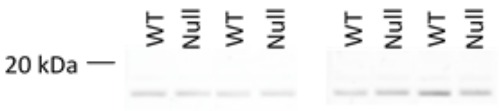

H) Myotubularin

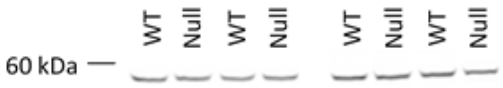

I) SRSF protein kinase 2

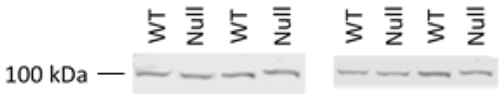

J) Pantothenate kinase 2, mitochondrial (PANK2)

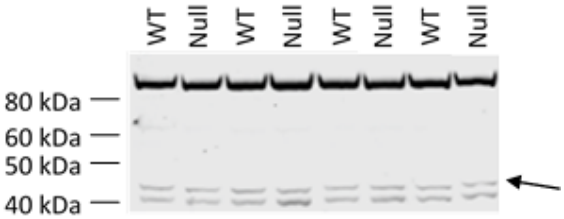

K) Solute carrier family 25 member 36 (SLC25A36)

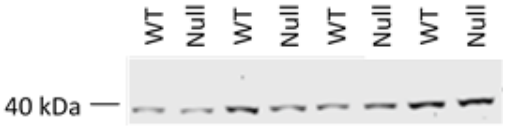

L)

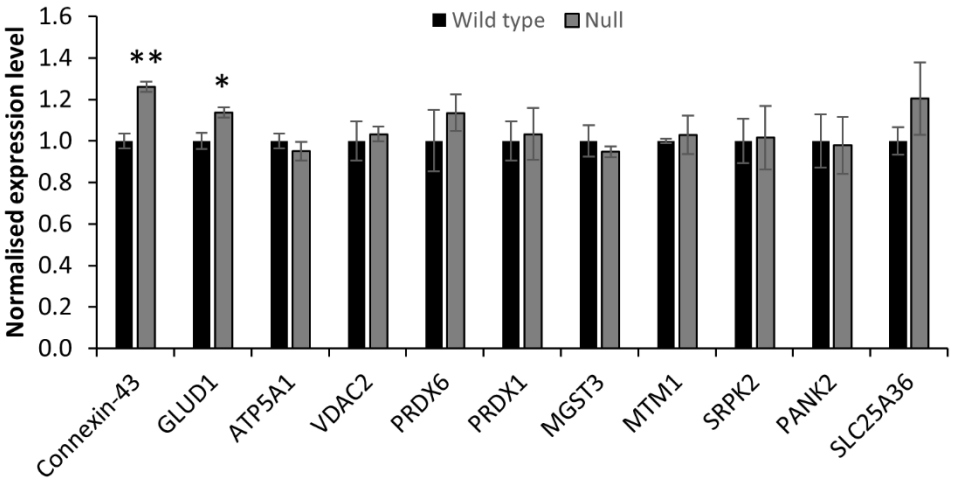

Figure 5.8 – Connexin-43 and glutamate dehydrogenase 1 confirmed as differentially expressed in PrP^{C}-null mouse forebrains compared with wild type controls

A-K) Representative images of western blots for 11 protein targets identified from proteomic and transcriptomic analyses of wild type (WT) and PrP^{C}-null mice. 4 WT and 4 PrP^{C}-null mouse forebrain homogenates were analysed in each case (2 of each sex for both

genotypes). Anti-connexin primary antibody was from Cell Signalling Technology (#3512) and anti-ATP5A1 was from Sigma (#SAB4502040). All the other primary antibodies were from AVIVA Systems Biology and had the following catalogue numbers: #ARP45709 **(B)**, #ARP35124 **(D)**, #ARP48267 **(E)**, #ARP48454 **(F)**, #ARP60342 **(G)**, #ARP56078 **(H)**, #ARP61851 **(I)**, #ARP43984 **(J)**, #ARP43984 **(K)**. **L)** Bar chart summarising quantification of immunostaining for the various protein targets. Arrows in images **D, E** and **J** indicate the bands that were quantified. For each membrane, after correction for loading errors, signals were normalised to the mean signal from the WT homogenates. Next, the mean normalised expression values from at least three technical replicates were calculated for each tissue. Finally, overall mean expression values for each genotype were calculated and these are indicated in the bar charts (+/- standard error of the mean). Expression differences between genotypes were tested for significance ($p < 0.05$) using unpaired, two-sample t-tests. Key: * for $p < 0.05$; ** for $p < 0.01$.

Before considering the implications of the western blotting data, the band patterns obtained by use of the antibodies to peroxiredoxin-6 (Figure 5.8e) and pantothenate kinase 2 (Figure 5.8j) should be explained further. Whilst a strong band was visible at ~33-34 kDa on blots for peroxiredoxin-6, the actual molecular weight of the protein matches the band at 25 kDa and this was also the apparent molecular weight reported by the antibody manufacturer. Therefore, the 25 kDa band was quantified and the identity of the higher molecular weight band remains unknown. The pantothenate kinase 2 antibody strongly detected a protein at ~90 kDa, which approximates to the molecular weight of the related protein pantothenate kinase 4 (92 kDa). Murine pantothenate kinase 2 has a molecular weight of 49 kDa and a previous publication reported detection of the protein at ~47 kDa in whole mouse brain homogenate (Brunetti et al., 2012). Therefore, I considered the fainter 45 kDa band to be pantothenate kinase 2. The higher band was also quantified but, like the 45 kDa band, there was no significant difference between genotypes (data not shown).

	Expression fold change (PrP^C-null vs WT)		
Protein target	**'Omics data (age)**	**P/T**	**Western data**
Connexin-43	+4.2 (700)	T	+1.26 (p = 0.0014)
GLUD1	+1.5/-2.4 (400)	P	+1.14 (p = 0.0306)
ATP5A1	-1.8 (700)	T	-1.05 (n.s)
VDAC2	-1.7 (700)	P	+1.03 (n.s)
Peroxiredoxin-6	-1.4 (700)	P	+1.13 (n.s)
Peroxiredoxin-1	-1.4 (700)	P	+1.03 (n.s)
MGST3	+1.6 (700)	T	-1.06 (n.s)
Myotubularin	+2.0 (700)	T	+1.03 (n.s)
SRSF protein kinase 2	+2.3 (700)	T	+1.02 (n.s)
PANK2	+2.2 (700)	T	-1.02 (n.s)
SLC25A36	+1.9 (700)	T	+1.20 (n.s)

Table 5.5 – Comparison of western blotting and proteomic/transcriptomic data

This table compares 'omics data for the 11 protein targets with the western blot data shown in **Figure 5.8**. Shown are the mean fold changes in expression in PrP^C-null mouse forebrains compared with wild type. The age shown in brackets for the 'omics data is the age in days of the mice at the point of culling. Also indicated is whether the 'omics fold change value came from proteomic (P) or transcriptomic (T) analyses. "n.s." = not significant. Full protein names are given in **Figure 5.8**.

Of the 11 targets analysed by western blotting, seven were chosen based on the transcriptomic data and only one (connexin-43) was validated as differentially expressed in PrP^C-null mouse forebrains at the protein level. This is, perhaps, to be expected, given that changes in mRNA abundance do not always translate into changes at the protein level. Indeed, the mRNA coding for connexin-43 displayed the largest fold change of all those identified from the microarray experiments and yet connexin-43 protein was only 1.26 fold upregulated in the PrP^C-null tissues. Furthermore, a systematic analysis of the transcriptome and proteome of a

mammalian cell line found that only 40 % of the variation in protein level can be explained by variation in mRNA abundance (Schwanhausser et al., 2011). Validation of the proteomic data obtained from mouse forebrain was not much more successful, however – one out of four proteins were confirmed as differentially expressed, whilst the other three were not. This may be a reflection of the relative unreliability of the 2-D gel-based proteomic method that was used for the forebrain tissues. In this approach, following 2-D separation of proteins, the end result is a gel that can be stained to identify protein spots. Images obtained from electrophoresis of different samples can be matched up and densitometric analysis of common spots carried out to detect any differential expression. The proteins present within in a spot can be determined by mass spectrometry but if the same spot contains multiple proteins then the expression ratios obtained will be inaccurate (Steen and Mann, 2004; Abdallah et al., 2012). Additionally, errors can be made when matching up the gel images, resulting in incorrect fold change estimates (Abdallah et al., 2012). These reasons could explain the opposing fold change estimates that were obtained for GLUD1, although it is conceivable that two distinct GLUD1 isoforms were detected.

In spite of the lack of validation of the proteomic/transcriptomic data from PrP^C-null mouse forebrains, it is still of note that the expression levels of two proteins were affected by PrP^C knockout, especially since some published proteomic studies did not identify a single differentially expressed protein in the brains of knockout mice compared with controls (Crecelius et al., 2008; Mehrabian et al., 2016). The upregulation of GLUD1 is intriguing given that it is involved in glutamate metabolism and PrP^C expression has been suggested to protect neurons from glutamate-mediated excitotoxicity (Sakurai-Yamashita et al., 2005; Frigg et al., 2006; Khosravani et al., 2008). Furthermore, GLUD1 can modulate cellular ATP production since it converts L-glutamate into alpha-ketoglutarate, an intermediate in the tricarboxylic acid cycle. Connexin-43, on the other hand, is a member of the connexin family of channel proteins that form cell-cell connections called gap junctions. These junctions provide cytoplasmic connections between neighbouring cells, allowing regulated intercellular transport of molecules (Evans and Martin, 2002). Gap junctions between neighbouring neurons, referred to as electrical

synapses, are widespread in the developing CNS. By allowing ions to flow between cells, electrical synapses enable primitive, synchronised firing of large neuronal networks. As the CNS matures, electrical synapses become rarer and chemical (neurotransmitter-driven) synapses seem to dominate (Arumugam et al., 2005). Therefore, higher connexin-43 expression in the adult forebrain, as was the case for the PrP^C-null mice, could be indicative of impaired maturation of the CNS, which, in turn, could be linked to the subtle learning and memory deficits previously reported in PrP^C-null mice (Bueler et al., 1992; Schmitz et al., 2014).

5.5.1 Altered expression levels of connexin-43 and glutamate dehydrogenase 1 in SH-SY5Y cells following PrP^C transfection

Connexin-43 and GLUD1 expression levels were analysed in the SH-SY5 cell line to investigate if they were altered upon PrP^C transfection in the same manner as they were in the forebrains of PrP^C-null mice. The aim was to obtain further evidence of the physiological relevance of the cell model. Again, as in previous experiments, cells were seeded into tissue culture plates and lysed 24 hours later. Connexin-43 levels were assessed by western blotting of five independently prepared sets of cell lysates and GLUD1 levels were similarly measured using four sets of lysates. Figure 5.9a shows that connexin-43 was dramatically upregulated (+23.2 fold) in clone 1G3 compared with $SH\text{-}SY5Y^{Untr}$. Connexin-43 expression by clone 2E3 was not significantly different from the level in the control cell line, although there was a trend towards upregulation (+4.37 fold; one-sample t-test: $p = 0.053$). Therefore, PrP^C appeared to upregulate connexin-43 expression in the cells, whilst downregulating it in mouse forebrain. This could be explained by the presence of binding sites in the connexin-43 promoter for numerous cell type-specific transcription factors. However, there are also binding sites for ubiquitous transcription factors, such as those activated by MAPK signalling pathways (Oyamada et al., 2013). PrP^C may modulate these pathways differently in SH-SY5Y cells compared with brain, perhaps, as has been suggested previously in this chapter, by affecting the cellular responses to specific growth factors.

A) Connexin-43

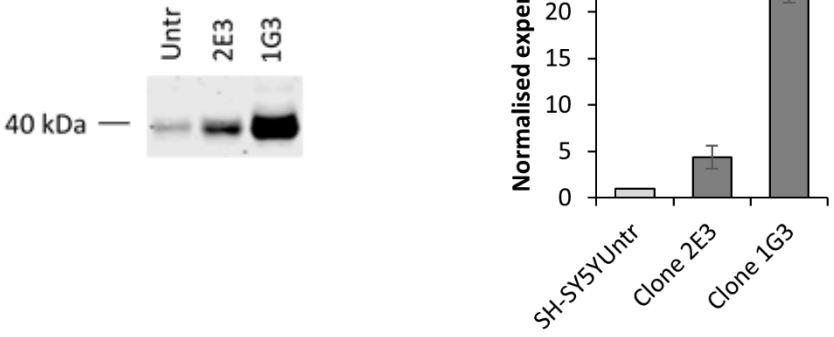

B) Glutamate dehydrogenase 1, mitochondrial

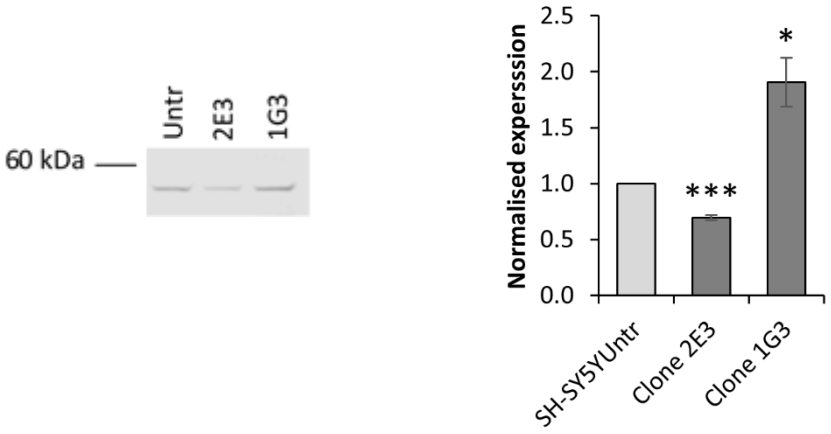

Figure 5.9 – Differential expression of connexin-43 and glutamate dehydrogenase 1 in stably transfected clones compared with untransfected cells

Representative western blot images and bar charts summarising quantification of immunostaining for connexin-43 **(A)** and GLUD1 **(B)** from at least four independently prepared sets of cell lysates. For each membrane, after correction for loading errors, data were normalised to the signal from the SH-SY5Y^{Untr} lane. The mean normalised expression values (+/- standard error of the mean) are displayed in the bar charts. Expression differences between the clones and SH-SY5Y^{Untr} were tested for significance ($p < 0.05$) using one-sample t-tests. Key: * for $p < 0.05$; *** for $p < 0.001$. Anti-connexin primary antibody was from Cell Signalling Technology (#3512) and anti-GLUD1 antibody was from AVIVA Systems Biology (#ARP45709).

Whilst the increased connexin-43 expression and the slower proliferation rate of the stably transfected clones could both have been consequences of altered growth factor signalling, it is possible that connexin-43 expression itself was the driver of the reduced proliferation. Connexin-43 is thought to repress proliferation by inhibiting the expression of S-phase kinase-associated protein 2 (SKP2) via gap junction-dependent and gap junction-independent mechanisms. Interestingly, SPK2 is a member of the same SCF ubiquitin ligase complex as SUGT1 (see section 5.4.2), which was downregulated in the stably transfected clones. SPK2 ubiquitinates cyclin-dependent kinase inhibitor 1B, thereby targeting it for degradation. Therefore, reduced levels of SPK2 lead to increased levels of the CDK inhibitor, in turn resulting in slower cell cycle progression (Zhang et al., 2003). The fact that connexin-43 expression was much less dramatically upregulated in clone 2E3 compared with SH-SY5Y^{Untr} than it was in clone 1G3 could, therefore, explain why clone 2E3 proliferated faster than clone 1G3.

GLUD1 expression was significantly higher in clone 1G3 (+1.91 fold) than in SH-SY5Y^{Untr} but was downregulated by 1.44 fold in clone 2E3 (Figure 5.9b). There is a paucity of information about how GLUD1 expression is regulated, although its activity is known to be enhanced by depletion of cellular ATP stores (Spanaki et al., 2012). If overall GLUD1 expression levels are similarly regulated then the higher expression in clone 1G3 might suggest a faster metabolic rate, since this would lead to quicker depletion of ATP. However, the reduced GLUD1 levels in clone 2E3 compared with SH-SY5Y^{Untr} argues against any regulation of overall metabolic rate by PrP^{C}.

5.6 Discussion

The proteomic datasets reported in section 4.2 of this thesis were combined to identify the proteins that were differentially expressed in stably transfected clones 2E3 and 1G3 compared with SH-SY5Y^{Untr} – we hypothesised that these changes were most likely to have resulted from PrP^C expression. Pathway analysis of these data suggested roles for PrP^C in cell cycle regulation, cytoskeletal organisation and ubiquitination, among other processes. Sections 5.2-5.4 of this chapter covered the follow-up studies that were undertaken to investigate these putative functions of PrP^C.

The stably transfected clones were shown to proliferate slower than the control line and transient knockdown of PrP^C expression using an siRNA partially rescued this phenotype. These results suggest that PrP^C is a negative regulator of proliferation in SH-SY5Y cells. An anti-proliferative role for PrP^C has been identified previously in several cell types (Kim et al., 2005; Morel et al., 2008; Bribian et al., 2012), although other studies have found that PrP^C promotes proliferation of neural precursors and mouse neuroblastoma cells (Steele et al., 2006; Llorens et al., 2013; Haigh and Collins, 2014). Interestingly, although PrP^C transfection did not seem to have affected overall levels of protein ubiquitination in the SH-SY5Y cells, specific ubiquitination processes may have been altered as a consequence of the changes to cell cycle regulation. For example, the E3 ubiquitin-protein ligase SUGT1, which is part of the SCF ubiquitin ligase complex that modulates the expression levels of elements of the cell cycle regulatory machinery, was downregulated in clones 2E3 and 1G3 compared with the control line.

Pathway analysis of the proteomic changes induced by PrP^C transfection suggested that proteins involved in cytoskeletal organisation were overrepresented. The upregulation of caldesmon expression in the stably transfected clones was particularly striking, since the protein is reportedly involved in Schwann cell migration during peripheral nerve regeneration (Han et al., 2007) and an adult-onset demyelination of the PNS has been observed in several PrP^C knockout mouse lines

(Bremer et al., 2010; Nuvolone et al., 2016). The intermediate filament protein vimentin was also upregulated in the clones but confocal analyses of the cells did not uncover obvious changes in the distribution of vimentin staining as a result of the differential expression. In contrast, changes to the actin cytoskeleton were evident in clone 1G3; specifically, the actin microfilaments seemed to be organised into fibres that were thicker than those of the SH-SY5Y^{Untr} cytoskeleton. Thicker actin stress fibres are associated with greater cytoskeletal stability and inhibition of neurite outgrowth (O'Connor et al., 1990; Troller and Larsson, 2006), which could explain why clone 1G3 (and clone 1F3) produced fewer neurite-like protrusions than the other lines, as was reported in Chapter 3. The alterations to the actin cytoskeleton that were observed in clone 1G3 may have been due to greater activation of the RhoA-ROCK pathway, which PrP^{C} has previously been reported to modulate (Loubet et al., 2012). However, this is not a complete explanation since this pathway is reported to promote proliferation (Yu and Brown, 2015) and yet clone 1G3 proliferated slower than SH-SY5Y^{Untr}. Interestingly, whilst the actin cytoskeleton of clone 2E3 appeared grossly similar to that of the control line, some of the molecular changes underlying the altered cytoskeletal architecture of clone 1G3 were shared by clone 2E3. The difference between the clones was that these expression changes were generally less dramatic in clone 2E3. Therefore, it is possible that clone 2E3 cells would have contained thicker stress fibres and produced fewer neurite-like protrusions had the relevant molecular changes been of greater magnitudes.

In spite of the apparent inhibition of neurite outgrowth in clone 1G3, several proteins that positively correlate with neurite outgrowth – annexin A2, neurosecretory protein VGF, zyxin and neuromodulin – were upregulated in all four stably transfected clones compared with SH-SY5Y^{Untr}. These molecular changes are in line with previous reports that PrP^{C} expression can promote neurite outgrowth (Graner et al., 2000; Loubet et al., 2012). Furthermore, a recent proteomic study found that the expression levels of neuromodulin and another component of the axonal growth cone, brain acid soluble protein 1, were perturbed by knockout or knockdown of PrP^{C} expression in more than one cell model (Mehrabian et al., 2016). It is unclear why PrP^{C} transfection resulted in proteomic alterations associated with increased

neurite outgrowth, whilst simultaneously causing molecular changes linked to its repression.

To complement the data obtained from the SH-SY5Y cell model, I followed up previous work carried out by my research group that had identified proteomic and transcriptomic changes that occurred in the forebrain as a result of PrP^C ablation in mice. A subset of targets from this study was chosen for validation by western blotting and, although the success of this was mixed at best, two proteins – GLUD1 and connexin-43 – were confirmed as upregulated in PrP^C-null tissues compared with wild type controls. Importantly, these forebrain tissues were from the Npu line of knockout mice, which is free from the issues of *Prnp* genotype-independent polymorphisms in neighbouring genes and ectopic doppel expression in the brain that affect some of the other knockout lines. Consequently, the differential expression of connexin-43 and GLUD1 is highly likely to have been caused by an absence of PrP^C expression. The increase in GLUD1 expression is of note given its role in glutamate metabolism and the previously reported role of PrP^C in protecting neurons from glutamate-mediated excitotoxicity (Sakurai-Yamashita et al., 2005; Frigg et al., 2006; Khosravani et al., 2008). Additionally, the upregulation of connexin-43 suggests that the PrP^C-null forebrains may have had a greater density of electrical synapses, perhaps reflecting a subtle impairment to the maturation of the CNS as a result of PrP^C knockout (Ben-Ari, 2001; Arumugam et al., 2005). This provides a potential alternative explanation for the reported deficits in learning and memory of PrP^C-null mice (Bueler et al., 1992; Schmitz et al., 2014). Furthermore, connexin-43 is thought to indirectly regulate cell cycle progression by affecting the expression of a subunit of the SCF ubiquitin ligase complex. Therefore, increased expression of connexin-43 in the PrP^C-null forebrain might indicate that PrP^C has a role in regulating proliferation *in vivo* as well as *in vitro*.

The results presented in this chapter show that the proliferation rate of SH-SY5Y cells was inhibited by PrP^C transfection and it appeared that the differential expression of specific ubiquitin ligases may have resulted from the changes to cell cycle regulation. One explanation for the ability of PrP^C to regulate proliferation is

that it modulates the cellular responses to specific growth factors. Growth factors can promote differentiation processes, which may involve changes to cell shape, potentially requiring reorganisation of cytoskeletal architecture. Therefore, the differential expression of proteins involved in cytoskeletal organisation that was observed in the stably transfected clones may have resulted from some kind of differentiation process. Links between PrP^C and growth factor signalling have been made before, although the evidence is rather limited. For example, PrP^C has been proposed to interact with the receptor for epidermal growth factor, thereby altering its responsiveness to its ligand (Llorens et al., 2013). PrP^C expression can also be induced by growth factors, such as NGF (Kuwahara et al., 2000; Zawlik et al., 2006) and insulin-like growth factor 1 (Liu et al., 2013). The putative connections between PrP^C and growth factor signalling are explored in more detail in Chapter 6.

Chapter 6: Investigating the links between PrP^C and growth factor signalling

6.1 Identifying upstream regulators of the proteomic changes induced by PrP^C transfection

Chapter 5 focused on the downstream consequences of transfecting the *Prnp* CDS into SH-SY5Y cells. The main findings were altered expression of various proteins linked to cytoskeletal organisation and slower proliferation of the stably transfected clones compared with $SH\text{-}SY5Y^{Untr}$. A potential explanation for these effects was that PrP^C was modulating the cellular response to specific growth factors, either those present in the foetal bovine serum (FBS) used to supplement the culture medium or any synthesised by the cells themselves. This hypothesis is supported by a small number of previous studies that have made connections between PrP^C and growth factor signalling. For example, PrP^C was shown to interact with the receptor for epidermal growth factor, thereby altering its responsiveness to its ligand (Llorens et al., 2013). PrP^C expression can also be induced by growth factors, such as NGF (Kuwahara et al., 2000; Zawlik et al., 2006) and insulin-like growth factor 1 (Liu et al., 2013).

This chapter covers the work carried out to determine the links between PrP^C and growth factor signalling. As a starting point, I returned to the dataset of proteins with altered expression levels in stably transfected clones 2E3 and 1G3 compared with $SH\text{-}SY5Y^{Untr}$ (Table 5.1). As described in detail in section 5.1, IPA was used for pathway analysis of this proteomic dataset. The core analysis suite of the software includes a feature that identifies the most likely upstream regulators of the proteomic changes. These regulator molecules could be transcription factors, proteins kinases, growth factors, microRNAs, endogenous chemicals, drugs etc. In a similar manner to other IPA features, the right-tailed Fisher exact test is used to determine whether there is significant ($p < 0.01$) overlap between the proteins/genes in the uploaded dataset and the proteins/genes that are known targets of the upstream regulator. If sufficient directional information about the interaction between a regulator and its target is available within the database used by the software (the Ingenuity Knowledge Base) then IPA can also predict whether the regulator molecule is more activated or more inhibited based on the expression change of the target protein/gene. IPA

combines these predictions for all the targets present in the uploaded dataset to generate an activation state z-score for the upstream regulator; these scores represent the degree of confidence that a particular regulator molecule is activated (positive value) or inhibited (negative value). Z-scores > 2 or < -2 are generally considered statistically significant but upstream regulators not meeting these thresholds might still warrant further investigation.

Table 6.1 reports the highest confidence upstream regulators of the PrP^{C} transfection-induced proteomic changes observed in SH-SY5Y cells. Following exclusion of chemical toxicants or drugs, which were considered irrelevant for this analysis, the top regulators, ranked by overlap p-value, are shown. Lower-ranked regulator molecules were not considered worthy of follow-up since most targeted only one or two of the 60 differentially expressed proteins in the dataset. A systematic search using the protein database Uniprot showed that many of the putative upstream regulators were involved in cell cycle regulation. For example, Table 6.1 contains members 1, 3, 4 and 5 of the E2F transcription factor family. E2Fs 1 and 3 are activators of cell cycle progression, whilst E2Fs 4 and 5 are repressors. E2F1 had the smallest overlap p-value of all the entries in Table 6.1 and was predicted to be less active in the stably transfected clones than $SH\text{-}SY5Y^{Untr}$ (activation state z-score of -1.710), as would be expected given the inhibitory effect of PrP^{C} expression on SH-SY5Y proliferation that was reported in section 5.2. The second-ranked upstream regulator, myc proto-oncogene protein, another positive regulator of proliferation, was also predicted to be inhibited in the stably transfected clones compared with $SH\text{-}SY5Y^{Untr}$. Additional putative upstream regulators involved in cell cycle regulation included the transcription factors retinoblastoma-like protein 1, T-box transcription factor TBX2 and N-myc proto-oncogene protein as well as protein kinases like ribosomal protein S6 kinase beta-1 and cyclin-dependent kinase inhibitor 1. However, since these proteins reside in the cytoplasm and/or nucleus, direct interactions with the mainly cell surface-associated PrP^{C} seemed unlikely; much more plausible were interactions with receptors (such as those for growth factors) at the cell membrane. For this reason as well as the potential link between…

Upstream regulator	Molecule type	Overlap p-value	Activation z-score	Target molecules in dataset
Transcription factor E2F1	Transcription regulator	1.36E-08	-1.710 (B)	11
Myc proto-oncogene protein	Transcription regulator	1.38E-06	-2.017	13
Transcription factor E2F4	Transcription regulator	1.78E-06	-	7
Hepatocyte nuclear factor 4-alpha	Transcription regulator	1.01E-05	-	17
Retinoblastoma-like protein 1	Transcription regulator	3.64E-05	-	4
T-box transcription factor TBX2	Transcription regulator	4.51E-05	-2.000	4
Protein max	Transcription regulator	6.41E-05	-	4
Heat shock factor protein 2	Transcription regulator	6.61E-05	-	3
Transcription factor AP-1	Transcription regulator	9.02E-05	-0.434 (B)	7
DNA (cytosine-5) methyltransferase 3B	Enzyme	9.21E-05	0.000	4
Vascular endothelial growth factor receptor 2	Kinase	1.15E-04	-	3
Osteonectin	Other	1.93E-04	2.000	4
Inosine	Chemical - endogenous mammalian	3.26E-04	-	3
Prostaglandin E synthase 3	Enzyme	3.45E-04	-	3
N-myc proto-oncogene protein	Transcription regulator	4.31E-04	-1.969	5
Let-7	MicroRNA	4.49E-04	0.555 (B)	4
Nuclear transcription factor Y	Transcription regulator	6.62E-04	-	5

Table 6.1 – Potential upstream regulators of the proteomic changes induced by PrP^C transfection

See following page for legend…

Upstream regulator	Molecule type	Overlap p-value	Activation z-score	Target molecules in dataset
Butyric acid	Chemical - endogenous mammalian	7.70E-04	-1.206	6
Transforming growth factor beta-1	Growth factor	8.71E-04	0.571	12
Tumor protein 63	Transcription regulator	8.88E-04	-1.069	5
Transcription factor E2F3	Transcription regulator	9.73E-04	-	3
Heat shock factor protein 1	Transcription regulator	1.20E-03	-2.000	4
Sphingosine-1-phosphate	Chemical - endogenous mammalian	1.22E-03	-	3
Nerve growth factor	Growth factor	1.31E-03	1.944 (B)	4
Ribosomal protein S6 kinase beta-1	Group	1.37E-03	-	2
Transcription factor E2F5	Transcription regulator	1.51E-03	-	2
Platelet-derived growth factor-AA	Complex	1.65E-03	-	2
Cyclin-dependent kinase inhibitor 1	Kinase	2.57E-03	-	4

Table 6.1 – Potential upstream regulators of the proteomic changes induced by PrP^{C} transfection

This table shows the molecules that IPA calculated to be the most likely upstream regulators of the PrP^{C} transfection-induced proteomic changes to the SH-SY5Y cells. Irrelevant entires (chemical drugs and toxicants) were removed from the list and are not shown. Ranking is based upon overlap p-value (right-tailed Fisher exact test for overrepresentation of the targets of the upstream regulator among the differentially expressed proteins). If IPA had sufficient directional information about the interactions between the upstream regulator and its targets in the dataset then an activation state z-score was calculated; these scores indicate the degree of confidence for increased (positive value) or decreased activation (negative value) of the putative upstream regulators. (B) indicates a biased z-score estimate, which can occur if a dataset contains greatly different numbers of upregulated and downregulated proteins (as was the case for this dataset).

…PrP^C and growth factor signalling that was suggested by the effect of PrP^C transfection on proliferation, the two growth factors present in Table 6.1, transforming growth factor beta-1 (TGFB1) and NGF, were of more interest. TGFB1 modulates proliferation, differentiation and other processes in various cell types (Massague, 2012) and 12 targets of TGFB1 signalling were among the proteins differentially expressed upon PrP^C transfection. Additionally, PrP^C reportedly modulates epithelial-mesenchymal transition processes driven by TGFB1 (Mehrabian et al., 2015) and potentially interacts directly with TGFB1 itself (Lappas Gimenez et al., 2015). However, of the 12 TGFB1 targets in the dataset, IPA determined that the expression changes to three proteins suggested activation of TGFB1, expression changes to a further two suggested inhibition and no predictions could be made from the remaining seven due to insufficient directional information about the interactions. Because of these data, the activation state z-score calculated for TGFB1 was not greatly different from zero (+0.571). Therefore, the proteomic alterations in the stably transfected clones were not obviously consistent with PrP^C enhancing or repressing TGFB1 signalling. NGF was, however, a better candidate. Although only four direct targets of NGF signalling were present in the dataset of differentially expressed proteins, these did include three of the five most upregulated proteins: neurosecretory protein VGF, neuromodulin and annexin A2 (see Table 5.1), which are all implicated in neurite outgrowth and/or cytoskeletal remodelling processes (Singh et al., 2004; Falsey et al., 2006; Sakamoto et al., 2015). CDK1, which was downregulated in the stably transfected clones and plays a key role in regulating the cell cycle (Santamaria et al., 2007), is also a target of NGF signalling. Furthermore, the directionality of the expression changes to the four NGF targets in the dataset all suggested activation of NGF signalling (overall activation state z-score for NGF of +1.944). These findings indicated that the slower proliferation of the stably transfected clones and at least some of the expression changes to proteins involved in cytoskeletal organisation or remodelling could be explained by PrP^C modulating NGF signalling pathways. Although there has been no direct evidence of such a role for PrP^C, as far as I am aware, a recent study found that PrP^C and TrkA, the high affinity receptor for NGF, both appear to interact with the ganglioside GM1 within lipid rafts (Mantuano et al., 2014). The authors proposed that PrP^C, TrkA,

GM1 and lipoprotein receptor-related protein-1 form a multimolecular complex that modulates neurite outgrowth and other cell signalling processes in neurons.

Before further exploring the putative connection between PrP^C and NGF signalling in the SH-SY5Y cells, we attempted to obtain additional evidence of the involvement of PrP^C in the pathway. The approach taken was to identify the genes with similar spatial expression patterns to *PRNP in vivo*, since genes are likely to be involved in the same processes as other genes that are similarly regulated. The following section summarises the results obtained from this analysis.

6.2 Investigating the genes displaying similar spatial expression patterns to *PRNP in vivo*

Upstream analysis of the proteomic changes induced by PrP^C transfection into SH-SY5Y cells suggested that the protein might modulate NGF signalling. To my knowledge, no direct effect of PrP^C on NGF signalling has been reported previously, although NGF does appear to induce PrP^C expression in neuronal cell lines (Kuwahara et al., 2000; Zawlik et al., 2006) and PrP^C has been proposed to be part of a multimolecular complex also containing the NGF receptor TrkA (Mantuano et al., 2014). To obtain further evidence of the processes potentially involving PrP^C, I aimed to identify the genes with similar spatial expression patterns to *PRNP in vivo*, since genes are likely to be involved in the same processes as other genes that are similarly regulated. Two publically available microarray datasets, both originally reported by Su et al. (2004), were used for this purpose: the GeneAtlas GNF1M and U133A datasets, which were both accessed through the BioGPS gene annotation portal (Wu et al., 2016). The GNF1M and U133A datasets contained baseline gene expression data from 61 young adult (2-3 month old) mouse tissues and 79 human tissues, respectively. The correlation tool on the BioGPS website was used to select those genes that were highly correlated[14] with *PRNP* in terms of their expression patterns (Pearson correlation coefficient > 0.75). Although neither NGF nor its receptors were among the highly coexpressed genes, the datasets were analysed using IPA to determine whether genes involved in NGF signalling or related pathways were overrepresented. IPA identified 267 analysis-ready genes for the mouse and 113 for the human coexpression datasets. These figures exclude any unannotated genes and duplicate entries (i.e. multiple microarray probes corresponding to the same gene) that were in the original data. Full tables of the analysis-ready genes are provided in Appendix III.

The IPA core analysis suite has a number of features, including those that identify the canonical pathways and molecular and cellular functions that are most

[14] Data from two microarray probes for detection of *PRNP* mRNA were available from the U133A dataset. For this thesis, data from the 201300_s_at probe was used.

overrepresented among the proteins/genes in the uploaded dataset. Canonical pathways are standard, well-characterised signalling pathways, whereas molecular and cellular functions are groupings of genes with similar functions, according to the Ingenuity Knowledge Base. Table 6.2 shows the top five canonical pathways and molecular and cellular functions identified from the genes that were highly coexpressed with *Prnp* in the mouse. The ranking is based upon overlap p-value (right-tailed Fisher exact test), which represents the statistical significance of the overrepresentation of the members of the pathway or function among the genes in the dataset. Most of the top canonical pathways identified were those important in the nervous system, as would be predicted from the high neuronal expression of PrP^C (Linden et al., 2008). The canonical pathway with the smallest overlap p-value was cyclin-dependent kinase 5 signalling, which regulates processes like neuronal migration and differentiation as well as synaptic development and function (Cheung and Ip, 2012). Cyclin-dependent kinase 5 is also vital for repressing cell cycle progression in neurons, thereby maintaining their post-mitotic state. This connection is striking given the links between PrP^C and proliferation of neuronal cells that have been reported in this thesis and elsewhere (Kim et al., 2005; Steele et al., 2006; Llorens et al., 2013). The fourth- and fifth-ranked canonical pathway identified from the mouse and human coexpression datasets, respectively, was melatonin signalling - melatonin is a hormone secreted by the pineal gland that plays a key role in regulating circadian rhythm. This result is in line with the disrupted circadian oscillation of melatonin production (Brown et al., 2002) and altered sleep patterns (Tobler et al., 1996; Sanchez-Alavez et al., 2007) that have been observed in PrP^C-null mice. Interestingly, the U133A transcriptomic data also indicates that the mRNA encoding the high affinity NGF receptor TrkA is expressed in the human pineal gland at much higher levels than in any other tissue.

The top five molecular and cellular functions identified from the genes highly coexpressed with *PRNP* in human tissues (Table 6.3) included three of the five most overrepresented functions among the proteins differentially expressed in…

Top molecular and cellular functions	p-values	# proteins	Proportion of dataset
Cell-to-cell signalling and interaction	5.13E-03 – 3.57E-20	80	30 %
Cellular development	4.60E-03 – 1.11E-12	65	24 %
Cellular assembly and organisation	4.92E-03 – 2.97E-12	95	36 %
Cellular function and maintenance	5.24E-03 – 2.97E-12	99	37 %
Cellular movement	5.12E-03 – 3.43E-11	31	12 %
Top canonical pathways	**p-value**	**Overlap**	
Cyclin-dependent-like kinase 5 signalling	3.27E-07	10/99 (10.1 %)	
Reelin signalling in neurons	4.56E-07	9/79 (11.4 %)	
Interleukin-1 signalling	1.53E-06	9/91 (9.9 %)	
Melatonin signalling	1.96E-06	8/70 (11.4 %)	
Amyloid processing	2.49E-06	7/51 (13.7 %)	

Table 6.2 – Summary of pathway analysis of the genes most highly coexpressed with *Prnp* in the mouse

This table shows the top five biofunctions that IPA calculated as most overrepresented among the dataset of genes with similar spatial expression patterns to *Prnp* in the mouse. Ranking is by p-value (right-tailed Fisher exact test) and ranges are given because p-values are calculated for each subfunction within the overall functional category. Also shown are the canonical pathways that had the most overlap with the genes in the dataset (overlap statistic indicates the proportion of genes in that pathway that were present in the dataset). Again, p-values were determined using the right-tailed Fisher exact test.

Top molecular and cellular functions	p-values	# proteins	Proportion of dataset
Cell-to-cell signalling and interaction	1.07E-02 – 3.60E-17	43	38 %
Cellular assembly and organisation	1.07E02 – 3.60E-17	60	53 %
Cell death and survival	1.07E-02 – 1.43E-12	41	36 %
Cellular function and maintenance	1.06E-02 – 6.13E-12	44	39 %
Cell morphology	9.79E-03 – 5.61E-07	36	32 %
Top canonical pathways	**p-value**	**Overlap**	
Reelin signalling in neurons	8.65E-04	4/79 (5.1 %)	
Tight junction signalling	2.08E-03	5/167 (3.0 %)	
Gonadotrophin-releasing hormone signalling	5.18E-03	4/129 (3.1 %)	
Gamma-aminobutyric acid receptor signalling	5.61E-03	3/67 (4.5 %)	
Melatonin signalling	6.34E-03	3/70 (4.3 %)	

Table 6.3 – Summary of pathway analysis of the genes most highly coexpressed with *PRNP* in humans

This table shows the top five biofunctions that IPA calculated as most overrepresented among the dataset of genes with similar spatial expression patterns to *PRNP* in humans. Ranking is by p-value (right-tailed Fisher exact test) and ranges are given because p-values are calculated for each subfunction within the overall functional category. Also shown are the canonical pathways that had the most overlap with the genes in the dataset (overlap statistic indicates the proportion of genes in that pathway that were present in the dataset). Again, p-values were determined using the right-tailed Fisher exact test.

…stably transfected clones 2E3 and 1G3 compared with SH-SY5Y^{Untr} (Table 5.2) – the functional categories in question were cellular assembly and organisation, cell death and survival, and cell morphology. These data, perhaps, provide some evidence of the physiological relevance of the proteomic alterations to SH-SY5Y cells that were induced by PrP^{C} transfection.

As described in section 6.1, IPA can suggest likely upstream regulators of the proteins/genes in a dataset. Again ranked by overlap p-value, Tables 6.4 and 6.5 show the 15 highest-confidence upstream regulators identified from the genes highly coexpressed with *PRNP* in mouse and human tissues, respectively. Given the links between PrP^{C} and cytoskeletal organisation that were reported in the previous chapter, it was striking that several of the putative regulator proteins had roles in cytoskeleton dynamics. For example, Nck-associated protein 1-like can regulate actin remodelling (Park et al., 2010a), whilst reticulon-4 and neurofascin are involved in neurite outgrowth processes. Reelin signalling, the second- and first-ranked canonical pathway in Tables 6.2 and 6.3, respectively, is also linked to neuritogenesis (D'Archangelo, 2014). Furthermore, although NGF was not among the highest-confidence upstream regulators identified from either dataset, the third-ranked protein in Table 6.4 is brain-derived neurotrophic factor (BDNF), which, like NGF, is a member of the neurotrophin family. BDNF and its high affinity receptor TrkB were also among the top 15 upstream regulators identified from the human coexpression dataset. Given that BDNF and NGF are both able to interact with the p75 neurotrophin receptor (p75^{NTR}), these results in combination with those reported in section 6.1 raise the possibility that PrP^{C} could influence cellular responses to all neurotrophins, not just NGF. The work carried out to further investigate the potential connection between PrP^{C} and NGF signalling is covered later in the chapter; the following section provides some background information on the downstream pathways and processes regulated by NGF.

Upstream regulator	Molecule type	Overlap p-value	Target molecules in dataset
MAP kinase-interacting serine/threonine-protein kinase 1	Kinase	8.66E-20	20
Microtubule-associated protein tau	Other	1.16E-15	24
Brain-derived neurotrophic factor	Growth factor	4.27E-14	24
Histone deacetylase 4	Transcription regulator	2.12E-12	15
Presenilin-1	Peptidase	4.53E-10	22
Amyloid precursor protein	Other	7.48E-09	31
RE1-silencing transcription factor	Transcription regulator	1.29E-08	12
PHD finger protein 21A	Enzyme	4.05E-08	5
L-dopamine	Chemical - endogenous mammalian	1.68E-07	25
Adenosine receptor A2a	G-protein coupled receptor	2.12E-07	11
Huntingtin	Transcription regulator	3.42E-07	25
Nck-associated protein 1-like	Other	4.74E-06	4
Reticulon-4	Other	2.44E-05	6
Neurofascin	Other	3.24E-05	4
Serine/threonine-protein kinase STK11	Kinase	8.25E-05	9

Table 6.4 – Upstream regulators of genes with spatial patterns of expression in the mouse that are similar to *Prnp*

This table shows the molecules that IPA calculated as the most likely upstream regulators of the genes with similar spatial expression patterns to *Prnp* in the mouse. The top 15 upstream regulators, after removal of irrelevant entries (chemical drugs and toxicants), are shown here. The ranking is based on overlap p-value (right-tailed Fisher exact test for overrepresentation of the targets of the upstream regulator among the differentially expressed proteins).

Upstream regulator	Molecule type	Overlap p-value	Target molecules in dataset
Double-strand-break repair protein Rad21 homolog	Transcription regulator	8.43E-12	7
Transcriptional repressor CTCF	Transcription regulator	2.07E-08	7
Adenosine receptor A2a	G-protein coupled receptor	2.11E-07	8
Neurofascin	Other	7.20E-05	3
Follicle-stimulating hormone	Complex	1.13E-04	9
Reticulon-4	Other	1.19E-04	4
High affinity brain derived neurotrophic factor/neurotrophin-3 receptor	Kinase	1.48E-04	4
Huntingtin	Transcription regulator	1.49E-04	12
Histone deacetylase 4	Transcription regulator	2.19E-04	5
Microtubule-associated protein tau	Other	2.33E-04	7
Bis(5'-adenosyl)-triphosphatase	Enzyme	3.34E-04	3
Brain-derived neurotrophic factor	Growth factor	6.12E-04	7
Presenilin	Group	6.41E-04	2
F-box only protein 2	Enzyme	6.41E-04	2
Disintegrin and metalloproteinase domain-containing protein 10	Peptidase	7.53E-04	4

Table 6.5 – Upstream regulators of genes with spatial patterns of expression in humans that are similar to *PRNP*

This table shows the molecules that IPA calculated as the most likely upstream regulators of the genes with similar spatial expression patterns to *PRNP* in humans. The top 15 upstream regulators, after removal of irrelevant entries (chemical drugs and toxicants), are shown here. The ranking is based on overlap p-value (right-tailed Fisher exact test for overrepresentation of the targets of the upstream regulator among the differentially expressed proteins).

6.3 Background on nerve growth factor signalling

NGF is a member of the neurotrophin family of growth factors that also includes BDNF, neurotrophin-3 (NT-3) and neurotrophin-4 (NT-4). Neurotrophins generally promote survival, growth and differentiation of specific neuronal populations. For example, a major role of NGF is to guide the development of sensory and sympathetic neurons in early life (Hefti et al., 2006). In the adult, NGF is still required for survival of the cholinergic neurons in the basal forebrain and is involved in nervous system repair processes after injury (Sofroniew et al., 2001; Chen et al., 2015). NGF also plays a key role as a pain mediator by increasing the sensitivity of nociceptive neurons to painful stimuli (Pezet and McMahon, 2006).

The canonical actions of the neurotrophins are mediated largely via high affinity interactions with receptor tyrosine kinases known as Trk receptors (*t*ropomyosin-*r*elated *k*inases). As shown in Figure 6.1, each neurotrophic factor binds to one Trk receptor with high affinity: NGF binds to TrkA, BDNF and NT-4 to TrkB, and NT-3 to TrkC. NT-3 can also form weaker interactions with TrkA and TrkB, and NT-4 can similarly interact with TrkC (Gilbert, 2006). In addition to the Trk receptors, all neurotrophins can bind to the receptor encoded by the *NGFR* gene. This protein is member 16 of the tumour necrosis factor receptor superfamily but is more commonly known as the p75 neurotrophin receptor ($p75^{NTR}$). Neurotrophins interact with $p75^{NTR}$ at considerably lower affinities than with the Trk receptors (Covaceuszach et al., 2009).

Mature neurotrophins are formed by proteolytic cleavage of precursor proteins known as pro-neurotrophins (Fahnestock et al., 2004). Relatively recently, these pro-neurotrophins were shown to be biologically active themselves (Arnett et al., 2007). For example, pro-NGF is known to bind to $p75^{NTR}$, although there are differences in opinion over whether NGF or pro-NGF is the preferred ligand (Lee et al., 2001b; Clewes et al., 2008). Pro-NGF can also activate signalling through TrkA, although it has a lower affinity for the receptor than NGF (Clewes et al., 2008). Furthermore, pro-NGF can interact via its "pro" domain with a third receptor called

sortilin (Nykjaer et al., 2004; Skeldal et al., 2012), which is a member of the vacuolar protein sorting 10 protein-domain receptor family (Willnow et al., 2008). The "mature" domain of pro-NGF can simultaneously bind to $p75^{NTR}$, reportedly leading to a crosslinking of the receptors that modulates downstream signalling (Nykjaer et al., 2004). Interestingly, pro-NGF seems to be more abundant than mature NGF in the adult brain (Arnett et al., 2007).

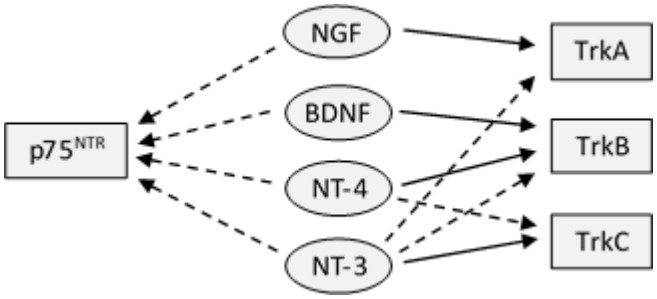

Figure 6.1 – Interactions between neurotrophins and their receptors

Adapted from a figure by Gilbert (2006), this diagram shows the receptor interactions of the four neurotrophins (NGF, BDNF, NT-3 and NT-4). Each neurotrophin binds one of the Trk receptors with high affinity (solid arrows), whilst all neurotrophins can form lower affinity interactions (dotted arrows) with $p75^{NTR}$. NT-3 and NT-4 can also bind other Trk receptors with relatively low affinities.

NGF binding to TrkA causes receptor dimerisation that activates the intracellular tyrosine kinase domains, leading to cross-phosphorylation of several tyrosine residues. This process is rapid – activation levels peak around five minutes after initiation of NGF stimulation (Chang et al., 2003). Phosphorylation of TrkA enables docking of adaptor proteins connected to various intracellular signalling pathways (Hefti et al., 2006). One key pathway is the MAPK cascade that culminates in phosphorylation of ERK1/2. Once activated, ERK1/2 can, in turn, activate transcription factors that promote neuronal differentiation, a process that includes induction of neurite outgrowth and cell cycle withdrawal (Huang and Reichardt, 2003). Another pathway downstream of TrkA is phosphatidylinositol-4,5-

bisphosphate 3-kinase (PI3K)-RAC-alpha serine/threonine-protein kinase (Akt) signalling. Although multifunctional, the PI3K-Akt pathway seems most important for NGF-mediated neuronal survival (Chang et al., 2003).

One role for $p75^{NTR}$ appears to be to interact with TrkA, thereby enhancing the affinity of TrkA for NGF (He and Garcia, 2004; Chen et al., 2009). However, if TrkA levels are low in comparison to $p75^{NTR}$ then NGF can initiate alternative signalling through $p75^{NTR}$ alone (Obata et al., 2006). Depending on the cellular context, this TrkA-independent signalling can either promote survival through PI3K-Akt and nuclear factor-kappa B pathways or apoptosis *via* activation of c-Jun N-terminal kinase and increased production of ceramide (Brann et al., 2002; Chen et al., 2009). It is thought that pro-apoptotic signalling mediated by $p75^{NTR}$ requires the presence of sortilin. Therefore, activation of these pathways by NGF may rely on the proposed weak interaction between NGF and sortilin (Nykjaer et al., 2004). Pro-NGF is more efficient than NGF at initiating apoptosis due to its higher affinity for sortilin that is conferred by its "pro" domain.

Although signalling pathways downstream of TrkA are usually considered responsible for NGF-mediated neurite outgrowth, some studies suggest that independent binding of NGF to $p75^{NTR}$ is more important. In the absence of neurotrophins, $p75^{NTR}$ is thought to be part of a receptor complex at the cell membrane that promotes activity of the RhoA-ROCK pathway, resulting in increased stability of the actin cytoskeleton (Mi et al., 2004; Chen et al., 2009). This disrupts the formation, extension and movement of filopodia, which are dynamic protrusions from the neurite growth cone that respond to extracellular signals to guide migration of the developing neurite (O'Connor et al., 1990). However, interactions between neurotrophins (and possibly pro-neurotrophins) and $p75^{NTR}$ seem to inhibit RhoA-ROCK signalling, which alleviates the block on neurite outgrowth (Gehler et al., 2004; Howard et al., 2013).

One feature that adds to the complexity of $p75^{NTR}$-mediated signalling is that the receptor can undergo sequential proteolytic cleavage events: firstly, alpha-cleavage

by disintegrin and metalloproteinase domain-containing protein 17 (ADAM17) releases the extracellular domain and leaves a C-terminal fragment (p75-CTF) at the cell membrane (Weskamp et al., 2004; Zampieri et al., 2005); secondly, p75-CTF is processed further by the gamma-secretase complex to allow the intracellular domain (p75-ICD) to move into the cytoplasm (Jung et al., 2003). Previously, it was thought that neurotrophins did not modulate $p75^{NTR}$ cleavage rates (Jung et al., 2003; Zampieri et al., 2005) but more recent *in vitro* data suggests that NGF can enhance p75-CTF (Coulson et al., 2008) and p75-ICD (Matusica et al., 2013) production. The mechanism seems to be NGF activating TrkA signalling, which promotes ADAM17 activity and, consequently, increases the rate of $p75^{NTR}$ cleavage (Kommaddi et al., 2011). The function of p75-CTF is still unclear: evidence suggests it can either be pro-survival (Verbeke et al., 2013) or pro-apoptotic (Coulson et al., 2008), perhaps depending on the cellular context. It has been proposed that p75-ICD is the active agent responsible for pro-apoptotic signalling induced by pro-neurotrophins (Kenchappa et al., 2006) and, interestingly, sortilin appears to enhance p75-ICD production, possibly by mediating the endocytosis of p75-CTF (Skeldal et al., 2012). Cleavage of the full length receptor to produce p75-ICD also reportedly prevents interaction with TrkA, leading to reduced affinity of TrkA for NGF (Jung et al., 2003). Contrastingly, another study suggests that only p75-ICD, not full length $p75^{NTR}$, can interact with TrkA (Matusica et al., 2013).

Overall, the NGF signalling pathways are highly complex and not fully understood. What is certain is that any protein modulating signalling through TrkA or $p75^{NTR}$ (or both) would have effects on a wide variety of different processes.

6.4 Investigating whether PrP^C expression alters the expression levels of neurotrophin receptors

6.4.1 Initial analysis of expression of neurotrophin receptors by SH-SY5Y cells

The proteomic changes observed in stably transfected clones 2E3 and 1G3 compared with SH-SY5Y^{Untr} suggested that PrP^C might modulate NGF signalling pathways. Additionally, analysis of the genes with similar expression patterns to PrP^C *in vivo* uncovered a potential link between PrP^C and BDNF signalling. These findings could be explained by PrP^C affecting neurotrophin signalling through the Trk receptors and/or $p75^{NTR}$. To follow up these results, I decided to investigate whether stable transfection of *Prnp* into SH-SY5Y cells had affected the expression levels of the relevant neurotrophin receptors. Firstly though, I needed to determine which of these receptors were expressed by the SH-SY5Y cells.

SH-SY5Y^{Untr} cells were seeded into a tissue culture plate and lysed 24 hours later. Next, expression of TrkA, TrkB and $p75^{NTR}$ were assessed by western blotting. Three main bands were detected by the anti-TrkA antibody (Figure 6.2a), the most intense of which was ~90 kDa. Human TrkA can be glycosylated at up to 13 sites, which greatly increases the molecular weight. Therefore, the diffuse band at ~120 kDa most likely corresponds to fully glycosylated TrkA, whilst the 90 kDa band is probably unglycosylated TrkA (actual molecular weight of 87.5 kDa). The lower band at ~80 kDa is most likely one of the additional TrkA isoforms that can be created by alternative splicing. Glycosylated bands on a western blot tend to be fuzzy and poorly defined because the glycans attached to a protein can vary in length (Gates et al., 2004); since the 80 kDa band is quite sharp, the TrkA isoform detected is probably unglycosylated.

Unglycoyslated TrkA is reported to be constitutively active in the absence of ligand and also seems unable to bind NGF, presumably because of a failure in trafficking…

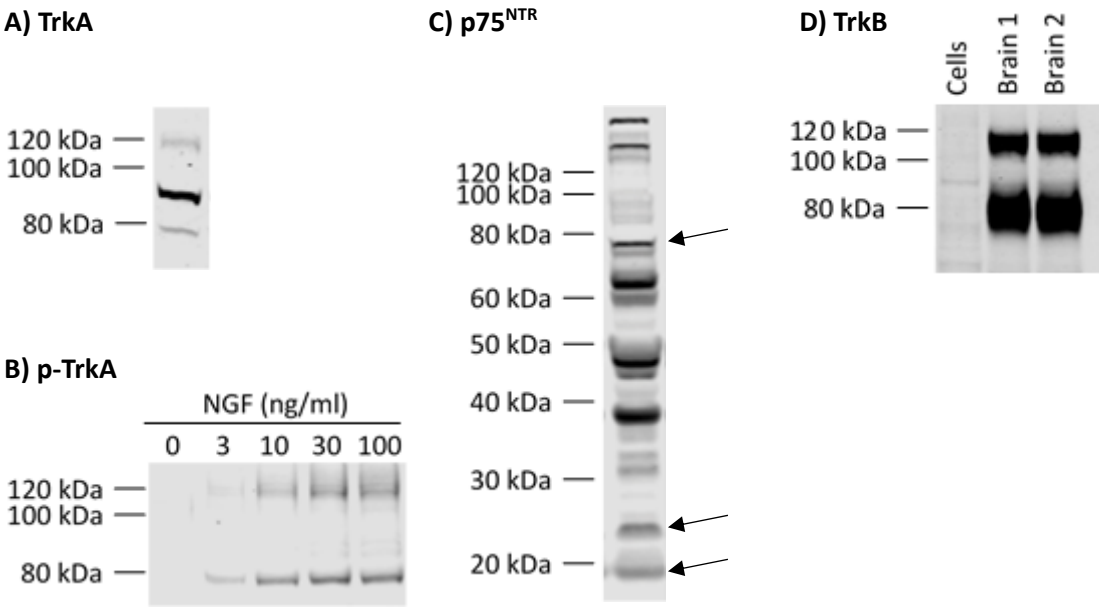

Figure 6.2 – SH-SY5Y cells expressed TrkA and p75^{NTR} but not TrkB

A) Western blot image showing detection in an SH-SY5Y^{Untr} lysate of three distinct bands (80, 90 and 120 kDa) corresponding to different forms of TrkA. **B)** Western blot image showing detection of phosphorylated TrkA (p-TrkA) in cell lysates prepared from clone 1G3 cells that had been stimulated with NGF for 5 min. This confirmed that the 80 and 120 kDa forms of TrkA were NGF-responsive and the 90 kDa form was not. **C)** Western blot image showing detection of p75^{NTR} in an SH-SY5Y^{Untr} lysate. Arrows indicate full length, glycosylated p75^{NTR} (78 kDa), the C-terminal fragment (24 kDa) and the intracellular domain (19 kDa). **D)** Western blot image showing absence of TrkB staining in an SH-SY5Y^{Untr} lysate. Mouse forebrain homogenates were used as positive controls for TrkB detection. p75^{NTR} was detected by use of 9992 antiserum (see main text for details). The other primary antibodies were from Cell Signalling Technology and had the following catalogue numbers: #2505 **(A)**, #4169 **(B**; specific for TrkA phosphorylated at Tyr785**)** and #4603 **(D).**

…of the receptor to the cell surface (Watson et al., 1999). Given the hypothesis that PrP^{C} modulates NGF signalling, it was important to determine which TrkA isoforms/glycoforms were responsive to NGF. This was achieved by culturing clone 1G3 cells in the absence of serum for 3.5 hours to allow TrkA phosphorylation to return to baseline prior to stimulating the cells with NGF concentrations of 3-

100 ng/ml for five minutes. At that point, the cells were lysed and levels of phosphorylated TrkA determined by western blotting. Figure 6.2b shows that, following NGF stimulation, bands at 80 and 120 kDa were detected at intensities that increased as NGF concentration increased. No 90 kDa band was identified, seemingly confirming that the unglycosylated TrkA was not phosphorylated in response to NGF, at least not by doses up to 100 ng/ml. However, in contrast to the findings of Watson et al. (1999), this result also suggested that the unglycosylated TrkA was not constitutively active. The most likely candidate for the 80 kDa band is the isoform designated TrkA-III (actual molecular weight of 77.1 kDa), which is also thought to be constitutively active and unresponsive to NGF (Luberg et al., 2015). Figure 6.2b indicates that both of these assumptions are incorrect for this band, at least in these cells. Nevertheless, both the 80 and 120 kDa forms of TrkA were activated by NGF stimulation and, therefore, were considered relevant for understanding how PrP^{C} expression was affecting the cellular response to NGF.

$p75^{NTR}$ was detected in the SH-SY5Y^{Untr} lysate using antiserum (designated 9992) originally produced by the research group of Prof. Moses V. Chao at New York University and provided as a gift by Dr Andrea Caporali of the University of Edinburgh. The antibody binds to the intracellular domain of $p75^{NTR}$, which enables it to detect the full length protein, p75-CTF and p75-ICD, although not the other fragments produced by each cleavage event. The protein was named $p75^{NTR}$ because it usually migrates to ~75 kDa in SDS-PAGE, mainly due to the presence of glycans that increase the molecular weight from the 45.2 kDa predicted by its amino acid sequence (Anastasia et al., 2015). Therefore, the band of ~78 kDa in Figure 6.2c was thought most likely to correspond to full length $p75^{NTR}$, although the sharpness of the band is unusual for a glycosylated protein. It is possible that the bands at ~24 and 19 kDa represent detection of p75-CTF and p75-ICD, respectively, because Zampieri et al. (2005) identified these $p75^{NTR}$ fragments at identical apparent molecular weights in human cell lysates when using the same antibody. The sharp band at ~47 kDa is probably unglycosylated $p75^{NTR}$ but the identities of the remaining bands in Figure 6.2c are unclear. Alternative splicing of $p75^{NTR}$ is thought to produce a 35.8 kDa isoform, so the bands at ~38 and 65 kDa could be unglycosylated and

glycosylated forms of that isoform, respectively. However, the shorter $p75^{NTR}$ isoform is reportedly unable to bind neurotrophins (Dechant and Barde, 2002), which makes it less relevant when investigating the links between PrP^C and NGF signalling.

The anti-TrkB antibody did not detect any bands in the SH-$SY5Y^{Untr}$ cell lysate (Figure 6.2d), although TrkB was present in large amounts in the mouse forebrain homogenates used as positive controls. TrkB is a similar size to TrkA and is glycosylated in a similar manner, so the band at ~110 kDa in the brain homogenates is probably the glycosylated form of the canonical isoform, whilst the lower band could be one of the numerous splice variants of the receptor.

6.4.2 Altered expression of TrkA and $p75^{NTR}$ in stably transfected clones compared with untransfected SH-SY5Y cells

The results in the previous section show that the SH-SY5Y cells expressed $p75^{NTR}$ and the high affinity NGF receptor TrkA but not the high affinity BDNF (and NT-4) receptor TrkB. Therefore, it seemed sensible to focus on the potential links between PrP^C and NGF signalling rather than any connection to BDNF signalling. Differences in the expression levels of TrkA and/or $p75^{NTR}$ between the stably transfected clones and SH-$SY5Y^{Untr}$ would be expected to alter the cellular response to NGF present in the culture medium – this NGF might derive from the FBS used to supplement the medium, which is thought to contain small amounts of the neurotrophin (Bonini et al., 2013), or from the SH-SY5Y cells themselves, which are purported to synthesise and secrete NGF (Tang et al., 2005). As in previous experiments, SH-$SY5Y^{Untr}$ and clones 2E3 and 1G3 were seeded into tissue culture plates and lysed 24 hours later. Expression levels of TrkA and $p75^{NTR}$ in five independently prepared sets of cell lysates were assessed by western blotting. Total TrkA levels (80, 90 and 120 kDa forms combined) did not vary significantly between SH-$SY5Y^{Untr}$ and the stably transfected clones (Figure 6.3a & b). However, Figure 6.3c indicates that the proportion of TrkA that was in the 120 kDa (glycoyslated) form was increased in clone 1G3 compared with SH-$SY5Y^{Untr}$ (19.9 vs 5.8 %) and by a lesser amount in clone 2E3 (10.5 vs 5.8 %). The difference between the two clones was also…

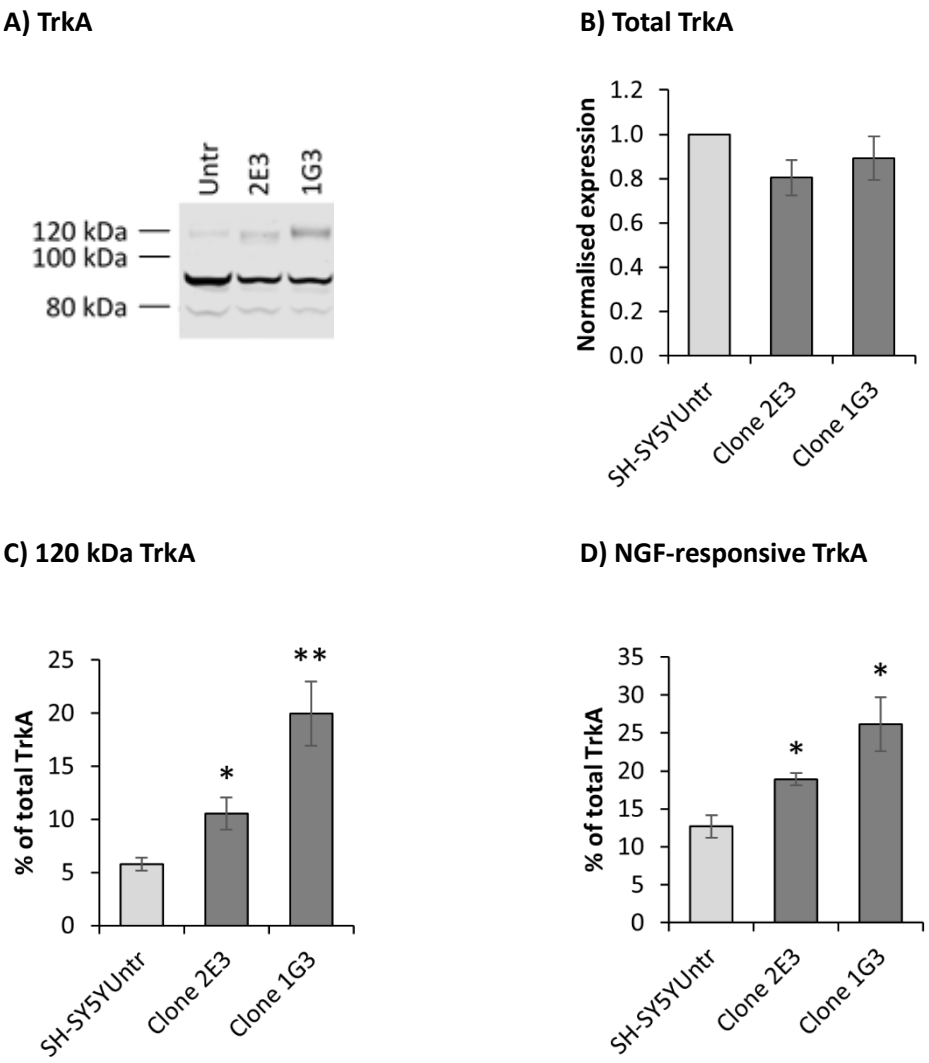

Figure 6.3 – Increased levels of glycosylated TrkA in stably transfected clones compared with untransfected SH-SY5Y cells

A) Representative western blot image showing TrkA immunostaining in SH-SY5Y cell lysates. The primary antibody used for TrkA detection was from Cell Signalling Technology (#2505). **B-D)** Bar charts summarising quantification of TrkA immunostaining from five independently prepared sets of cell lysates. Charts **B** shows total TrkA expression (all three bands combined), chart **C** shows the percentage of TrkA that was in the 120 kDa (glycosylated) form and chart **D** shows the percentage of TrkA that was NGF-responsive (80 and 120 kDa bands combined). For each membrane, after correction or loading errors, data were normalised to the signal from the SH-SY5Y^{Untr} lane. The mean normalised expression values (or percentages) are displayed in the bar charts (+/- standard error of the mean). Expression differences between the clones and SH-SY5Y^{Untr} were tested for significance ($p < 0.05$) using

one-sample or unpaired, two-sample t-tests as appropriate. Key: * for $p < 0.05$; ** for $p < 0.01$.

…statistically significant (unpaired, two-sample t-test: $p = 0.033$). Since data presented in the previous section showed that both the 80 and 120 kDa forms of TrkA were phosphorylated following NGF stimulation, the signal intensities of these bands were combined to enable calculation of the percentage of TrkA that was NGF-responsive. Again, this percentage was significantly increased in stably transfected clones 2E3 and 1G3 compared with SH-SY5Y^{Untr} (Figure 6.3d). In contrast, the level of full length, glycosylated p75^{NTR} (78 kDa) was reduced by almost 50 % in clone 1G3 compared with SH-SY5Y^{Untr}, although it was unchanged in clone 2E3 (Figure 6.4b). Additionally, Figure 6.4c shows that both stably transfected clones had reduced levels of the ~24 kDa band thought to correspond to p75-CTF. A similar trend was evident for the putative p75-ICD band at ~19 kDa (Figure 6.4d) but the reductions were not statistically significant in this case.

It has been proposed that p75^{NTR} molecules can self-assemble into trimeric complexes that are less able to mediate downstream signalling than the monomeric form (Anastasia et al., 2015). Although the intense bands at the very top of the Figure 6.4a western blot (~200 kDa) could represent detection of trimeric p75^{NTR}, the blotted samples were prepared under denaturing and reducing conditions that should disassemble protein complexes. It is, however, possible that this process may not have been completely effective. Alternatively, the putative trimers could have been artefactually created when heating the samples prior to loading the SDS-PAGE gels – certain membrane proteins are known to be prone to this form of aggregation (Sagne et al., 1996). Either way, the quantification of the levels of full length p75^{NTR} shown in Figure 6.4b may be incomplete, because it was only based upon the 78 kDa bands. However, the ~200 kDa bands were towards the top end of the western blot membrane, at a position where the transfer quality was poor and seemingly quite variable between lanes. Because of this, I decided that any quantification of the ~200 kDa bands would not be accurate.

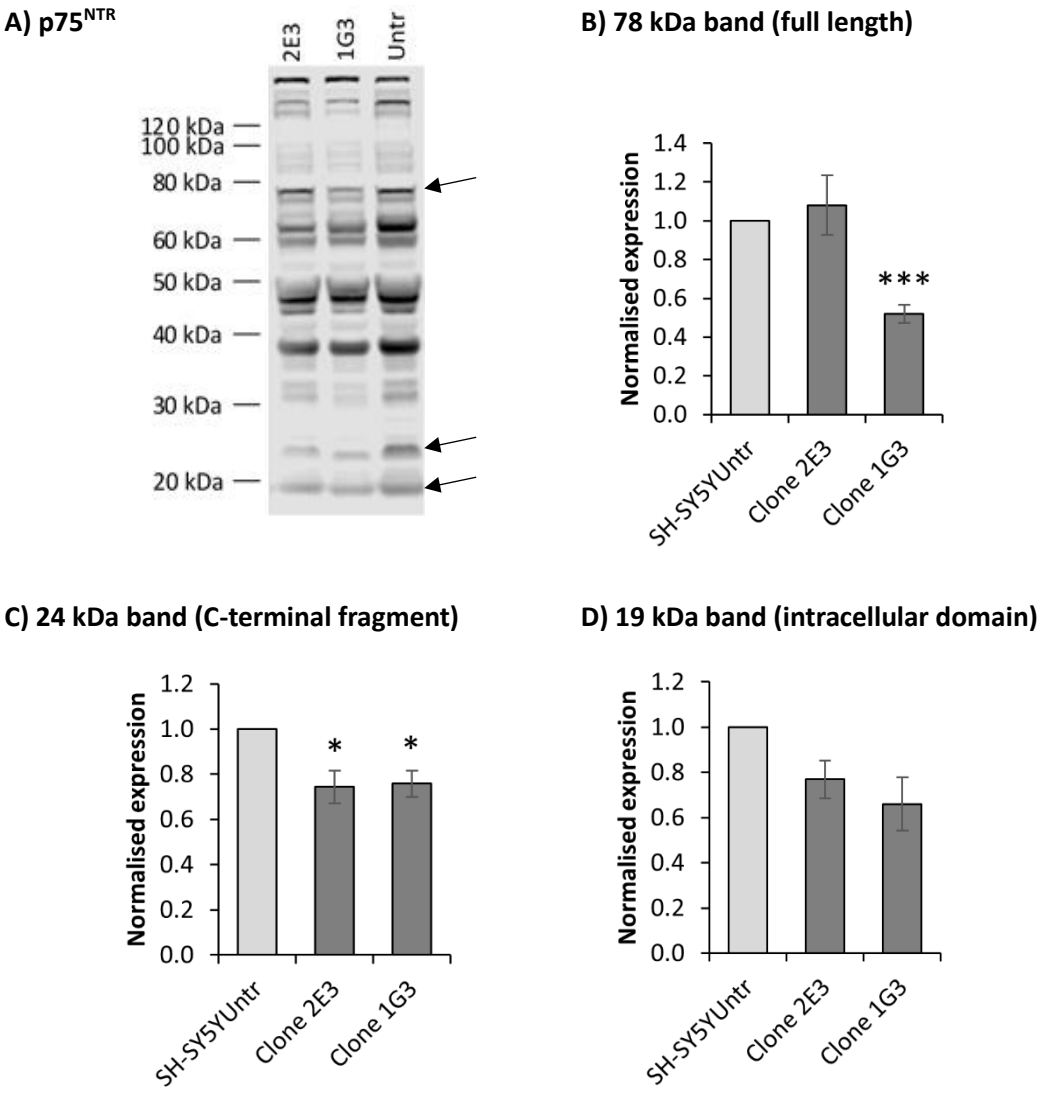

Figure 6.4 – Reduced levels of p75^{NTR} C-terminal fragment in stably transfected clones compared with untransfected SH-SY5Y cells

A) Representative western blot image showing p75^{NTR} immunostaining in SH-SY5Y cell lysates. Rabbit 9992 anti-serum was used for p75^{NTR} detection (see **Appendix I** for details). **B-D)** Bar charts summarising quantification of p75^{NTR} immunostaining from five independently prepared sets of cell lysates. Charts **B, C** and **D** show the data for the 78 kDa (full length, glycosylated), 24 kDa (p75-CTF) and 19 kDa (p75-ICD) forms of p75^{NTR}, respectively. For each membrane, after correction for loading errors, data were normalised to the signal from the SH-SY5Y^{Untr} lane. The mean normalised expression values (+/- standard error of the mean) are indicated in the bar charts. Expression differences between clones and SH-SY5Y^{Untr} were tested for significance ($p < 0.05$) using one-sample t-tests. Key: * for $p < 0.05$; *** for $p < 0.001$.

Overall, the data presented in this section indicate that PrP^C transfection increased the amount of NGF-responsive TrkA, specifically by increasing the levels of the 120 kDa glycoform. Although altered expression of full length $p75^{NTR}$ was only found in clone 1G3, levels of p75-CTF did appear to be reduced in both clones tested compared with SH-$SY5Y^{Untr}$. Combined, these results suggest that PrP^C expression might tip the balance in favour of NGF signalling through TrkA rather than $p75^{NTR}$.

Pro-apoptotic signalling mediated by $p75^{NTR}$ seems to require expression of the sortilin receptor (Nykjaer et al., 2004). Therefore, the levels of this receptor were also relevant when considering the effect of PrP^C expression on the cellular response to NGF, especially given a recent report that sortilin interacts with PrP^C directly in order to mediate its endocytosis (Uchiyama and Sakaguchi, 2016). Western blot…

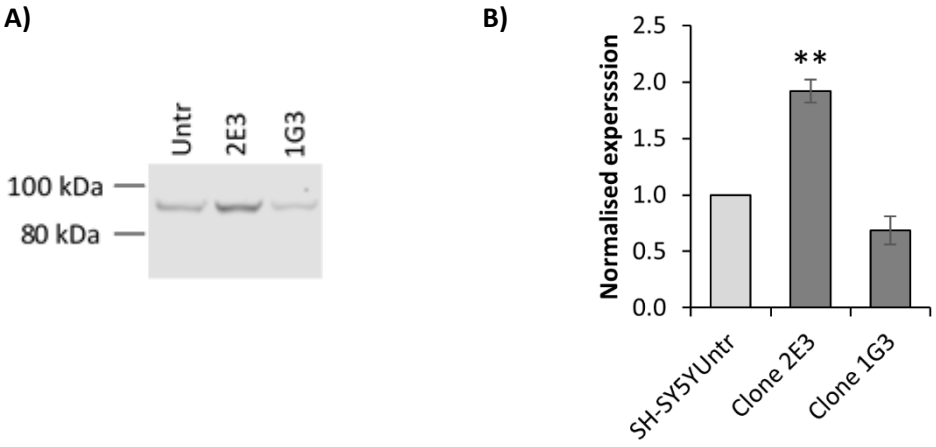

Figure 6.5 – Altered sortilin expression in stably transfected clones compared with untransfected SH-SY5Y cells

A & B) Representative western blot image and bar chart summarising quantification of sortilin immunostaining from four independently prepared sets of SH-SY5Y cell lysates. The primary antibody for sortilin detection was from Proteintech (#12369-1-AP). For each experiment, after correction for loading errors, data were normalised to the signal from the SH-$SY5Y^{Untr}$ lane. The mean normalised expression values (+/- standard error of the mean) are displayed in the bar charts. Expression differences between clones and SH-$SY5Y^{Untr}$ were tested for significance ($p < 0.05$) using one-sample t-tests. Key: ** for $p < 0.01$.

...analysis of four independently prepared sets of lysates determined that sortilin expression was higher in clone 2E3 (+1.92 fold) compared with SH-SY5Y^{Untr} (Figure 6.5). No significant change was observed in clone 1G3, although the trend was in the opposite direction to clone 2E3. The implications of these results are unclear, given the lack of consistent change to sortilin expression induced by PrP^{C} transfection. Higher sortilin levels in clone 2E3 compared with SH-SY5Y^{Untr} might suggest a greater tendency towards pro-apoptotic signalling in response to neurotrophins (both the "pro" and mature forms) but the increase in NGF-responsive TrkA could counteract this.

6.4.3 Knockdown of PrP^{C} did not reverse the changes to p75^{NTR} expression that seemed to have been induced by PrP^{C} transfection

Stably transfected clones 2E3 and 1G3 displayed increased levels of the 120 kDa TrkA glycoform and also appeared to express lower levels of p75-CTF compared with SH-SY5Y^{Untr}. The assumption was that these changes were induced by PrP^{C} expression, so, in an attempt to confirm this, I investigated the effects of knocking down PrP^{C} expression in the clones. PrP^{C} knockdown was achieved by use of the PrP siRNA (designated s72188) that was introduced in section 4.1. To make the experiments manageable from a technical point of view, the effects of PrP^{C} knockdown on TrkA and p75^{NTR} expression were assessed only in clone 1G3 and SH-SY5Y^{Untr} cultures. Cells were subjected to one of three treatments: 1) transient transfection with 15 nM PrP siRNA; 2) transient transfection with 15 nM of a negative control siRNA with "no significant sequence similarity to mouse, rat, or human gene sequences" (Thermo Fisher Scientific, [n.d.]-b); or 3) exposure only to the carrier medium for the transfection reagent-siRNA complexes. The culture medium was refreshed the day after transfection and the cells were subcultured into fresh plates two days later to ensure the SH-SY5Y^{Untr} and clone 1G3 cultures were at similar densities – this was necessary due to the faster proliferation rate of SH-SY5Y^{Untr}. Lysis was performed the following day i.e. four days post-transfection,

which should have allowed sufficient time for any effect of reduced PrP^C levels on NGF receptor expression to take place.

Prior to carrying out these experiments, I noted that when the effects of PrP^C knockdown on the proliferation rates of the SH-SY5Y cell lines were assessed (see section 5.2) the culture medium contained a small amount (roughly 9 % (v/v)) of OptiMEM medium, which is the recommended carrier solution for formation of the complexes between the siRNAs and the transfection reagent. The cells were cultured in this OptiMEM-containing medium for the duration of those proliferation assays to avoid any detachment from the plates that might have occurred during medium changes. Although the presence of OptiMEM seemed unimportant at the time, OptiMEM contains insulin, in addition to its other components (Thermo Fisher Scientific, [n.d.]-a). Given the putative connection between PrP^C and NGF signalling and the reported involvement of $p75^{NTR}$ in insulin signalling pathways (Passino et al., 2007; Baeza-Raja et al., 2013), it seemed worth investigating whether the presence or absence of OptiMEM had any influence on the effect of PrP^C knockdown on expression levels of the NGF receptors. Ultimately, including OptiMEM in the medium did not alter the results (data not shown) and, because one more experimental replicate was performed in OptiMEM-containing medium, the data from those experiments are the results presented here.

Western blotting of clone 1G3 lysates confirmed that PrP^C expression was greatly reduced by the PrP siRNA, whilst the negative control siRNA had no effect (Figure 6.6a). Unfortunately, because of the low initial seeding density required for efficient transfection, it was difficult to reliably obtain cell lysates at sufficient protein concentrations for western blot detection of the 120 kDa TrkA glycoform (data not shown). It was, however, possible to analyse the levels of $p75^{NTR}$ expression, and western blotting data obtained from…

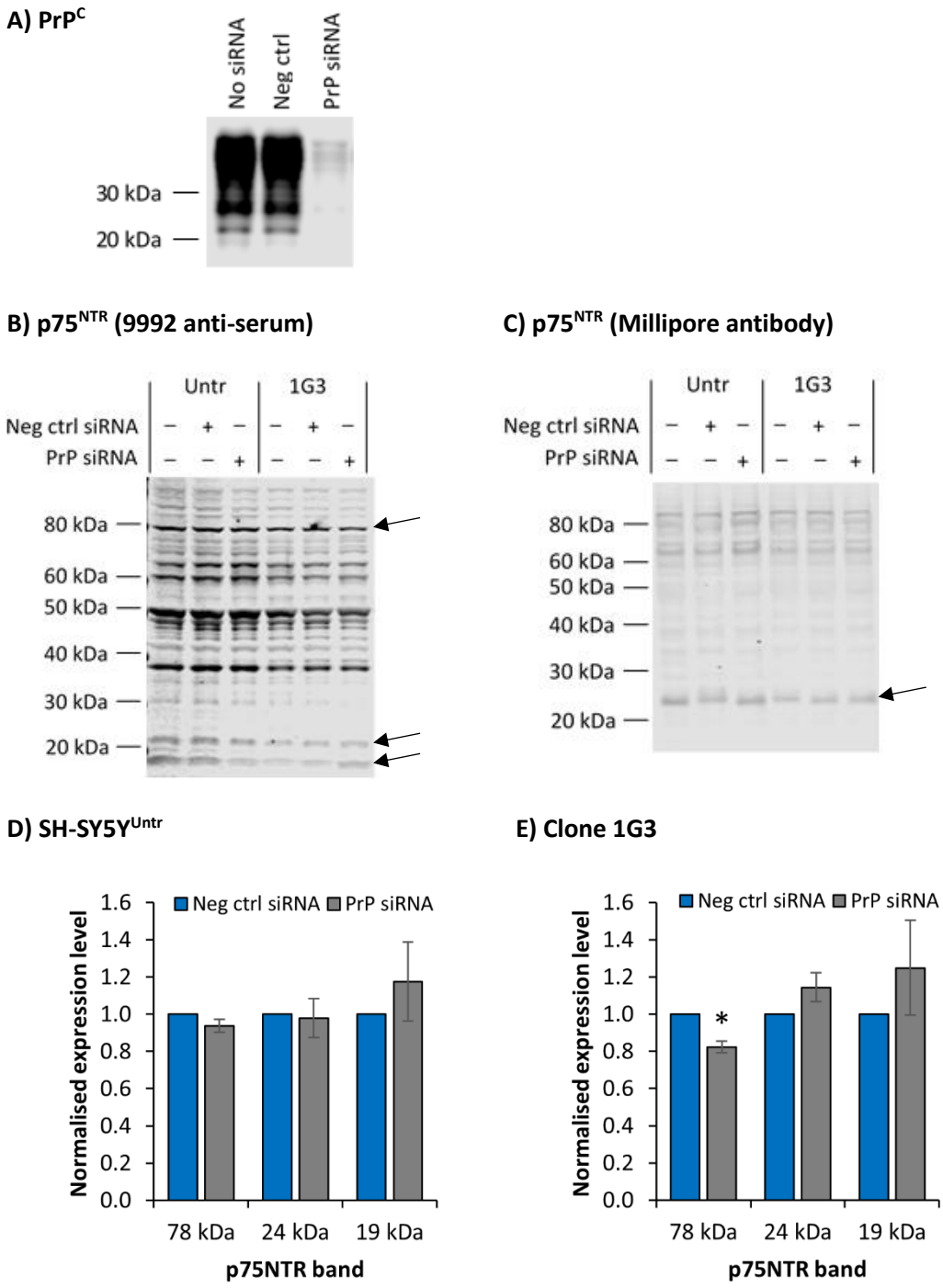

Figure 6.6 – PrP^C knockdown did not rescue the difference in levels of p75^{NTR} C-terminal fragment between clone 1G3 and untransfected SH-SY5Y cells

A) Representative western blot image showing markedly reduced PrP^C immunostaining from a clone 1G3 lysate prepared four days after transient transfection with the PrP siRNA s72188 compared with lysates prepared from cells either transiently transfected with a

negative control siRNA (neg ctrl) or not transfected with any siRNA at all (nor exposed to the transfection reagent). PrP^C was detected by use of the BC6 anti-PrP^C primary antibody (McCutcheon et al., 2014). **B & C)** Representative western blot images showing $p75^{NTR}$ immunostaining in the same lysates as in image **A** as well as in lysates of SH-$SY5Y^{Untr}$ cells that had undergone the same treatments. The relevant bands are shown with arrows. 9992 antiserum (see **Appendix I** for more details) was used for $p75^{NTR}$ detection in the case of image **B.** Image **C** shows the pattern obtained when using a primary antibody from Millipore (#07-046; see explanation in footnote 15). Only p75-CTF (24 kDa) was conclusively detected by the commercial antibody. **D & E)** Bar charts summarising quantification of $p75^{NTR}$ immunostaining in SH-$SY5Y^{Untr}$ **(D)** and clone 1G3 **(E)** lysates obtained from four independent experiments. For each experiment, after correction for loading errors, data were normalised to the signal from the negative control siRNA-transfected lysate. The mean normalised expression values (+/- standard error of the mean) are indicated in the bar charts. Expression differences between negative control siRNA- and PrP siRNA-transfected cells were tested for significance ($p < 0.05$; indicated with *) using one-sample t-tests.

…four independent experiments[15] are presented in Figure 6.6b-e. Initially, the data were normalised to the SH-$SY5Y^{Untr}$ "no siRNA" lanes but it was difficult to isolate any effects of the PrP siRNA from the assay-to-assay variability in the expression levels of $p75^{NTR}$ by SH-$SY5Y^{Untr}$ and clone 1G3. Therefore, for each cell type, the band intensities for $p75^{NTR}$ and its cleavage fragments in the PrP siRNA-transfected lysates were normalised to those from the negative control siRNA-transfected lysates. Figure 6.6d shows that transfection of the PrP siRNA did not significantly alter the levels in SH-$SY5Y^{Untr}$ of the bands thought to correspond to full length $p75^{NTR}$, p75-CTF and p75-ICD, which was as expected due to the lack of detectable PrP^C expression in those cells normally. For clone 1G3, knockdown of PrP^C expression slightly but significantly ($p = 0.033$) reduced the abundance of the ~78 kDa band thought to be full length $p75^{NTR}$ (Figure 6.6e). This change was

[15] The fourth experiment required the use of a commercial $p75^{NTR}$ antibody since no more of the 9992 $p75^{NTR}$ antiserum was available. Figure 6.6c shows that the commercial antibody only detected p75-CTF conclusively. A ~78 kDa band corresponding to full length $p75^{NTR}$ was just about visible but not quantifiable, whilst p75-ICD was not detected at all. Therefore, the bar charts in Figure 6.6 summarise data from only three experiments for full length $p75^{NTR}$ and p75-ICD.

opposite to the expected direction given the already lower levels of full length $p75^{NTR}$ in clone 1G3 compared with SH-SY5Y^{Untr}. However, non-significant trends towards increased levels of the ~24 and 19 kDa bands possibly corresponding to the $p75^{NTR}$ cleavage fragments were noticeable in the PrP siRNA-transfected clone 1G3 cells. These effects could be relevant considering that both p75-CTF and p75-ICD are thought to be functionally active (Kenchappa et al., 2006; Coulson et al., 2008; Matusica et al., 2013; Verbeke et al., 2013). Indeed, one could speculate that four days of reduced PrP^{C} expression is insufficient to affect overall levels of $p75^{NTR}$ but does increase cleavage rates to bring the levels of p75-CTF and p75-ICD closer to those observed in SH-SY5Y^{Untr}.

As described above, knocking down PrP^{C} did not conclusively prove that the differential expression of the NGF receptors in the stably transfected clones was the result of PrP^{C} expression in the SH-SY5Y cells. However, another obvious question to ask was whether the altered expression levels translated into differences in the activities of downstream signalling pathways. One way to assess this was to measure the levels of activated NGF receptors in the cells. The activation status of $p75^{NTR}$ is difficult to determine directly: whilst the receptor can be phosphorylated, this is not thought to occur in response to ligand binding. Moreover, phosphorylation of $p75^{NTR}$ may only occur when receptor molecules are transported along axons (Butowt and von Bartheld, 2009) and, although SH-SY5Y cells do extend neurite-like processes, they do not have axons. Since p75-CTF and p75-ICD are biologically active, cleavage rates could be considered correlates of receptor activation but, again, the cleavage processes do not appear to be induced by neurotrophin binding to $p75^{NTR}$. However, TrkA activation is much easier to assess. In response to NGF stimulation, TrkA is phosphorylated at a number of tyrosine residues, which activates the receptor and, consequently, initiates downstream signalling.

I performed western blotting experiments using an antibody specific to the phosphorylated form of TrkA (p-TrkA) in order to assess baseline levels of TrkA activation in SH-SY5Y cells growing in their standard culture medium. As explained previously, the NGF required for receptor activation would either have come from

the FBS used to supplement the medium (Bonini et al., 2013) or from its secretion by the cells themselves (Tang et al., 2005). Bands at ~120 kDa, perhaps corresponding to the 120 kDa TrkA glycoform, were detected by the p-TrkA antibody in SH-SY5Y^{Untr} lysates but were too faint to quantify accurately (data not shown). However, this finding did suggest that NGF-TrkA signalling was occurring at low levels in the SH-SY5Y cells. An alternative approach for investigating whether baseline p-TrkA levels were higher in clones 2E3 and 1G3 than SH-SY5Y^{Untr} was to quantify TrkA phosphorylation in response to NGF stimulation. If p-TrkA were more abundant in the stably transfected clones following exposure to exogenous NGF then p-TrkA levels would also be predicted to be higher when the cells were cultured normally in serum-containing medium (which is thought to contain some NGF). Unfortunately, there was not enough time to optimise these NGF stimulation assays. Therefore, I was unable to confirm that PrP^{C} transfection into SH-SY5Y cells had caused increased baseline levels of TrkA activation.

6.4.4 Neurotrophin receptors expressed at similar levels in wild type and PrP^{C}-null mouse forebrains

The data presented in section 6.4.2 indicate that PrP^{C} transfection altered expression of NGF receptors in the SH-SY5Y cells. Because of the availability of homogenised forebrain tissues from age- and sex-matched wild type and PrP^{C}-null mice (see sections 5.3 and 5.5 for more information), I decided to investigate whether the expression changes identified in SH-SY5Y cells were also present in *ex vivo* tissues. In addition to TrkA and p75^{NTR}, TrkB expression was also assessed, because analysis of the genes usually coexpressed with *PRNP* suggested a potential link between PrP^{C} and BDNF signalling, as reported in section 6.2. Moreover, mouse forebrain tissues had already been shown to express TrkB (Figure 6.2d) unlike the SH-SY5Y cells.

Figure 6.7a shows that the glycosylated form of TrkA was detected in the forebrain homogenates, although at a slightly higher molecular weight (~130 kDa) than in the cells, presumably as a result of differential glycosylation. However, western blot…

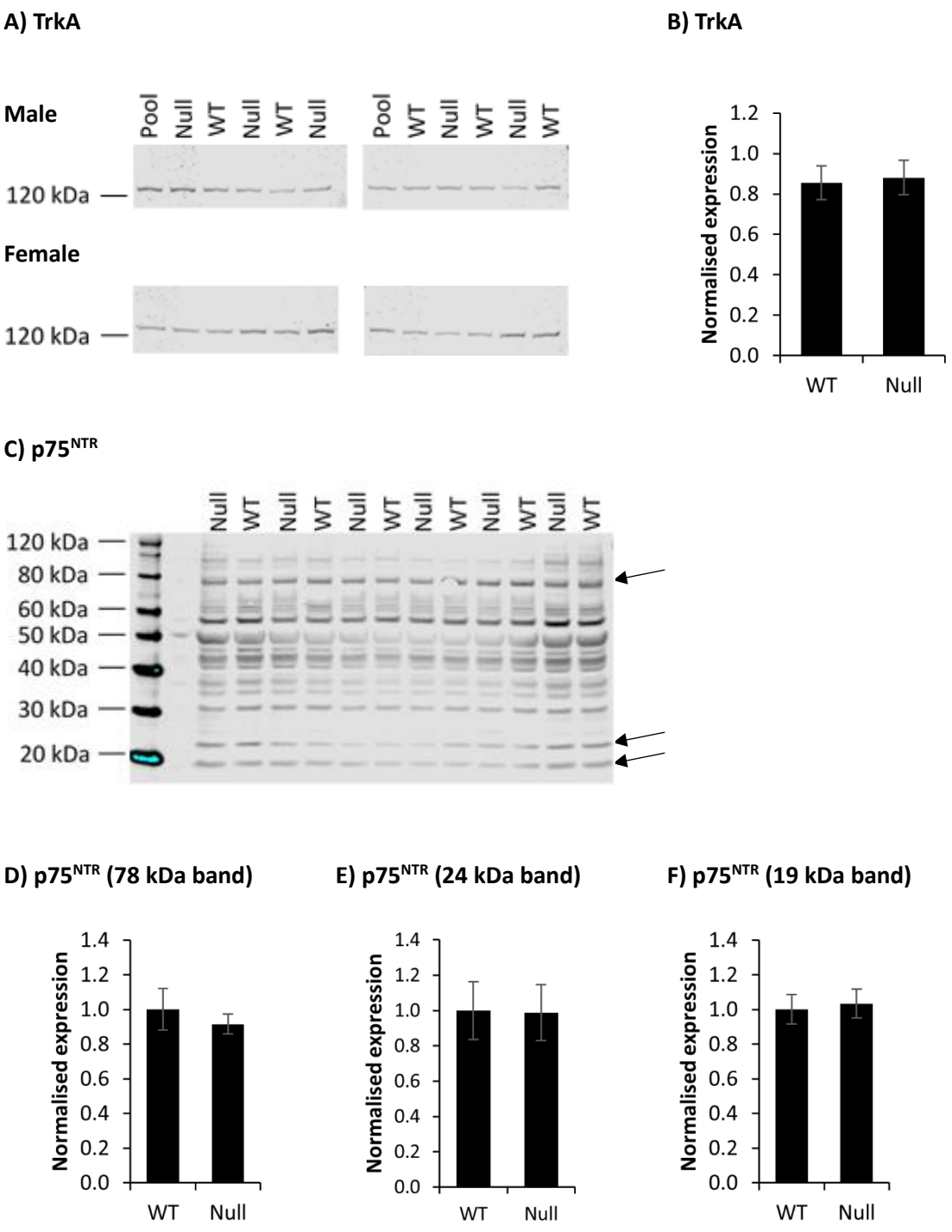

Figure 6.7 – Expression levels of neurotrophin receptors did not vary between wild type and PrP^{C}-null mouse forebrains

See following page for legend…

G) TrkB

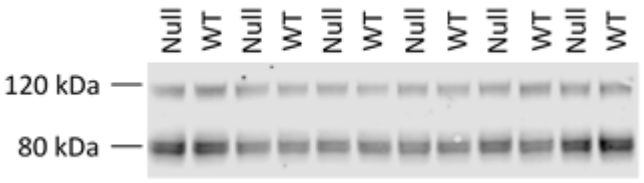

H) TrkB

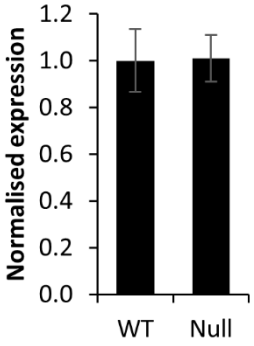

Figure 6.7 – Expression levels of neurotrophin receptors did not vary between wild type and PrP^{C}-null mouse forebrains

A, C & G) Representative Images of western blots of wild type (WT) and PrP^{C}-null mouse forebrain homogenates that were probed for TrkA, p75^{NTR} and TrkB, respectively. The relevant bands on image **C** are shown with arrows. Rabbit 9992 anti-serum (see **Appendix I** for more details) was used for p75^{NTR} detection. Anti-TrkA and anti-TrkB primary antibodies were from Cell Signalling Technology (#2505 and #4603, respectively). **B)** Bar chart summarising quantification of TrkA immunostaining from 10 tissues of each genotype (5 male, 5 female). After correction for loading errors, signals on each membrane were normalised to a fixed reference sample – a "pool" consisting of equal amounts of all 20 brain homogenates. **D-F)** Bar charts summarising quantification of p75^{NTR} immunostaining from six tissues of each genotype. After correction for loading errors, the data were normalised to the mean signal from the WT tissues. Bar charts **D**, **E** and **F** show the data for the 78 kDa (full length, glycosylated), 24 kDa (p75-CTF) and 19 kDa (p75-ICD) bands, respectively. For bar chart **D**, the 78 kDa band in the 5th lane from the right was not quantified due to presence of an air bubble. **H)** Bar chart summarising quantification of TrkB immunostaining from six tissues of each genotype (signals from 80 and 120 kDa bands were combined). After correction for loading errors, the data were normalised to the mean signal from the WT tissues. **B, D-F & H)** Overall mean normalised expression values for each genotype were calculated and these are indicated in the bar charts (+/- standard error of the mean). Expression differences between genotypes were tested for significance ($p < 0.05$) using unpaired, two-sample t-tests but no comparisons met the threshold.

…analysis of 10 wild type and 10 PrP^C-null tissues identified no differences in TrkA expression between the genotypes (Figure 6.7b). No other specific bands were detected by the anti-TrkA antibody. To save on the time required for these experiments, $p75^{NTR}$ expression was initially assessed in just six tissues of each genotype and the results showed that levels of the bands thought to correspond to the full length receptor and its cleavage fragments did not vary between PrP^C-null and wild type control tissues (Figure 6.7c-f). Western blots for TrkB showed a single at band around 120 kDa and a doublet at 80 kDa (Figure 6.7g) – TrkB can be glycosylated much like TrkA, which suggests that the higher band is the glycosylated form of the canonical isoform. The 80 kDa TrkB bands are probably the result of alternative splicing, since the Uniprot entry (#Q16620) for human TrkB indicates that multiple isoforms exist. Figure 6.7h shows quantification of TrkB expression based on the combined signal intensities of the 80 and 120 kDa bands, because the results were virtually identical when each set of bands were analysed separately (data not shown). In a similar manner to TrkA and $p75^{NTR}$, TrkB levels did not vary according to PrP^C genotype.

The lack of *in vivo* confirmation of *in vitro* results is a common theme in the study of PrP^C function. For example, in spite of cell culture experiments performed by various groups identifying numerous putative roles for PrP^C, one proteomic study did not identify a single protein that was differentially expressed between wild type and PrP^C-null mouse brain homogenates (Crecelius et al., 2008). Others have explained similar results by suggesting that PrP^C regulates processes in a cell type-specific manner, leading to an averaging out of these effects over an entire tissue (Mehrabian et al., 2014; Mehrabian et al., 2016). Alternatively, the role of PrP^C in the immature, neuronal precursor-like SH-SY5Y cells (Kovalevich and Langford, 2013) may not be the same as its role in the forebrains of aged mice – the tissues used in these analyses were from mice culled at around 550 days old. A final potential explanation for the lack of differences in neurotrophin receptor expression levels between genotypes is that absence of PrP^C in the knockout mice could be compensated for by other proteins, as has been suggested previously (Shmerling et al., 1998; Hajj et al., 2007).

6.5 Investigating the effects of PrP^C expression on the activities of growth factor signalling pathways

6.5.1 PrP^C transfection into SH-SY5Y cells alters activities of growth factor signalling pathways

As explained in section 6.4.3, I was unable to confirm that the higher levels of NGF-responsive TrkA in the stably transfected clones compared with SH-SY5Y^{Untr} led to equivalent increases in p-TrkA. The levels of activated $p75^{NTR}$ could also not be determined directly due to the lack of a well-defined marker for its activation. An alternative approach was to assess the activities of signalling pathways downstream of the NGF receptors. I decided to focus on the PI3K/Akt and ERK1/2 pathways, which play important roles in facilitating the neurotrophic activity of NGF that is initiated by binding to TrkA (Huang and Reichardt, 2003). Independent binding of NGF to $p75^{NTR}$ can also activate PI3K/Akt signalling (Chen et al., 2009).

Akt and ERK1/2 are activated by phosphorylation mediated by upstream protein kinases. Therefore, levels of phosphorylated Akt (p-Akt) and ERK1/2 (p-ERK1/2) in the SH-SY5Y cell lines were assessed by western blotting, making use of an antibody that specifically detects Akt phosphorylated at Ser473 and another antibody specific for the Thr202 and Tyr204 phosphorylation sites of ERK1 and the Thr185 and Tyr187 sites of ERK2. Total levels of Akt and ERK1/2 were also quantified using antibodies able to pick up all forms of the proteins. As in similar experiments, cells were seeded into plates and cultured in their standard, serum-containing medium for 24 hours prior to lysis. Western blot analysis of four independently prepared sets of cell lysates revealed intense p-Akt and total Akt bands that migrated to around the expected molecular weight of 56 kDa (Figure 6.8a & b). Figure 6.8c shows that overall Akt expression did not vary significantly between SH-SY5Y^{Untr} and stably transfected clones 2E3 and 1G3. However, the p-Akt/total Akt ratio was significantly reduced by 17 % in clone 2E3 and by 31 % in clone 1G3 compared with the control cell line (Figure 6.8d).

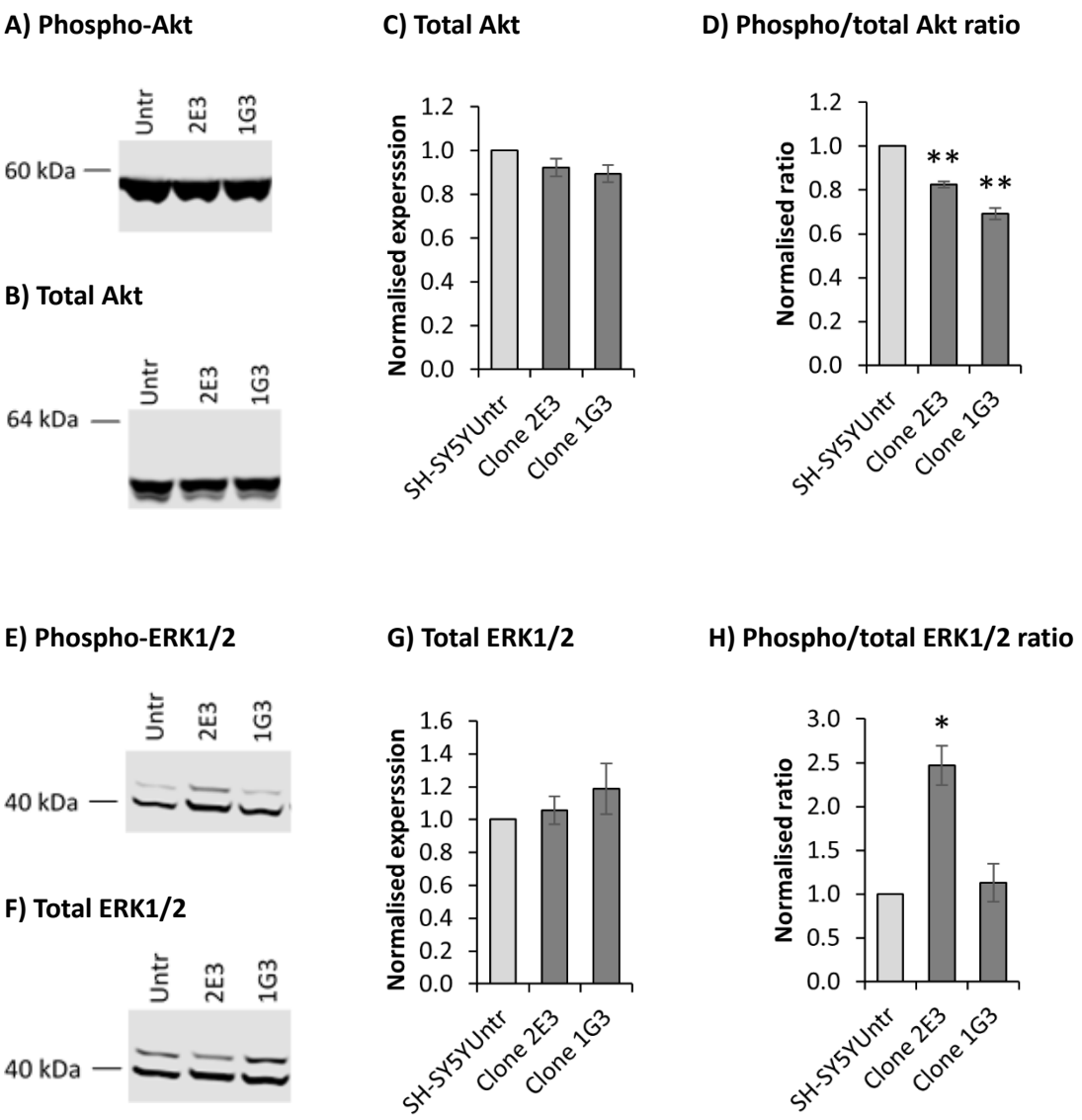

Figure 6.8 – Decreased activation of Akt in clones 2E3 and 1G3 and increased activation of ERK1/2 in clone 2E3 compared with untransfected SH-SY5Y cells

Representative images of western blots of SH-SY5Y cell lysates that were simultaneously probed for Akt phosphorylated at Ser473 and total Akt **(A & B)** or phosphorylated ERK1/2 (Thr202/Tyr204 for ERK1 and Thr185/Tyr187 for ERK2) and total ERK1/2 **(E & F)**, respectively. Primary antibodies were all from Cell Signalling Technology and had the following catalogue numbers: #4060 **(A)**, #2920 **(B)**, #4370 **(E)** and #9107 **(F)**. Also shown are bar charts summarising quantification of total Akt **(C)** and total ERK1/2 **(G)** immunostaining from at least three independently prepared sets of cell lysates as well as normalised ratios of phospho-/total Akt **(D)** and phospho-/total ERK1/2 **(H)** levels. For ERK1/2 blots, signals from ERK1 (42 kDa) and ERK2 (40 kDa) bands were combined. For each

membrane, after correction for loading errors, total Akt or total ERK1/2 band signals were normalised to the signal from the SH-SY5Y^{Untr} lane. Normalised phospho/total ratios were calculated by normalising the ratios for each lane to the ratio from the SH-SY5Y^{Untr} lane. The overall mean normalised expression values/ratios (+/- standard error of the mean) are displayed in the bar charts. Expression differences between clones and SH-SY5Y^{Untr} were tested for significance ($p < 0.05$) using one-sample t-tests. Key: * for $p < 0.05$; ** for $p < 0.01$.

The ~42 and 40 kDa bands detected by the ERK1/2 antibodies correspond to ERK1 and ERK2, respectively (Figure 6.8e & f). For quantification, the signal intensities of these bands were combined because ERK1 and 2 are thought to have very similar functions and to be regulated similarly, at least in most cell types (Wortzel and Seger, 2011). Western blot analysis of three independently prepared sets of cell lysates showed that total ERK1/2 levels were similar among the cell lines (Figure 6.8g), as was the case for Akt. In contrast, the p-ERK1/2/total ERK1/2 ratio was increased in clone 2E3 by 147 % compared with SH-SY5Y^{Untr}, although no such effect was evident in clone 1G3, which displayed similar levels of p-ERK1/2 to the control cell line.

The PI3K/Akt pathway is considered a positive regulator of proliferation. Moreover, high levels of p-Akt have been shown to block cell cycle arrest induced by NGF stimulation (Bang et al., 2001). Therefore, the reduced Akt signalling activity in the stably transfected clones is in agreement with their slower proliferation compared with SH-SY5Y^{Untr}, as was reported in section 5.2. Akt activation was also greater in clone 2E3 than in clone 1G3 (unpaired, two-sample t-test: $p = 0.008$), which could explain the faster proliferation rate of clone 2E3. Intriguingly, these differences between the clones are in line with the data for the 120 kDa TrkA glycoform, which was more upregulated in clone 1G3 compared with SH-SY5Y^{Untr} than it was in clone 2E3.

At first glance, reduced Akt signalling in the stably transfected clones seems strange given that NGF, whether signalling through TrkA or $p75^{NTR}$, is usually considered to activate Akt. One conclusion could be that PrP^{C} expression makes SH-SY5Y cells less responsive to NGF but, as reported in section 6.1, pathway analysis of the proteomic data suggested that NGF signalling pathways were more active in the stably transfected clones, not less. However, whilst NGF does cause an initial increase in p-Akt, rapid dephosphorylation then seems to occur and Akt activity drops back to a much lower, constant level if NGF stimulation is maintained (Bang et al., 2001). This situation may have applied to the experiments reported in Figure 6.8, given that the cells had been cultured in serum-containing medium for 24 hours prior to lysis and, therefore, would have been exposed for that time period to any NGF present. Therefore, in this context, lower levels of p-Akt may not necessarily indicate that the stably transfected clones were less responsive to NGF.

ERK1/2 signalling is thought to be the key driver of NGF-mediated neuronal differentiation (Klesse et al., 1999). Therefore, the increased ERK1/2 activity in clone 2E3 compared with $SH\text{-}SY5Y^{Untr}$ is in agreement with the proposed increased activity of NGF signalling pathways in the PrP^{C}-transfected cells. The counter evidence is that the degree of ERK1/2 activation was similar in clone 1G3 and in the control cell line, suggesting that the increase in clone 2E3 may not have been caused by PrP^{C} expression. Strangely, enhanced ERK1/2 signalling in clone 2E3 compared with clone 1G3 would suggest that clone 2E3 had the more neuronal phenotype and yet several lines of evidence indicated that this was not the case. Firstly, cell cycle arrest is required for complete neuronal differentiation, since neurons are post-mitotic, and yet, as eluded to earlier, clone 1G3 proliferated slower than clone 2E3. Secondly, as reported in section 4.2.2, it was clone 1G3 not 2E3 that displayed increased expression of neuroblast differentiation-associated protein AHNAK and reduced expression of the immature neuronal marker proliferation cell nuclear antigen compared with $SH\text{-}SY5Y^{Untr}$. Thirdly, another feature of neuronal differentiation is neurite outgrowth and, although Figure 3.9 in section 3.3.3 clearly shows that clone 2E3 extended more neuritic processes than clone 1G3, $SH\text{-}SY5Y^{Untr}$ seemed to produce just as many of these processes as clone 2E3 in

spite of having much lower p-ERK1/2 levels. The explanation for this confusing picture is probably the involvement in neuronal differentiation of other signalling pathways not considered in these analyses.

6.5.2 Knockdown of PrP^C did not appear to rescue the alterations to growth factor signalling pathways that were induced by PrP^C transfection

Whilst the effects of PrP^C transfection on ERK1/2 activity were not consistent, the reduced levels of p-Akt in stably transfection clones 2E3 *and* 1G3 in the absence of any significant changes to total Akt expression did suggest that PrP^C expression may have altered the cellular response to specific growth factors. In an attempt to gather more evidence for the direct involvement of PrP^C in this process, I assessed how depleting PrP^C expression in the stably transfected clones affected Akt activation. The method used was the same as per the experiments to determine whether PrP^C knockdown rescued the altered $p75^{NTR}$ expression in clone 1G3 – cells were either transiently transfected with the PrP siRNA s72188 or the negative control siRNA or were exposed only to the carrier medium for the transfection reagent-siRNA complexes. Again, the culture medium was refreshed the day after transfection and the cells were subcultured into fresh plates two days later to ensure all the cultures were at similar densities. Cell lysis was performed on the fourth day post transfection. For the experiments to be technically manageable it was only possible to include SH-$SY5Y^{Untr}$ and clone 1G3 cultures and, due to time limitations, Akt activation could only be assessed in two independent experiments, which limits the conclusions that can be made from the data.

Quantitative western blotting indicated that total Akt levels and p-Akt/total Akt ratios in SH-$SY5Y^{Untr}$ and clone 1G3 cells not transfected with either siRNA were similar to the results presented in the previous section (Figure 6.9a-d). The data also indicated that transfection with the PrP siRNA did not increase Akt activation in clone 1G3; if anything, there was a tendency towards a lower p-Akt/total Akt ratio compared with negative control siRNA-transfected clone 1G3 cells (Figure 6.9d).

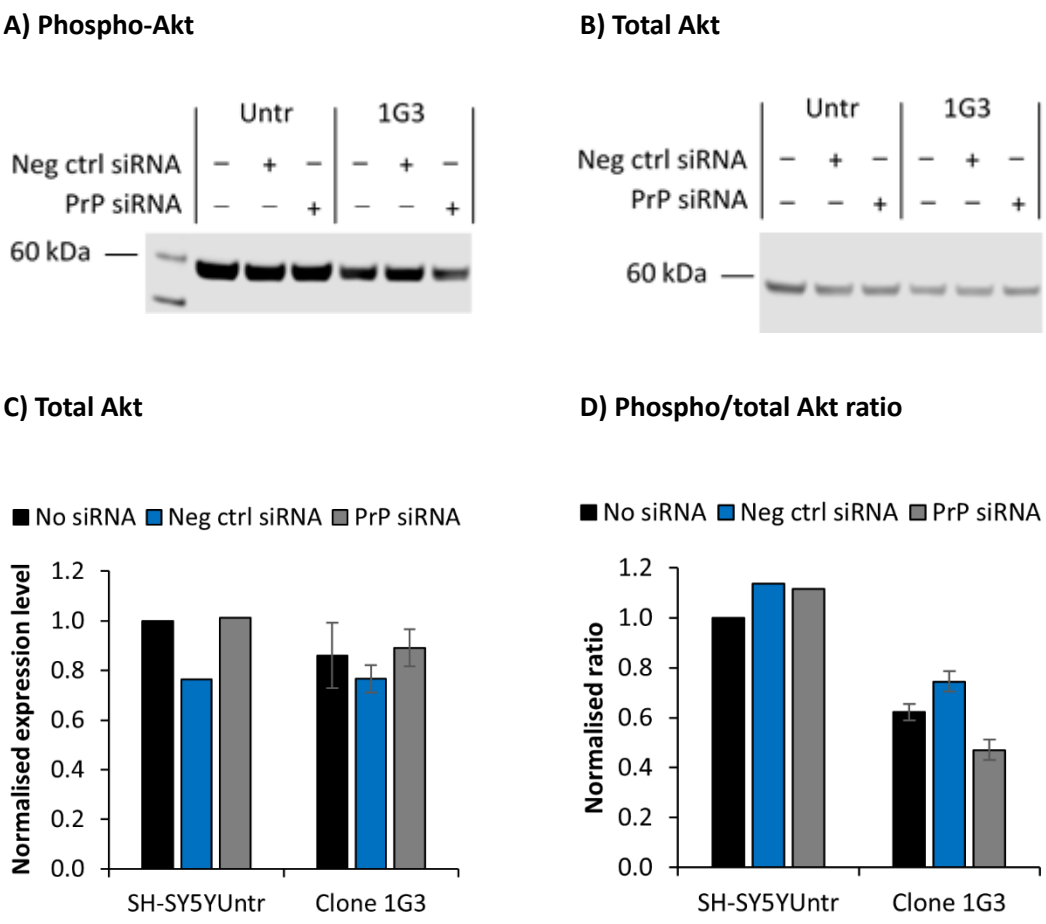

Figure 6.9 – PrP^C knockdown did not appear to rescue the differences in Akt activation between clone 1G3 and untransfected SH-SY5Y cells

Representative images of western blots of SH-SY5Y cell lysates that were simultaneously probed for Akt phosphorylated at Ser473 and total Akt **(A & B)**. Lysates had been prepared 4 days after $SH\text{-}SY5Y^{Untr}$ and clone 1G3 cells were transiently transfected either with the PrP-specific siRNA s72188 or a negative control siRNA. Control lysates were also prepared from cells not exposed to the transfection reagent. Primary antibodies were from Cell Signalling Technology and had the following catalogue numbers: #4060 **(A)** and #2920 **(B)**. Also shown are bar charts summarising quantification of total Akt **(C)** immunostaining in lysates obtained from two independent experiments as well as normalised ratios of phospho-/total Akt **(D)** levels. For each membrane, after correction for loading errors, total Akt band signals were normalised to the signal from $SH\text{-}SY5Y^{Untr}$ cells not exposed to the transfection reagent. Normalised phospho/total ratios were calculated by normalising the ratios for each lane to the ratio from the $SH\text{-}SY5Y^{Untr}$ lane. The overall mean normalised

expression values/ratios (+/- standard error of the mean) are displayed in the bar charts. Error bars are shown only for the clone 1G3 cultures, because siRNA transfections of SH-SY5Y^{Untr} were performed only for one of the experimental replicates.

Neither siRNA noticeably affected Akt activation in SH-SY5Y^{Untr} cultures nor total Akt levels in either cell line. As previously mentioned, the data in Figure 6.9 are only suggestive, because just two experimental replicates could be performed. Nevertheless, there was little evidence for PrP^{C} knockdown rescuing the altered Akt signalling displayed by clone 1G3. This was definitely not due to a lack of activity of the PrP siRNA, because PrP^{C} expression had already been shown to be knocked down effectively when using this method (Figure 6.6a). One possibility is that transient reduction of PrP^{C} expression is not sufficient to reverse the effects of stably transfecting SH-SY5Y cells with a protein they do not normally express, at least not at detectable levels. Indeed, a previous study found that complete knockout of PrP^{C} in an epithelial cell line had rather different effects compared to a transient knockdown of expression (Mehrabian et al., 2015). Whatever the reason for the lack of effect of PrP^{C} knockdown, what can be said is that, compared with SH-SY5Y^{Untr}, Akt activation was reduced in the stably transfected clones and differential activation of the PI3K-Akt pathway fits reasonably well with the altered expression of the NGF receptors TrkA and p75^{NTR}, although the PI3K/Akt pathway can also be modulated by growth factors other than NGF.

6.6 No evidence for direct interactions between PrP^C and receptors for nerve growth factor

The data presented in this chapter so far suggest that transfection of PrP^C into SH-SY5Y cells increased TrkA glycosylation and reduced p75-CTF levels, which may, in turn, have caused reduced activation of the PI3K/Akt pathway. What has yet to be addressed is how PrP^C could have altered expression of the NGF receptors. An indirect effect is plausible; for example, PrP^C could have affected the cellular response to a growth factor other than NGF, thereby affecting the expression of TrkA and $p75^{NTR}$. However, of the growth factors suggested by IPA as potential upstream regulators of the PrP^C transfection-induced proteomic changes (see section 6.1), NGF was the best candidate because it had a high activation state z-score. A second possibility is that PrP^C expression slowed down cell cycle progression by some other mechanism and, as a consequence, the proportions of the cells in each stage of the cell cycle were altered. This might have affected the overall expression levels of the NGF receptors in the cultures, since TrkA in preferentially expressed in the M and late G_1 phases and $p75^{NTR}$ in the S, G_2 and early G_1 phases (Urdiales et al., 1998; Bono et al., 1999). It was TrkA glycosylation, though, rather than its overall expression level that seemed to be altered in the stably transfected clones. TrkA is N-glycosylated, so a global effect of PrP^C expression on protein N-glycosylation could have been responsible for the increased levels of the 120 kDa TrkA glycoform. However, there was no evidence in the proteomic data obtained from the SH-SY5Y cell lines of any altered expression of enzymes involved in the early stages of N-glycosylation. For example, three subunits of the oligosaccharyltransferase enzyme complex that transfers glycan precursors to polypeptide chains being synthesised in the ER were identified in the proteomic datasets and were expressed at similar levels among the cell lines – the mean fold changes compared with $SH\text{-}SY5Y^{Untr}$ for these subunits were +1.12, +1.15 and +1.03 in clone 2E3 and -1.04, +1.03 and -1.05 in clone 1G3. Therefore, it is more likely that the differential glycosylation of TrkA was specific to that protein. Unfortunately, exactly what regulates whether a TrkA receptor does or does not get glycosylated within the ER seems to be unknown.

Activation of certain signalling pathways downstream of $p75^{NTR}$, such as the nuclear factor-kappa B pathway, seems to increase $p75^{NTR}$ expression (Choi and Friedman, 2009), thereby further enhancing signalling in a positive feedback loop. Therefore, if PrP^{C} were interacting with $p75^{NTR}$ directly and consequently altering its affinity for NGF and/or TrkA, downstream signalling would be affected and this might lead to a change in $p75^{NTR}$ expression. One problem with this idea is that expression of full length $p75^{NTR}$ was reduced only in clone 1G3 compared with SH-$SY5Y^{Untr}$, not in clone 2E3. p75-CTF levels appeared to be reduced in both clones, which might suggest that PrP^{C} inhibits alpha-cleavage of $p75^{NTR}$ but, because of its lower expression of the full length receptor, the proportion of $p75^{NTR}$ that was cleaved by clone 1G3 may actually have been higher than in SH-$SY5Y^{Untr}$. Nonetheless, it still seemed likely that if PrP^{C} were causing the altered expression of the NGF receptors, it would be by direct interaction, especially because PrP^{C}, $p75^{NTR}$ and TrkA are all found in the same cell membrane microdomains known as lipid rafts (Vey et al., 1996; Huang et al., 1999). To investigate putative interactions between PrP^{C} and the NGF receptors, analyses of the proteins that co-immunoprecipitated with PrP^{C} were performed. In the absence of cross-linking, cell lysis prior to co-immunoprecipitation (co-IP) has to be performed under non-denaturing conditions to maintain the existing protein-protein interactions. However, non-denaturing detergents like Triton X-100 may insufficiently solubilise proteins residing in lipid rafts. Therefore, a buffer containing 1 % (v/v) Triton, 0.25 % (w/v) sodium deoxycholate (SDA) and 1.5 % (w/v) N-octyl glucopyranoside was initially used for lysis. SDA effectively solubilises membrane proteins (Zhou et al., 2006), although it can also be denaturing, which meant the concentration had to be kept low. N-octyl glucopyranoside is also known to improve extraction of membrane proteins (Kan et al., 2013) but is not thought to disrupt protein-protein interactions. After lysis, the anti-PrP^{C} antibody BC6 (McCutcheon et al., 2014) was used for immunoprecipitation of PrP^{C} along with any interacting partners. Protein G-conjugated magnetic beads were used to extract the antibody-protein complexes and, following washes to remove non-specific binders, the remaining proteins were eluted from the beads and analysed by western blotting. Because initial experiments showed that a large proportion of the PrP^{C} in the original cell lysates was not carried through to the final samples (data

not shown), SDA was removed from the lysis buffer in case it was disrupting the interactions between protein G and the antibody or between the antibody and PrP^C. Figure 6.10 mainly shows the data from co-IP experiments performed on lysates prepared without SDA in the buffer. Loss of PrP^C from the final samples was reduced by this method – Figure 6.10a demonstrates that PrP^C was present at high levels in a BC6 co-IP sample prepared from a clone 1G3 lysate, whilst minimal staining was observed in the sample prepared using an isotype control antibody (IgG_1). The ~50 kDa bands near the top of Figure 6.10a represent detection of the heavy chains of the antibodies used for co-IP by the secondary antibody used for western blotting. Figure 6.10b & c indicate that all the TrkA iso/glycoforms and the various forms of $p75^{NTR}$ were detectable in the original cell lysates but did not co-immunoprecipitate with PrP^C – any staining from the BC6 co-IP sample was also present in the isotype control co-IP sample. Again, the bands at 25 and 50 kDa in Figure 6.10c are from the antibodies used for co-IP (light and heavy chains, respectively).

Sortilin can interact with $p75^{NTR}$ to modulate NGF signalling (Nykjaer et al., 2004) and was recently reported to interact with PrP^C (Uchiyama and Sakaguchi, 2016). Therefore, whether sortilin co-immunoprecipitated with the PrP^C expressed by the…

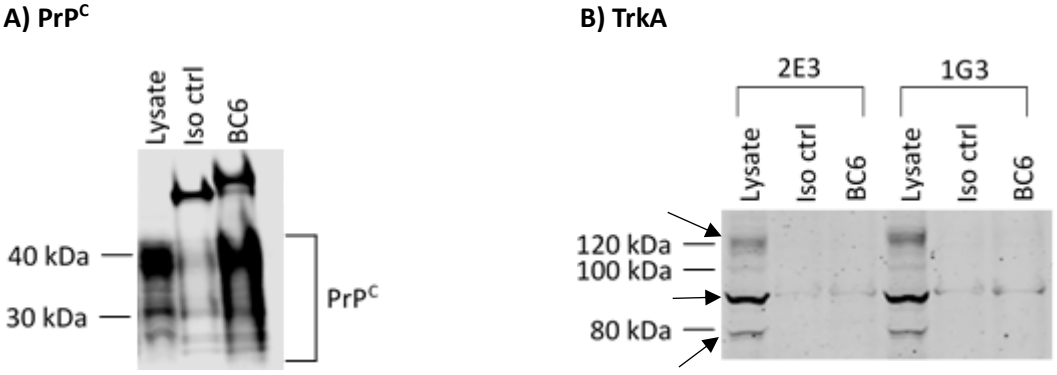

Figure 6.10 – Nerve growth factor receptors did not co-immunoprecipitate with PrP^C

See following page for legend…

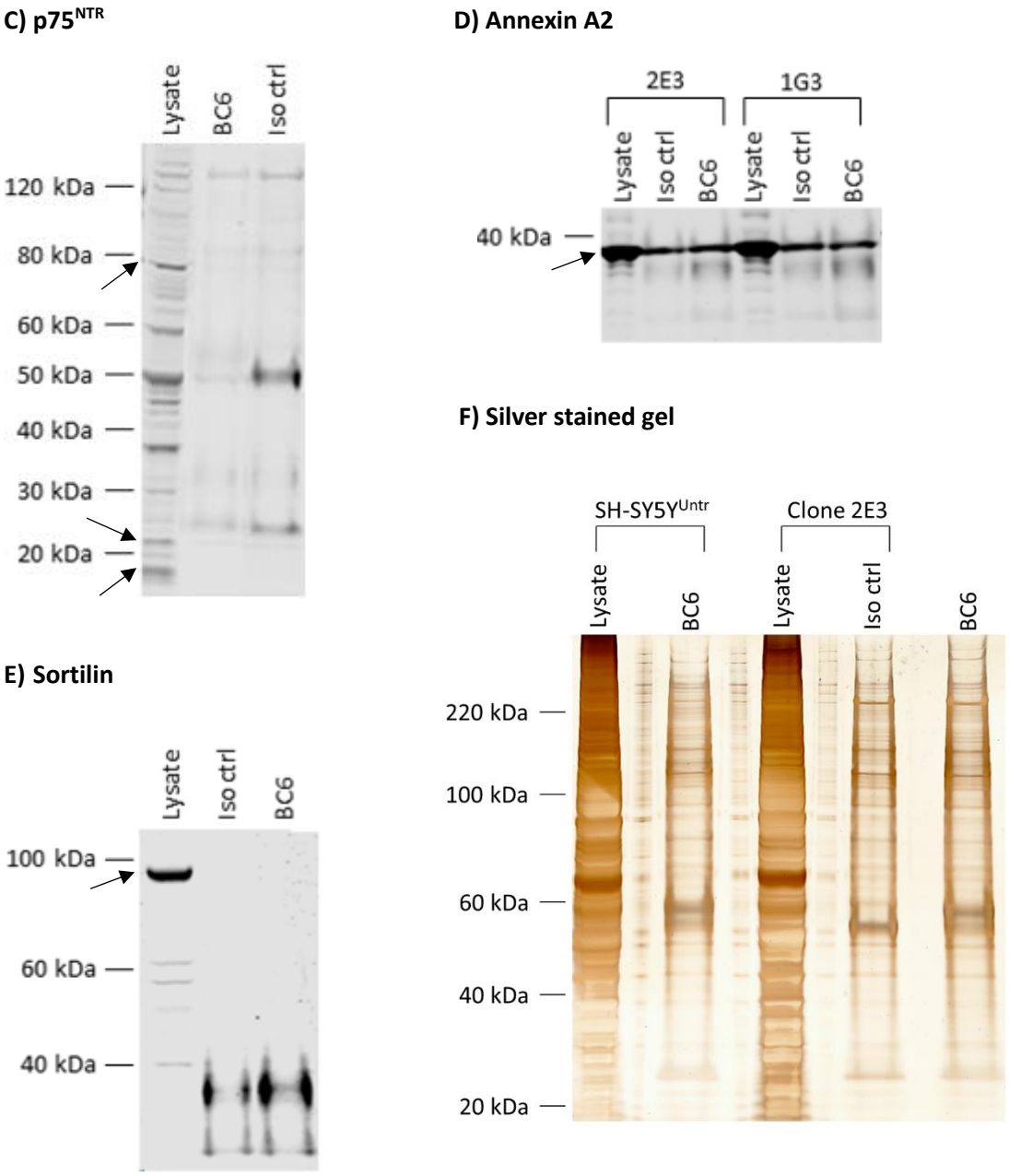

Figure 6.10 – Nerve growth factor receptors did not co-immunoprecipitate with PrP^{C}

A-E) Images of western blots from PrP^{C} co-IP experiments that were probed for PrP^{C} **(A)**, TrkA **(B)**, p75^{NTR} **(C)**, annexin A2 **(D)** or sortilin **(E)** using the following antibodies: **A)** BC6 anti-PrP^{C} (McCutcheon et al., 2014), **B)** Cell Signalling Technology #2505, **C)** rabbit 9992 anti-serum (see **Appendix I** for details), **D)** Cell Signalling Technology #8235, and **E)** Proteintech #12369-1AP. The relevant bands are indicated with arrows. In each case, the samples

obtained following PrP^C immunoprecipitation from cell lysates using the BC6 anti-PrP^C antibody were analysed alongside samples of the isotype control (IgG_1) reaction (antibody from Cell Signalling Technology, #5415) and the original cell lysate. Image **A** shows data from clone 1G3 cells, images **C** and **E** the data from clone 2E3 cells. **B)** PrP^C was strongly detected in the BC6 co-IP reaction and the original lysate, whilst minimal staining was observed in the isotype control lane. **C-E)** Any specific immunostaining was found equally in the BC6 and isotype control co-IP reactions. **F)** Image of a representative silver-stained gel from a PrP^C co-IP experiment.

…stably transfected SH-SY5Y cells was investigated. Figure 6.10e shows that sortilin was easily detectable in the original cell lysate (clone 2E3) but was not present in the BC6 co-IP sample. In a further attempt to validate the co-IP assay, a western blot of the co-IP samples was probed for annexin A2. This protein is thought to be an interacting of partner of PrP^C (Morel et al., 2008) and, therefore, would be expected to co-immunoprecipitate with PrP^C. However, Figure 6.10d indicates that, although the BC6 co-IP sample contained a small amount of annexin A2, it was also present in the isotype control co-IP sample. The lack of specific detection in the BC6 co-IP sample of two proteins that reportedly interact with PrP^C is strange, since the non-specific co-IP of limited amounts of annexin A2 seemingly rules out the possibility that the bead washes were so "harsh" that the proteins interacting with PrP^C were simply washed away. Interestingly, when analysing the co-IP samples on a gel and silver staining to detect protein bands (Figure 6.10f), the most intense bands corresponded to antibody heavy and light chains, whilst the fainter bands all appeared to be non-specific contaminants, since they were present in both BC6 and isotype control co-IP samples. This raises the question of whether any proteins were co-immunoprecipitated with PrP^C in sufficient amounts for western blot detection. Because of this, the results of these co-IP experiments are inconclusive: it is still plausible that PrP^C interacts with a receptor for NGF but the interaction may be too weak and/or transient for detection by this method. A future approach might be to use a cross-linking reagent to stabilise the interactions between proteins prior to lysis, which would be more effective for identifying weaker interactions. Additionally, it

would be useful to repeat the co-IP experiments with another PrP^C antibody that recognises a different epitope of the protein, since it may be that the epitope bound by BC6 is obscured by interactions with other proteins, leading to immunoprecipitation of only the PrP^C molecules not involved in any interactions at that time.

In spite of the lack of data for a direct interaction between PrP^C and one or more of the receptors for NGF, several lines of evidence reported in this chapter do support the idea that PrP^C modulates NGF signalling pathways. Such a role for PrP^C gives rise to a number of predictions for phenotypes one would expect to observe in PrP^C-null mice. In this vein, Chapter 6 ends by covering preliminary experiments to investigate whether PrP^C knockout affects the expression of key proteins in certain metabolic processes that are known to be regulated by $p75^{NTR}$.

6.7 No evidence for PrP^C knockout affecting specific metabolic processes *in vivo*

If PrP^C can modulate NGF signalling then PrP^C-null mice would be expected to display certain phenotypes consistent with deregulation of NGF signalling. As previously described, $p75^{NTR}$ is perhaps the most likely target for modulation by PrP^C. Among other roles, $p75^{NTR}$ appears to be part of a network of proteins, the circadian clock, that work together to regulate circadian rhythms (Baeza-Raja et al., 2013). Metabolic processes are typically regulated in a circadian manner (Dibner et al., 2010), which may explain why knockout of $p75^{NTR}$ in mice results in several metabolic defects; for instance, Baeza-Raja et al. (2013) showed that mRNA expression levels of solute carrier family 2, facilitated glucose transporter member 4 (GLUT4) were increased and the levels of phosphoenolpyruvate carboxykinase, cytosolic (PCK1) and fatty acid synthase (FASN) decreased in the livers of $p75^{NTR}$-null mice compared with wild type controls. GLUT4 is the main insulin-responsive glucose transporter – insulin promotes its translocation from the cytoplasm to the cell membrane where its function is to transport glucose into the cell (Herman and Kahn, 2006). PCK1 is also involved in glucose homeostasis, since it is one of the rate-limiting enzymes in gluconeogenesis (Yoon et al., 2001), the process that synthesises glucose from non-carbohydrate substrates. Finally, FASN is a multi-enzyme protein that catalyses *de novo* production of fatty acids from other metabolites (Menendez and Lupu, 2007). These molecular changes, and others, result in hypersensitivity to insulin and altered glucose metabolism in $p75^{NTR}$-null mice (Baeza-Raja et al., 2012; Baeza-Raja et al., 2013). $p75^{NTR}$ knockout also disrupts the ability of the liver to repair itself after injury (Passino et al., 2007). Interestingly, *Prnp* mRNA levels oscillate in a circadian manner in the brain (Cagampang et al., 1999) and PrP^C-null mice display circadian rhythm disruption, including impaired melatonin production (Brown et al., 2002), altered sleep structure and altered response to sleep deprivation (Tobler et al., 1996; Sanchez-Alavez et al., 2007). Moreover, there are indications that PrP^C-null mice also have altered responsiveness to insulin, though in this case they are hyposensitive, which leads to an impaired ability to control blood glucose (Strom et al., 2011; Brito et al., 2013).

Given the changes to glucose homeostasis that reportedly arise from both $p75^{NTR}$ and PrP^{C} knockout, I decided to perform a simple pilot experiment to determine whether similar molecular changes to those observed in $p75^{NTR}$-null livers were also found in the livers of mice lacking PrP^{C}. Firstly, four PrP^{C}-null and four wild type mice were culled and their livers removed and snap frozen in liquid nitrogen. These steps were performed by Ms. Rebecca Hogan, a senior animal technician within the Roslin Institute's Biological Resource Facility. The liver tissues were from relatively young (3-4 months of age), adult mice of the same lines (Manson et al., 1994) as the forebrain tissues used in previous experiments (see sections 5.3, 5.5 and 6.4.4). Next, the livers were homogenised by following the same method as was used for brain homogenisation, and PrP^{C} expression was assessed by western blotting. An earlier study found a lack of PrP^{C} expression in healthy liver tissue (Savas et al., 2010), although detection at the protein level has been reported in diseased human livers (Savas et al., 2010), probably as a result of its upregulation in liver injury-activated hepatic stellate cells (Ikeda et al., 1998). My analysis showed that PrP^{C} was, in fact, expressed in the wild type livers, albeit in small amounts, and was absent from the PrP^{C}-null livers as expected (Figure 6.11a). $p75^{NTR}$ expression was also investigated to determine if it varied according to *Prnp* genotype. Use of the 9992 $p75^{NTR}$ antibody produced a noticeably different band pattern to that obtained from the forebrain tissues (see Figure 6.7c for image of the blot from the brains). Figure 6.11b shows that the most intense band was detected at ~45 kDa, presumably corresponding to unglycosylated $p75^{NTR}$. No clear band for the glycosylated, full length protein could be identified at the expected 78 kDa, although the ~19 and 24 kDa bands thought to correspond to the $p75^{NTR}$ cleavage fragments were detected. In any case, Figure 6.11c demonstrates that none of the various forms of $p75^{NTR}$ varied in their expression between the livers of PrP^{C}-null and wild type control mice. Finally, TrkA expression in the liver tissues was investigated but the receptor was not present in sufficient amounts for quantification (data not shown).

The next step was to investigate the expression of GLUT4, FASN and PCK1, which were reportedly differentially expressed at the transcript level in $p75^{NTR}$-null mice, as described previously. I was able to detect all three proteins in the liver tissues, as…

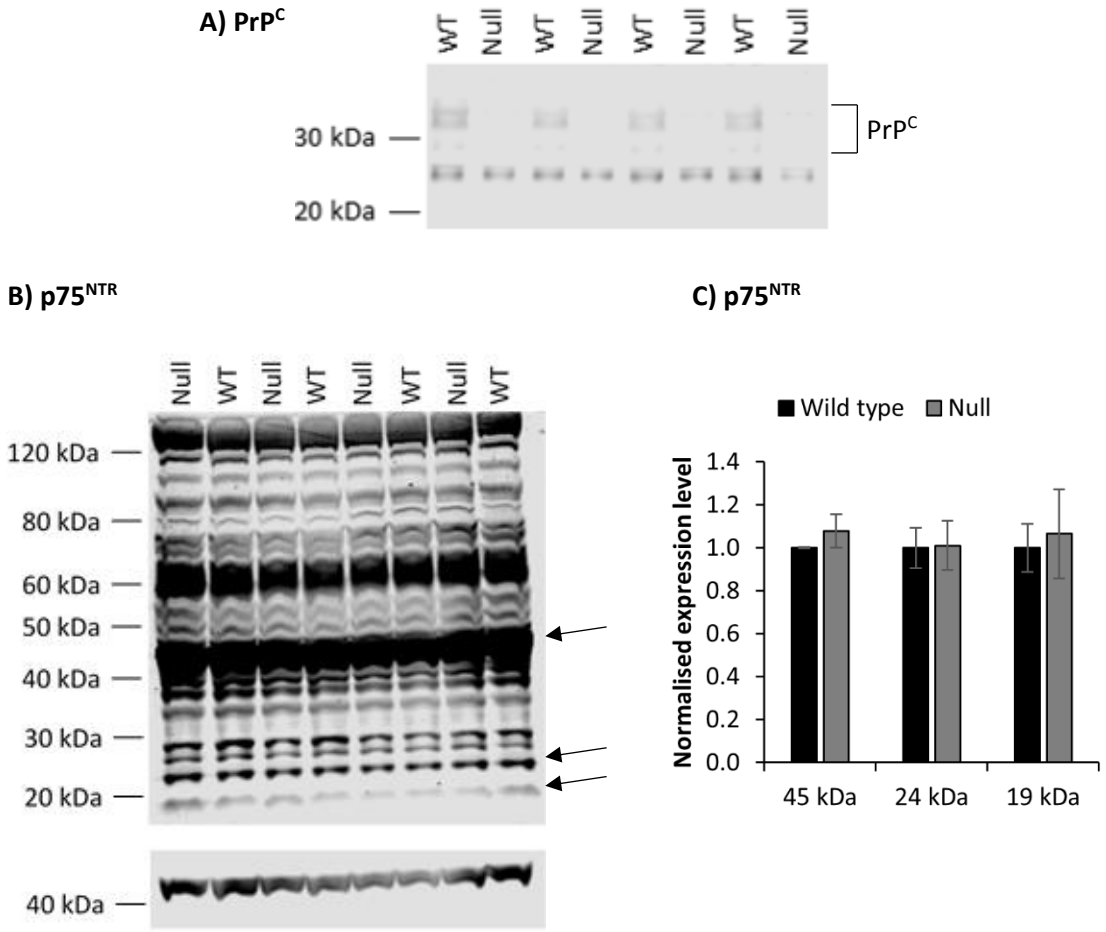

Figure 6.11 – p75^{NTR} expression did not vary between wild type and PrP^{C}-null mouse livers

A) Western blot image showing detection of PrP^{C} immunostaining in 4 wild type (WT) but not 4 PrP^{C}-null liver homogenates. PrP^{C} was detected by use of the BC6 anti-PrP^{C} primary antibody (McCutcheon et al., 2014). **B)** Image of a western blot of the same homogenates that was probed for p75^{NTR} using the 9992 antiserum (see **Appendix I** for more details). The bottom part is the same image but focusing on the approximately 45 kDa bands with the brightness setting reduced. **C)** Bar chart summarising quantification of p75^{NTR} immunostaining in image **B**. Data is shown for the 45 kDa, 24 kDa (p75-CTF) and 19 kDa (p75-ICD) bands. After correction for loading errors, the data were normalised to the mean signal from the WT homogenates. Overall mean normalised expression values for each genotype were calculated and are indicated in the charts (+/- standard error of the mean). Expression differences between genotypes were tested for significance ($p < 0.05$) using unpaired, two-sample t-tests but no comparisons met the threshold.

demonstrated in Figure 6.12a-c – the relevant bands are shown with arrows. The bands at 25 kDa and just over 50 kDa on the GLUT4 blot (Figure 6.12a) are the light and heavy chains of antibodies present in the homogenised livers. Since the actual molecular weight of GLUT4 is 54.8 kDa it is possible that GLUT4 staining was masked by the antibody heavy chain. However, previous studies have shown that the apparent molecular weight of GLUT4 on a western blot can be ~45 kDa (Brosius et al., 1992; Stuart et al., 2009), so the bands at approximately that molecular weight in Figure 6.12a were presumed to be GLUT4 and were quantified. The apparent molecular weight of PCK1 on a western blot was predicted to be 63 kDa according to the antibody manufacturer. Therefore, the higher of the two bands on Figure 6.12b was quantified. The identity of the lower band is unclear, since the Uniprot entry for PCK1 (#Q9Z2V4) does not report any other isoforms for the protein. Figure 6.12d demonstrates that none of GLUT4, PCK1 and FASN were significantly altered in their expression in PrP^C-null livers compared with wild type controls. Given the putative opposing effects of $p75^{NTR}$ and PrP^C knockout on insulin resistance, the apparent increase in GLUT4 expression in $p75^{NTR}$-null mice might suggest a decrease in expression in mice lacking PrP^C. Although non-significant (unpaired, two-sample t-test: $p = 0.187$), there was a trend towards reduced GLUT4 levels in the PrP^C-null mice compared with wild type controls (-1.12 fold change). Unfortunately, there was not enough time to expand this analysis to encompass more than four tissues of each genotype, which might have revealed a significant difference in GLUT4 expression.

Because forebrain homogenates from wild type and PrP^C-null mice had already been prepared for other experiments reported in this thesis, it seemed worthwhile to also assess GLUT4, PCK1 and FASN expression in these tissues, particularly because 10 tissues of each genotype had been homogenised, providing greater potential statistical power than the analyses of the liver tissues. Initially though, expression levels of the three target proteins were assessed in six forebrain homogenates (three male, three female) of each genotype, again by western blotting. Figure 6.13a shows that, for many of the homogenates, the 45 kDa GLUT4 bands were weaker relative…

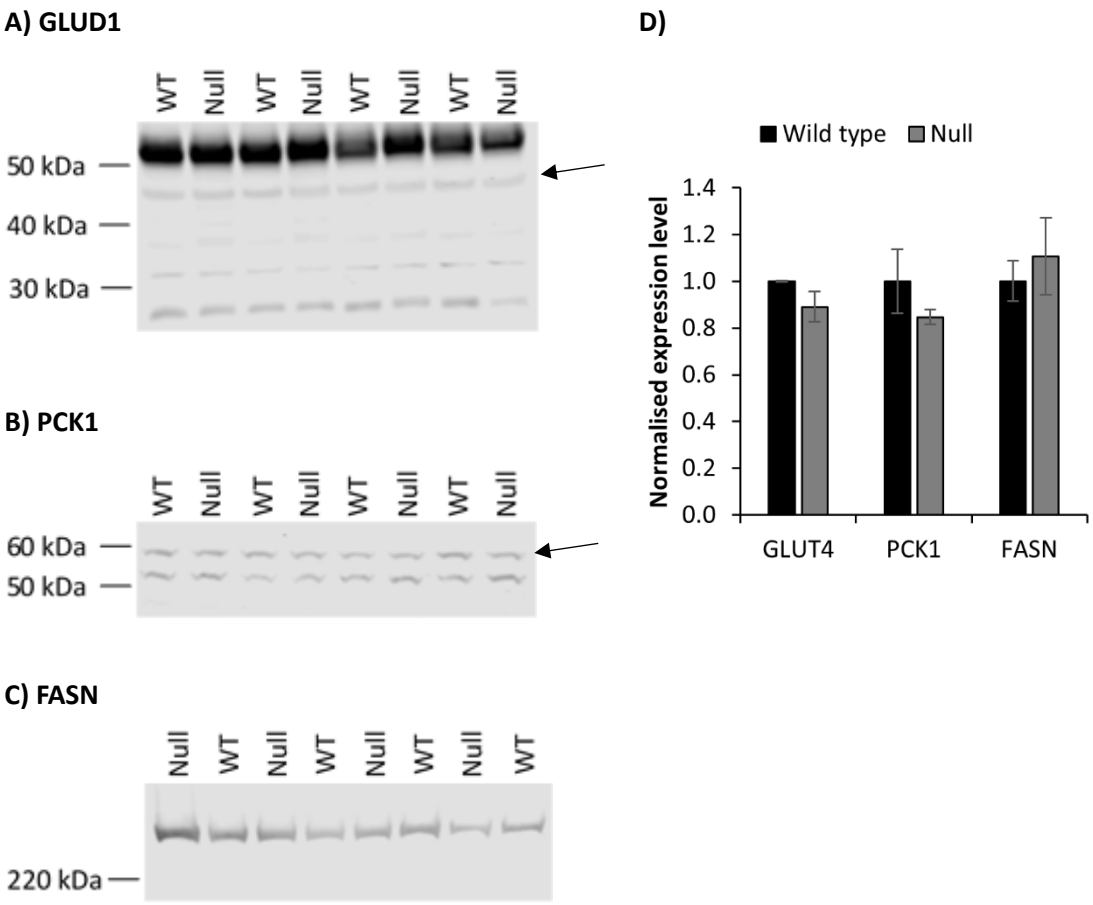

Figure 6.12 – Expression levels of key proteins involved in glucose homeostasis and lipogenesis did not vary between wild type and PrP^C-null mouse livers

Representative images of western blots of 4 wild type (WT) and 4 PrP^C-null mouse liver homogenates that were probed for GLUT4 **(A)**, PCK1 **(B)** or FASN **(C)**. The relevant bands are indicated with arrows. Primary antibodies were all from Cell Signalling Technology and had the following catalogue numbers: #2213 **(A)**, #12940 **(B)** and #3180 **(C)**. **D)** Bar chart summarising quantification of GLUT4, PCK1 and FASN immunostaining. For each membrane, after correction for loading errors, the data were normalised to the mean signal from the WT tissues. Next, the means of the normalised expression values from at least two technical replicates were calculated for each tissue. Overall mean normalised expression values for each genotype were calculated and are indicated in the bar charts (+/- standard error of the mean). Expression differences between genotypes were tested for significance ($p < 0.05$) using unpaired, two-sample t-tests but no comparisons met the threshold.

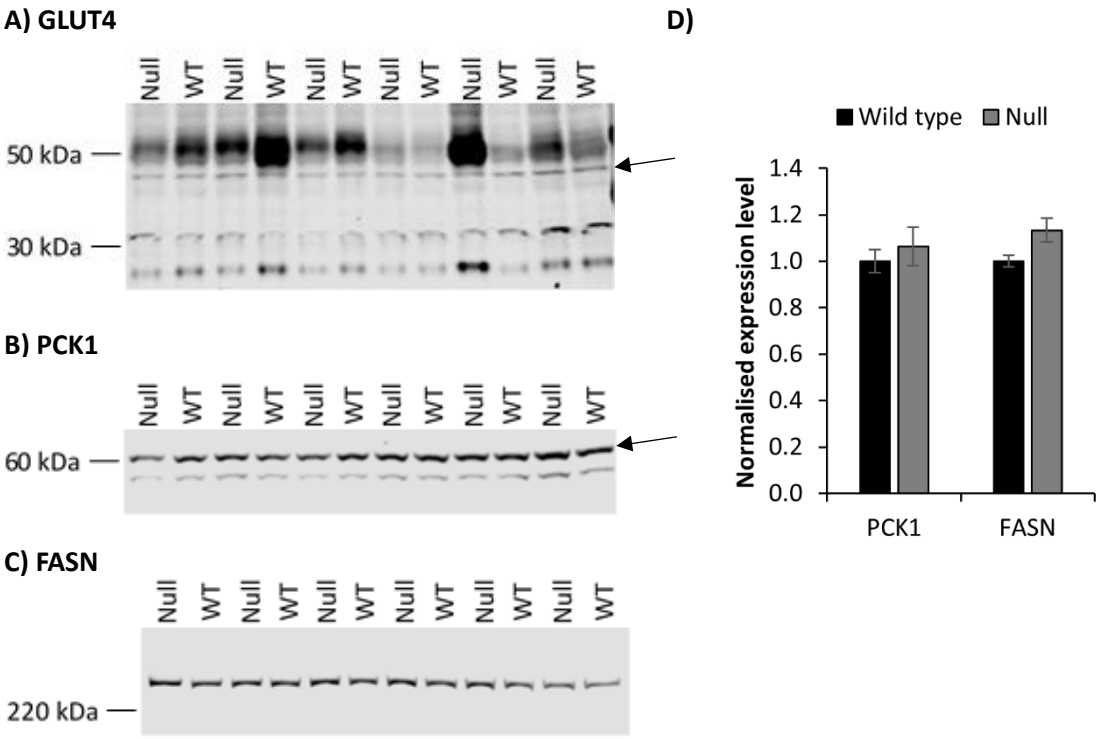

Figure 6.13 – Expression levels of key proteins involved in glucose homeostasis and lipogenesis did not vary between wild type and PrP^C-null mouse forebrains

Representative images of western blots of 6 wild type (WT) and 6 PrP^C-null mouse forebrain homogenates that were probed for GLUT4 **(A)**, PCK1 **(B)** or FASN **(C)**. The relevant bands are indicated with arrows. Primary antibodies were all from Cell Signalling Technology and had the following catalogue numbers: #2213 **(A)**, #12940 **(B)** and #3180 **(C)**. **D)** Bar chart summarising quantification of PCK1 and FASN immunostaining. For each membrane, after correction for loading errors, the data were normalised to the mean signal from the WT tissues. Next, the means of the normalised expression values from two technical replicates were calculated for each tissue. Overall mean normalised expression values for each genotype were calculated and are indicated in the bar charts (+/- standard error of the mean). Expression differences between genotypes were tested for significance ($p < 0.05$) using unpaired, two-sample t-tests but no comparisons met the threshold.

…to the ~50 kDa antibody heavy chain bands than they were in blots of the liver homogenates. The result was that the antibody heavy chain bands interfered with

quantification of the 45 kDa bands in some of the lanes, making reliable assessment of GLUT4 levels impossible. PCK1 and FASN were easily detectable in the forebrain homogenates (Figure 6.13b & c) but, as was the case for the analyses of the liver tissues, their expression levels did not vary significantly according to genotype (Figure 6.13d), although FASN displayed a trend towards upregulation in the PrP^{C}-null tissues (+1.13 fold) that was close to significance (unpaired two-sample t-test: $p = 0.051$).

In conclusion, no compelling evidence was obtained for PrP^{C} knockout significantly affecting expression levels of GLUT4, PCK1 and FASN in either liver or forebrain tissues, although GLUT4 levels could not be quantified accurately in mouse forebrain. However, levels of *Glut4*, *Pck1* and *Fasn* transcripts are reportedly subject to circadian oscillations and the differential expression of these genes between $p75^{NTR}$-null and wild type control mice fluctuated similarly (Baeza-Raja et al., 2013). Analysing the expression of GLUT4, PCK1 and FASN in livers of mice culled at different times of the day/night would therefore provide more conclusive data.

6.8 Discussion

The previous chapter explored the downstream effects of PrP^C transfection into SH-SY5Y cells, which included altered expression of proteins involved in cytoskeletal organisation and reduced proliferation rates. This chapter has focused on a potential upstream mechanism to explain these changes, specifically that PrP^C modulates NGF signalling. This hypothesis arose from pathway analysis of the proteomic changes induced by PrP^C transfection, which showed that several targets of NGF were differentially expressed in a manner that hinted at altered regulation of NGF signalling pathways. Subsequent analysis of the expression levels of NGF receptors in the SH-SY5Y cells found that, although overall levels of the high affinity receptor TrkA were unaffected by PrP^C expression, the amount of TrkA that was glycosylated seemed to be increased. This change did not appear to be due to a global effect on protein N-glycosylation, although how PrP^C expression could regulate TrkA glycosylation specifically is not clear. PrP^C knockout had no effect on TrkA expression in the mouse forebrain but, interestingly, only the glycosylated form of the receptor was detected – this finding questions the physiological relevance of the results from the SH-SY5Y cells, in which the majority of TrkA was unglycosylated. Consequently, it would be useful to investigate whether there are any tissues that do express some TrkA in the unglycosylated form.

Unglycosylated TrkA is unresponsive to NGF, as shown in this thesis and by others (Watson et al., 1999), whilst the glycosylated receptor is phosphorylated and, therefore, activated by binding of NGF. Consequently, increased expression of glycosylated TrkA in the stably transfected clones compared with $SH\text{-}SY5Y^{Untr}$ suggested that p-TrkA levels would be similarly increased in response to any NGF present in the culture medium. However, this could not be proved because, whilst p-TrkA could just about be detected on a western blot, the bands were too faint for accurate quantification. Measuring p-TrkA levels following stimulation with exogenous NGF at a range of concentrations would the best way to obtain conclusive evidence for increased TrkA activation following PrP^C transfection.

In addition to the altered TrkA glycosylation, western blotting results suggested that p75-CTF, which is produced by alpha-cleavage of the $p75^{NTR}$ receptor, was downregulated in the stably transfected clones compared with $SH\text{-}SY5Y^{Untr}$. p75-CTF can be further processed to produce p75-ICD, which showed similar trends towards downregulation in clones 2E3 and 1G3, although these were not significant. The lack of statistical significance seemed to be because the levels of p75-ICD varied between experimental replicates more than the levels of p75-CTF, possibly because of the greater instability of p75-ICD (Zampieri et al., 2005). Whether cleavage of $p75^{NTR}$ is required for initiation of downstream signalling is unclear; certainly both p75-CTF and p75-ICD are bio-active, although there are conflicting reports of their exact functions (Jung et al., 2003; Kenchappa et al., 2006; Coulson et al., 2008; Matusica et al., 2013; Verbeke et al., 2013). Interestingly, compared with its cleavage fragments, full length $p75^{NTR}$ seemed to be affected quite differently by PrP^{C} transfection – it appeared to be downregulated in clone 1G3 compared with $SH\text{-}SY5Y^{Untr}$ but unaffected in clone 2E3. However, this may not be the full story because $p75^{NTR}$ receptors can self-assemble into homotrimeric complexes (Anastasia et al., 2015) and bands approximately matching the expected molecular weight of trimeric $p75^{NTR}$ were detected in western blots of SH-SY5Y cell lysates. Whether these bands were physiologically generated trimers, artefacts of the western blot process, or not $p75^{NTR}$ at all is unclear. In any case, the bands were detected at the very top of the western blot membranes, which meant that the transfer quality was too variable for accurate quantification. Nevertheless, the presence of trimeric $p75^{NTR}$ in addition to the monomeric form that was quantified could explain why the apparent expression trends for full length $p75^{NTR}$ were different from those for the cleavage fragments.

The PI3K/Akt and ERK1/2 pathways are key downstream mediators of the cellular response to various growth factors, including NGF. Given that NGF signalling via TrkA can modulate both pathways (Huang and Reichardt, 2003) and independent signalling through $p75^{NTR}$ can affect the PI3K/Akt pathway (Chen et al., 2009), it seemed possible that the altered expression of the NGF receptors in the stably transfected clones would translate into differential activation of these downstream

pathways. Akt activation was indeed shown to be affected by PrP^C transfection but ERK1/2 activation was altered only in clone 2E3 compared with SH-SY5Y^{Untr}, not in clone 1G3. These findings suggest that PrP^C modulates the PI3K-Akt pathway in SH-SY5Y cells but may not have any direct effect on ERK1/2 signalling. The PI3K-Akt signalling pathway promotes proliferation, so the reduced Akt activation in the stably transfected clones was in agreement with their slower proliferation compared with SH-SY5Y^{Untr}. Furthermore, since this pathway is considered important for neuronal survival (Chang et al., 2003), lower levels of Akt phosphorylation could explain the enhanced susceptibility to serum deprivation that resulted from PrP^C transfection (see section 3.4). This is because when cells are transferred to serum-free medium, p-Akt levels would be expected to drop due to the loss of growth factors present in the serum. In cells with lower baseline Akt activity it might take less time for p-Akt levels to reduce sufficiently for induction of apoptosis, potentially explaining why the stably transfected clones were less viable than SH-SY5Y^{Untr} after the same period of serum deprivation. Furthermore, the p-Akt/total Akt ratio was significantly lower in clone 1G3 than in clone 2E3, which is in line with the more pronounced sensitivity to serum deprivation of clone 1G3.

siRNA-mediated knockdown of PrP^C in the stably transfected clones was used in an attempt to confirm that the changes in expression of the NGF receptors and in the activity of the PI3K-Akt signalling pathway were under the control of PrP^C. No convincing evidence of PrP^C knockdown rescuing these phenotypes was obtained, although I did not have time to perform sufficient experimental replicates to determine conclusively the impacts on Akt activation, whilst some technical issues meant that the levels of glycosylated TrkA could not be quantified. It is also possible that transiently reducing PrP^C levels, albeit by a large amount, was not sufficient to reverse the original changes induced by stable transfection of PrP^C. This might especially be the case if PrP^C expression had driven the SH-SY5Y cells towards a more neuronal phenotype via increased NGF signalling. Such differentiation processes might not be reversible at all, even if PrP^C were knocked out completely. However, it is notable that, in spite of the lack of impact of PrP^C knockdown on Akt activation, the slower proliferation of the stably transfected clones was partially

rescued by knocking down PrP^C expression. Consequently, reduced activation of the Akt signalling pathway may not have been responsible for the slower proliferation of the clones.

One way for PrP^C to modulate NGF signalling pathways is by directly interacting with one or more of the NGF receptors. This is a credible hypothesis since PrP^C, $p75^{NTR}$ and TrkA all mainly reside in the lipid raft microdomains of the cell membrane (Vey et al., 1996; Huang et al., 1999). However, I found that neither TrkA nor $p75^{NTR}$ nor the $p75^{NTR}$ co-receptor sortilin co-immunoprecipitated with the PrP^C expressed by the stably transfected SH-SY5Y cells. These experiments do not rule out such interactions though: further experiments employing cross-linking of proteins prior to cell lysis as well as use of additional PrP^C antibodies recognising different epitopes of the protein would be useful for clarifying the situation. An interaction between PrP^C and full length $p75^{NTR}$ still seems plausible, especially because analysis of the genes with similar expression patterns to PrP^C *in vivo* hinted at involvement of PrP^C in BDNF signalling and both NGF and BDNF can bind to $p75^{NTR}$. By interacting with $p75^{NTR}$, PrP^C could modulate downstream signalling by affecting the affinity of $p75^{NTR}$ for NGF and/or TrkA. This, combined with the existence of feedback loops that connect activities of the downstream pathways to expression levels of the receptors (Lei and Parada, 2007; Choi and Friedman, 2009), could result in altered expression of TrkA and $p75^{NTR}$, although it would not explain why TrkA glycosylation was affected by PrP^C transfection.

Aside from the data obtained from the SH-SY5Y cells, the results of earlier studies *in vivo* also hint at a connection between PrP^C and $p75^{NTR}$ signalling. For example, $p75^{NTR}$-null mice displayed alterations to glucose homeostasis and other metabolic processes that may stem from the putative role of $p75^{NTR}$ in generating circadian rhythms (Baeza-Raja et al., 2012; Baeza-Raja et al., 2013). Similarly, PrP^C-null mice show signs of impaired blood glucose control (Strom et al., 2011; Brito et al., 2013) and have disrupted sleep patterns (Tobler et al., 1996; Sanchez-Alavez et al., 2007), which also links PrP^C to the regulation of circadian rhythm. An underlying mechanism of the changes to glucose homeostasis in $p75^{NTR}$-null mice is reported to

be altered expression in the liver of two key proteins: GLUT4 and PCK1. Therefore, the expression levels of these proteins and of FASN, which is involved in lipogenesis and was also differentially expressed in $p75^{NTR}$-null mice, were assessed in PrP^{C}-null and wild type livers. PrP^{C} genotype had no significant effects on the levels of these proteins in liver or on PCK1 and FASN expression in mouse forebrain – technical reasons meant that GLUT4 could not be quantified accurately in the brain tissues. However, these were just pilot experiments and, since GLUT4, PCK1 and FASN expression levels in the liver vary considerably throughout the day (Baeza-Raja et al., 2013), it would be more informative to analyse expression in livers isolated at different times of the day/night. Furthermore, the expression changes to these proteins may have been too small to detect from what were rather small sample sizes.

Chapter 7: Final conclusions and future directions

7.1 Conclusions

7.1.1 Lack of direct stress protection by PrP^C

PrP^C has previously been associated with numerous functions, including stress protection, neurite outgrowth, circadian rhythm generation and myelin maintenance. However, understanding of the basic molecular mechanisms controlled by PrP^C is still limited. The aim of my project was to investigate these mechanisms to shed light on the physiological function of PrP^C. I began by stably transfecting the SH-SY5Y neuroblastoma cell line with the *Prnp* CDS and isolating monoclonal, PrP^C-expressing lines. Initial characterisation work confirmed that the exogenous PrP^C was correctly targeted to the cell surface and that the four clones used in subsequent experiments expressed PrP^C at similar levels. Next, the putative role of PrP^C as a stress-protective protein was assessed by exposing the cells to several forms of stress. Two of four stably transfected clones (named 1G3 and 1F3) displayed significantly improved survival compared with SH-SY5Y^{Untr} in response to treatment with three chemical toxins: the oxidative toxin paraquat, the broad-spectrum protein kinase inhibitor staurosporine and the ER stress-inducer tunicamycin. However, the other two clones (2E3 and 1B5) were generally no more resistant to these toxins than the control line. The clone-specific nature of the altered stress responses meant that further evidence for the involvement of PrP^C was required. These follow-up experiments showed that transient knockdown of PrP^C expression did not affect the response to stress, suggesting that the enhanced resistance to the toxins that was displayed by clones 1G3 and 1F3 may have been independent of PrP^C expression. It is possible that a transient reduction in PrP^C levels was not sufficient to rescue the changes induced by stable transfection but this does not explain why the other two clones were no more resistant to the toxins than SH-SY5Y^{Untr}. Moreover, all four stably transfected clones displayed reduced viability in response to serum deprivation compared with SH-SY5Y^{Untr}. The observation that PrP^C transfection reduced the baseline activation state of Akt, a key player in the PI3K-Akt signalling pathway that is considered important for neuronal survival (Chang et al., 2003), could explain the increased sensitivity to serum

withdrawal. This is because in the absence of serum growth factors that stimulate the PI3K-Akt pathway, it is conceivable that a lower baseline level of signalling would result in the activity of the pathway reducing more quickly to a level that results in the induction of apoptosis. Additionally, analysis of proteomic data demonstrated that proteins involved in cell death and survival processes were overrepresented among the proteins differentially expressed upon PrP^{C} transfection. Furthermore, the directionality of these expression changes suggested that the stably transfected clones were less viable than SH-SHY5Y^{Untr} under standard culture conditions.

Overall, the data reported in this thesis are not consistent with a role for PrP^{C} in stress protection. It is, perhaps, not overly surprising that PrP^{C} expression failed to confer robust protection against staurosporine treatment or paraquat-induced oxidative stress given the contradictory reports in the literature – whilst many studies report that PrP^{C} expression is protective (Brown et al., 2002; Senator et al., 2004; Lopes et al., 2005), several others found no evidence of stress protection or even that PrP^{C} expression enhances sensitivity to these forms of stress (Paitel et al., 2004; Vassallo et al., 2005; Guillot-Sestier et al., 2009; Steinacker et al., 2010). However, the observation that PrP^{C} transfection reduces the viability of SH-SY5Y cells in response to serum deprivation does contradict the majority of studies that suggest a protective role for PrP^{C} (Kuwahara et al., 1999; Bounhar et al., 2001; Kim et al., 2004; Roucou et al., 2005; Krebs et al., 2007; Wu et al., 2008). The results from several of these studies (Kuwahara et al., 1999; Kim et al., 2004; Wu et al., 2008) are questionable though due to expression of doppel, another member of the prion protein family, by the hippocampal neuronal cell line used in the experiments. Publically available transcriptomic data (GeneAtlas U133A dataset (Su et al., 2004) accessed through BioGPS (Wu et al., 2016)) indicate that doppel expression is normally confined to the testes. Moreover, doppel was not detected in proteomic analyses of the SH-SY5Y cells used for the experiments reported in this thesis. Therefore, my data support the hypothesis that the stress-protective effect of PrP^{C} expression observed in the doppel-expressing hippocampal cell line was a result of PrP^{C} interacting with doppel to suppress its reported neurotoxic properties (Moore et al., 1999; Sakudo et al., 2005; Qin et al., 2006). This is unlikely to be a

physiologically relevant function of PrP^C given that PrP^C and doppel are not typically expressed in the same tissues.

Proteomic analyses of the SH-SY5Y cells were carried out to identify the pathways and processes affected by PrP^C transfection and to investigate why the stably transfected clones varied in their responses to stress in spite of similar PrP^C expression levels and localisation patterns. These experiments consisted of separate comparisons between SH-$SY5Y^{Untr}$ and clone 1G3, a clone that displayed enhanced resistance to the three chemical toxins, and between SH-$SY5Y^{Untr}$ and clone 2E3, a clone that was generally no more resistant than the control line. The proteomic data contained some indications that clone 1G3 was more differentiated towards a mature neuronal phenotype than clone 2E3 or SH-$SY5Y^{Untr}$; for example, neuroblast differentiation-associated protein AHNAK was upregulated by almost three fold in clone 1G3 compared with SH-$SY5Y^{Untr}$ but essentially unchanged in its expression in clone 2E3. However, neuromodulin and neurosecretory protein VGF, which are involved in neurite outgrowth processes, were upregulated in both clones compared with SH-$SY5Y^{Untr}$. Additionally, almost no neurite-like protrusions could be identified in phase contrast images of clone 1G3, whereas these structures were abundant in clone 2E3 and SH-$SY5Y^{Untr}$ cultures. Given that neurite outgrowth is a key feature of neuronal differentiation, these results were not consistent with clone 1G3 displaying a more mature neuronal phenotype. Therefore, to investigate further the differences between the clones in their responses to stress, additional proteomic experiments were carried out to identify the proteins differentially expressed following staurosporine treatment in SH-$SY5Y^{Untr}$ and in clones 2E3 and 1G3. In agreement with the cell viability data, pathway analysis of these datasets demonstrated that the molecular signatures of cell death were less pronounced in clone 1G3 than in either SH-$SY5Y^{Untr}$ or clone 2E3 in response to staurosporine exposure. Furthermore, the same analysis indicated that activity of the ERK1/2 signalling pathway, which normally promotes cell survival (Mebratu and Tesfaigzi, 2009), was reduced in clone 2E3 and SH-$SY5Y^{Untr}$ during stress but was possibly less affected in clone 1G3. One potential explanation was that the baseline expression level of STAT3, a pro-survival transcription factor activated by ERK1/2,

seemed to be higher in clone 1G3 compared with clone 2E3 and SH-SY5Y^{Untr}. This suggested that the pathway may have been more active under normal culture conditions in clone 1G3, thereby leading to its increased resistance to the protein kinase inhibitor staurosporine. However, western blotting data showed that baseline p-ERK1/2/total ERK1/2 ratios were similar in clone 1G3 and SH-SY5Y^{Untr}, whilst ERK1/2 activation in clone 2E3 was significantly greater than in both clone 1G3 and SH-SY5Y^{Untr}. Therefore, differential activation of the ERK1/2 signalling pathway does not explain the differing stress responses among the clones and no obvious alternative explanation could be identified from the proteomic data.

7.1.2 Downstream processes regulated by PrP^{C}

The proteomic datasets separately comparing SH-SY5Y^{Untr} with clones 2E3 and 1G3 were combined to select only the proteins differentially expressed in both stably transfected clones compared with SH-SY5Y^{Untr} – we hypothesised that these changes were the most likely to have resulted from PrP^{C} expression. Pathway analysis of these data suggested roles for PrP^{C} in cell cycle regulation, cytoskeletal organisation and ubiquitination, among other processes. Follow-up studies showed that the stably transfected clones proliferated more slowly than SH-SY5Y^{Untr}, a phenotype that was partially rescued by transient knockdown of PrP^{C} expression. A role for PrP^{C} as a negative regulator of proliferation has been observed previously in oligodendrocyte precursors, a neuronal cell line, and in cells derived from the intestinal epithelium (Kim et al., 2005; Morel et al., 2008; Bribian et al., 2012). In contrast, other studies have found that PrP^{C} promotes proliferation of neural precursors and mouse neuroblastoma cells (Steele et al., 2006; Llorens et al., 2013; Haigh and Collins, 2014).

No effects of PrP^{C} transfection on overall levels of protein ubiquitination were identified from western blotting experiments that made use of an antibody able to detect monomeric, unconjugated ubiquitin as well as ubiquitinated proteins. However, further analysis of the proteomic data showed that two E3 ubiquitin-protein ligases, SUGT1 and PRPF19, were downregulated in clones 2E3 and 1G3

compared with SH-SY5Y^{Untr}. The reduced SUGT1 expression may have been a consequence of the slower proliferation of the stably transfected clones, since SUGT1 is a member of the SCF ubiquitin ligase complex that controls the turnover of proteins involved in cell cycle regulation (Kitagawa et al., 1999). PRPF19 has a very different role – it ubiquitinates certain splicing factors to modify spliceosome function (Chanarat and Strasser, 2013). Other proteins involved in pre-mRNA splicing were also expressed at lower levels in the PrP^{C}-transfected cells, which could suggest a reduction in overall spliceosome activity. Although the mechanism for such an effect is not immediately clear, it is possible that the rate of protein synthesis is lower in slower-proliferating cells, which may result in a reduced requirement for spliceosome activity.

Western blotting of cell lysates showed that expression levels of three proteins involved in cytoskeletal organisation, seemed to be increased by PrP^{C} transfection – compared with SH-SY5Y^{Untr}, vimentin, caldesmon and zyxin were significantly upregulated in two, three and four stably transfected clones, respectively. Trends towards upregulation of vimentin and caldesmon that were close to significance were also observed in the remaining clones. The increase in caldesmon expression is particularly striking, since this protein is reportedly involved in Schwann cell migration during peripheral nerve regeneration (Han et al., 2007) and an adult-onset demyelination of the PNS has been observed in several PrP^{C} knockout mouse lines (Bremer et al., 2010; Nuvolone et al., 2016). To follow up this observation, caldesmon levels were assessed in age- and sex-matched wild type and PrP^{C}-null mouse forebrains but no significant difference between the genotypes was observed, perhaps because cell type-specific effects of PrP^{C} expression were averaged out over the entire tissue. Moreover, since the demyelinating phenotype of the PrP^{C}-null mice appears restricted to the PNS (Bremer et al., 2010), assessing caldesmon expression in peripheral nerves may be more informative. Such tissues were not immediately available however.

Confocal imaging showed that the actin cytoskeleton of clone 1G3 differed from clone 2E3 and SH-SY5Y^{Untr} – clone 1G3 cells seemed to contain thick stress fibres,

which are associated with reduced cell motility and greater cytoskeletal stability (Troller and Larsson, 2006). Increased stability of actin microfilaments disrupts the formation, extension and movement of filopodia, which are dynamic protrusions from the neurite growth cone that respond to extracellular signals to guide migration of developing neurites (O'Connor et al., 1990). This may explain why clone 1G3 produced fewer neurite-like protrusions than the other cell lines. The RhoA-ROCK signalling pathway, which PrP^{C} has previously been reported to modulate, is known to promote the formation of stress fibres and inhibit neurite outgrowth (Altun-Gultekin et al., 1998; Loubet et al., 2012), so this pathway may have been more active in clone 1G3. However, this is not a complete explanation, since activated RhoA is reported to promote proliferation (Yu and Brown, 2015), whereas clone 1G3 proliferated slower than SH-$SY5Y^{Untr}$ and clone 2E3. Interestingly, neuromodulin, annexin A2, neurosecretory protein VGF and zyxin – proteins that positively correlate with neurite outgrowth in their expression – were generally more abundant in the stably transfected clones than in SH-$SY5Y^{Untr}$. It is unclear why PrP^{C} transfection induced proteomic alterations associated with increased neurite outgrowth at the same time as causing other molecular changes linked to its repression.

In spite of the tendency towards increased caldesmon expression in the PrP^{C}-transfected SH-SY5Y cells, differential expression was not observed between PrP^{C}-null and wild type forebrains. Similarly, no genotype-dependent alterations in the expression levels of annexin A2, neurosecretory protein VGF or zyxin were identified in the same tissues. These results are in line with published proteomic studies that found no differentially expressed proteins in the brains of PrP^{C} knockout mice compared with controls (Crecelius et al., 2008; Mehrabian et al., 2016). However, I was able to identify two proteins that were upregulated in the mouse forebrain as a result of PrP^{C} knockout; these were connexin-43 and GLUD1. These proteins were targeted as a part of an attempt to validate an earlier study performed by my research group that identified proteomic and transcriptomic changes in the forebrain resulting from PrP^{C} ablation in the mouse. Importantly, these forebrain tissues were from the Npu line of PrP^{C} knockout mice, which is free from the issues

of mixed genetic background and ectopic doppel expression in the brain that affect most of the other knockout lines. Consequently, the differential expression of connexin-43 and GLUD1 is highly likely to have been caused by an absence of PrP^C expression. GLUD1 is involved in the metabolism of glutamate, which is of note given that PrP^C has been suggested previously to protect neurons from excitotoxic cell death caused by hyperactivation of glutamate receptors (Sakurai-Yamashita et al., 2005; Frigg et al., 2006; Khosravani et al., 2008). Connexin-43 is part of a protein family that forms gap junctions, which provide cytoplasmic connections between neighbouring cells and allow regulated intercellular transport of molecules, including calcium ions (Evans and Martin, 2002). Gap junctions between neurons, known as electrical synapses, enable the synchronised firing of large neuronal networks that is characteristic of the immature CNS (Ben-Ari, 2001). The upregulation of connexin-43 suggests that PrP^C-null mice could have a greater density of electrical synapses and, since this form of synapse becomes rarer as the CNS develops (Arumugam et al., 2005), it may be that PrP^C knockout subtly impairs the maturation of the CNS. This could provide an alternative explanation for the reported learning and memory deficits of PrP^C-null mice (Rial et al., 2009; Schmitz et al., 2014). Furthermore, PrP^C downregulating connexin-43 expression in the brain could be the reason why connexin-43 levels are reportedly increased in mouse models of TSEs (Lee et al., 2015), since PrP^C levels tend to fall as disease progresses (Mays et al., 2014).

7.1.3 Connections between PrP^C and NGF/neurotrophin signalling

Pathway analysis of the aforementioned proteomic datasets suggested that altered activity of NGF signalling pathways could explain some of the proteomic changes induced by PrP^C transfection into the SH-SY5Y cells. Additionally, analysis of publically available microarray data from various tissues and cell types showed that targets of BDNF were overrepresented among the genes with similar spatial expression patterns to *PRNP* in both mice and humans. Taken together, these results suggested that PrP^C might modulate the cellular response to neurotrophins. Since SH-SY5Y cells do not express TrkB, the high affinity receptor for BDNF, subsequent

experiments focused solely on NGF signalling. Firstly, I examined the expression levels of the NGF receptors and found that, although overall TrkA expression was unaffected by PrP^C transfection, the levels of NGF-responsive TrkA were increased, mainly because a greater proportion of TrkA was glycosylated. A further examination of the proteomic datasets suggested that any alteration to TrkA glycosylation was unlikely to have resulted from a global effect of PrP^C expression on N-glycosylation, since key components of this pathway did not vary in their expression between the stably transfected clones and SH-SY5Y^{Untr}. Therefore, TrkA glycosylation may have been affected specifically, although no information about the regulation of TrkA glycosylation could be identified from the literature. In contrast to the effects on TrkA expression, western blotting data suggested that levels of p75-CTF were lower in the stably transfected clones compared with SH-SY5Y^{Untr}. p75-ICD expression seemed to vary similarly, although these changes were not statistically significant. Furthermore, it was not possible to determine conclusively the expression levels of full length $p75^{NTR}$ by western blotting due to the tendency of the receptor to self-assemble into trimers. As a consequence, I cannot be certain whether PrP^C transfection reduced the rate of $p75^{NTR}$ cleavage or lowered the overall expression level of $p75^{NTR}$. It should also be cautioned that the "messy" nature of the $p75^{NTR}$ immunostaining pattern made it difficult to identify the relevant bands with certainty. Treatment of cells with compounds that induce $p75^{NTR}$ processing events or use of a negative control sample when western blotting would have helped to confirm specificity of the antibody.

The impact on downstream signalling of the differential expression of the NGF receptors was assessed by quantifying the activation states of key protein kinases in the pathways that mediate NGF-induced neuronal survival and differentiation (Huang and Reichardt, 2003). These data demonstrated that p-Akt/total Akt ratios were reduced by PrP^C transfection, indicating that the PI3K-Akt pathway that promotes survival and proliferation was less active. Whilst this finding is consistent with the slower proliferation of the stably transfected clones compared with SH-SY5Y^{Untr}, reduced Akt activity cannot easily be explained by the altered expression of the NGF receptors – the PI3K-Akt pathway is reportedly activated by

NGF binding to TrkA (Chang et al., 2003; Huang and Reichardt, 2003) and PrP^{C} transfection into the SH-SY5Y cells resulted in a greater proportion of TrkA being NGF-responsive. Of course it is possible that, in spite of expressing more NGF-responsive TrkA, NGF-TrkA signalling could have been less active in the stably transfected clones than in SH-SY5Y^{Untr}.

A credible hypothesis to explain the putative effect of PrP^{C} expression on NGF signalling pathways is that PrP^{C} interacts directly with one of the NGF receptors, especially given that PrP^{C}, TrkA and $p75^{NTR}$ all reside mainly in lipid rafts (Vey et al., 1996; Huang et al., 1999). Such an interaction might alter the affinity of the receptor for NGF or affect how it activates in response to NGF binding, for example. Consequently, the effect of PrP^{C} expression on the activities of downstream pathways would vary between cell types because of differences in the relative expression levels of TrkA, $p75^{NTR}$ and also the $p75^{NTR}$ co-receptor sortilin. This idea could explain why PrP^{C} has been associated with such a diverse array of functions and also how PrP^{C} expression can have opposing effects on the same process, such as proliferation, in different types of cell. In the case of the SH-SY5Y cells used in my experiments, a change in NGF signalling caused by PrP^{C} transfection may have resulted in altered expression of the NGF receptors via positive or negative feedback loops. For example, $p75^{NTR}$ expression is known to be upregulated by nuclear factor-kappa B signalling, a pathway that is activated through $p75^{NTR}$ itself (Chen et al., 2009; Choi and Friedman, 2009).

Preliminary PrP^{C} co-IP experiments performed under non-denaturing conditions did not identify any interactions with TrkA or $p75^{NTR}$ or with the cleavage fragments p75-CTF or p75-ICD in PrP^{C}-transfected SH-SY5Y cells. Additionally, neither sortilin nor annexin A2 co-immunoprecipitated with PrP^{C} in spite of previous evidence of interactions between PrP^{C} and these proteins (Morel et al., 2008; Uchiyama and Sakaguchi, 2016). However, whilst the use of non-denaturing conditions minimises the detection of false positives, weak or transient interactions that may still be biologically relevant are unlikely to be detectable; incorporating

cross-linking prior to lysis to maintain protein-protein interactions would help to identify these less stable interactions.

One way to investigate the wider impact of the putative link between PrP^C and NGF signalling is to make use of PrP^C-knockout animals, which would be expected to display phenotypes consistent with deregulation of NGF signalling and potentially of those pathways controlled by other neurotrophins. In this regard, the adult-onset demyelination of the PNS in PrP^C-null mice is striking (Bremer et al., 2010; Nuvolone et al., 2016), given the reported involvement of $p75^{NTR}$ in signalling processes mediated by myelin components (Ahmed et al., 2006; Park et al., 2010b; Palandri et al., 2015) and the impairment of remyelination after peripheral nerve injury that is observed in $p75^{NTR}$ knockout mice (Song et al., 2006). Furthermore, $p75^{NTR}$ is proposed to be part of the circadian clock network that generates circadian rhythms (Baeza-Raja et al., 2013), and it is conceivable that PrP^C has a similar role given the report of circadian oscillation of *Prnp* expression in the brain (Cagampang et al., 1999) and the disrupted sleep observed in PrP^C-knockout mice (Tobler et al., 1996; Tobler et al., 1997; Sanchez-Alavez et al., 2007). This sleep disruption probably arises from deregulation of melatonin production (Brown et al., 2002) and it is interesting to note that my analysis of publically available microarray data from human and mouse tissues/cell types showed that components of the melatonin signalling pathway were overrepresented among the genes highly coexpressed with *PRNP*. The microarray data also indicate that TrkA gene expression was higher in the pineal gland, which produces melatonin, than it was in any other tissues.

Metabolic processes are regulated in a circadian manner (Dibner et al., 2010), which may explain why both $p75^{NTR}$ and PrP^C knockout mice display signs of disrupted glucose homeostasis (Strom et al., 2011; Baeza-Raja et al., 2012; Brito et al., 2013). The molecular changes underlying the altered glucose homeostasis of $p75^{NTR}$-null mice were reported to be differential expression of GLUT1 and PCK1 in the liver (Baeza-Raja et al., 2013). Therefore, the expression levels of these proteins and of FASN, which is involved in lipogenesis and also displayed altered expression upon $p75^{NTR}$ knockout (Baeza-Raja et al., 2013), were assessed in liver and brain tissues

from PrP^C-null and wild type control mice. No significant effects of PrP^C knockout on the expression levels of these proteins were identified in these pilot experiments. However, it is possible that differential expression would be revealed by analysing tissues isolated at different times of the day/night, since GLUT4, PCK1 and FASN expression levels oscillate according to circadian rhythms (Baeza-Raja et al., 2013).

7.1.4 Limitations of the data

As is the case for any scientific project, there are caveats associated with the results obtained from some of the experiments. Several of these limitations have been described in the previous sections of this chapter; some additional caveats are mentioned here. Firstly, it must be acknowledged that much of the data reported in this thesis was obtained from *in vitro* experiments, which puts the physiological relevance of the conclusions up for debate. However, there were several valid reasons for adopting such an approach, not least that this project aimed to identify the molecular mechanisms underlying PrP^C function. Numerous studies have identified phenotypes of PrP^C-null mice but it is the mechanistic understanding that is lacking, and this work is much more practical to carry out *in vitro*. A second potential criticism is that, rather than using a cell line, I could have investigated PrP^C function using primary neuronal cultures. However, culturing primary neurons is technical demanding and there are issues surrounding reproducibility and genetically manipulating these cells in culture (Karra and Dahm, 2010). Furthermore, any compensatory mechanisms active during the development of PrP^C-knockout mice might complicate analysis of PrP^C function in cells derived from those mice. Indeed, examples of mechanisms compensating for a lack of PrP^C expression during development have been reported previously (Shmerling et al., 1998; Hajj et al., 2007).

One potential criticism of the format of the *in vitro* experiments is that untransfected SH-SY5Y cells were not proper controls for the PrP^C-independent effects of transfection. However, whilst it makes sense to use cells transfected with the empty vector to control for presence of the antibiotic resistance gene and other vector

components in a transient transfection experiment, when stably transfecting cells such an approach does not control for the consequences of the vector integrating into the genome, since this will almost certainly occur at different sites for each clone. To alleviate this problem, I would have needed to derive and use multiple empty vector-transfected clones, which would have made the logistics of carrying out experiments very difficult. Therefore, on balance, untransfected cells matched to the stably transfected clones in terms of weeks in culture were considered acceptable controls.

Another potential issue with the cell model was that the transgenic PrP^C expressed by the stably transfected clones was abnormally glycosylated – specifically, the glycans on the di-glycosylated form of transgenic PrP^C had a greater combined molecular weight than the glycans on mouse brain PrP^C. However, such alterations to glycosylation are reported to occur frequently in cell lines but are thought to have few biological consequences (Varki and Lowe, 2009). Additionally, aside from the differences in glycan size, the majority of PrP^C expressed by the stably transfected clones was di-glycosylated as was the case in mouse forebrain.

The data reported in this thesis do not support a direct role for PrP^C in protecting cells from stress. Clones 1G3 and 1F3 did display increased viability and cytotoxicity in response to three chemical toxins compared with SH-SY5Y^{Untr} but the lack of effect of PrP^C knockdown on this phenotype suggests that it was not a result of PrP^C expression. However, whilst detailed characterisation of the cells suggested that PrP^C expression levels and localisation patterns were similar among the clones, a single western blot, performed prior to preparing frozen stocks of each clone, showed that PrP^C expression may have initially been higher in clones 1G3 and 1F3 than in clones 2E3 and 1B5. Later, PrP^C expression may have normalised to a stable level that was relatively consistent among the clones. If this were the case then it is conceivable that PrP^C expression in clones 1G3 and 1F3 may have initially exceeded some kind of threshold that resulted in a change to the cells that persisted even after a subsequent reduction in PrP^C expression. This might especially be the case if PrP^C expression had driven the SH-SY5Y cells towards a more neuronal phenotype via increased NGF signalling. Such a differentiation process might not be reversible even if PrP^C

expression was subsequently knocked out completely, which could explain the lack of effects of siRNA-mediated PrP^C knockdown. Nevertheless, aside from that initial western blot seemingly showing differences in PrP^C expression among the clones, there is little evidence to support the above speculation.

Western blot analyses of the SH-SY5Y cells showed that PrP^C transfection perturbed the expression of proteins involved in cytoskeletal organisation or neurite outgrowth and also affected expression of receptors for NGF. However, these molecular changes were not confirmed by experiments comparing PrP^C-null and wild type mouse forebrain tissues. In some ways, this was not surprising given that, in spite of numerous roles for PrP^C that have been identified from cell models by various groups, two published proteomic studies failed to identify a single differentially expressed protein when comparing PrP^C-null mouse brain homogenates with wild type controls (Crecelius et al., 2008; Mehrabian et al., 2016). One explanation that has been put forward is that PrP^C regulates processes in a cell type-specific manner, leading to an averaging out of these effects over an entire tissue (Mehrabian et al., 2014; Mehrabian et al., 2016). Additionally, absence of PrP^C expression in the knockout mice could be compensated for by other proteins, as has been suggested previously (Shmerling et al., 1998; Hajj et al., 2007). Finally, and specifically to my data, the role of PrP^C in the immature, neuronal precursor-like SH-SY5Y cell line may not be the same as its role in the forebrain of an aged mice – for reasons explained in section 5.5, the tissues used in the experiments reported in this thesis were from mice culled at ~550 days of age.

7.2 Future directions

7.2.1 Further investigating the molecular details of the putative modulation of NGF/neurotrophin signalling by PrP^C

Putting aside concerns over the specificity of the anti-$p75^{NTR}$ antibody, western blotting data suggested that levels of p75-CTF were significantly lower in the stably

transfected clones than in SH-SY5Y^{Untr}. However, expression of the full length receptor could not be quantified accurately due to the previously described issue of trimer formation. Therefore, it is not clear whether the putative downregulation of p75-CTF resulted from a reduced rate of p75^{NTR} alpha-cleavage or from an overall reduction in the expression of p75^{NTR}. One way to check would be to analyse the subcellular distribution of expression of p75^{NTR} and its cleavage fragments by confocal microscopy. If p75^{NTR} cleavage rates were reduced then one might expect the staining in the clones to be more confined to the cell membrane than in SH-SY5Y^{Untr}, because p75-ICD is present in the cytoplasm, whereas p75-CTF and the full length receptors are normally associated with the cell membrane (Weskamp et al., 2004; Zampieri et al., 2005). On the other hand, if PrP^{C} transfection affects overall p75^{NTR} expression levels then the staining pattern should be similar irrespective of whether or not the cells express PrP^{C}.

Interactions between PrP^{C} and TrkA, p75^{NTR} or sortilin were not identified in preliminary co-IP experiments. As previously mentioned, one potential follow-up experiment would be to use cross-linking prior to cell lysis to enable detection of weaker or more transient interactions, should they exist. A second approach would be to immunoprecipitate PrP^{C} using an antibody that binds to a different epitope, since the epitope recognised by the BC6 antibody used in the experiments reported in this thesis could have been obscured by interactions between PrP^{C} and other proteins. Such a situation might result in immunoprecipitation of only the PrP^{C} molecules not involved in any interactions at that time. The BC6 epitope is reported to be amino acids 144-154 in the C-terminal domain of PrP^{C} (McCutcheon et al., 2014), so the use of an antibody that binds to the N-terminal domain would be one option. This would also enable immunoprecipitation of the N1 fragment that is released from cells following alpha-cleavage of PrP^{C} – initial characterisation of the PrP^{C}-transfected SH-SY5Y cells confirmed that alpha-cleavage of PrP^{C} did occur and an interaction between N1 and one of the NGF receptors is plausible, especially since N1 has been specifically implicated in some of the functions ascribed to PrP^{C} (Guillot-Sestier et al., 2009; Haigh and Collins, 2014; Haigh et al., 2015b). Finally, if it is the cleavage rate of p75^{NTR} that is affected by PrP^{C} transfection then one could investigate

whether PrP^C interacts with ADAM17, the enzyme reportedly responsible for $p75^{NTR}$ alpha-cleavage (Weskamp et al., 2004).

One way for PrP^C to affect signalling pathways downstream of TrkA or $p75^{NTR}$ would be to interact with one of these receptors to modulate their response to NGF binding. In addition to assessing these putative interactions by co-IP experiments, activation of the receptors and/or downstream protein kinases in response to stimulation with exogenous NGF could be investigated. For example, a PrP^C transfection-dependent alteration in the half-maximal effective concentration of NGF for induction of TrkA phosphorylation would indicate that PrP^C affects the response of TrkA to NGF.

Instead of interacting with a receptor for NGF, PrP^C could modulate NGF signalling pathways by upregulating the expression of NGF itself; this could be assessed by quantifying the NGF present in conditioned media from transfected and untransfected SH-SY5Y cells. Since neuronal cell lines have been shown to upregulate PrP^C expression upon NGF stimulation (Kuwahara et al., 2000; Zawlik et al., 2006), PrP^C could have a similar effect on NGF expression via a positive feedback loop. However, an interaction between PrP^C and another as yet unknown protein would be required for PrP^C to initiate the downstream signalling pathways that would affect NGF gene transcription.

7.2.2 Further investigation of the consequences *in vivo* of a role for PrP^C in modulating NGF/neurotrophin signalling

NGF signalling is important for the proper development of sensory neurons with cell bodies in the dorsal root ganglia (DRGs) (Hefti et al., 2006). PrP^C may play a similar role, since its expression has been observed in the dorsal and ventral root ganglia of the developing spinal cord (Tremblay et al., 2007; Peralta et al., 2012; Ganley et al., 2015) as well as in sensory and motor axons (Manson et al., 1992) and associated Schwann cells (Follet et al., 2002). Furthermore, interactions between PrP^C and the extracellular matrix protein vitronectin are reported to promote the developmental

growth of axons that project from DRGs (Hajj et al., 2007), whilst vitronectin also seems to be important for the neurite outgrowth displayed by the neuronal cell line PC12 following exposure to NGF (Grabham et al., 1992). PrP^C knockout does not appear to affect neurite outgrowth from cultured DRG neurons; however, this is reportedly because integrins substitute for PrP^C in interactions with vitronectin (Hajj et al., 2007). This putative compensatory mechanism may not be completely effective though, since PrP^C knockout has been reported to alter pain sensitivity (Meotti et al., 2007; Gadotti and Zamponi, 2011). NGF is a key pain mediator, partly because it is required for the development and survival of nociceptive neurons but also because it can alter neuronal excitability directly. For example, spinal cord NMDARs, which are important for the onward processing of pain signals (Petrenko et al., 2003), can be phosphorylated in response to signals from NGF and other neurotrophins, potentially affecting NMDAR activity (Di Luca et al., 2001; Slack et al., 2004; Salter et al., 2009). Modulation of neurotrophin signalling by PrP^C could explain why an NMDAR inhibitor rescued an increase in pain sensitivity that resulted from PrP^C knockout (Gadotti and Zamponi, 2011) and also provides an alternative explanation for the finding that PrP^C affects NMDAR activity in the brain (Khosravani et al., 2008). To investigate this apparent connection in more detail, one could analyse whether NMDAR phosphorylation and/or expression in the spinal cord is affected by PrP^C knockout. Additionally, one might expect disrupted NGF signalling to affect the numbers of nociceptive neurons, and sensory neurons in general, that develop and survive into adulthood. This could be assessed in PrP^C-null mice by examining the morphologies of their DRGs and by quantifying the numbers of neuronal cell bodies present.

Several proteins involved in cytoskeletal organisation and/or neurite outgrowth were altered in their expression in the stably transfected clones compared with $SH\text{-}SY5Y^{Untr}$. However, the expression levels of these proteins did not vary significantly between PrP^C-null and wild type forebrains, possibly because cell type-specific effects of PrP^C were averaged out or "diluted" when analysing homogenates of the entire tissue. A more effective approach might be to study different regions of the brain separately, especially focusing on areas where NGF signalling is important

for neuronal survival, such as the basal forebrain (Sofroniew et al., 2001). Alternatively, the effects of PrP^C knockout on the expression of proteins involved in cytoskeletal organisation might be more noticeable in peripheral nerves due to the aforementioned function of NGF in the development of sensory neurons.

As mentioned previously, a comprehensive analysis of GLUT4, PCK1 and FASN expression levels in liver tissues from mice culled at different times of the day/night might reveal an effect of PrP^C knockout. Additionally, analysing expression at the mRNA level could be more effective at detecting differences associated with *Prnp* genotype. Assuming that any effects of PrP^C expression on metabolic processes derive from a role in generating circadian rhythms, possibly linked to modulation of signalling through $p75^{NTR}$, it would be useful to confirm that PrP^C expression is subject to circadian oscillation in the suprachiasmatic nucleus at the protein level; as far as I am aware, oscillations have only been identified in *Prnp* mRNA levels (Cagampang et al., 1999). Furthermore, since $p75^{NTR}$ knockout reportedly disrupts circadian oscillations in the expression of other clock network genes, one could investigate whether PrP^C knockout has a similar effect. A better understanding of the putative role of PrP^C in generating circadian rhythms would help to determine whether a loss of PrP^C function is involved in the pathogenesis of the TSE known as fatal familial insomnia, the clinical phase of which is characterised by disruptions to sleep-wake patterns (Collins et al., 2001).

PrP^C is highly expressed by mast cells and can be shed from the cell surface in the form of the N3 fragment. Shedding seems to occur at a low level constitutively but when mast cells are activated by inflammatory stimuli a large amount of N3 can be released (Haddon et al., 2009). Strikingly, NGF can activate mast cells and is also released from the cells upon their activation (Stempelj and Ferjan, 2005; Cantarella et al., 2011), which suggests an autocrine or paracrine positive feedback mechanism, potentially involving PrP^C, that further increases mast cell activity. Therefore, one might expect PrP^C knockout to impair mast cell function. Since activated mast cells release various inflammatory mediators, including histamine, prostaglandins and cytokines (Stempelj and Ferjan, 2005), the production of these compounds by mast

cells isolated from PrP^C-null and wild type mice could be compared following exposure to compounds that induce activation.

PrP^C expression has been detected in human teeth, including within the odontoblasts that form and calcify dentin. Furthermore, variations in dentin structure have been identified between PrP^C-null and wild type mice (Schneider et al., 2007). If PrP^C is expressed by odontoblasts then it may also be found in osteoblasts, which form bone. Intriguingly, targets of a protein called osteonectin were overrepresented among the proteins differentially expressed in PrP^C-transfected cells compared with $SH\text{-}SY5Y^{Untr}$. Although multifunctional, a major role of osteonectin is to promote bone mineralisation and the production of new osteoblasts (Ribeiro et al., 2014). A role for PrP^C in bone homeostasis can be explained by an involvement in NGF signalling pathways, since $p75^{NTR}$ knockout mice display decreased bone mineral content (IMPC, [n.d.]) and pro-NGF reportedly promotes bone regeneration by stimulating osteoblast and inhibiting osteoclast differentiation from precursors in bone marrow (Mediero et al., 2014). In order to investigate whether PrP^C has a function in bone, the structure and mineral content of bones from PrP^C-null and wild type mice could be examined. Additionally, one could investigate whether a lack of PrP^C expression affects the ability of precursor cells to differentiate into osteoblasts or osteoclasts in culture.

Whilst a complete description of PrP^C function is some way off, this thesis contributes towards our understanding of the molecular mechanisms regulated by PrP^C. Firstly, the data presented suggests that PrP^C is not involved in stress protection directly, which is in contrast to much of the published literature. Secondly, PrP^C expression inhibits proliferation of the SH-SY5Y cell line and alters the expression levels of proteins involved in cytoskeletal organisation and/or neurite outgrowth. Thirdly, changes to the expression of receptors for NGF and to the activities of downstream growth factor signalling pathways suggested that the phenotypes induced by PrP^C transfection may have resulted from modulation of NGF signalling pathways by PrP^C. A role for PrP^C in modulating NGF signalling, or neurotrophin signalling more generally, has the potential to explain many of the diverse

phenotypic observations in PrP^C-null mice, could indicate that loss of PrP^C function is an important part of TSE pathogenesis, and opens up various avenues for future investigation of the pathways and processes regulated by PrP^C.

Bibliography

Abcam. 2012. LDH-Cytotoxicity Assay Kit II. Available: http://www.abcam.com/ps/products/65/ab65393/documents/ab65393%20LDH%20Cytotoxicity%20Assay%20Kit%20II%20Protocol%20v4%20(website).pdf [Accessed 28/09/2015].

Abdallah, C., Dumas-Gaudot, E., Renaut, J., and Sergeant, K. (2012). Gel-based and gel-free quantitative proteomics approaches at a glance. *International journal of plant genomics* 2012**,** 494572-494572. doi: 10.1155/2012/494572.

Adle-Biassette, H., Verney, C., Peoc'h, K., Dauge, M.C., Razavi, F., Choudat, L., et al. (2006). Immunohistochemical expression of prion protein (PrPC) in the human forebrain during development. *Journal of Neuropathology and Experimental Neurology* 65(7)**,** 698-706.

Agholme, L., Lindstrom, T., Kagedal, K., Marcusson, J., and Hallbeck, M. (2010). An In Vitro Model for Neuroscience: Differentiation of SH-SY5Y Cells into Cells with Morphological and Biochemical Characteristics of Mature Neurons. *Journal of Alzheimers Disease* 20(4)**,** 1069-1082. doi: 10.3233/jad-2010-091363.

Ahmed, Z., Mazibrada, G., Seabright, R.J., Dent, R.G., Berry, M., and Logan, A. (2006). TACE-induced cleavage of NgR and p75(NTR) in dorsal root ganglion cultures disinhibits outgrowth and promotes branching of neurites in the presence of inhibitory CNS myelin. *Faseb Journal* 20(11)**,** 1939-+. doi: 10.1096/fj.05-5339fje.

Alfaidy, N., Chauvet, S., Donadio-Andrei, S., Salomon, A., Saoudi, Y., Richaud, P., et al. (2013). Prion Protein Expression and Functional Importance in Developmental Angiogenesis: Role in Oxidative Stress and Copper Homeostasis. *Antioxidants & Redox Signaling* 18(4)**,** 400-411. doi: 10.1089/ars.2012.4637.

Alper, T. (1985). SCRAPIE AGENT UNLIKE VIRUSES IN SIZE AND SUSCEPTIBILITY TO INACTIVATION BY IONIZING OR ULTRAVIOLET-RADIATION. *Nature* 317(6039)**,** 750-750. doi: 10.1038/317750a0.

Alper, T., Haig, D.A., and Clarke, M.C. (1966). EXCEPTIONALLY SMALL SIZE OF SCRAPIE AGENT. *Biochemical and Biophysical Research Communications* 22(3)**,** 278-&. doi: 10.1016/0006-291x(66)90478-5.

Alper, T., Haig, D.A., and Clarke, M.C. (1978). SCRAPIE AGENT - EVIDENCE AGAINST ITS DEPENDENCE FOR REPLICATION ON INTRINSIC NUCLEIC-ACID. *Journal of General Virology* 41(DEC)**,** 503-516. doi: 10.1099/0022-1317-41-3-503.

Altmeppen, H.C., Prox, J., Krasemann, S., Puig, B., Kruszewski, K., Dohler, F., et al. (2015). The sheddase ADAM10 is a potent modulator of prion disease. *Elife.* 4.(doi)**,** 10.7554/eLife.04260.

Altmeppen, H.C., Prox, J., Puig, B., Dohler, F., Falker, C., Krasemann, S., et al. (2013). Roles of endoproteolytic alpha-cleavage and shedding of the prion protein in neurodegeneration. *Febs Journal* 280(18)**,** 4338-4347. doi: 10.1111/febs.12196.

Altun-Gultekin, Z.F., Chandriani, S., Bougeret, C., Ishizaki, T., Narumiya, S., de Graaf, P., et al. (1998). Activation of Rho-dependent cell spreading and focal adhesion biogenesis by the v-Crk adaptor protein. *Molecular and Cellular Biology* 18(5)**,** 3044-3058.

Anantharam, V., Kanthasamy, A., Choi, C.J., Martin, D.P., Latchoumycandane, C., Richt, J.A., et al. (2008). Opposing roles of prion protein in oxidative stress- and ER stress-induced apoptotic signaling. *Free Radical Biology and Medicine* 45(11)**,** 1530-1541. doi: 10.1016/j.freeradbiomed.2008.08.028.

Anastasia, A., Barker, P.A., Chao, M.V., and Hempstead, B.L. (2015). Detection of p75(NTR) Trimers: Implications for Receptor Stoichiometry and Activation. *Journal of Neuroscience* 35(34)**,** 11911-11920. doi: 10.1523/jneurosci.0591-15.2015.

Arnett, M.G., Ryas, J.M., and Wright, D.E. (2007). pro-NGF, sortilin, and p75(NTR): Potential mediators of injury-induced apoptosis in the mouse dorsal root ganglion. *Brain Research* 1183**,** 32-42. doi: 10.1016/j.brainres.2007.09.051.

Arora, A.S., Zafar, S., Schmitz, M., and Zerr, I. (2013). Differential proteome analysis of cytoskeleton associated proteins in the liver of PrP knockout mice. *Prion* 7(sup1)**,** 69-69. doi: 10.4161/pri.24865

Arumugam, H., Liu, X.H., Colombo, P.J., Corriveau, R.A., and Belousov, A.B. (2005). NMDA receptors regulate developmental gap junction uncoupling via CREB signaling. *Nature Neuroscience* 8(12)**,** 1720-1726. doi: 10.1038/nn1588.

ATCC ([n.d.]). *SH-SY5Y (ATCC® CRL-2266™)* [Online]. Available: http://www.lgcstandards-atcc.org/products/all/CRL-2266.aspx?geo_country=gb#culturemethod [Accessed 25/09/2015].

Aude-Garcia, C., Villiers, C., Candeias, S.M., Garrel, C., Bertrand, C., Collin, V., et al. (2011). Enhanced susceptibility of T lymphocytes to oxidative stress in the absence of the cellular prion protein. *Cellular and Molecular Life Sciences* 68(4)**,** 687-696. doi: 10.1007/s00018-010-0477-5.

Baeza-Raja, B., Eckel-Mahan, K., Zhang, L.Y., Vagena, E., Tsigelny, I.F., Sassone-Corsi, P., et al. (2013). p75 Neurotrophin Receptor Is a Clock Gene That Regulates Oscillatory Components of Circadian and Metabolic Networks. *Journal of Neuroscience* 33(25)**,** 10221-10234. doi: 10.1523/jneurosci.2757-12.2013.

Baeza-Raja, B., Li, P.P., Le Moan, N., Sachs, B.D., Schachtrup, C., Davalos, D., et al. (2012). p75 neurotrophin receptor regulates glucose homeostasis and insulin sensitivity. *Proceedings of the National Academy of Sciences of the United States of America* 109(15)**,** 5838-5843. doi: 10.1073/pnas.1103638109.

Bailly, Y., Haeberle, A.M., Blanquet-Grossard, F., Chasserot-Golaz, S., Grant, N., Schulze, T., et al. (2004). Prion protein (PrPc) immunocytochemistry and expression of the green fluorescent protein reporter gene under control of the bovine PrP gene promoter in the mouse brain. *Journal of Comparative Neurology* 473(2)**,** 244-269. doi: 10.1002/cne.20117.

Bakkebo, M.K., Mouillet-Richard, S., Espenes, A., Goldmann, W., Tatzelt, J., and Tranulis, M.A. (2015). The cellular prion protein: a player in immunological quiescence. *Frontiers in Immunology* 6. doi: 10.3389/fimmu.2015.00450.

Bang, O.S., Park, E.K., Yang, S.I., Lee, S.R., Franke, T.F., and Kang, S.S. (2001). Overexpression of Akt inhibits NGF-induced growth arrest and neuronal differentiation of PC12 cells. *Journal of Cell Science* 114(1)**,** 81-88.

Barbieri, G., Palumbo, S., Gabrusiewicz, K., Azzalin, A., Marchesi, N., Spedito, A., et al. (2011). Silencing of cellular prion protein (PrPC) expression by DNA-antisense oligonucleotides induces autophagy-dependent cell death in glioma cells. *Autophagy* 7(8)**,** 840-853. doi: 10.4161/auto.7.8.15615.

Basler, K., Oesch, B., Scott, M., Westaway, D., Walchli, M., Groth, D.F., et al. (1986). SCRAPIE AND CELLULAR PRP ISOFORMS ARE ENCODED BY THE SAME CHROMOSOMAL GENE. *Cell* 46(3)**,** 417-428. doi: 10.1016/0092-8674(86)90662-8.

Beland, M., Bedard, M., Tremblay, G., Lavigne, P., and Roucou, X. (2014). A beta induces its own prion protein N-terminal fragment (PrPN1)-mediated neutralization in amorphous aggregates. *Neurobiology of Aging* 35(7)**,** 1537-1548. doi: 10.1016/j.neurobiolaging.2014.02.001.

Beland, M., Motard, J., Barbarin, A., and Roucou, X. (2012). PrPC Homodimerization Stimulates the Production of PrPC Cleaved Fragments PrPN1 and PrPC1. *Journal of Neuroscience* 32(38)**,** 13255-13263. doi: 10.1523/jneurosci.2236-12.2012.

Beland, M., and Roucou, X. (2013). Homodimerization as a molecular switch between low and high efficiency PrPC cell surface delivery and neuroprotective activity. *Prion* 7(2)**,** 170-174. doi: 10.1523/jneurosci.2236-12.2012.

Ben-Ari, Y. (2001). Developing networks play a similar melody. *Trends in Neurosciences* 24(6)**,** 353-360. doi: 10.1016/s0166-2236(00)01813-0.

Benestad, S.L., Austbo, L., Tranulis, M.A., Espenes, A., and Olsaker, I. (2012). Healthy goats naturally devoid of prion protein. *Veterinary Research* 43. doi: 10.1186/1297-9716-43-87.

Beraldo, F.H., Arantes, C.P., Santos, T.G., Machado, C.F., Roffe, M., Hajj, G.N., et al. (2011). Metabotropic glutamate receptors transduce signals for neurite outgrowth after binding of the prion protein to laminin gamma 1 chain. *Faseb Journal* 25(1)**,** 265-279. doi: 10.1096/fj.10-161653.

Beraldo, F.H., Arantes, C.P., Santos, T.G., Queiroz, N.G.T., Young, K., Rylett, R.J., et al. (2010). Role of alpha 7 Nicotinic Acetylcholine Receptor in Calcium Signaling Induced by Prion Protein Interaction with Stress-inducible Protein 1. *Journal of Biological Chemistry* 285(47)**,** 36542-36550. doi: 10.1074/jbc.M110.157263.

Bertuchi, F.R., Bourgeon, D.M.G., Landemberger, M.C., Martins, V.R., and Cerchiaro, G. (2012). PrPC displays an essential protective role from oxidative stress in an astrocyte cell line derived from PrPC knockout mice. *Biochemical and Biophysical Research Communications* 418(1)**,** 27-32. doi: 10.1016/j.bbrc.2011.12.098.

Besnier, L.S., Cardot, P., Da Rocha, B., Simon, A., Loew, D., Klein, C., et al. (2015). The cellular prion protein PrPc is a partner of the Wnt pathway in intestinal epithelial cells. *Molecular Biology of the Cell* 26(18)**,** 3313-3328. doi: 10.1091/mbc.E14-11-1534.

Biedler, J.L., Helson, L., and Spengler, B.A. (1973). MORPHOLOGY AND GROWTH, TUMORIGENICITY, AND CYTOGENETICS OF HUMAN NEUROBLASTOMA CELLS IN CONTINUOUS CULTURE. *Cancer Research* 33(11)**,** 2643-2652.

Biedler, J.L., Rofflertarlov, S., Schachner, M., and Freedman, L.S. (1978). MULTIPLE NEUROTRANSMITTER SYNTHESIS BY HUMAN NEUROBLASTOMA CELL LINES AND CLONES. *Cancer Research* 38(11)**,** 3751-3757.

Bjelfman, C., Meyerson, G., Cartwright, C.A., Mellstrom, K., Hammerling, U., and Pahlman, S. (1990). EARLY ACTIVATION OF ENDOGENOUS PP60SRC KINASE-ACTIVITY DURING NEURONAL DIFFERENTIATION OF CULTURED HUMAN NEUROBLASTOMA-CELLS. *Molecular and Cellular Biology* 10(1)**,** 361-370.

Boersema, P.J., Raijmakers, R., Lemeer, S., Mohammed, S., and Heck, A.J.R. (2009). Multiplex peptide stable isotope dimethyl labeling for quantitative proteomics. *Nature Protocols* 4(4)**,** 484-494. doi: 10.1038/nprot.2009.21.

Bondy, S.C., and Lee, D.K. (1993). OXIDATIVE STRESS-INDUCED BY GLUTAMATE RECEPTOR AGONISTS. *Brain Research* 610(2)**,** 229-233. doi: 10.1016/0006-8993(93)91405-h.

Bonini, M., Fioretti, D., Sargentini, V., Del Giacco, S., Rinaldi, M., Tranquilli, C., et al. (2013). Increased Nerve Growth Factor Serum Levels in Top Athletes. *Clinical Journal of Sport Medicine* 23(3)**,** 228-231. doi: 10.1097/JSM.0b013e31827ee6d5.

Bono, F., Lamarche, I., Bornia, J., Savi, P., Della Valle, G., and Herbert, J.M. (1999). Nerve growth factor (NGF) exerts its pro-apoptotic effect via the P75(NTR) receptor in a cell cycle-dependent manner. *Febs Letters* 457(1)**,** 93-97. doi: 10.1016/s0014-5793(99)01006-6.

Bounhar, Y., Zhang, Y., Goodyer, C.G., and LeBlanc, A. (2001). Prion protein protects human neurons against Bax-mediated apoptosis. *Journal of Biological Chemistry* 276(42)**,** 39145-39149. doi: 10.1074/jbc.C100443200.

Brann, A.B., Tcherpakov, M., Williams, I.M., Futerman, A.H., and Fainzilber, M. (2002). Nerve growth factor-induced p75-mediated death of cultured hippocampal neurons is age-dependent and transduced through ceramide generated by neutral sphingomyelinase. *Journal of Biological Chemistry* 277(12)**,** 9812-9818. doi: 10.1074/jbc.M109862200.

Bravard, A., Auvre, F., Fantini, D., Bernardino-Sgherri, J., Sissoeff, L., Daynac, M., et al. (2015). The prion protein is critical for DNA repair and cell survival after genotoxic stress. *Nucleic Acids Research* 43(2)**,** 904-916. doi: 10.1093/nar/gku1342.

Breitling, L.P., Muller, H., Stegmaier, C., Kliegel, M., and Brenner, H. (2012). Association of prion protein with cognitive functioning in humans. *Experimental Gerontology* 47(12)**,** 919-924. doi: 10.1016/j.exger.2012.08.001.

Bremer, J., Baumann, F., Tiberi, C., Wessig, C., Fischer, H., Schwarz, P., et al. (2010). Axonal prion protein is required for peripheral myelin maintenance. *Nature Neuroscience* 13(3)**,** 310-U319. doi: 10.1038/nn.2483.

Bribian, A., Fontana, X., Llorens, F., Gavin, R., Reina, M., Garcia-Verdugo, J.M., et al. (2012). Role of the Cellular Prion Protein in Oligodendrocyte Precursor Cell Proliferation and Differentiation in the Developing and Adult Mouse CNS. *Plos One* 7(4). doi: 10.1371/journal.pone.0033872.

Brito, G., Roffe, M., Lupinacci, F., Santos, T., Beraldo, F., Martins, V.R., et al. (2013). The role of cellular prion protein in the regulation of insulin signaling. *Molecular Biology of the Cell* 24(24)**,** 3775-3775. doi: 10.1091/mbc.E13-10-0584.

Brosius, F.C., Briggs, J.P., Marcus, R.G., Baracnieto, M., and Charron, M.J. (1992). INSULIN-RESPONSIVE GLUCOSE TRANSPORTER EXPRESSION IN RENAL MICROVESSELS AND GLOMERULI. *Kidney International* 42(5)**,** 1086-1092. doi: 10.1038/ki.1992.391.

Brown, D.R., and Mohn, C.M. (1999). Astrocytic glutamate uptake and prion protein expression. *Glia* 25(3)**,** 282-292. doi: 10.1002/(sici)1098-1136(19990201)25:3<282::aid-glia8>3.0.co;2-n.

Brown, D.R., Nicholas, R.S.J., and Canevari, L. (2002). Lack of prion protein expression results in a neuronal phenotype sensitive to stress. *Journal of Neuroscience Research* 67(2)**,** 211-224. doi: 10.1002/jnr.10118.

Brown, D.R., Qin, K.F., Herms, J.W., Madlung, A., Manson, J., Strome, R., et al. (1997a). The cellular prion protein binds copper in vivo. *Nature* 390(6661)**,** 684-687.

Brown, D.R., SchulzSchaeffer, W.J., Schmidt, B., and Kretzschmar, H.A. (1997b). Prion protein-deficient cells show altered response to oxidative stress due to decreased SOD-1 activity. *Experimental Neurology* 146(1)**,** 104-112. doi: 10.1006/exnr.1997.6505.

Brunetti, D., Dusi, S., Morbin, M., Uggetti, A., Moda, F., Damato, I., et al. (2012). Pantothenate kinase-associated neurodegeneration: altered mitochondria membrane potential and defective respiration in Pank2 knock-out mouse model. *Human Molecular Genetics* 21(24)**,** 5294-5305. doi: 10.1093/hmg/dds380.

Bueler, H., Aguzzi, A., Sailer, A., Greiner, R.A., Autenried, P., Aguet, M., et al. (1993). MICE DEVOID OF PRP ARE RESISTANT TO SCRAPIE. *Cell* 73(7)**,** 1339-1347. doi: 10.1016/0092-8674(93)90360-3.

Bueler, H., Fischer, M., Lang, Y., Bluethmann, H., Lipp, H.P., Dearmond, S.J., et al. (1992). NORMAL DEVELOPMENT AND BEHAVIOR OF MICE LACKING THE NEURONAL CELL-SURFACE PRP PROTEIN. *Nature* 356(6370)**,** 577-582. doi: 10.1038/356577a0.

Butowt, R., and von Bartheld, C.S. (2009). Fates of Neurotrophins after Retrograde Axonal Transport: Phosphorylation of p75NTR Is a Sorting Signal for Delayed Degradation. *Journal of Neuroscience* 29(34)**,** 10715-10729. doi: 10.1523/jneurosci.2512-09.2009.

Caetano, F.A., Lopes, M.H., Hajj, G.N.M., Machado, C.F., Arantes, C.P., Magalhaes, A.C., et al. (2008). Endocytosis of prion protein is required for ERK1/2 signaling induced by stress-inducible protein 1. *Journal of Neuroscience* 28(26)**,** 6691-6702. doi: 10.1523/jneurosci.1701-08.2008.

Cagampang, F.R.A., Whatley, S.A., Mitchell, A.L., Powell, J.F., Campbell, I.C., and Coen, C.W. (1999). Circadian regulation of prion protein messenger RNA in the rat forebrain: A widespread and synchronous rhythm. *Neuroscience* 91(4)**,** 1201-1204. doi: 10.1016/s0306-4522(99)00092-5.

Campbell, L., Gill, A.C., McGovern, G., Jalland, C.M.O., Hopkins, J., Tranulis, M.A., et al. (2013). The PrPC Cl fragment derived from the ovine A(136)R(154)R(171) PRNP allele is highly abundant in sheep brain and inhibits fibrillisation of full-length PrPC protein in vitro. *Biochimica Et Biophysica Acta-Molecular Basis of Disease* 1832(6)**,** 826-836. doi: 10.1016/j.bbadis.2013.02.020.

Cantarella, G., Scollo, M., Lempereur, L., Saccani-Jotti, G., Basile, F., and Bernardini, R. (2011). Endocannabinoids inhibit release of nerve growth factor by inflammation-activated mast cells. *Biochemical Pharmacology* 82(4)**,** 380-388. doi: 10.1016/j.bcp.2011.05.004.

Carulla, P., Bribian, A., Rangel, A., Gavin, R., Ferrer, I., Caelles, C., et al. (2011). Neuroprotective role of PrPC against kainate-induced epileptic seizures and cell death depends on the modulation of JNK3 activation by GluR6/7-PSD-95 binding. *Molecular Biology of the Cell* 22(17)**,** 3041-3054. doi: 10.1091/mbc.E11-04-0321.

Chakrabarti, O., Ashok, A., and Hegde, R.S. (2009). Prion protein biosynthesis and its emerging role in neurodegeneration. *Trends in Biochemical Sciences* 34(6)**,** 287-295. doi: 10.1016/j.tibs.2009.03.001.

Chanarat, S., and Strasser, K. (2013). Splicing and beyond: The many faces of the Prp19 complex. *Biochimica Et Biophysica Acta-Molecular Cell Research* 1833(10)**,** 2126-2134. doi: 10.1016/j.bbamcr.2013.05.023.

Chang, J.H., Mellon, E., Schanen, N.C., and Twiss, J.L. (2003). Persistent TrkA activity is necessary to maintain transcription in neuronally differentiated PC12 cells. *Journal of Biological Chemistry* 278(44)**,** 42877-42885. doi: 10.1074/jbc.M308155200.

Chen, S.G., Teplow, D.B., Parchi, P., Teller, J.K., Gambetti, P., and Autiliogambetti, L. (1995). TRUNCATED FORMS OF THE HUMAN PRION PROTEIN IN NORMAL BRAIN AND IN PRION DISEASES. *Journal of Biological Chemistry* 270(32)**,** 19173-19180.

Chen, S.G., Yadav, S.P., and Surewicz, W.K. (2010). Interaction between Human Prion Protein and Amyloid-beta (A beta) Oligomers ROLE OF N-TERMINAL RESIDUES. *Journal of Biological Chemistry* 285(34)**,** 26377-26383. doi: 10.1074/jbc.M110.145516.

Chen, W.H., Mao, C.Q., Zhuo, L.L., and Ong, J.L. (2015). Beta-nerve growth factor promotes neurogenesis and angiogenesis during the repair of bone defects. *Neural Regeneration Research* 10(7)**,** 1159-1165. doi: 10.4103/1673-5374.160114.

Chen, Y., Zeng, J., Chen, Y., Wang, X., Yao, G., Wang, W., et al. (2009). Multiple Roles of the p75 Neurotrophin Receptor in the Nervous System. *Journal of International Medical Research* 37(2)**,** 281-288.

Cheung, N.K.V., and Dyer, M.A. (2013). Neuroblastoma: developmental biology, cancer genomics and immunotherapy. *Nature Reviews Cancer* 13(6)**,** 397-411. doi: 10.1038/nrc3526.

Cheung, Z.H., and Ip, N.Y. (2012). Cdk5: a multifaceted kinase in neurodegenerative diseases. *Trends in Cell Biology* 22(3)**,** 169-175. doi: 10.1016/j.tcb.2011.11.003.

Choi, S., and Friedman, W.J. (2009). Inflammatory cytokines IL-1 beta and TNF-alpha regulate p75(NTR) expression in CNS neurons and astrocytes by distinct cell-type-specific signalling mechanisms. *Asn Neuro* 1(2). doi: 10.1042/an20090009.

Cichon, A.-C., and Brown, D.R. (2014). Nrf-2 regulation of prion protein expression is independent of oxidative stress. *Molecular and Cellular Neuroscience* 63**,** 31-37. doi: 10.1016/j.mcn.2014.09.001.

Cingaram, P.K.R., Nyeste, A., Dondapati, D.T., Fodor, E., and Welker, E. (2015). Prion Protein Does Not Confer Resistance to Hippocampus-Derived Zpl Cells against the Toxic Effects of Cu2+, Mn2+, Zn2+ and Co2+ Not Supporting a General Protective Role for PrP in Transition Metal Induced Toxicity. *Plos One* 10(10). doi: 10.1371/journal.pone.0139219.

Cisse, M., Duplan, E., Guillot-Sestier, M.V., Rumigny, J., Bauer, C., Pages, G., et al. (2011). The Extracellular Regulated Kinase-1 (ERK1) Controls Regulated alpha-Secretase-mediated Processing, Promoter Transactivation, and mRNA Levels of the Cellular Prion Protein. *Journal of Biological Chemistry* 286(33)**,** 29192-29206. doi: 10.1074/jbc.M110.208249.

Cisse, M.A., Louis, K., Braun, U., Mari, B., Leitges, M., Slack, B.E., et al. (2008). Isoform-specific contribution of protein kinase C to prion processing. *Molecular and Cellular Neuroscience* 39(3)**,** 400-410. doi: 10.1016/j.mcn.2008.07.013.

Clewes, O., Fahey, M.S., Tyler, S.J., Watson, J.J., Seok, H., Catania, C., et al. (2008). Human ProNGF: biological effects and binding profiles at TrkA, P75(NTR) and sortilin. *Journal of Neurochemistry* 107(4)**,** 1124-1135. doi: 10.1111/j.1471-4159.2008.05698.x.

Collinge, J., Whittington, M.A., Sidle, K.C.L., Smith, C.J., Palmer, M.S., Clarke, A.R., et al. (1994). PRION PROTEIN IS NECESSARY FOR NORMAL SYNAPTIC FUNCTION. *Nature* 370(6487)**,** 295-297. doi: 10.1038/370295a0.

Collins, S., McLean, C.A., and Masters, C.L. (2001). Gerstmann-Straussier-Scheinker syndrome, fatal familial insomnia, and kuru: a review of these less common human transmissible spongiform encephalopathies. *Journal of Clinical Neuroscience* 8(5)**,** 387-397. doi: 10.1054/jocn.2001.0919.

Collins, S.J., Lawson, V.A., and Masters, C.L. (2004). Transmissible spongiform encephalopathies. *Lancet* 363(9402)**,** 51-61. doi: 10.1016/s0140-6736(03)15171-9.

Coulson, E.J., May, L.M., Osborne, S.L., Reid, K., Underwood, C.K., Meunier, F.A., et al. (2008). p75 neurotrophin receptor mediates neuronal cell death by activating GIRK channels through phosphatidylinositol 4,5-bisphosphate. *Journal of Neuroscience* 28(1)**,** 315-324. doi: 10.1523/jneurosci.2699-07.2008.

Covaceuszach, S., Capsoni, S., Ugolini, G., Spirito, F., Vignone, D., and Cattaneo, A. (2009). Development of a Non Invasive NGF-Based Therapy for Alzheimer's Disease. *Current Alzheimer Research* 6(2)**,** 158-170.

Crecelius, A.C., Helmstetter, D., Strangmann, J., Mitteregger, G., Frohlich, T., Arnold, G.J., et al. (2008). The brain proteome profile is highly conserved between Prnp(-/-) and Prnp(+/+) mice. *Neuroreport* 19(10)**,** 1027-1031.

D'Archangelo, G. (2014). Reelin in the Years: Controlling Neuronal Migration and Maturation in the Mammalian Brain. *Advances in Neuroscience* 2014.

Daude, N., Marella, M., and Chabry, J. (2003). Specific inhibition of pathological prion protein accumulation by small interfering RNAs. *Journal of Cell Science* 116(13)**,** 2775-2779. doi: 10.1242/jcs.00494.

Dechant, G., and Barde, Y.A. (2002). The neurotrophin receptor p75(NTR): novel functions and implications for diseases of the nervous system. *Nature Neuroscience* 5(11)**,** 1131-1136. doi: 10.1038/nn1102-1131.

Deckwerth, T.L., Elliott, J.L., Knudson, C.M., Johnson, E.M., Snider, W.D., and Korsmeyer, S.J. (1996). BAX is required for neuronal death after trophic factor deprivation and during development. *Neuron* 17(3)**,** 401-411. doi: 10.1016/s0896-6273(00)80173-7.

Dery, M.A., Jodoin, J., Ursini-Siegel, J., Aleynikova, O., Ferrario, C., Hassan, S., et al. (2013). Endoplasmic reticulum stress induces PRNP prion protein gene expression in breast cancer. *Breast Cancer Research* 15(2). doi: 10.1186/bcr3398.

Di Luca, M., Gardoni, F., Finardi, A., Pagliardini, S., Cattabeni, F., Battaglia, G., et al. (2001). NMDA receptor subunits are phosphorylated by activation of neurotrophin receptors in PSD of rat spinal cord. *Neuroreport* 12(6)**,** 1301-1305. doi: 10.1097/00001756-200105080-00049.

Dibner, C., Schibler, U., and Albrecht, U. (2010). "The Mammalian Circadian Timing System: Organization and Coordination of Central and Peripheral Clocks," in *Annual Review of Physiology*.), 517-549.

Dohler, F., Sepulveda-Falla, D., Krasemann, S., Altmeppen, H., Schluter, H., Hildebrand, D., et al. (2014). High molecular mass assemblies of amyloid-beta oligomers bind prion protein in patients with Alzheimer's disease. *Brain* 137**,** 873-886. doi: 10.1093/brain/awt375.

Dupiereux, I., Falisse-Poirrier, N., Zorzi, W., Watt, N.T., Thellin, O., Zorzi, D., et al. (2008). Protective effect of prion protein via the N-terminal region in mediating a protective effect on paraquat-induced oxidative injury in neuronal cells. *Journal of Neuroscience Research* 86(3)**,** 653-659. doi: 10.1002/jnr.21506.

Durig, J., Giese, A., Schulz-Schaeffer, W., Rosenthal, C., Schmucker, U., Bieschke, J., et al. (2000). Differential constitutive and activation-dependent expression of prion protein in human peripheral blood leucocytes. *British Journal of Haematology* 108(3)**,** 488-496. doi: 10.1046/j.1365-2141.2000.01881.x.

Eaton, S.L., Roche, S.L., Hurtado, M.L., Oldknow, K.J., Farquharson, C., Gillingwater, T.H., et al. (2013). Total Protein Analysis as a Reliable Loading Control for Quantitative Fluorescent Western Blotting. *Plos One* 8(8). doi: 10.1371/journal.pone.0072457.

Ehsani, S., Huo, H.R., Salehzadeh, A., Pocanschi, C.L., Watts, J.C., Wille, H., et al. (2011). Family reunion - The ZIP/prion gene family. *Progress in Neurobiology* 93(3)**,** 405-420. doi: 10.1016/j.pneurobio.2010.12.001.

Ehsani, S., Mehrabian, M., Pocanschi, C.L., and Schmitt-Ulms, G. (2012). The ZIP-prion connection. *Prion* 6(4)**,** 317-321. doi: 10.1371/journal.pone.e0026800.

Encinas, M., Iglesias, M., Liu, Y.H., Wang, H.Y., Muhaisen, A., Cena, V., et al. (2000). Sequential treatment of SH-SY5Y cells with retinoic acid and brain-derived neurotrophic factor gives rise to fully differentiated, neurotrophic factor-dependent, human neuron-like cells. *Journal of Neurochemistry* 75(3)**,** 991-1003. doi: 10.1046/j.1471-4159.2000.0750991.x.

Evans, W.H., and Martin, P.E.M. (2002). Gap junctions: structure and function (Review). *Molecular Membrane Biology* 19(2)**,** 121-136. doi: 10.1080/09687680210139839.

Fahnestock, M., Yu, G., Michalski, B., Mathew, S., Colquhoun, A., Ross, G.M., et al. (2004). The nerve growth factor precursor proNGF exhibits neurotrophic activity but is less active than mature nerve growth factor. *Journal of Neurochemistry* 89(3)**,** 581-592. doi: 10.1111/j.1471-4159.2004.02340.x.

Falsey, R.R., Marron, M.T., Gunaherath, G., Shirahatti, N., Mahadevan, D., Gunatilaka, A.A.L., et al. (2006). Actin microfilament aggregation induced by withaferin A is mediated by annexin II. *Nature Chemical Biology* 2(1)**,** 33-38. doi: 10.1038/nchembio755.

Fernandez-Borges, N., Chianini, F., Erana, H., Vidal, E., Eaton, S.L., Pintado, B., et al. (2012). Naturally prion resistant mammals A utopia? *Prion* 6(5)**,** 425-429. doi: 10.4161/pri.22057.

Figueiredo-Pereira, M.E., Rockwell, P., Schmidt-Glenewinkel, T., and Serrano, P. (2015). Neuroinflammation and J2 prostaglandins: linking impairment of the ubiquitin-proteasome pathway and mitochondria to neurodegeneration. *Frontiers in Molecular Neuroscience* 7. doi: 10.3389/fnmol.2014.00104.

Fleisch, V.C., Leighton, P.L.A., Wang, H., Pillay, L.M., Ritz, R.G., Bhinder, G., et al. (2013). Targeted mutation of the gene encoding prion protein in zebrafish reveals a conserved role in neuron excitability. *Neurobiology of Disease* 55**,** 11-25. doi: 10.1016/j.nbd.2013.03.007.

Follet, J., Lemaire-Vieille, C., Blanquet-Grossard, F., Podevin-Dimster, V., Lehmann, S., Chauvin, J.P., et al. (2002). PrP expression and replication by Schwann cells: Implications in prion spreading. *Journal of Virology* 76(5)**,** 2434-2439. doi: 10.1128/jvi.76.5.2434-2439.2002.

Frigg, R., Wenzel, A., Samardzija, M., Oesch, B., Wariwoda, H., Navarini, A.A., et al. (2006). The prion protein is neuroprotective against retinal degeneration in vivo. *Experimental Eye Research* 83(6)**,** 1350-1358. doi: 10.1016/j.exer.2006.07.010.

Fujita, Y., Yamaguchi, A., Hata, K., Endo, M., Yamaguchi, N., and Yamashita, T. (2009). Zyxin is a novel interacting partner for SIRT1. *Bmc Cell Biology* 10. doi: 10.1186/1471-2121-10-6.

Gadotti, V.M., and Zamponi, G.W. (2011). Cellular prion protein protects from inflammatory and neuropathic pain. *Molecular Pain* 7. doi: 10.1186/1744-8069-7-59.

Ganley, R.P., Iwagaki, N., del Rio, P., Baseer, N., Dickie, A.C., Boyle, K.A., et al. (2015). Inhibitory Interneurons That Express GFP in the PrP-GFP Mouse Spinal Cord Are Morphologically Heterogeneous, Innervated by Several Classes of Primary Afferent and Include Lamina I Projection Neurons among Their Postsynaptic Targets. *Journal of Neuroscience* 35(19)**,** 7626-7642. doi: 10.1523/jneurosci.0406-15.2015.

Gasperini, L., Meneghetti, E., Pastore, B., Benetti, F., and Legname, G. (2015). Prion Protein and Copper Cooperatively Protect Neurons by Modulating NMDA Receptor Through S-nitrosylation. *Antioxidants & Redox Signaling* 22(9)**,** 772-784. doi: 10.1089/ars.2014.6032.

Gates, R., Rathbone, E., Masterson, L., Wright, I., and Electricwala, A. (2004). "Glycoprotein Analysis: Manual". 1st ed.: Sigma-Aldrich).

Gehler, S., Gallo, G., Veien, E., and Letourneau, P.C. (2004). p75 Neurotrophin receptor signaling regulates growth cone filopodial dynamics through modulating RhoA activity. *Journal of Neuroscience* 24(18)**,** 4363-4372. doi: 10.1523/jneurosci.0404-04.2004.

Gerlai, R. (1996). Gene-targeting studies of mammalian behavior: Is it the mutation or the background genotype? *Trends in Neurosciences* 19(5)**,** 177-181. doi: 10.1016/s0166-2236(96)20020-7.

Gilbert, S.F. (2006). *Developmental Biology*. Sunderland: Sinaeur Associates Inc. .

Goedert, M. (2015). Alzheimer's and Parkinson's diseases: The prion concept in relation to assembled A beta, tau, and alpha-synuclein. *Science* 349(6248). doi: 10.1126/science.1255555.

Goh, A.X.H., Li, C.Y., Sy, M.S., and Wong, B.S. (2007). Altered prion protein glycosylation in the aging mouse brain. *Journal of Neurochemistry* 100(3)**,** 841-854. doi: 10.1111/j.1471-4159.2006.04268.x.

Gold, M.S., and Gebhart, G.F. (2010). Nociceptor sensitization in pain pathogenesis. *Nature Medicine* 16(11)**,** 1248-1257. doi: 10.1038/nm.2235.

Gorman, A.M. (2008). Neuronal cell death in neurodegenerative diseases: recurring themes around protein handling. *Journal of Cellular and Molecular Medicine* 12(6A)**,** 2263-2280. doi: 10.1111/j.1582-4934.2008.00402.x.

Gourdain, P., Ballerini, C., Nicot, A.B., and Carnaud, C. (2012). Exacerbation of experimental autoimmune encephalomyelitis in prion protein (PrPc)-null mice: evidence for a critical role of the central nervous system. *Journal of Neuroinflammation* 9. doi: 10.1186/1742-2094-9-25.

Grabham, P.W., Gallimore, P.H., and Grand, R.J.A. (1992). VITRONECTIN IS THE MAJOR SERUM-PROTEIN ESSENTIAL FOR NGF-MEDIATED NEURITE OUTGROWTH FROM PC12 CELLS. *Experimental Cell Research* 202(2)**,** 337-344. doi: 10.1016/0014-4827(92)90083-k.

Graner, E., Mercadante, A.F., Zanata, S.M., Forlenza, O.V., Cabral, A.L.B., Veiga, S.S., et al. (2000). Cellular prion protein binds laminin and mediates neuritogenesis. *Molecular Brain Research* 76(1)**,** 85-92. doi: 10.1016/s0169-328x(99)00334-4.

Grosheva, I., Vittitow, J.L., Goichberg, P., Gabelt, B.T., Kaufman, P.L., Borras, T., et al. (2006). Caldesmon effects on the actin cytoskeleton and cell adhesion in cultured HTM cells. *Experimental Eye Research* 82(6)**,** 945-958. doi: 10.1016/j.exer.2006.01.006.

Guillot-Sestier, M.V., Sunyach, C., Druon, C., Scarzello, S., and Checler, F. (2009). The alpha-Secretase-derived N-terminal Product of Cellular Prion, N1, Displays Neuroprotective Function in Vitro and in Vivo. *Journal of Biological Chemistry* 284(51)**,** 35973-35986. doi: 10.1074/jbc.M109.051086.

Gygi, S.P., Rochon, Y., Franza, B.R., and Aebersold, R. (1999). Correlation between protein and mRNA abundance in yeast. *Molecular and Cellular Biology* 19(3)**,** 1720-1730.

Haddon, D.J., Hughes, M.R., Antignano, F., Westaway, D., Cashman, N.R., and McNagny, K.M. (2009). Prion Protein Expression and Release by Mast Cells After Activation. *Journal of Infectious Diseases* 200(5)**,** 827-831. doi: 10.1086/605022.

Hagiwara, K., Hara, H., and Hanada, K. (2013). Species-barrier phenomenon in prion transmissibility from a viewpoint of protein science. *Journal of Biochemistry* 153(2)**,** 139-145. doi: 10.1093/jb/mvs148.

Hagstrom, K.A., and Meyer, B.J. (2003). Condensin and cohesin: More than chromosome compactor and glue. *Nature Reviews Genetics* 4(7)**,** 520-534. doi: 10.1038/nrg1110.

Haigh, C., and Collins, S. (2014). Oxidative Modulation of Neural Stem Cell Growth by Prion Protein Cleavage Fragments. *Free Radical Biology and Medicine* 76**,** S24-S24. doi: 10.1016/j.freeradbiomed.2014.10.476.

Haigh, C.L., McGlade, A.R., and Collins, S.J. (2015a). MEK1 transduces the prion protein N2 fragment antioxidant effects. *Cellular and Molecular Life Sciences* 72(8)**,** 1613-1629. doi: 10.1007/s00018-014-1777-y.

Haigh, C.L., Tumpach, C., Drew, S.C., and Collins, S.J. (2015b). The Prion Protein N1 and N2 Cleavage Fragments Bind to Phosphatidylserine and Phosphatidic Acid; Relevance to Stress-Protection Responses. *Plos One* 10(8). doi: 10.1371/journal.pone.0134680.

Haire, L.F., Whyte, S.M., Vasisht, N., Gill, A.C., Verma, C., Dodson, E.J., et al. (2004). The crystal structure of the globular domain of sheep prion protein. *Journal of Molecular Biology* 336(5)**,** 1175-1183. doi: 10.1016/j.jmb.2003.12.059.

Hajj, G.N.M., Lopes, M.H., Mercadante, A.F., Veiga, S.S., da Silveira, R.B., Santos, T.G., et al. (2007). Cellular prion protein interaction with vitronectin supports axonal growth and is compensated by integrins. *Journal of Cell Science* 120(11)**,** 1915-1926. doi: 10.1242/jcs.03459.

Haldar, S., Tripathi, A., Qian, J., Beserra, A., Suda, S., McElwee, M., et al. (2015). Prion Protein Promotes Kidney Iron Uptake via Its Ferrireductase Activity. *Journal of Biological Chemistry* 290(9)**,** 5512-5522. doi: 10.1074/jbc.M114.607507.

Halliday, M., and Mallucci, G.R. (2014). Targeting the unfolded protein response in neurodegeneration: A new approach to therapy. *Neuropharmacology* 76**,** 169-174. doi: 10.1016/j.neuropharm.2013.08.034.

Han, I.S., Seo, T.B., Kim, K.H., Yoon, J.H., Yoon, S.J., and Namgung, U. (2007). Cdc2-mediated Schwann cell migration during peripheral nerve regeneration. *Journal of Cell Science* 120(2)**,** 246-255. doi: 10.1242/jcs.03322.

Harris, D.A., Huber, M.T., Vandijken, P., Shyng, S.L., Chait, B.T., and Wang, R. (1993). PROCESSING OF A CELLULAR PRION PROTEIN - IDENTIFICATION OF N-TERMINAL AND C-TERMINAL CLEAVAGE SITES. *Biochemistry* 32(4)**,** 1009-1016. doi: 10.1021/bi00055a003.

Hartmann, C.A., Martins, V.R., and Lima, F.R.S. (2013). High levels of Cellular Prion Protein improve astrocyte development. *Febs Letters* 587(2)**,** 238-244. doi: 10.1016/j.febslet.2012.11.032.

Hayakawa, A., Babour, A., Sengmanivong, L., and Dargemont, C. (2012). Ubiquitylation of the nuclear pore complex controls nuclear migration during mitosis in S. cerevisiae. *Journal of Cell Biology* 196(1)**,** 19-27. doi: 10.1083/jcb.201108124.

He, X.L., and Garcia, K.C. (2004). Structure of nerve growth factor complexed with the shared neurotrophin receptor p75. *Science* 304(5672)**,** 870-875. doi: 10.1126/science.1095190.

Head, M.W. (2013). Human prion diseases: Molecular, cellular and population biology. *Neuropathology* 33(3)**,** 221-236. doi: 10.1111/neup.12016.

Hefti, F.F., Rosenthal, A., Walicke, P.A., Wyatt, S., Vergara, G., Shelton, D.L., et al. (2006). Novel class of pain drugs based on antagonism of NGF. *Trends in Pharmacological Sciences* 27(2)**,** 85-91. doi: 10.1016/j.tips.2005.12.001.

Hegde, R.S., Mastrianni, J.A., Scott, M.R., DeFea, K.A., Tremblay, P., Torchia, M., et al. (1998). A transmembrane form of the prion protein in neurodegenerative disease. *Science* 279(5352)**,** 827-834. doi: 10.1126/science.279.5352.827.

Helfman, D.M., Levy, E.T., Berthier, C., Shtutman, M., Riveline, D., Grosheva, I., et al. (1999). Caldesmon inhibits nonmuscle cell contractility and interferes with the formation of focal adhesions. *Molecular Biology of the Cell* 10(10)**,** 3097-3112.

Herman, M.A., and Kahn, B.B. (2006). Glucose transport and sensing in the maintenance of glucose homeostasis and metabolic harmony. *Journal of Clinical Investigation* 116(7)**,** 1767-1775. doi: 10.1172/jci129027.

Hirata, H., Tatsumi, H., and Sokabe, M. (2008). Zyxin emerges as a key player in the mechanotransduction at cell adhesive structures. *Communicative & integrative biology* 1(2)**,** 192-195.

Hornshaw, M.P., McDermott, J.R., and Candy, J.M. (1995a). COPPER-BINDING TO THE N-TERMINAL TANDEM REPEAT REGIONS OF MAMMALIAN AND AVIAN PRION PROTEIN. *Biochemical and Biophysical Research Communications* 207(2)**,** 621-629. doi: 10.1006/bbrc.1995.1233.

Hornshaw, M.P., McDermott, J.R., Candy, J.M., and Lakey, J.H. (1995b). COPPER-BINDING TO THE N-TERMINAL TANDEM REPEAT REGION OF MAMMALIAN AND AVIAN PRION PROTEIN - STRUCTURAL STUDIES USING SYNTHETIC PEPTIDES. *Biochemical and Biophysical Research Communications* 214(3)**,** 993-999. doi: 10.1006/bbrc.1995.2384.

Horwich, A.L., and Weissman, J.S. (1997). Deadly conformations - Protein misfolding in prion disease. *Cell* 89(4)**,** 499-510. doi: 10.1016/s0092-8674(00)80232-9.

Howard, L., Wyatt, S., Nagappan, G., and Davies, A.M. (2013). ProNGF promotes neurite growth from a subset of NGF-dependent neurons by a p75(NTR)-dependent mechanism. *Development* 140(10)**,** 2108-2117. doi: 10.1242/dev.085266.

Hu, W., Nessler, S., Hemmer, B., Eagar, T.N., Kane, L.P., Leliveld, S.R., et al. (2010). Pharmacological prion protein silencing accelerates central nervous system autoimmune disease via T cell receptor signalling. *Brain* 133**,** 375-388. doi: 10.1093/brain/awp298.

Huang, C., Zhou, J., Feng, A.K., Lynch, C.C., Klumperman, J., DeArmond, S.J., et al. (1999). Nerve growth factor signaling in caveolae-like domains at the plasma membrane. *Journal of Biological Chemistry* 274(51)**,** 36707-36714. doi: 10.1074/jbc.274.51.36707.

Huang, E.J., and Reichardt, L.F. (2003). Trk receptors: Roles in neuronal signal transduction. *Annual Review of Biochemistry* 72**,** 609-642. doi: 10.1146/annurev.biochem.72.121801.161629.

Hutter, G., Heppner, F.L., and Aguzzi, A. (2003). No superoxide dismutase activity of cellular prion protein in vivo. *Biological Chemistry* 384(9)**,** 1279-1285. doi: 10.1515/bc.2003.142.

Ikeda, K., Kawada, N., Wang, Y.Q., Kadoya, H., Nakatani, K., Sato, M., et al. (1998). Expression of cellular prion protein in activated hepatic stellate cells. *American Journal of Pathology* 153(6)**,** 1695-1700. doi: 10.1016/s0002-9440(10)65683-0.

IMPC ([n.d.]). *Phenotype associations for Ngfr* [Online]. Available: http://www.mousephenotype.org/data/genes/MGI:97323 [Accessed 06/09/2016].

Ingenuity Systems. 2005. IPA Network Generation Algorithm. Available: https://www.ingenuity.com/wp-content/themes/ingenuity-qiagen/pdf/ipa/IPA-netgen-algorithm-whitepaper.pdf [Accessed 31/05/2016].

Ingenuity Systems. [n.d.]. Ingenuity Upstream Regulator Analysis in IPA. Available: http://pages.ingenuity.com/rs/ingenuity/images/0812%20upstream_regulator_analysis_whitepaper.pdf [Accessed 31/05/2016].

Invitrogen (2012). "PrestoBlue FAQ".).

Iwatsuki, M., Mimori, K., Sato, T., Toh, H., Yokobori, T., Tanaka, F., et al. (2010). Overexpression of SUGT1 in human colorectal cancer and its clinicopathological significance. *International Journal of Oncology* 36(3)**,** 569-575. doi: 10.3892/ijo_00000531.

Jung, K.M., Tan, S., Landman, N., Petrova, K., Murray, S., Lewis, R., et al. (2003). Regulated intramembrane proteolysis of the p75 neurotrophin receptor modulates its association with the TrkA receptor. *Journal of Biological Chemistry* 278(43)**,** 42161-42169. doi: 10.1074/jbc.M306028200.

Kan, A., Mohamedali, A., Tan, S.H., Cheruku, H.R., Slapetova, I., Lee, L.Y., et al. (2013). An improved method for the detection and enrichment of low-abundant membrane and lipid raft-residing proteins. *Journal of Proteomics* 79**,** 299-304. doi: 10.1016/j.jprot.2012.11.019.

Karra, D., and Dahm, R. (2010). Transfection Techniques for Neuronal Cells. *Journal of Neuroscience* 30(18)**,** 6171-6177. doi: 10.1523/jneurosci.0183-10.2010.

Kenchappa, R.S., Zampieri, N., Chao, M.V., Barker, P.A., Teng, H.K., Hempstead, B.L., et al. (2006). Ligand-dependent cleavage of the P75 neurotrophin receptor is necessary for NRIF nuclear translocation and apoptosis in sympathetic neurons. *Neuron* 50(2)**,** 219-232. doi: 10.1016/j.neuron.2006.03.011.

Khosravani, H., Zhang, Y.F., Tsutsui, S., Hameed, S., Altier, C., Hamid, J., et al. (2008). Prion protein attenuates excitotoxicity by inhibiting NMDA receptors. *Journal of Cell Biology* 181(3)**,** 551-565. doi: 10.1083/jcb.200711002.

Kim, B.H., Kim, J.I., Choi, E.K., Carp, R.I., and Kim, Y.S. (2005). A neuronal cell line that does not express either prion or doppel proteins. *Neuroreport* 16(5)**,** 425-429. doi: 10.1097/00001756-200504040-00002.

Kim, B.H., Lee, H.G., Choi, J.K., Kim, J.I., Choi, E.K., Carp, R.I., et al. (2004). The cellular prion protein (PrPC) prevents apoptotic neuronal cell death and mitochondrial dysfunction induced by serum deprivation. *Molecular Brain Research* 124(1)**,** 40-50. doi: 10.1016/j.molbrainres.2004.02.005.

Kim, Y., Lee, J., and Lee, C. (2008). In silico, comparative analysis of DNA and amino acid sequences for prion protein gene. *Transboundary and Emerging Diseases* 55(2)**,** 105-114. doi: 10.1111/j.1865-1682.2007.00997.x.

Kitagawa, K., Skowyra, D., Elledge, S.J., Harper, J.W., and Hieter, P. (1999). SGT1 encodes an essential component of the yeast kinetochore assembly pathway and a novel subunit of the SCF ubiquitin ligase complex. *Molecular Cell* 4(1)**,** 21-33. doi: 10.1016/s1097-2765(00)80184-7.

Kitamoto, T., Tateishi, J., Tashima, T., Takeshita, I., Barry, R.A., Dearmond, S.J., et al. (1986). AMYLOID PLAQUES IN CREUTZFELDT-JAKOB DISEASE STAIN WITH PRION PROTEIN ANTIBODIES. *Annals of Neurology* 20(2)**,** 204-208. doi: 10.1002/ana.410200205.

Kleene, R., Loers, G., Langer, J., Frobert, Y., Buck, F., and Schachner, M. (2007). Prion protein regulates glutamate-dependent lactate transport of Astrocytes. *Journal of Neuroscience* 27(45)**,** 12331-12340. doi: 10.1523/jneurosci.1358-07.2007.

Klesse, L.J., Meyers, K.A., Marshall, C.J., and Parada, L.F. (1999). Nerve growth factor induces survival and differentiation through two distinct signaling cascades in PC12 cells. *Oncogene* 18(12)**,** 2055-2068. doi: 10.1038/sj.onc.1202524.

Komander, D., and Rape, M. (2012). "The Ubiquitin Code," in *Annual Review of Biochemistry, Vol 81*, ed. R.D. Kornberg.), 203-229.

Kommaddi, R.P., Thomas, R., Ceni, C., Daigneault, K., and Barker, P.A. (2011). Trk-dependent ADAM17 activation facilitates neurotrophin survival signaling. *Faseb Journal* 25(6)**,** 2061-2070. doi: 10.1096/fj.10-173740.

Kovalevich, J., and Langford, D. (2013). "Considerations for the Use of SH-SY5Y Neuroblastoma Cells in Neurobiology," in *Neuronal Cell Culture: Methods and Protocols*, eds. S. Amini & M.K. White.), 9-21.

Krebs, B., Wiebelitz, A., Balitzki-Korte, B., Vassallo, N., Paluch, S., Mitteregger, G., et al. (2007). Cellular prion protein modulates the intracellular calcium response to hydrogen peroxide. *Journal of Neurochemistry* 100(2)**,** 358-367. doi: 10.1111/j.1471-4159.2006.04256.x.

Kuffer, A., Lakkaraju, A.K., Mogha, A., Petersen, S.C., Airich, K., Doucerain, C., et al. (2016). The prion protein is an agonistic ligand of the G protein-coupled receptor Adgrg6. *Nature* 536(7617)**,** 464-468. doi: 10.1038/nature19312.

Kuner, R. (2010). Central mechanisms of pathological pain. *Nature Medicine* 16(11)**,** 1258-1266. doi: 10.1038/nm.2231.

Kuwahara, C., Kubosaki, A., Nishimura, T., Nasu, Y., Nakamura, Y., Saeki, K., et al. (2000). Enhanced expression of cellular prion protein gene by insulin or nerve growth factor in immortalized mouse neuronal precursor cell lines. *Biochemical and Biophysical Research Communications* 268(3)**,** 763-766. doi: 10.1006/bbrc.2000.2152.

Kuwahara, C., Takeuchi, A.M., Nishimura, T., Haraguchi, K., Kubosaki, A., Matsumoto, Y., et al. (1999). Prions prevent neuronal cell-line death. *Nature* 400(6741)**,** 225-226. doi: 10.1038/22241.

Laffont-Proust, I., Hassig, R., Haik, S., Simon, S., Grassi, J., Fonta, C., et al. (2006). Truncated PrPc in mammalian brain: interspecies variation and location in membrane rafts. *Biological Chemistry* 387(3)**,** 297-300. doi: 10.1515/bc.2006.039.

Lappas Gimenez, A.P., Luciani Richter, L.M., Atherino, M.C., Branco Beirao, B.C., Favaro, C., Jr., Moura Costa, M.D., et al. (2015). Identification of novel putative-binding proteins for cellular prion protein and a specific interaction with the STIP1 homology and U-Box-containing protein 1. *Prion* 9(5)**,** 355-366. doi: 10.1080/19336896.2015.1075347.

Lauren, J., Gimbel, D.A., Nygaard, H.B., Gilbert, J.W., and Strittmatter, S.M. (2009). Cellular prion protein mediates impairment of synaptic plasticity by amyloid-beta oligomers. *Nature* 457(7233)**,** 1128-U1184. doi: 10.1038/nature07761.

Le Belle, J.E., Orozco, N.M., Paucar, A.A., Saxe, J.P., Mottahedeh, J., Pyle, A.D., et al. (2011). Proliferative Neural Stem Cells Have High Endogenous ROS Levels that Regulate Self-Renewal and Neurogenesis in a PI3K/Akt-Dependant Manner. *Cell Stem Cell* 8(1)**,** 59-71. doi: 10.1016/j.stem.2010.11.028.

Lee, G.H., Jang, B., Choi, H.S., Kim, H.J., Park, J.H., Jeon, Y.C., et al. (2015). Upregulation of Connexin 43 Expression Via C-Jun N-Terminal Kinase Signaling in Prion Disease. *Journal of Alzheimers Disease* 49(4)**,** 1005-1019. doi: 10.3233/jad-150283.

Lee, K.S., Magalhaes, A.C., Zanata, S.M., Brentani, R.R., Martins, V.R., and Prado, M.A.M. (2001a). Internalization of mammalian fluorescent cellular prion protein and N-terminal deletion mutants in living cells. *Journal of Neurochemistry* 79(1)**,** 79-87. doi: 10.1046/j.1471-4159.2001.00529.x.

Lee, R., Kermani, P., Teng, K.K., and Hempstead, B.L. (2001b). Regulation of cell survival by secreted proneurotrophins. *Science* 294(5548)**,** 1945-1948. doi: 10.1126/science.1065057.

Lee, Y.J., and Baskakov, I.V. (2013). The cellular form of the prion protein is involved in controlling cell cycle dynamics, self-renewal, and the fate of human embryonic stem cell differentiation. *Journal of Neurochemistry* 124(3)**,** 310-322. doi: 10.1111/j.1471-4159.2012.07913.x.

Lee, Y.J., and Baskakov, I.V. (2014). The cellular form of the prion protein guides the differentiation of human embryonic stem cells into neuron-, oligodendrocyte-, and astrocyte-committed lineages. *Prion* 8(3)**,** 266-275. doi: 10.4161/pri.32079.

Lei, L., and Parada, L.F. (2007). Transcriptional regulation of Trk family neurotrophin receptors. *Cellular and Molecular Life Sciences* 64(5)**,** 522-532. doi: 10.1007/s00018-006-6328-8.

Lewis, V., Whitehouse, I.J., Baybutt, H., Manson, J.C., Collins, S.J., and Hooper, N.M. (2012). Cellular Prion Protein Expression Is Not Regulated by the Alzheimer's Amyloid Precursor Protein Intracellular Domain. *Plos One* 7(2). doi: 10.1371/journal.pone.0031754.

Lima, F.R.S., Arantes, C.P., Muras, A.G., Nomizo, R., Brentani, R.R., and Martins, V.R. (2007). Cellular prion protein expression in astrocytes modulates neuronal survival and differentiation. *Journal of Neurochemistry* 103(6)**,** 2164-2176. doi: 10.1111/j.1471-4159.2007.04904.x.

Linden, R., Martins, V.R., Prado, M.A.M., Cammarota, M., Izquierdo, I., and Brentani, R.R. (2008). Physiology of the prion protein. *Physiological Reviews* 88(2)**,** 673-728. doi: 10.1152/physrev.00007.2007.

Liu, T., Yi, W.J., Feng, B.Y., Zhou, Z., and Xiao, G.F. (2013). IGF-1-Induced Enhancement of PRNP Expression Depends on the Negative Regulation of Transcription Factor FOXO3a. *Plos One* 8(8). doi: 10.1371/journal.pone.0071896.

Lledo, P.M., Tremblay, P., Dearmond, S.J., Prusiner, S.B., and Nicoll, R.A. (1996). Mice deficient for prion protein exhibit normal neuronal excitability and synaptic transmission in the hippocampus. *Proceedings of the National Academy of Sciences of the United States of America* 93(6)**,** 2403-2407. doi: 10.1073/pnas.93.6.2403.

Llorens, F., Carulla, P., Villa, A., Torres, J.M., Fortes, P., Ferrer, I., et al. (2013). PrPC regulates epidermal growth factor receptor function and cell shape dynamics in Neuro2a cells. *Journal of Neurochemistry* 127(1)**,** 124-138. doi: 10.1111/jnc.12283.

Lobao-Soares, B., Bianchin, M.M., Linhares, M.N., Carqueja, C.L., Tasca, C.I., Souza, M., et al. (2005). Normal brain mitochondrial respiration in adult mice lacking cellular prion protein. *Neuroscience Letters* 375(3)**,** 203-206. doi: 10.1016/j.neulet.2004.11.012.

Lopes, M.H., Hajj, G.N.M., Muras, A.G., Mancini, G.L., Castro, R., Ribeiro, K.C.B., et al. (2005). Interaction of cellular prion and stress-inducible protein 1 promotes neuritogenesis and neuroprotection by distinct signaling pathways. *Journal of Neuroscience* 25(49)**,** 11330-11339. doi: 10.1523/jneurosci.2313-05.2005.

Loubet, D., Dakowski, C., Pietri, M., Pradines, E., Bernard, S., Callebert, J., et al. (2012). Neuritogenesis: the prion protein controls beta 1 integrin signaling activity. *Faseb Journal* 26(2)**,** 678-690. doi: 10.1096/fj.11-185579.

Luberg, K., Park, R., Aleksejeva, E., and Timmusk, T. (2015). Novel transcripts reveal a complex structure of the human TRKA gene and imply the presence of multiple protein isoforms. *Bmc Neuroscience* 16. doi: 10.1186/s12868-015-0215-x.

Luo, S., Schaefer, A.M., Dour, S., and Nonet, M.L. (2014). The conserved LIM domain-containing focal adhesion protein ZYX-1 regulates synapse maintenance in Caenorhabditis elegans. *Development* 141(20)**,** 3922-3933. doi: 10.1242/dev.108217.

Mabbott, N.A., Brown, K.L., Manson, J., and Bruce, M.E. (1997). T-lymphocyte activation and the cellular form of the prion protein. *Immunology* 92(2)**,** 161-165. doi: 10.1046/j.1365-2567.1997.00331.x.

Magalhaes, A.C., Silva, J.A., Lee, K.S., Martins, V.R., Prado, V.F., Ferguson, S.S.G., et al. (2002). Endocytic intermediates involved with the intracellular trafficking of a fluorescent cellular prion protein. *Journal of Biological Chemistry* 277(36)**,** 33311-33318. doi: 10.1074/jbc.M203661200.

Mahal, S.P., Asante, E.A., Antoniou, M., and Collinge, J. (2001). Isolation and functional characterisation of the promoter region of the human prion protein gene. *Gene* 268(1-2)**,** 105-114. doi: 10.1016/s0378-1119(01)00424-3.

Makowska, K.A., Hughes, R.E., White, K.J., Wells, C.M., and Peckham, M. (2015). Specific Myosins Control Actin Organization, Cell Morphology, and Migration in Prostate Cancer Cells. *Cell Reports* 13(10)**,** 2118-2125. doi: 10.1016/j.celrep.2015.11.012.

Mange, A., Beranger, F., Poec'h, K., Onodera, T., Frobert, Y., and Lehmann, S. (2004). Alpha- and beta- cleavages of the amino-terminus of the cellular prion protein. *Biology of the Cell* 96(2)**,** 125-132. doi: 10.1016/j.biolcel.2003.11.007.

Manson, J., West, J.D., Thomson, V., McBride, P., Kaufman, M.H., and Hope, J. (1992). THE PRION PROTEIN GENE - A ROLE IN MOUSE EMBRYOGENESIS. *Development* 115(1)**,** 117-122.

Manson, J.C., Clarke, A.R., Hooper, M.L., Aitchison, L., McConnell, I., and Hope, J. (1994). 129/OLA MICE CARRYING A NULL MUTATION IN PRP THAT ABOLISHES MESSENGER-RNA PRODUCTION ARE DEVELOPMENTALLY NORMAL. *Molecular Neurobiology* 8(2-3)**,** 121-127. doi: 10.1007/bf02780662.

Mantuano, E., Tasciotti, V., Garofalo, T., Sorice, M., Misasi, R., and Mattei, V. (2014). PrPC associates with a multimolecular complex including LRP1 and glycosphingolipids within lipid rafts. *Faseb Journal* 28(1).

Marechal, A., Li, J.M., Ji, X.Y., Wu, C.S., Yazinski, S.A., Nguyen, H.D., et al. (2014). PRP19 Transforms into a Sensor of RPA-ssDNA after DNA Damage and Drives ATR Activation via a Ubiquitin-Mediated Circuitry. *Molecular Cell* 53(2)**,** 235-246. doi: 10.1016/j.molcel.2013.11.002.

Massague, J. (2012). TGF beta signalling in context. *Nature Reviews Molecular Cell Biology* 13(10)**,** 616-630. doi: 10.1038/nrm3434.

Mastrianni, J.A. (2010). The genetics of prion diseases. *Genetics in Medicine* 12(4)**,** 187-195. doi: 10.1097/GIM.0b013e3181cd7374.

Mattei, V., Garofalo, T., Misasi, R., Circella, A., Manganelli, V., Lucania, G., et al. (2004). Prion protein is a component of the multimolecular signaling complex involved in T cell activation. *Febs Letters* 560(1-3)**,** 14-18. doi: 10.1016/s0014-5793(04)00029-8.

Matusica, D., Skeldal, S., Sykes, A.M., Palstra, N., Sharma, A., and Coulson, E.J. (2013). An Intracellular Domain Fragment of the p75 Neurotrophin Receptor (p75(NTR)) Enhances Tropomyosin Receptor Kinase A (TrkA) Receptor Function. *Journal of Biological Chemistry* 288(16)**,** 11144-11154. doi: 10.1074/jbc.M112.436469.

Mays, C.E., Kim, C., Haldiman, T., van der Merwe, J., Lau, A., Yang, J., et al. (2014). Prion disease tempo determined by host-dependent substrate reduction. *Journal of Clinical Investigation* 124(2)**,** 847-858. doi: 10.1172/jci72241.

McCutcheon, S., Langeveld, J.P.M., Tan, B.C., Gill, A.C., de Wolf, C., Martin, S., et al. (2014). Prion Protein-Specific Antibodies that Detect Multiple TSE Agents with High Sensitivity. *Plos One* 9(3). doi: 10.1371/journal.pone.0091143.

McDonald, A.J., Dibble, J.P., Evans, E.G.B., and Millhauser, G.L. (2014). A New Paradigm for Enzymatic Control of alpha-Cleavage and beta-Cleavage of the Prion Protein. *Journal of Biological Chemistry* 289(2)**,** 803-813. doi: 10.1074/jbc.M113.502351.

McHugh, P.C., Wright, J.A., Williams, R.J., and Brown, D.R. (2012). Prion protein expression alters APP cleavage without interaction with BACE-1. *Neurochemistry International* 61(5)**,** 672-680. doi: 10.1016/j.neuint.2012.07.002.

McKinley, M.P., Bolton, D.C., and Prusiner, S.B. (1983). A PROTEASE-RESISTANT PROTEIN IS A STRUCTURAL COMPONENT OF THE SCRAPIE PRION. *Cell* 35(1)**,** 57-62. doi: 10.1016/0092-8674(83)90207-6.

McKinnon, C., Goold, R., Andre, R., Devoy, A., Ortega, Z., Moonga, J., et al. (2016). Prion-mediated neurodegeneration is associated with early impairment of the ubiquitin-proteasome system. *Acta Neuropathologica* 131(3)**,** 411-425. doi: 10.1007/s00401-015-1508-y.

McMahon, H.E.M., Mange, A., Nishida, N., Creminon, C., Casanova, D., and Lehmann, S. (2001). Cleavage of the amino terminus of the prion protein by reactive oxygen species. *Journal of Biological Chemistry* 276(3)**,** 2286-2291. doi: 10.1074/jbc.M007243200.

Mebratu, Y., and Tesfaigzi, Y. (2009). How ERK1/2 activation controls cell proliferation and cell death is subcellular localization the answer? *Cell Cycle* 8(8)**,** 1168-1175.

Mediero, A., Hempstead, B., and Cronstein, B.N. (2014). Pro-Nerve Growth Factor (ProNGF) Stimulates Bone Growth By Stimulating Osteoblasts and Inhibiting Osteoclast Differentiation, an Explanation for Anti-NGF-Mediated Osteonecrosis; Prongf Is a Novel Therapeutic Target for Treatment of Osteonecrosis and Charcot's Arthropathy. *Arthritis & Rheumatology* 66**,** S14-S15.

Meggio, F., Deana, A.D., Ruzzene, M., Brunati, A.M., Cesaro, L., Guerra, B., et al. (1995). DIFFERENT SUSCEPTIBILITY OF PROTEIN-KINASES TO STAUROSPORINE INHIBITION - KINETIC-STUDIES AND MOLECULAR-BASES FOR THE RESISTANCE OF PROTEIN-KINASE CK2. *European Journal of Biochemistry* 234(1)**,** 317-322. doi: 10.1111/j.1432-1033.1995.317_c.x.

Megison, M.L., Gillory, L.A., and Beierle, E.A. (2013). Cell Survival Signaling in Neuroblastoma. *Anti-Cancer Agents in Medicinal Chemistry* 13(4)**,** 563-575.

Mehrabian, M., Brethour, D., MacIsaac, S., Kim, J.K., Gunawardana, C.G., Wang, H., et al. (2014). CRISPR-Cas9-Based Knockout of the Prion Protein and Its Effect on the Proteome. *Plos One* 9(12). doi: 10.1371/journal.pone.0114594.

Mehrabian, M., Brethour, D., Wang, H., Xi, Z., Rogaeva, E., and Schmitt-Ulms, G. (2015). The Prion Protein Controls Polysialylation of Neural Cell Adhesion Molecule 1 during Cellular Morphogenesis. *Plos One* 10(8). doi: 10.1371/journal.pone.0133741.

Mehrabian, M., Brethour, D., Williams, D., Wang, H.S., Arnould, H., Schneider, B., et al. (2016). Prion Protein Deficiency Causes Diverse Proteome Shifts in Cell Models That Escape Detection in Brain Tissue. *Plos One* 11(6). doi: 10.1371/journal.pone.0156779.

Mendez, M.G., Kojima, S.-I., and Goldman, R.D. (2010). Vimentin induces changes in cell shape, motility, and adhesion during the epithelial to mesenchymal transition. *Faseb Journal* 24(6)**,** 1838-1851. doi: 10.1096/fj.09-151639.

Menendez, J.A., and Lupu, R. (2007). Fatty acid synthase and the lipogenic phenotype in cancer pathogenesis. *Nature Reviews Cancer* 7(10)**,** 763-777. doi: 10.1038/nrc2222.

Meotti, F.C., Carqueja, C.L., Gadotti, V.D., Tasca, C.I., Walz, R., and Santos, A.R.S. (2007). Involvement of cellular prion protein in the nociceptive response in mice. *Brain Research* 1151**,** 84-90. doi: 10.1016/j.brainres.2007.03.024.

Mi, S., Lee, X., Shao, Z.H., Thill, G., Ji, B.X., Relton, J., et al. (2004). LINGO-1 is a component of the Nogo-66 receptor/p75 signaling complex. *Nature Neuroscience* 7(3)**,** 221-228. doi: 10.1038/nn1188.

Miele, G., Jeffrey, M., Turnbull, D., Manson, J., and Clinton, M. (2002). Ablation of cellular prion protein expression affects mitochondrial numbers and morphology. *Biochemical and Biophysical Research Communications* 291(2)**,** 372-377. doi: 10.1006/bbrc.2002.6460.

Moore, R.C., Lee, I.Y., Silverman, G.L., Harrison, P.M., Strome, R., Heinrich, C., et al. (1999). Ataxia in prion protein (PrP)-deficient mice is associated with upregulation of the novel PrP-like protein Doppel. *Journal of Molecular Biology* 292(4)**,** 797-817. doi: 10.1006/jmbi.1999.3108.

Moore, R.C., Redhead, N.J., Selfridge, J., Hope, J., Manson, J.C., and Melton, D.W. (1995). DOUBLE REPLACEMENT GENE TARGETING FOR THE PRODUCTION OF A SERIES OF MOUSE STRAINS WITH DIFFERENT PRION PROTEIN GENE ALTERATIONS. *Bio-Technology* 13(9)**,** 999-1004. doi: 10.1038/nbt0995-999.

Morel, E., Fouquet, S., Strup-Perrot, C., Thievend, C.P., Petit, C., Loew, D., et al. (2008). The Cellular Prion Protein PrPc Is Involved in the Proliferation of Epithelial Cells and in the Distribution of Junction-Associated Proteins. *Plos One* 3(8). doi: 10.1371/journal.pone.0003000.

Moser, M., Colello, R.J., Pott, U., and Oesch, B. (1995). DEVELOPMENTAL EXPRESSION OF THE PRION PROTEIN GENE IN GLIAL-CELLS. *Neuron* 14(3)**,** 509-517. doi: 10.1016/0896-6273(95)90307-0.

Muller, W.E.G., Ushijima, H., Schroder, H.C., Forrest, J.M.S., Schatton, W.F.H., Rytik, P.G., et al. (1993). CYTOPROTECTIVE EFFECT OF NMDA RECEPTOR ANTAGONISTS ON PRION PROTEIN (PRION(SC))-INDUCED TOXICITY IN RAT CORTICAL CELL-CULTURES. *European Journal of Pharmacology-Molecular Pharmacology Section* 246(3)**,** 261-267. doi: 10.1016/0922-4106(93)90040-g.

Nah, J., Pyo, J.O., Jung, S., Yoo, S.M., Kam, T.I., Chang, J., et al. (2013). BECN1/Beclin 1 is recruited into lipid rafts by prion to activate autophagy in response to amyloid beta 42. *Autophagy* 9(12)**,** 2009-2021. doi: 10.4161/auto.26118.

Nathanson, N., Wilesmith, J., and Griot, C. (1997). Bovine spongiform encephalopathy (BSE): Causes and consequences of a common source epidemic. *American Journal of Epidemiology* 145(11)**,** 959-969.

Nikles, D., Vana, K., Gauczynski, S., Knetsch, H., Ludewigs, H., and Weiss, S. (2008). Subcellular localization of prion proteins and the 37 kDa/67 kDa laminin receptor fused to fluorescent proteins. *Biochimica Et Biophysica Acta-Molecular Basis of Disease* 1782(5)**,** 335-340. doi: 10.1016/j.bbadis.2008.02.003.

Nishida, N., Tremblay, P., Sugimoto, T., Shigematsu, K., Shirabe, S., Petromilli, C., et al. (1999). A mouse prion protein transgene rescues mice deficient for the prion protein gene from Purkinje cell degeneration and demyelination. *Laboratory Investigation* 79(6)**,** 689-697.

Nishimura, T., Sakudo, A., Hashiyama, Y., Yachi, A., Saeki, K., Matsumoto, Y., et al. (2007). Serum withdrawal-induced apoptosis in Zrchl prion protein (PrP) gene-deficient neuronal cell line is suppressed by PrP, independent of Doppel. *Microbiology and Immunology* 51(4)**,** 457-466. doi: 10.1111/j.1348-0421.2007.tb03920.x.

Nuvolone, M., Hermann, M., Sorce, S., Russo, G., Tiberi, C., Schwarz, P., et al. (2016). Strictly co-isogenic C57BL/6J-Prnp(-/-) mice: A rigorous resource for prion science. *Journal of Experimental Medicine* 213(3)**,** 313-327. doi: 10.1084/jem.20151610.

Nuvolone, M., Kana, V., Hutter, G., Sakata, D., Mortin-Toth, S.M., Russo, G., et al. (2013). SIRP alpha polymorphisms, but not the prion protein, control phagocytosis of apoptotic cells. *Journal of Experimental Medicine* 210(12)**,** 2539-2552. doi: 10.1084/jem.20131274.

Nykjaer, A., Lee, R., Teng, K.K., Jansen, P., Madsen, P., Nielsen, M.S., et al. (2004). Sortilin is essential for proNGF-induced neuronal cell death. *Nature* 427(6977)**,** 843-848. doi: 10.1038/nature02319.

O'Connor, T.P., Duerr, J.S., and Bentley, D. (1990). PIONEER GROWTH CONE STEERING DECISIONS MEDIATED BY SINGLE FILOPODIAL CONTACTS INSITU. *Journal of Neuroscience* 10(12)**,** 3935-3946.

Obata, K., Katsura, H., Sakurai, J., Kobayashi, K., Yamanaka, H., Dai, Y., et al. (2006). Suppression of the p75 neurotrophin receptor in uninjured sensory neurons reduces neuropathic pain after nerve injury. *Journal of Neuroscience* 26(46)**,** 11974-11986. doi: 10.1523/jneurosci.3188-06.2006.

Oh, J.M., Shin, H.Y., Park, S.J., Kim, B.H., Choi, J.K., Choi, E.K., et al. (2008). The involvement of cellular prion protein in the autophagy pathway in neuronal cells. *Molecular and Cellular Neuroscience* 39(2)**,** 238-247. doi: 10.1016/j.mcn.2008.07.003.

Onischenko, E.A., Gubanova, N.V., Kiseleva, E.V., and Hallberg, E. (2005). Cdk1 and okadaic acid-sensitive phosphatases control assembly of nuclear pore complexes in Drosophila embryos. *Molecular Biology of the Cell* 16(11)**,** 5152-5162. doi: 10.1091/mbc.E05-07-0642.

Opattova, A., Cente, M., Novak, M., and Filipcik, P. (2015). The ubiquitin proteasome system as a potential therapeutic target for treatment of neurodegenerative diseases. *General Physiology and Biophysics* 34(4)**,** 337-352. doi: 10.4149/gpb_2015024.

Orsi, A., Fioriti, L., Chiesa, R., and Sitia, R. (2006). Conditions of endoplasmic reticulum stress favor the accumulation of cytosolic prion protein. *Journal of Biological Chemistry* 281(41)**,** 30431-30438. doi: 10.1074/jbc.M605320200.

Ostapchenko, V.G., Beraldo, F.H., Mohammad, A.H., Xie, Y.F., Hirata, P.H.F., Magalhaes, A.C., et al. (2013). The Prion Protein Ligand, Stress-Inducible Phosphoprotein 1, Regulates Amyloid-beta Oligomer Toxicity. *Journal of Neuroscience* 33(42)**,** 16552-16564. doi: 10.1523/jneurosci.3214-13.2013.

Oyamada, M., Takebe, K., and Oyamada, Y. (2013). Regulation of connexin expression by transcription factors and epigenetic mechanisms. *Biochimica Et Biophysica Acta-Biomembranes* 1828(1)**,** 118-133. doi: 10.1016/j.bbamem.2011.12.031.

Pahlman, S., Odelstad, L., Larsson, E., Grotte, G., and Nilsson, K. (1981). PHENOTYPIC CHANGES OF HUMAN NEURO-BLASTOMA CELLS IN CULTURE INDUCED BY 12-0-TETRADECANOYL-PHORBOL-13-ACETATE. *International Journal of Cancer* 28(5)**,** 583-589. doi: 10.1002/ijc.2910280509.

Paitel, E., da Costa, C.A., Vilette, D., Grassi, J., and Checler, F. (2002). Overexpression of PrPc triggers caspase 3 activation: potentiation by proteasome inhibitors and blockade by anti-PrP antibodies. *Journal of Neurochemistry* 83(5)**,** 1208-1214. doi: 10.1046/j.1471-4159.2002.01234.x.

Paitel, E., Fahraeus, R., and Checler, F. (2003). Cellular prion protein sensitizes neurons to apoptotic stimuli through Mdm2-regulated and p53-dependent caspase 3-like activation. *Journal of Biological Chemistry* 278(12)**,** 10061-10066. doi: 10.1074/jbc.M211580200.

Paitel, E., Sunyach, C., da Costa, C.A., Bourdon, J.C., Vincent, B., and Checler, F. (2004). Primary cultured neurons devoid of cellular prion display lower responsiveness to Staurosporine through the control of p53 at both transcriptional and post-transcriptional levels. *Journal of Biological Chemistry* 279(1)**,** 612-618. doi: 10.1074/jbc.M310453200.

Palandri, A., Salvador, V.R., Wojnacki, J., Vivinetto, A.L., Schnaar, R.L., and Lopez, P.H.H. (2015). Myelin-associated glycoprotein modulates apoptosis of motoneurons during early postnatal development via NgR/p75(NTR) receptor-mediated activation of RhoA signaling pathways. *Cell Death & Disease* 6. doi: 10.1038/cddis.2015.228.

Pan, K.M., Baldwin, M., Nguyen, J., Gasset, M., Serban, A., Groth, D., et al. (1993). CONVERSION OF ALPHA-HELICES INTO BETA-SHEETS FEATURES IN THE FORMATION OF THE SCRAPIE PRION PROTEINS. *Proceedings of the National Academy of Sciences of the United States of America* 90(23)**,** 10962-10966. doi: 10.1073/pnas.90.23.10962.

Park, H., Chan, M.M., and Iritani, B.M. (2010a). Hem-1: Putting the "WAVE" into actin polymerization during an immune response. *Febs Letters* 584(24)**,** 4923-4932. doi: 10.1016/j.febslet.2010.10.018.

Park, K.J., Grosso, C.A., Aubert, I., Kaplan, D.R., and Miller, F.D. (2010b). p75NTR-dependent, myelin-mediated axonal degeneration regulates neural connectivity in the adult brain. *Nature Neuroscience* 13(5)**,** 559-U552. doi: 10.1038/nn.2513.

Parkin, E.T., Watt, N.T., Hussain, I., Eckman, E.A., Eckman, C.B., Manson, J.C., et al. (2007). Cellular prion protein regulates beta-secretase cleavage of the Alzheimer's amyloid precursor protein. *Proceedings of the National Academy of Sciences of the United States of America* 104(26)**,** 11062-11067. doi: 10.1073/pnas.0609621104.

Passino, M.A., Adams, R.A., Sikorski, S.L., and Akassoglou, K. (2007). Regulation of hepatic stellate cell differentiation by the neurotrophin receptor p75(NTR). *Science* 315(5820)**,** 1853-1856. doi: 10.1126/science.1137603.

Pastore, A., and Zagari, A. (2007). A Structural Overview of the Vertebrate Prion Proteins. *Prion* 1(3)**,** 185-197. doi: 10.4161/pri.1.3.5281.

Paterson, A.W.J., Curtis, J.C., and MacLeod, N.K. (2008). Complex I specific increase in superoxide formation and respiration rate by PrP-null mouse brain mitochondria. *Journal of Neurochemistry* 105(1)**,** 177-191. doi: 10.1111/j.1471-4159.2007.5123.x.

Peralta, O.A., and Eyestone, W.H. (2009). Quantitative and qualitative analysis of cellular prion protein (PrPC) expression in bovine somatic tissues. *Prion* 3(3)**,** 161-170. doi: 10.4161/pri.3.3.9772

Peralta, O.A., Huckle, W.R., and Eyestone, W.H. (2012). Developmental expression of the cellular prion protein (PrPC) in bovine embryos. *Molecular Reproduction and Development* 79(7)**,** 488-498. doi: 10.1002/mrd.22057.

Perera, W.S.S., and Hooper, N.M. (1999). Proteolytic fragmentation of the murine prion protein: role of Tyr-128 and His-177. *Febs Letters* 463(3)**,** 273-276. doi: 10.1016/s0014-5793(99)01648-8.

Petrenko, A.B., Yamakura, T., Baba, A., and Shimoji, K. (2003). The role of N-methyl-D-aspartate (NMDA) receptors in pain: A review. *Anesthesia and Analgesia* 97(4)**,** 1108-1116. doi: 10.1213/01.ane.0000081061.12235.55.

Pezet, S., and McMahon, S.B. (2006). "Neurotrophins: Mediators and modulators of pain," in *Annual Review of Neuroscience*.), 507-538.

Presgraves, S.P., Ahmed, T., Borwege, S., and Joyce, J.N. (2004). Terminally differentiated SH-SY5Y cells provide a model system for studying neuroprotective effects of dopamine agonists. *Neurotoxicity Research* 5(8)**,** 579-598.

Prince, J.A., and Oreland, L. (1997). Staurosporine differentiated human SH-SY5Y neuroblastoma cultures exhibit transient apoptosis and trophic factor independence. *Brain Research Bulletin* 43(6)**,** 515-523. doi: 10.1016/s0361-9230(97)00328-6.

Promega. 2009. pCI-neo Mammalian Expression Vector: Instructions for Use. Available: https://www.promega.co.uk/~/media/files/resources/protocols/technical%20bulletins/0/pci%20neo%20mammalian%20expression%20vector%20protocol.pdf [Accessed 10/09/15].

Provansal, M., Roche, S., Pastore, M., Casanova, D., Belondrade, M., Alais, S., et al. (2010). Proteomic consequences of expression and pathological conversion of the prion protein in inducible neuroblastoma N2a cells. *Prion* 4(4)**,** 292-301. doi: 10.4161/pri.4.4.13435.

Prusiner, S., Oesch, B., Walchli, M., Westaway, D., McKinley, M., Teplow, D., et al. (1985). MOLECULAR-CLONING STUDIES DEMONSTRATE THAT CELLULAR GENOMIC DNA ENCODES THE SCRAPIE PRION PROTEIN. *Clinical Research* 33(2)**,** A565-A565.

Prusiner, S.B. (1982). NOVEL PROTEINACEOUS INFECTIOUS PARTICLES CAUSE SCRAPIE. *Science* 216(4542)**,** 136-144. doi: 10.1126/science.6801762.

Prusiner, S.B., Bolton, D.C., Groth, D.F., Bowman, K.A., Cochran, S.P., and McKinley, M.P. (1982). FURTHER PURIFICATION AND CHARACTERIZATION OF SCRAPIE PRIONS. *Biochemistry* 21(26)**,** 6942-6950. doi: 10.1021/bi00269a050.

Prusiner, S.B., Groth, D., Serban, A., Koehler, R., Foster, D., Torchia, M., et al. (1993). ABLATION OF THE PRION PROTEIN (PRP) GENE IN MICE PREVENTS SCRAPIE AND FACILITATES PRODUCTION OF ANTI-PRP ANTIBODIES. *Proceedings of the National Academy of Sciences of the United States of America* 90(22)**,** 10608-10612. doi: 10.1073/pnas.90.22.10608.

Prusiner, S.B., Woerman, A.L., Mordes, D.A., Watts, J.C., Rampersaud, R., Berry, D.B., et al. (2015). Evidence for alpha-synuclein prions causing multiple system atrophy in humans with parkinsonism. *Proceedings of the National Academy of Sciences of the United States of America* 112(38)**,** E5308-E5317. doi: 10.1073/pnas.1514475112.

Puckett, C., Concannon, P., Casey, C., and Hood, L. (1991). GENOMIC STRUCTURE OF THE HUMAN PRION PROTEIN GENE. *American Journal of Human Genetics* 49(2)**,** 320-329.

Qin, K., Zhao, L., Tang, Y., Bhatta, S., Simard, J.M., and Zhao, R.Y. (2006). Doppel-induced apoptosis and counteraction by cellular prion protein in neuroblastoma and astrocytes. *Neuroscience* 141(3)**,** 1375-1388. doi: 10.1016/j.neuroscience.2006.04.068.

Rachidi, W., Vilette, D., Guiraud, P., Arlotto, M., Riondel, J., Laude, H., et al. (2003). Expression of prion protein increases cellular copper binding and antioxidant enzyme activities but not copper delivery. *Journal of Biological Chemistry* 278(11)**,** 9064-9072. doi: 10.1074/jbc.M211830200.

Rambold, A.S., Muller, V., Ron, U., Ben-Tal, N., Winklhofer, K.F., and Tatzelt, J. (2008). Stress-protective signalling of prion protein is corrupted by scrapie prions. *Embo Journal* 27(14)**,** 1974-1984. doi: 10.1038/emboj.2008.122.

Ramljak, S., Asif, A.R., Armstrong, V.W., Wrede, A., Groschup, M.H., Buschman, A., et al. (2008). Physiological role of the cellular prion protein (PrPc): Protein profiling study in two cell culture systems. *Journal of Proteome Research* 7(7)**,** 2681-2695. doi: 10.1021/pr7007187.

Rappsilber, J., Mann, M., and Ishihama, Y. (2007). Protocol for micro-purification, enrichment, pre-fractionation and storage of peptides for proteomics using StageTips. *Nature Protocols* 2(8)**,** 1896-1906. doi: 10.1038/nprot.2007.261.

Reiten, M.R., Bakkebo, M.K., Tranulis, M.A., Espenes, A., and Boysen, P. (2015). Hematological shift but no evidence of immunological impairment in goat kids naturally devoid of the cellular prion protein (PrPC). *Prion* 9**,** S81-S81. doi: 10.1080/19336896.2015.1033248

Rial, D., Duarte, F.S., Xikota, J.C., Schmitz, A.E., Dafre, A.L., Figueiredo, C.P., et al. (2009). CELLULAR PRION PROTEIN MODULATES AGE-RELATED BEHAVIORAL AND NEUROCHEMICAL ALTERATIONS IN MICE. *Neuroscience* 164(3)**,** 896-907. doi: 10.1016/j.neuroscience.2009.09.005.

Rial, D., Pandolfo, P., Bitencourt, R.M., Pamplona, F.A., Moreira, K.M., Hipolide, D., et al. (2014). Cellular prion protein (PrPC) modulates ethanol-induced behavioral adaptive changes in mice. *Behavioural Brain Research* 271**,** 325-332. doi: 10.1016/j.bbr.2014.05.067.

Ribeiro, N., Sousa, S.R., Brekken, R.A., and Monteiro, F.J. (2014). Role of SPARC in Bone Remodeling and Cancer-Related Bone Metastasis. *Journal of Cellular Biochemistry* 115(1)**,** 17-26. doi: 10.1002/jcb.24649.

Richt, J.A., Kasinathan, P., Hamir, A.N., Castilla, J., Sathiyaseelan, T., Vargas, F., et al. (2007). Production of cattle lacking prion protein. *Nature Biotechnology* 25(1)**,** 132-138. doi: 10.1038/nbt1271.

Riek, R., Hornemann, S., Wider, G., Billeter, M., Glockshuber, R., and Wuthrich, K. (1996). NMR structure of the mouse prion protein domain PrP(121-231). *Nature* 382(6587)**,** 180-182. doi: 10.1038/382180a0.

Ritchie, D.L., Boyle, A., McConnell, I., Head, M.W., Ironside, J.W., and Bruce, M.E. (2009). Transmissions of variant Creutzfeldt-Jakob disease from brain and lymphoreticular tissue show uniform and conserved bovine spongiform encephalopathy-related phenotypic properties on primary and secondary passage in wild-type mice. *Journal of General Virology* 90**,** 3075-3082. doi: 10.1099/vir.0.013227-0.

Roffe, M., Beraldo, F.H., Bester, R., Nunziante, M., Bach, C., Mancini, G., et al. (2010). Prion protein interaction with stress-inducible protein 1 enhances neuronal protein synthesis via mTOR. *Proceedings of the National Academy of Sciences of the United States of America* 107(29)**,** 13147-13152. doi: 10.1073/pnas.1000784107.

Rossi, D., Cozzio, A., Flechsig, E., Klein, M.A., Rulicke, T., Aguzzi, A., et al. (2001). Onset of ataxia and Purkinje cell loss in PrP null mice inversely correlated with Dpl level in brain. *Embo Journal* 20(4)**,** 694-702. doi: 10.1093/emboj/20.4.694.

Roucou, X., Giannopoulos, P.N., Zhang, Y., Jodoin, J., Goodyer, C.G., and LeBlanc, A. (2005). Cellular prion protein inhibits proapoptotic Bax conformational change in human neurons and in breast carcinoma MCF-7 cells. *Cell Death and Differentiation* 12(7)**,** 783-795. doi: 10.1038/sj.cdd.4401629.

Ruegg, U.T., and Burgess, G.M. (1989). STAUROSPORINE, K-252 AND UCN-01 - POTENT BUT NONSPECIFIC INHIBITORS OF PROTEIN-KINASES. *Trends in Pharmacological Sciences* 10(6)**,** 218-220. doi: 10.1016/0165-6147(89)90263-0.

Sagne, C., Isambert, M.F., Henry, J.P., and Gasnier, B. (1996). SDS-resistant aggregation of membrane proteins: Application to the purification of the vesicular monoamine transporter. *Biochemical Journal* 316**,** 825-831.

Sakaguchi, S., Katamine, S., Nishida, N., Moriuchi, R., Shigematsu, K., Sugimoto, T., et al. (1996). Loss of cerebellar Purkinje cells in aged mice homozygous for a disrupted Prp gene. *Nature* 380(6574)**,** 528-531. doi: 10.1038/380528a0.

Sakamoto, M., Miyazaki, Y., Kitajo, K., and Yamaguchi, A. (2015). VGF, Which Is Induced Transcriptionally in Stroke Brain, Enhances Neurite Extension and Confers Protection Against Ischemia In Vitro. *Translational Stroke Research* 6(4)**,** 301-308. doi: 10.1007/s12975-015-0401-2.

Sakudo, A., Lee, D.C., Nakamura, I., Taniuchi, Y., Saeki, K., Matsumoto, Y., et al. (2005). Cell-autonomous PrP-Doppel interaction regulates apoptosis in PrP gene-deficient neuronal cells. *Biochemical and Biophysical Research Communications* 333(2)**,** 448-454. doi: 10.1016/j.bbrc.2005.05.128.

Sakudo, A., Lee, D.C., Saeki, K., Nakamura, Y., Inoue, K., Matsumoto, Y., et al. (2003). Impairment of superoxide dismutase activation by N-terminally truncated prion protein (PrP) in PrP-deficient neuronal cell line. *Biochemical and Biophysical Research Communications* 308(3)**,** 660-667. doi: 10.1016/s0006-29ix(03)01459-1.

Sakudo, A., Xue, G.A., Kawashita, N., Ano, Y., Takagi, T., Shintani, H., et al. (2010). Structure of the Prion Protein and Its Gene: An Analysis Using Bioinformatics and Computer Simulation. *Current Protein & Peptide Science* 11(2)**,** 166-179. doi: 10.2174/138920310790848386.

Sakurai-Yamashita, Y., Sakaguchi, S., Yoshikawa, D., Okimura, N., Masuda, Y., Katamine, S., et al. (2005). Female-specific neuroprotection against transient brain ischemia observed in mice devoid of prion protein is abolished by ectopic expression of prion protein-like protein. *Neuroscience* 136(1)**,** 281-287. doi: 10.1016/j.neuroscience.2005.06.095.

Sales, N., Hassig, R., Rodolfo, K., Di Giamberardino, L., Traiffort, E., Ruat, M., et al. (2002). Developmental expression of the cellular prion protein in elongating axons. *European Journal of Neuroscience* 15(7)**,** 1163-1177. doi: 10.1046/j.1460-9568.2002.01953.x.

Sales, N., Rodolfo, K., Hassig, R., Faucheux, B., Di Giamberardino, L., and Moya, K.L. (1998). Cellular prion protein localization in rodent and primate brain. *European Journal of Neuroscience* 10(7)**,** 2464-2471. doi: 10.1046/j.1460-9568.1998.00258.x.

Salter, M.W., Dong, Y.N., Kalia, L.V., Liu, X.J., and Pitcher, G. (2009). Regulation of NMDA Receptors by Kinases and Phosphatases. *Biology of the Nmda Receptor***,** 123-148.

Sanchez-Alavez, M., Conti, B., Moroncini, G., and Criado, J.R. (2007). Contributions of neuronal prion protein on sleep recovery and stress response following sleep deprivation. *Brain Research* 1158**,** 71-80. doi: 10.1016/j.brainres.2007.05.010.

Santamaria, D., Barriere, C., Cerqueira, A., Hunt, S., Tardy, C., Newton, K., et al. (2007). Cdk1 is sufficient to drive the mammalian cell cycle. *Nature* 448(7155)**,** 811-U818. doi: 10.1038/nature06046.

Santuccione, A., Sytnyk, V., Leshchyns'ka, I., and Schachner, M. (2005). Prion protein recruits its neuronal receptor NCAM to lipid rafts to activate p59(fyn) and to enhance neurite outgrowth. *Journal of Cell Biology* 169(2)**,** 341-354. doi: 10.1083/jcb.200409127.

Saunders, S.E., Bartelt-Hunt, S.L., and Bartz, J.C. (2012). Occurrence, Transmission, and Zoonotic Potential of Chronic Wasting Disease. *Emerging Infectious Diseases* 18(3)**,** 369-376. doi: 10.3201/eid1803.110685.

Savas, M.C., Koruk, I., Koruk, M., Kadayifci, A., and Sari, I. (2010). Association of Prion Protein with the Stage of Liver Fibrosis in Chronic Viral Hepatitis. *Trakya Universitesi Tip Fakultesi Dergisi* 27(4)**,** 373-377. doi: 10.5174/tutfd.2009.02284.1.

Scalabrino, G., Veber, D., De Giuseppe, R., and Roncaroli, F. (2015). LOW LEVELS OF COBALAMIN, EPIDERMAL GROWTH FACTOR, AND NORMAL PRIONS IN MULTIPLE SCLEROSIS SPINAL CORD. *Neuroscience* 298**,** 293-301. doi: 10.1016/j.neuroscience.2015.04.020.

Schmitt-Ulms, G., Ehsani, S., Watts, J.C., Westaway, D., and Wille, H. (2009). Evolutionary Descent of Prion Genes from the ZIP Family of Metal Ion Transporters. *Plos One* 4(9). doi: 10.1371/journal.pone.0007208.

Schmitz, M., Greis, C., Ottis, P., Silva, C.J., Schulz-Schaeffer, W.J., Wrede, A., et al. (2014). Loss of Prion Protein Leads to Age-Dependent Behavioral Abnormalities and Changes in Cytoskeletal Protein Expression. *Molecular Neurobiology* 50(3)**,** 923-936. doi: 10.1007/s12035-014-8655-3.

Schneider, K., Korkmaz, Y., Addicks, K., Lang, H., and Raab, W.H.M. (2007). Prion protein (PrP) in human teeth: An unprecedented pointer to PrP's function. *Journal of Endodontics* 33(2)**,** 110-113. doi: 10.1016/j.joen.2006.11.010.

Schwanhausser, B., Busse, D., Li, N., Dittmar, G., Schuchhardt, J., Wolf, J., et al. (2011). Global quantification of mammalian gene expression control. *Nature* 473(7347)**,** 337-342. doi: 10.1038/nature10098.

Senator, A., Rachidi, W., Lehmann, S., Favier, A., and Benboubetra, M. (2004). Prion protein protects against DNA damage induced by paraquat in cultured cells. *Free Radical Biology and Medicine* 37(8)**,** 1224-1230. doi: 10.1016/j.freeradbiomed.2004.07.006.

Shin, H.Y., Park, J.H., Carp, R.I., Choi, E.K., and Kim, Y.S. (2014). Deficiency of prion protein induces impaired autophagic flux in neurons. *Frontiers in Aging Neuroscience* 6. doi: 10.3389/fnagi.2014.00207.

Shmerling, D., Hegyi, I., Fischer, M., Blattler, T., Brandner, S., Gotz, J., et al. (1998). Expression of amino-terminally truncated PrP in the mouse leading to ataxia and specific cerebellar lesions. *Cell* 93(2)**,** 203-214. doi: 10.1016/s0092-8674(00)81572-x.

Shyng, S.L., Huber, M.T., and Harris, D.A. (1993). A PRION PROTEIN CYCLES BETWEEN THE CELL-SURFACE AND AN ENDOCYTIC COMPARTMENT IN CULTURED NEUROBLASTOMA-CELLS. *Journal of Biological Chemistry* 268(21)**,** 15922-15928.

Shyng, S.L., Moulder, K.L., Lesko, A., and Harris, D.A. (1995). THE N-TERMINAL DOMAIN OF A GLYCOLIPID-ANCHORED PRION PROTEIN IS ESSENTIAL FOR ITS ENDOCYTOSIS VIA CLATHRIN-COATED PITS. *Journal of Biological Chemistry* 270(24)**,** 14793-14800.

Sigma-Aldrich ([n.d.]). *Tunicamycin from Streptomyces sp.* [Online]. Available: http://www.sigmaaldrich.com/catalog/product/sigma/t7765?lang=en&region=GB [Accessed 21/09/2015].

Silber, B.M., Gever, J.R., Rao, S., Li, Z., Renslo, A.R., Widjaja, K., et al. (2014). Novel compounds lowering the cellular isoform of the human prion protein in cultured human cells. *Bioorganic & Medicinal Chemistry* 22(6)**,** 1960-1972. doi: 10.1016/j.bmc.2014.01.001.

Silverman, G.L., Qin, K.F., Moore, R.C., Yang, Y., Mastrangelo, P., Tremblay, P., et al. (2000). Doppel is an N-glycosylated, glycosylphosphatidylinositol-anchored protein - Expression in testis and ectopic production in the brains of Prnp(o/o) mice predisposed to Purkinje cell loss. *Journal of Biological Chemistry* 275(35)**,** 26834-26841. doi: 10.1074/jbc.M003888200.

Singh, A., Haldar, S., Horback, K., Tom, C., Zhou, L., Meyerson, H., et al. (2013). Prion Protein Regulates Iron Transport by Functioning as a Ferrireductase. *Journal of Alzheimers Disease* 35(3)**,** 541-552. doi: 10.3233/jad-130218.

Singh, A., Kong, Q.Z., Luo, X., Petersen, R.B., Meyerson, H., and Singh, N. (2009). Prion Protein (PrP) Knock-Out Mice Show Altered Iron Metabolism: A Functional Role for PrP in Iron Uptake and Transport. *Plos One* 4(7). doi: 10.1371/journal.pone.0006115.

Singh, T.K., Abonyo, B., Narasaraju, T.A., and Liu, L. (2004). Reorganization of cytoskeleton during surfactant secretion in lung type II cells: a role of annexin II. *Cellular Signalling* 16(1)**,** 63-70. doi: 10.1016/s0898-6568(03)00089-5.

Skeldal, S., Sykes, A.M., Glerup, S., Matusica, D., Palstra, N., Autio, H., et al. (2012). Mapping of the Interaction Site between Sortilin and the p75 Neurotrophin Receptor Reveals a Regulatory Role for the Sortilin Intracellular Domain in p75 Neurotrophin Receptor Shedding and Apoptosis. *Journal of Biological Chemistry* 287(52)**,** 43798-43809. doi: 10.1074/jbc.M112.374710.

Slack, S.E., Pezet, S., McMahon, S.B., Thompson, S.W.N., and Malcangio, M. (2004). Brain-derived neurotrophic factor induces NMDA receptor subunit one phosphorylation via ERK and PKC in the rat spinal cord. *European Journal of Neuroscience* 20(7)**,** 1769-1778. doi: 10.1111/j.1460-9568.2004.03656.x.

Smith, M.A., Blankman, E., Gardel, M.L., Luettjohann, L., Waterman, C.M., and Beckerle, M.C. (2010). A Zyxin-Mediated Mechanism for Actin Stress Fiber Maintenance and Repair. *Developmental Cell* 19(3)**,** 365-376. doi: 10.1016/j.devcel.2010.08.008.

Sofroniew, M.V., Howe, C.L., and Mobley, W.C. (2001). Nerve growth factor signaling, neuroprotection, and neural repair. *Annual Review of Neuroscience* 24**,** 1217-1281. doi: 10.1146/annurev.neuro.24.1.1217.

Sorice, M., Mattei, V., Tasciotti, V., Manganelli, V., Garofalo, T., and Misasi, R. (2012). Trafficking of PrPC to mitochondrial raft-like microdomains during cell apoptosis. *Prion* 6(4)**,** 354-358. doi: 10.4161/pri.20479.

Spanaki, C., Zaganas, I., Kounoupa, Z., and Plaitakis, A. (2012). The complex regulation of human glud1 and glud2 glutamate dehydrogenases and its implications in nerve tissue biology. *Neurochemistry International* 61(4)**,** 470-481. doi: 10.1016/j.neuint.2012.05.020.

Steele, A.D., Emsley, J.G., Ozdinler, P.H., Lindquist, S., and Macklis, J.D. (2006). Prion protein (PrPc) positively regulates neural precursor proliferation during developmental and adult mammalian neurogenesis. *Proceedings of the National Academy of Sciences of the United States of America* 103(9)**,** 3416-3421. doi: 10.1073/pnas.0511290103.

Steele, A.D., Lindquist, S., and Aguzzi, A. (2007). The Prion Protein Knockout Mouse A Phenotype Under Challenge. *Prion* 1(2)**,** 83-93.

Steen, H., and Mann, M. (2004). The ABC's (and XYZ's) of peptide sequencing. *Nature Reviews Molecular Cell Biology* 5(9)**,** 699-711. doi: 10.1038/nrm1468.

Steinacker, P., Hawlik, A., Lehnert, S., Jahn, O., Meier, S., Gorz, E., et al. (2010). Neuroprotective Function of Cellular Prion Protein in a Mouse Model of Amyotrophic Lateral Sclerosis. *American Journal of Pathology* 176(3)**,** 1409-1420. doi: 10.2353/ajpath.2010.090355.

Stella, R., Cifani, P., Peggion, C., Hansson, K., Lazzari, C., Bendz, M., et al. (2012). Relative Quantification of Membrane Proteins in Wild-Type and Prion Protein (PrP)-Knockout Cerebellar Granule Neurons. *Journal of Proteome Research* 11(2)**,** 523-536. doi: 10.1021/pr200759m.

Stempelj, M., and Ferjan, I. (2005). Signaling pathway in nerve growth factor induced histamine release from rat mast cells. *Inflammation Research* 54(8)**,** 344-349. doi: 10.1007/s00011-005-1364-7.

Stewart, R.S., Drisaldi, B., and Harris, D.A. (2001). A transmembrane form of the prion protein contains an uncleaved signal peptide and is retained in the endoplasmic reticululm. *Molecular Biology of the Cell* 12(4)**,** 881-889.

Stewart, R.S., Piccardo, P., Ghetti, B., and Harris, D.A. (2005). Neurodegenerative illness in transgenic mice expressing a transmembrane form of the prion protein. *Journal of Neuroscience* 25(13)**,** 3469-3477. doi: 10.1523/jneurosci.0105-05.2005.

Strom, A., Wang, G.S., and Scott, F.W. (2011). Impaired Glucose Tolerance in Mice Lacking Cellular Prion Protein. *Pancreas* 40(2)**,** 229-232. doi: 10.1097/MPA.0b013e3181f7e547.

Stuart, C.A., Howell, M.E.A., Zhang, Y., and Yin, D.L. (2009). Insulin-Stimulated Translocation of Glucose Transporter (GLUT) 12 Parallels That of GLUT4 in Normal Muscle. *Journal of Clinical Endocrinology & Metabolism* 94(9)**,** 3535-3542. doi: 10.1210/jc.2009-0162.

Su, A.I., Wiltshire, T., Batalov, S., Lapp, H., Ching, K.A., Block, D., et al. (2004). A gene atlas of the mouse and human protein-encoding transcriptomes. *Proceedings of the National Academy of Sciences of the United States of America* 101(16)**,** 6062-6067. doi: 10.1073/pnas.0400782101.

Sunyach, C., Cisse, M.A., da Costa, C.A., and Checler, F. (2007). The C-terminal products of cellular prion protein processing, C1 and C2, exert distinct influence on p53-dependent staurosporine-induced caspase-3 activation. *Journal of Biological Chemistry* 282(3)**,** 1956-1963. doi: 10.1074/jbc.M609663200.

Sunyach, C., Jen, A., Deng, J., Fitzgerald, K.T., Frobert, Y., Grassi, J., et al. (2003). The mechanism of internalization of glycosylphosphatidylinositol-anchored prion protein. *Embo Journal* 22(14)**,** 3591-3601. doi: 10.1093/emboj/cdg344.

Tang, L.L., Wang, R., and Tang, X.C. (2005). Huperzine A protects SHSY5Y neuroblastoma cells against oxidative stress damage via nerve growth factor production. *European Journal of Pharmacology* 519(1-2)**,** 9-15. doi: 10.1016/j.ejphar.2005.06.026.

Taylor, D.R., Parkin, E.T., Cocklin, S.L., Ault, J.R., Ashcroft, A.E., Turner, A.J., et al. (2009). Role of ADAMs in the Ectodomain Shedding and Conformational Conversion of the Prion Protein. *Journal of Biological Chemistry* 284(34)**,** 22590-22600. doi: 10.1074/jbc.M109.032599.

Thermo Fisher Scientific ([n.d.]-a). *OptiMEM I Reduced Serum Medium* [Online]. Available: https://www.thermofisher.com/order/catalog/product/31985070 [Accessed 13/06/2016].

Thermo Fisher Scientific ([n.d.]-b). *Silencer® Negative Control No. 1 siRNA* [Online]. Available: https://www.thermofisher.com/order/catalog/product/AM4636 [Accessed 10/03/2016].

Thermo Fisher Scientific ([n.d.]-c). *Technical Resources: N-2 Supplement (100X) liquid* [Online]. Available: http://www.thermofisher.com/uk/en/home/technical-resources/media-formulation.166.html [Accessed 19/09/2015].

Tobler, I., Deboer, T., and Fischer, M. (1997). Sleep and sleep regulation in normal and prion protein-deficient mice. *Journal of Neuroscience* 17(5)**,** 1869-1879.

Tobler, I., Gaus, S.E., Deboer, T., Achermann, P., Fischer, M., Rulicke, T., et al. (1996). Altered circadian activity rhythms and sleep in mice devoid of prion protein. *Nature* 380(6575)**,** 639-642. doi: 10.1038/380639a0.

Tojkander, S., Gateva, G., and Lappalainen, P. (2012). Actin stress fibers - assembly, dynamics and biological roles. *Journal of Cell Science* 125(8)**,** 1855-1864. doi: 10.1242/jcs.098087.

Tremblay, P., Bouzamondo-Bernstein, E., Heinrich, C., Prusiner, S.B., and DeArmond, S.J. (2007). Developmental expression of PrP in the post-implantation embryo. *Brain Research* 1139**,** 60-67. doi: 10.1016/j.brainres.2006.12.055.

Tripathi, A.K., Haldar, S., Qian, J., Beserra, A., Suda, S., Singh, A., et al. (2015). Prion protein functions as a ferrireductase partner for ZIP14 and DMT1. *Free Radical Biology and Medicine* 84**,** 322-330. doi: 10.1016/j.freeradbiomed.2015.03.037.

Troller, U., and Larsson, C. (2006). Cdc42 is involved in PKC epsilon- and delta-induced neurite outgrowth and stress fibre dismantling. *Biochemical and Biophysical Research Communications* 349(1)**,** 91-98. doi: 10.1016/j.bbrc.2006.07.200.

Tsutsui, S., Hahn, J.N., Johnson, T.A., Ali, Z., and Jirik, F.R. (2008). Absence of the cellular prion protein exacerbates and prolongs neuroinflammation in experimental autoimmune encephalomyelitis. *American Journal of Pathology* 173(4)**,** 1029-1041. doi: 10.2353/ajpath.2008.071062.

Uchiyama, K., and Sakaguchi, S. (2016). Sorting of prion protein and PrPSc accumulation. *Prion* 10**,** S124-S125.

Ugalde, C.L., Finkelstein, D.I., Lawson, V.A., and Hill, A.F. (2016). Pathogenic mechanisms of prion protein, amyloid-beta and alpha-synuclein misfolding: the prion concept and neurotoxicity of protein oligomers. *Journal of Neurochemistry* 139(2)**,** 162-180. doi: 10.1111/jnc.13772.

Urdiales, J.L., Becker, E., Andrieu, M., Thomas, A., Jullien, J., van Grunsven, L.A., et al. (1998). Cell cycle phase-specific surface expression of nerve growth factor receptors TrkA and p75(NTR). *Journal of Neuroscience* 18(17)**,** 6767-6775.

Van Kolen, K., Bruinzeel, W., He, W., De Kimpe, N., Van Puyvelde, L., Cik, M., et al. (2013). Investigation of signalling cascades induced by neurotrophic synaptolepis factor K7 reveals a

critical role for novel PKC epsilon. *European Journal of Pharmacology* 701(1-3)**,** 73-81. doi: 10.1016/j.ejphar.2013.01.004.

Varki, A., and Lowe, J.B. (2009). "Biological Roles of Glycans", in: *Essentials of Glycobiology*. (eds.) A. Varki, R. Cummings, J.D. Esko, H.H. Freeze, P. Stanley, C.R. Bertozzi, G.W. Hart & M.E. Etzler. 2nd ed. (Cold Spring Harbor (NY): Cold Spring Harbor Laboratory Press).

Vassallo, N., Herms, J., Behrens, C., Krebs, B., Saeki, K., Onodera, T., et al. (2005). Activation of phosphatidylinositol in 3-kinase by cellular prion protein and its role cell survival. *Biochemical and Biophysical Research Communications* 332(1)**,** 75-82. doi: 10.1016/j.bbrc.2005.04.099.

Verbeke, S., Tomellini, E., Dhamani, F., Meignan, S., Adriaenssens, E., and Xuefen, L. (2013). Extracellular cleavage of the p75 neurotrophin receptor is implicated in its pro-survival effect in breast cancer cells. *Febs Letters* 587(16)**,** 2591-2596. doi: 10.1016/j.febslet.2013.06.039.

Vergara, C., Ordonez-Gutierrez, L., Wandosell, F., Ferrer, I., del Rio, J.A., and Gavin, R. (2015). Role of PrPC Expression in Tau Protein Levels and Phosphorylation in Alzheimer's Disease Evolution. *Molecular Neurobiology* 51(3)**,** 1206-1220. doi: 10.1007/s12035-014-8793-7.

Vey, M., Pilkuhn, S., Wille, H., Nixon, R., Dearmond, S.J., Smart, E.J., et al. (1996). Subcellular colocalization of the cellular and scrapie prion proteins in caveolae-like membranous domains. *Proceedings of the National Academy of Sciences of the United States of America* 93(25)**,** 14945-14949. doi: 10.1073/pnas.93.25.14945.

Vincent, B., Paitel, E., Frobert, Y., Lehmann, S., Grassi, J., and Checler, F. (2000). Phorbol ester-regulated cleavage of normal prion protein in HEK293 human cells and murine neurons. *Journal of Biological Chemistry* 275(45)**,** 35612-35616. doi: 10.1074/jbc.M004628200.

Vincent, B., Paitel, E., Saftig, P., Frobert, Y., Hartmann, D., De Strooper, B., et al. (2001). The disintegrins ADAM10 and TACE contribute to the constitutive and phorbol ester-regulated normal cleavage of the cellular prion protein. *Journal of Biological Chemistry* 276(41)**,** 37743-37746. doi: 10.1074/jbc.M105677200.

Vincent, B., Sunyach, C., Orzechowski, H.D., St George-Hyslop, P., and Checler, F. (2009). p53-Dependent Transcriptional Control of Cellular Prion by Presenilins. *Journal of Neuroscience* 29(20)**,** 6752-6760. doi: 10.1523/jneurosci.0789-09.2009.

Walmsley, A.R., Watt, N.T., Taylor, D.R., Perera, W.S.S., and Hooper, N.M. (2009). alpha-cleavage of the prion protein occurs in a late compartment of the secretory pathway and is independent of lipid rafts. *Molecular and Cellular Neuroscience* 40(2)**,** 242-248. doi: 10.1016/j.mcn.2008.10.012.

Wang, X., Dong, C.F., Shi, Q., Shi, S., Wang, G.R., Lei, Y.J., et al. (2009). Cytosolic prion protein induces apoptosis in human neuronal cell SH-SY5Y via mitochondrial disruption pathway. *Bmb Reports* 42(7)**,** 444-449.

Watson, F.L., Porcionatto, M.A., Bhattacharyya, A., Stiles, C.D., and Segal, R.A. (1999). TrkA glycosylation regulates receptor localization and activity. *Journal of Neurobiology* 39(2)**,** 323-336. doi: 10.1002/(sici)1097-4695(199905)39:2<323::aid-neu15>3.0.co;2-4.

Watt, N.T., Routledge, M.N., Wild, C.P., and Hooper, N.M. (2007). Cellular prion protein protects against reactive-oxygen-species-induced DNA damage. *Free Radical Biology and Medicine* 43(6)**,** 959-967. doi: 10.1016/j.freeradbiomed.2007.06.004.

Watt, N.T., Taylor, D.R., Gillott, A., Thomas, D.A., Perera, W.S.S., and Hooper, N.M. (2005). Reactive oxygen species-mediated beta-cleavage of the prion protein in the cellular response to oxidative stress. *Journal of Biological Chemistry* 280(43)**,** 35914-35921. doi: 10.1074/jbc.M507327200.

Watts, J.C., Drisaldi, B., Ng, V., Yang, J., Strome, B., Horne, P., et al. (2007). The CNS glycoprotein Shadoo has PrPC-like protective properties and displays reduced levels in prion infections. *Embo Journal* 26(17)**,** 4038-4050. doi: 10.1038/sj.emboj.7601830.

Weiss, E., Ramljak, S., Asif, A.R., Ciesielczyk, B., Schmitz, M., Gawinecka, J., et al. (2010). CELLULAR PRION PROTEIN OVEREXPRESSION DISTURBS CELLULAR HOMEOSTASIS IN SH-SY5Y NEUROBLASTOMA CELLS BUT DOES NOT ALTER p53 EXPRESSION: A PROTEOMIC STUDY. *Neuroscience* 169(4)**,** 1640-1650. doi: 10.1016/j.neuroscience.2010.06.013.

Weskamp, G., Schlondorff, J., Lum, L., Becherer, J.D., Kim, T.W., Saftig, P., et al. (2004). Evidence for a critical role of the tumor necrosis factor alpha convertase (TACE) in ectodomain shedding of the p75 neurotrophin receptor (p75(NTR)). *Journal of Biological Chemistry* 279(6)**,** 4241-4249. doi: 10.1074/jbc.M307974200.

Whitehead, K.A., Dahlman, J.E., Langer, R.S., and Anderson, D.G. (2011). "Silencing or Stimulation? siRNA Delivery and the Immune System," in *Annual Review of Chemical and Biomolecular Engineering, Vol 2*, ed. J.M. Prausnitz.), 77-96.

Whitehouse, I.J., Jackson, C., Turner, A.J., and Hooper, N.M. (2010). Prion Protein is Reduced in Aging and in Sporadic but not in Familial Alzheimer's Disease. *Journal of Alzheimers Disease* 22(3)**,** 1023-1031. doi: 10.3233/jad-2010-101071.

Whitehouse, I.J., Miners, J.S., Glennon, E.B.C., Kehoe, P.G., Love, S., Kellett, K.A.B., et al. (2013). Prion Protein Is Decreased in Alzheimer's Brain and Inversely Correlates with BACE1 Activity, Amyloid-beta Levels and Braak Stage. *Plos One* 8(4). doi: 10.1371/journal.pone.0059554.

Wik, L., Klingeborn, M., Willander, H., and Linne, T. (2012). Separate mechanisms act concurrently to shed and release the prion protein from the cell. *Prion* 6(5)**,** 498-509. doi: 10.4161/pri.22588.

Will, R.G., Ironside, J.W., Zeidler, M., Cousens, S.N., Estibeiro, K., Alperovitch, A., et al. (1996). A new variant of Creutzfeldt-Jakob disease in the UK. *Lancet* 347(9006)**,** 921-925. doi: 10.1016/s0140-6736(96)91412-9.

Williams, W.M., Stadtman, E.R., and Moskovitz, J. (2004). Ageing and exposure to oxidative stress in vivo differentially affect cellular levels of PrPc in mouse cerebral microvessels and brain parenchyma. *Neuropathology and Applied Neurobiology* 30(2)**,** 161-168. doi: 10.1111/j.1365-2990.2004.00523.x.

Willnow, T.E., Petersen, C.M., and Nykjaer, A. (2008). VPS10P-domain receptors - regulators of neuronal viability and function. *Nature Reviews Neuroscience* 9(12)**,** 899-909. doi: 10.1038/nrn2516.

Witusik, M., Gresner, S.M., Hulas-Bigoszewska, K., Krynska, B., Azizi, S.A., Liberski, P.P., et al. (2007). Neuronal and astrocytic cells, obtained after differentiation of human neural GFAP-positive progenitors, present heterogeneous expression of PrPc. *Brain Research* 1186**,** 65-73. doi: 10.1016/j.brainres.2007.10.039.

Wortzel, I., and Seger, R. (2011). The ERK Cascade: Distinct Functions within Various Subcellular Organelles. *Genes & Cancer* 2(3)**,** 195-209.

Wu, C.L., Jin, X.F., Tsueng, G., Afrasiabi, C., and Su, A.I. (2016). BioGPS: building your own mash-up of gene annotations and expression profiles. *Nucleic Acids Research* 44(D1)**,** D313-D316. doi: 10.1093/nar/gkv1104.

Wu, G., Nakajima, K., Takeyama, N., Yukawa, M., Taniuchi, Y., Sakudo, A., et al. (2008). Species-specific anti-apoptotic activity of cellular prion protein in a mouse PrP-deficient neuronal cell line transfected with mouse, hamster, and bovine Prnp. *Neuroscience Letters* 446(1)**,** 11-15. doi: 10.1016/j.neulet.2008.09.020.

Xicoy, H., Wieringa, B., and Martens, G.J.M. (2017). The SH-SY5Y cell line in Parkinson's disease research: a systematic review. *Molecular Neurodegeneration* 12. doi: 10.1186/s13024-017-0149-0.

Yokoyama, T., Kimura, K.M., Ushiki, Y., Yamada, S., Morooka, A., Nakashiba, T., et al. (2001). In vivo conversion of cellular prion protein to pathogenic isoforms, as monitored by conformation-specific antibodies. *Journal of Biological Chemistry* 276(14)**,** 11265-11271. doi: 10.1074/jbc.M008734200.

Yoon, J.C., Puigserver, P., Chen, G.X., Donovan, J., Wu, Z.D., Rhee, J., et al. (2001). Control of hepatic gluconeogenesis through the transcriptional coactivator PGC-1. *Nature* 413(6852)**,** 131-138. doi: 10.1038/35093050.

Yu, O.M., and Brown, J.H. (2015). G Protein-Coupled Receptor and RhoA-Stimulated Transcriptional Responses: Links to Inflammation, Differentiation, and Cell Proliferation. *Molecular Pharmacology* 88(1)**,** 171-180. doi: 10.1124/mol.115.097857.

Yusuf, M., Leung, K., Morris, K.J., and Volpi, E.V. (2013). Comprehensive cytogenomic profile of the in vitro neuronal model SH-SY5Y. *Neurogenetics* 14(1)**,** 63-70. doi: 10.1007/s10048-012-0350-9.

Zafar, S., Asif, A.R., Ramljak, S., Tahir, W., Schmitz, M., and Zerr, I. (2014). Anchorless 23-230 PrPC Interactomics for Elucidation of PrPC Protective Role. *Molecular Neurobiology* 49(3)**,** 1385-1399. doi: 10.1007/s12035-013-8616-2.

Zampieri, N., Xu, C.F., Neubert, T.A., and Chao, M.V. (2005). Cleavage of p75 neurotrophin receptor by alpha-secretase and gamma-secretase requires specific receptor domains. *Journal of Biological Chemistry* 280(15)**,** 14563-14571. doi: 10.1074/jbc.M412957200.

Zanetti, F., Carpi, A., Menabo, R., Giorgio, M., Schulz, R., Valen, G., et al. (2014). The cellular prion protein counteracts cardiac oxidative stress. *Cardiovascular Research* 104(1)**,** 93-102. doi: 10.1093/cvr/cvu194.

Zawlik, I., Witusik, M., Hulas-Bigoszewska, K., Piaskowski, S., Szybka, M., Golanska, E., et al. (2006). Regulation of PrPc expression: Nerve growth factor (NGF) activates the prion gene promoter through the MEK1 pathway in PC12 cells. *Neuroscience Letters* 400(1-2)**,** 58-62. doi: 10.1016/j.neulet.2006.02.021.

Zeng, F.N., Watt, N.T., Walmsley, A.R., and Hooper, N.M. (2003). Tethering the N-terminus of the prion protein compromises the cellular response to oxidative stress. *Journal of Neurochemistry* 84(3)**,** 480-490. doi: 10.1046/j.1471-4159.2003.01529.x.

Zhang, L., Karsten, P., Hamm, S., Pogson, J.H., Mueller-Rischart, A.K., Exner, N., et al. (2013). TRAP1 rescues PINK1 loss-of-function phenotypes. *Human Molecular Genetics* 22(14)**,** 2829-2841. doi: 10.1093/hmg/ddt132.

Zhang, X.D., Gillespie, S.K., and Hersey, P. (2004). Staurosporine induces apoptosis of melanoma by both caspase-dependent and -independent apoptotic pathways. *Molecular Cancer Therapeutics* 3(2)**,** 187-197.

Zhang, Y.W., Kaneda, M., and Morita, I. (2003). The gap junction-independent tumor-suppressing effect of connexin 43. *Journal of Biological Chemistry* 278(45)**,** 44852-44856. doi: 10.1074/jbc.M305072200.

Zhou, J., Zhou, T.Y., Cao, R., Liu, Z., Shen, J.Y., Chen, P., et al. (2006). Evaluation of the application of sodium deoxycholate to proteomic analysis of rat hippocampal plasma membrane. *Journal of Proteome Research* 5(10)**,** 2547-2553. doi: 10.1021/pr060112a.

Appendices

Appendix I: Primary antibodies

Target protein	Company & catalogue no.	Dilution factor/concentration
phospho-Akt (Ser473)	CST #4060	1:2000 to 1:4000
Akt (pan)	CST #2920	1:2000 to 1:4000
Annexin A2	CST #8235	1:2000
ATP synthase subunit alpha, mitochondrial	Sigma #SAB4502040	1:1000
E3 ubiquitin-protein ligase BRE1A	CST #11974	1:2000
Caldesmon	CST #12503	1:2000
Connexin-43	CST #3512	1:1000 to 1:2000
Eukaryotic translation initiation factor 1	CST #12496	1:2000
phospho-ERK1/2 (Thr202/Tyr204 for ERK1 and Thr185/Tyr187 for ERK2)	CST #4370	1:2000 to 1:4000
ERK1/2	CST #9107	1:2000 to 1:4000
FASN	CST #3180	1:1000
Glutamate dehydrogenase 1, mitochondrial	AVIVA #ARP45709	1:1000 to 1:2000
GLUT4	CST #2213	1:1000
Microsomal glutathione S-transferase 3	AVIVA #ARP60342	1:2000
Myotubularin	AVIVA #ARP56078	1:2000
$p75^{NTR}$	N/A[16]	1:2000 to 1:5000
$p75^{NTR}$	Millipore #07-046	1:4000
Pantothenate kinase 2, mitochondrial	AVIVA #ARP43984	1:2000
PCK1	CST #12940	1:2000
Proliferation cell nuclear antigen	CST #13110	1:2000
Peroxiredoxin-1	AVIVA #ARP48454	1:2000
Peroxiredoxin-6	AVIVA #ARP48267	1:1000
Protein kinase C alpha type	CST #2056	1:2000
PrP^{C}	N/A[17]	0.15-0.2 µg/ml
PrP^{C}	Thermo #7500996	1:1000 (IF)
Neuromodulin	CST #5307	1:1000
Ribonucleoside-diphosphate reductase large subunit	CST #8637	1:2000
Solute carrier family 25 member 36	AVIVA #ARP43984	1:4000
Sortilin	Proteintech #12369-1-AP	1:1000
SRSF protein kinase 2	AVIVA #ARP61851	1:2000
phospho-TrkA (Tyr785) /phospho-TrkB (Tyr816)	CST #4168	1:1000

[16] This anti-$p75^{NTR}$ antibody (9992 antiserum), originally developed in the lab of Prof. Moses V. Chao from New York University, was a gift from Dr Andrea Caporali of the University of Edinburgh.
[17] This anti-PrP^{C} antibody, known as BC6, was developed in house, as described by McCutcheon et al. (2014).

Target protein	Company & catalogue no.	Dilution factor/concentration
TrkA	CST #2505	1:1000
TrkB	CST #4603	1:1000
Ubiquitin	Millipore #MAB1510	1:1600
Voltage-dependent anion-selective channel protein 2	AVIVA #ARP35124	1:2000 to 1:4000
Vimentin	CST #5741	1:2000 or 1:100 (IF)
Neurosecretory protein VGF	Abcam #ab74140	1:1000
Zyxin	CST #3553	1:2000

Supplementary Table 1 – Primary antibodies used for western blotting and immunofluorescence

Antibodies were used for western blotting except for those marked with (IF); these were used for immunofluorescence. Company abbreviations are as follows: AVIVA Systems Biology (AVIVA), Cell Signalling Technology (CST), Sigma-Aldrich (Sigma) and Thermo Fisher Scientific (Thermo).

Appendix II: Datasets from proteomic experiments

Uniprot ID	Protein	Mean FC	Uniprot ID	Protein	Mean FC
Q9Y371	Endophilin-B1	+3.66	O15240	Neurosecretory protein VGF	+2.46
P07355	Annexin A2	+3.50	Q14315	Filamin-C	+2.46
P17677	Neuromodulin	+3.48	P60660	Myosin light polypeptide 6	+2.41
P22570	NADPH:adrenodoxin oxidoreductase, mitochondrial	+3.36	Q8NBJ7	Sulfatase-modifying factor 2	+2.41
P31949	Protein S100-A11	+3.36	P10643	Complement component C7	+2.40
O75369	Filamin-B	+3.31	P09493	Tropomyosin alpha-1 chain	+2.36
P35579	Myosin-9	+3.25	J3KMY5	Epididymal secretory protein E1	+2.35
E7EPJ7	Triple functional domain protein	+3.23	P50552	Vasodilator-stimulated phosphoprotein	+2.34
P18206	Vinculin	+2.91	P05556	Integrin beta-1	+2.33
F8WAD8	Disintegrin and metalloproteinase domain-containing protein 22	+2.87	H7C3P4	N-acetylglucosamine-6-sulfatase	+2.30
Q09666	Neuroblast differentiation-associated protein AHNAK	+2.82	Q05682	Caldesmon	+2.29
P09525	Annexin A4	+2.81	Q2M2I8	AP2-associated protein kinase 1	+2.28
Q9UDY2	Tight junction protein ZO-2	+2.80	P13797	Plastin-3	+2.26
Q9UDT6	CAP-Gly domain-containing linker protein 2	+2.77	P02545	Prelamin-A/C	+2.26
Q99439	Calponin-2	+2.75	K7EKL3	Paragranulin	+2.23
Q9GZT9	Egl nine homolog 1	+2.63	P07858	Cathepsin B	+2.17
Q9C0C2	182 kDa tankyrase-1-binding protein	+2.63	P09382	Galectin-1	+2.15
Q9NR12	PDZ and LIM domain protein 7	+2.60	Q9NR46	Endophilin-B2	+2.13
O95302	Peptidyl-prolyl cis-trans isomerase FKBP9	+2.54	Q5T123	SH3 domain-binding glutamic acid-rich-like protein 3	+2.13
Q53GG5	PDZ and LIM domain protein 3	+2.50	G3V4F2	Acyl-coenzyme A thioesterase 1	+2.11

Supplementary table 2 – List of proteins differentially expressed in clone 1G3 compared with untransfected SH-SY5Y cells

Table continues on the following pages – legend displayed on the final page of the table.

Uniprot ID	Protein	Mean FC
Q96HC4	PDZ and LIM domain protein 5	+2.06
P08574	Cytochrome c1, heme protein, mitochondrial	+2.05
P14923	Junction plakoglobin	+2.05
Q53FA7	Quinone oxidoreductase PIG3	+2.05
Q9UBG0	C-type mannose receptor 2	+2.04
P11216	Glycogen phosphorylase, brain form	+2.04
E7EPV7	Alpha-synuclein	+2.04
H3BPK3	Hydroxyacylglutathione hydrolase, mitochondrial	+2.03
P21333	Filamin-A	+2.00
Q8WX93	Palladin	+2.00
Q07065	Cytoskeleton-associated protein 4	+1.99
Q08257	Quinone oxidoreductase	+1.98
O15143	Actin-related protein 2/3 complex subunit 1B	+1.98
Q14847	LIM and SH3 domain protein 1	+1.96
P22695	Cytochrome b-c1 complex subunit 2, mitochondrial	+1.96
Q15149	Plectin	+1.94
P49748	Very long-chain specific acyl-CoA dehydrogenase, mitochondrial	+1.92
Q9BWM7	Sideroflexin-3	+1.91
O95490	Latrophilin-2	+1.91
P55263	Adenosine kinase	+1.90
P17252	Protein kinase C alpha type	+1.89
O43707	Alpha-actinin-4	+1.89
Q32P28	Prolyl 3-hydroxylase 1	+1.88
O95865	N(G),N(G)-dimethylarginine dimethylaminohydrolase 2	+1.88
Q96AC1	Fermitin family homolog 2	+1.87
A0A087WT27	Phosphoacetylglucosamine mutase	+1.86
Q9P2E9	Ribosome-binding protein 1	+1.86
Q6VY07	Phosphofurin acidic cluster sorting protein 1	+1.85
P12814	Alpha-actinin-1	+1.83
P20810	Calpastatin	+1.82
S4R3Q6	Vacuolar protein sorting-associated protein 26A	+1.80
O43852	Calumenin	+1.79
P42574	Caspase-3	+1.77
Q8N8S7	Protein enabled homolog	+1.77
Q9Y2H6	Fibronectin type-III domain-containing protein 3A	+1.77
Q14195	Dihydropyrimidinase-related protein 3	+1.76
P48681	Nestin	+1.75
Q9NPH2	Inositol-3-phosphate synthase 1	+1.74
Q9BR76	Coronin-1B	+1.74
Q14195-2	Isoform LCRMP-4 of Dihydropyrimidinase-related protein 3	+1.73
F8VQX6	Methyltransferase-like protein 7A	+1.71
P50454	Serpin H1	+1.70
P37802	Transgelin-2	+1.69
A1X283	SH3 and PX domain-containing protein 2B	+1.69

Supplementary table 2 – List of proteins differentially expressed in clone 1G3 compared with untransfected SH-SY5Y cells

Table continues on the following pages – legend displayed on the final page of the table.

Uniprot ID	Protein	Mean FC
P10253	Lysosomal alpha-glucosidase	+1.69
Q96AB3	Isochorismatase domain-containing protein 2, mitochondrial	+1.69
P35580	Myosin-10	+1.68
Q16527	Cysteine and glycine-rich protein 2	+1.67
Q13740	CD166 antigen	+1.67
Q8NBJ5	Procollagen galactosyltransferase 1	+1.66
P31930	Cytochrome b-c1 complex subunit 1, mitochondrial	+1.66
P04899	Guanine nucleotide-binding protein G(i) subunit alpha-2	+1.66
Q9UH99	SUN domain-containing protein 2	+1.65
P08758	Annexin A5	+1.63
Q32MZ4	Leucine-rich repeat flightless-interacting protein 1	+1.63
Q92626	Peroxidasin homolog	+1.63
P68133	Actin, alpha skeletal muscle	+1.63
P13489	Ribonuclease inhibitor	+1.63
P67936	Tropomyosin alpha-4 chain	+1.62
O60664	Perilipin-3	+1.61
P50416	Carnitine O-palmitoyltransferase 1, liver isoform	+1.60
Q13045	Protein flightless-1 homolog	+1.60
P52292	Importin subunit alpha-1	-2.47
Q92598	Heat shock protein 105 kDa	-2.38

Uniprot ID	Protein	Mean FC
Q12765	Secernin-1	+1.56
O75083	WD repeat-containing protein 1	+1.56
P46940	Ras GTPase-activating-like protein IQGAP1	+1.55
Q9UMS6	Synaptopodin-2	+1.55
Q8NBS9	Thioredoxin domain-containing protein 5	+1.55
P36957	Dihydrolipoyllysine-residue succinyltransferase component of 2-oxoglutarate dehydrogenase complex, mitochondrial	+1.53
Q07812	Apoptosis regulator BAX	+1.53
O00159	Unconventional myosin-Ic	+1.52
Q9UNZ2	NSFL1 cofactor p47	+1.50
P30101	Protein disulfide-isomerase A3	+1.50
Q15417	Calponin-3	+1.50
O60701	UDP-glucose 6-dehydrogenase	+1.48
Q9Y696	Chloride intracellular channel protein 4	+1.48
O60568	Procollagen-lysine,2-oxoglutarate 5-dioxygenase 3	+1.47
Q6ZNB6	NF-X1-type zinc finger protein NFXL1	+1.47
F5GX14	Malectin	+1.44
P27816	Microtubule-associated protein 4	+1.40
A0A087WV66	Antigen KI-67	-2.35
Q9BZE4	Nucleolar GTP-binding protein 1	-2.35

Supplementary table 2 – List of proteins differentially expressed in clone 1G3 compared with untransfected SH-SY5Y cells

Table continues on the following pages – legend displayed on the final page of the table.

Uniprot ID	Protein	Mean FC	Uniprot ID	Protein	Mean FC
P30405	Peptidyl-prolyl cis-trans isomerase F, mitochondrial	-2.35	P31350	Ribonucleoside-diphosphate reductase subunit M2	-2.00
Q9BVP2	Guanine nucleotide-binding protein-like 3	-2.33	P63092	Guanine nucleotide-binding protein G(s) subunit alpha isoforms short	-2.00
Q14676	Mediator of DNA damage checkpoint protein 1	-2.33	E9PDE8	Heat shock 70 kDa protein 4L	-1.98
O43719	HIV Tat-specific factor 1	-2.33	O75717	WD repeat and HMG-box DNA-binding protein 1	-1.98
A0A087WW59	Uncharacterized protein C11orf96	-2.30	Q9HB71	Calcyclin-binding protein	-1.98
P09622	Dihydrolipoyl dehydrogenase, mitochondrial	-2.22	P33991	DNA replication licensing factor MCM4	-1.96
P23921	Ribonucleoside-diphosphate reductase large subunit	-2.20	Q14978	Nucleolar and coiled-body phosphoprotein 1	-1.96
P49736	DNA replication licensing factor MCM2	-2.17	Q9BRT6	Protein LLP homolog	-1.96
P33993	DNA replication licensing factor MCM7	-2.17	O75223	Gamma-glutamylcyclotransferase	-1.96
O95239	Chromosome-associated kinesin KIF4A	-2.15	Q9UJA5	tRNA (adenine(58)-N(1))-methyltransferase non-catalytic subunit TRM6	-1.96
O43795	Unconventional myosin-Ib	-2.15	P18754	Regulator of chromosome condensation	-1.96
Q02790	Peptidyl-prolyl cis-trans isomerase FKBP4	-2.13	Q01469	Fatty acid-binding protein, epidermal	-1.96
Q03701	CCAAT/enhancer-binding protein zeta	-2.13	P11388	DNA topoisomerase 2-alpha	-1.94
Q9NW13	RNA-binding protein 28	-2.13	B1AHB1	DNA replication licensing factor MCM5	-1.94
P12004	Proliferating cell nuclear antigen	-2.08	H0Y4R1	Inosine-5'-monophosphate dehydrogenase 2	-1.94
P25205	DNA replication licensing factor MCM3	-2.08	I3L1L3	Myb-binding protein 1A	-1.94
P08243	Asparagine synthetase [glutamine-hydrolyzing]	-2.06	Q08752	Peptidyl-prolyl cis-trans isomerase D	-1.94
Q99615	DnaJ homolog subfamily C member 7	-2.04	Q9H0A0	N-acetyltransferase 10	-1.94
O00566	U3 small nucleolar ribonucleoprotein protein MPP10	-2.04	Q16537	Serine/threonine-protein phosphatase 2A 56 kDa regulatory subunit epsilon isoform	-1.94
Q9Y5J1	U3 small nucleolar RNA-associated protein 18 homolog	-2.02	Q14566	DNA replication licensing factor MCM6	-1.92

Supplementary table 2 – List of proteins differentially expressed in clone 1G3 compared with untransfected SH-SY5Y cells

Table continues on the following pages – legend displayed on the final page of the table.

Uniprot ID	Protein	Mean FC	Uniprot ID	Protein	Mean FC
A0A087WV73	Probable 28S rRNA (cytosine(4447)-C(5))-methyltransferase	-1.90	P22234	Multifunctional protein ADE2	-1.80
Q9Y4C2	Protein FAM115A	-1.90	Q13283	Ras GTPase-activating protein-binding protein 1	-1.79
P06744	Glucose-6-phosphate isomerase	-1.90	O75152	Zinc finger CCCH domain-containing protein 11A	-1.79
P11171	Protein 4.1	-1.90	Q9NQZ2	Something about silencing protein 10	-1.79
Q5JRC6	PHD finger protein 6	-1.89	Q09028	Histone-binding protein RBBP4	-1.79
Q9NR30	Nucleolar RNA helicase 2	-1.87	P17844	Probable ATP-dependent RNA helicase DDX5	-1.79
Q13310	Polyadenylate-binding protein 4	-1.87	M0R0P1	rRNA 2'-O-methyltransferase fibrillarin	-1.77
J3KQN4	60S ribosomal protein L36a	-1.87	C9J4W5	Eukaryotic translation initiation factor 5A-2	-1.77
K7EQA1	Programmed cell death protein 5	-1.87	P12277	Creatine kinase B-type	-1.77
P06493	Cyclin-dependent kinase 1	-1.87	B7Z6D5	Probable ATP-dependent RNA helicase DDX27	-1.75
Q9H4L7	SWI/SNF-related matrix-associated actin-dependent regulator of chromatin subfamily A containing DEAD/H box 1	-1.87	P15121	Aldose reductase	-1.75
P24752	Acetyl-CoA acetyltransferase, mitochondrial	-1.87	Q9Y262	Eukaryotic translation initiation factor 3 subunit L	-1.75
O95433	Activator of 90 kDa heat shock protein ATPase homolog 1	-1.87	Q86YP4	Transcriptional repressor p66-alpha	-1.75
P31689	DnaJ homolog subfamily A member 1	-1.85	O43396	Thioredoxin-like protein 1	-1.75
Q15181	Inorganic pyrophosphatase	-1.85	O75534	Cold shock domain-containing protein E1	-1.74
K7EM18	Eukaryotic translation initiation factor 1	-1.83	Q8WXI9	Transcriptional repressor p66-beta	-1.74
O76003	Glutaredoxin-3	-1.83	P45973	Chromobox protein homolog 5	-1.74
Q9UHD1	Cysteine and histidine-rich domain-containing protein 1	-1.80	Q8IY81	pre-rRNA processing protein FTSJ3	-1.74
P07196	Neurofilament light polypeptide	-1.80	F5GWX5	Chromodomain-helicase-DNA-binding protein 4	-1.74
E9PD53	Structural maintenance of chromosomes protein	-1.80	Q9UMS4	Pre-mRNA-processing factor 19	-1.74
P78347	General transcription factor II-I	-1.80	Q92769	Histone deacetylase 2	-1.72
J3QSV6	Ribosomal L1 domain-containing protein 1	-1.80	P49915	GMP synthase [glutamine-hydrolyzing]	-1.72

Supplementary table 2 – List of proteins differentially expressed in clone 1G3 compared with untransfected SH-SY5Y cells

Table continues on the following pages – legend displayed on the final page of the table.

Uniprot ID	Protein	Mean FC
P21281	V-type proton ATPase subunit B, brain isoform	-1.72
Q9Y2Z0	Suppressor of G2 allele of SKP1 homolog	-1.71
Q15021	Condensin complex subunit 1	-1.71
Q9UKX7	Nuclear pore complex protein Nup50	-1.71
P98179	Putative RNA-binding protein 3	-1.71
Q06203	Amidophosphoribosyltransferase	-1.71
Q9UQ80	Proliferation-associated protein 2G4	-1.71
Q9BQ39	ATP-dependent RNA helicase DDX50	-1.71
Q5VTR2	E3 ubiquitin-protein ligase BRE1A	-1.69
O00267	Transcription elongation factor SPT5	-1.69
P62495	Eukaryotic peptide chain release factor subunit 1	-1.69
Q6FI81	Anamorsin	-1.69
P26358	DNA (cytosine-5)-methyltransferase 1	-1.69
P38606	V-type proton ATPase catalytic subunit A	-1.69
O95347	Structural maintenance of chromosomes protein 2	-1.68
O14745	Na(+)/H(+) exchange regulatory cofactor NHE-RF1	-1.68
G3V4F7	Signal recognition particle 54 kDa protein	-1.68
Q9UKD2	mRNA turnover protein 4 homolog	-1.68
Q15393	Splicing factor 3B subunit 3	-1.68
M0QXM4	Amino acid transporter	-1.67
Q9UKK9	ADP-sugar pyrophosphatase	-1.67
Q7Z4S6	Kinesin-like protein KIF21A	-1.67
P61081	NEDD8-conjugating enzyme Ubc12	-1.67
K7ERF1	Eukaryotic translation initiation factor 3 subunit K	-1.67
Q7L014	Probable ATP-dependent RNA helicase DDX46	-1.67
Q5VT52	Regulation of nuclear pre-mRNA domain-containing protein 2	-1.67
O00303	Eukaryotic translation initiation factor 3 subunit F	-1.67
O00743	Serine/threonine-protein phosphatase 6 catalytic subunit	-1.65
P60842	Eukaryotic initiation factor 4A-I	-1.65
P39748	Flap endonuclease 1	-1.65
P29144	Tripeptidyl-peptidase 2	-1.65
P49458	Signal recognition particle 9 kDa protein	-1.65
O75643	U5 small nuclear ribonucleoprotein 200 kDa helicase	-1.65
Q9BXJ9	N-alpha-acetyltransferase 15, NatA auxiliary subunit	-1.65
Q53GQ0	Estradiol 17-beta-dehydrogenase 12	-1.65
P33316	Deoxyuridine 5'-triphosphate nucleotidohydrolase, mitochondrial	-1.64
P43246	DNA mismatch repair protein Msh2	-1.64
P43487	Ran-specific GTPase-activating protein	-1.64
Q9HAV0	Guanine nucleotide-binding protein subunit beta-4	-1.64
P30154	Serine/threonine-protein phosphatase 2A 65 kDa regulatory subunit A beta isoform	-1.64
P41227	N-alpha-acetyltransferase 10	-1.64
P22102	Trifunctional purine biosynthetic protein adenosine-3	-1.64

Supplementary table 2 – List of proteins differentially expressed in clone 1G3 compared with untransfected SH-SY5Y cells

Table continues on the following pages – legend displayed on the final page of the table.

Uniprot ID	Protein	Mean FC
P63173	60S ribosomal protein L38	-1.63
Q14684	Ribosomal RNA processing protein 1 homolog B	-1.63
P30520	Adenylosuccinate synthetase isozyme 2	-1.63
O43143	Putative pre-mRNA-splicing factor ATP-dependent RNA helicase DHX15	-1.63
A0A087X1W2	Protein arginine N-methyltransferase 1	-1.63
P24666	Low molecular weight phosphotyrosine protein phosphatase	-1.63
B4DUR8	T-complex protein 1 subunit gamma	-1.61
P40227	T-complex protein 1 subunit zeta	-1.61
P05388	60S acidic ribosomal protein P0	-1.61
O94776	Metastasis-associated protein MTA2	-1.61
O43447	Peptidyl-prolyl cis-trans isomerase H	-1.61
Q9Y3F4	Serine-threonine kinase receptor-associated protein	-1.61
Q29RF7	Sister chromatid cohesion protein PDS5 homolog A	-1.61
Q9UPQ0	LIM and calponin homology domains-containing protein 1	-1.61
Q14690	Protein RRP5 homolog	-1.60
P11940	Polyadenylate-binding protein 1	-1.60
Q9UQE7	Structural maintenance of chromosomes protein 3	-1.60
Q12931	Heat shock protein 75 kDa, mitochondrial	-1.60
P55060	Exportin-2	-1.60
Q13185	Chromobox protein homolog 3	-1.59
P52701	DNA mismatch repair protein Msh6	-1.59

Uniprot ID	Protein	Mean FC
J3KR24	Isoleucine--tRNA ligase, cytoplasmic	-1.59
P48643	T-complex protein 1 subunit epsilon	-1.59
P08107	Heat shock 70 kDa protein 1A/1B	-1.59
Q8NC51	Plasminogen activator inhibitor 1 RNA-binding protein	-1.59
P17987	T-complex protein 1 subunit alpha	-1.59
P08195	4F2 cell-surface antigen heavy chain	-1.59
Q9Y314	Nitric oxide synthase-interacting protein	-1.57
O00410	Importin-5	-1.57
P00338	L-lactate dehydrogenase A chain	-1.57
P38117	Electron transfer flavoprotein subunit beta	-1.57
Q9UN86	Ras GTPase-activating protein-binding protein 2	-1.57
G5E9W3	Cleavage and polyadenylation specific factor 3, 73kDa, isoform CRA_b	-1.56
F5H3U9	Protein mago nashi homolog 2	-1.56
P51532	Transcription activator BRG1	-1.56
P60228	Eukaryotic translation initiation factor 3 subunit E	-1.56
B5MCF9	Pescadillo homolog	-1.56
P55884	Eukaryotic translation initiation factor 3 subunit B	-1.56
Q9H0S4	Probable ATP-dependent RNA helicase DDX47	-1.56
P50991	T-complex protein 1 subunit delta	-1.55
Q96I25	Splicing factor 45	-1.55
P50990	T-complex protein 1 subunit theta	-1.55

Supplementary table 2 – List of proteins differentially expressed in clone 1G3 compared with untransfected SH-SY5Y cells

See following page for legend…

Uniprot ID	Protein	Mean FC
O75400	Pre-mRNA-processing factor 40 homolog A	-1.55
O75821	Eukaryotic translation initiation factor 3 subunit G	-1.55
E9PJD9	60S ribosomal protein L27a	-1.54
Q9H9B1	Histone-lysine N-methyltransferase EHMT1	-1.54
Q14444	Caprin-1	-1.54
A0A087X1S2	Nuclease-sensitive element-binding protein 1	-1.54
P48634	Protein PRRC2A	-1.54
Q9UHV9	Prefoldin subunit 2	-1.53
Q92922	SWI/SNF complex subunit SMARCC1	-1.53
P46778	60S ribosomal protein L21	-1.53
B5MBZ0	Echinoderm microtubule-associated protein-like 4	-1.52
P11586	C-1-tetrahydrofolate synthase, cytoplasmic	-1.52
G8JLG1	Structural maintenance of chromosomes protein 1A	-1.52
Q9BWD1	Acetyl-CoA acetyltransferase, cytosolic	-1.50
Q9Y520	Protein PRRC2C	-1.50
Q9Y266	Nuclear migration protein nudC	-1.50
Q92879	CUGBP Elav-like family member 1	-1.50
Q9BWF3	RNA-binding protein 4	-1.50
O60828	Polyglutamine-binding protein 1	-1.49
Q08945	FACT complex subunit SSRP1	-1.49
P20290	Transcription factor BTF3	-1.49
O95373	Importin-7	-1.49
E9PHA2	Condensin complex subunit 2	-1.48
Q13247	Serine/arginine-rich splicing factor 6	-1.47
Q9Y383	Putative RNA-binding protein Luc7-like 2	-1.46
Q8WWM7	Ataxin-2-like protein	-1.45
P11142	Heat shock cognate 71 kDa protein	-1.44
O43765	Small glutamine-rich tetratricopeptide repeat-containing protein alpha	-1.44
Q14166	Tubulin--tyrosine ligase-like protein 12	-1.44
Q04637	Eukaryotic translation initiation factor 4 gamma 1	-1.44
Q9HAV4	Exportin-5	-1.43

Supplementary table 2 – List of proteins differentially expressed in clone 1G3 compared with untransfected SH-SY5Y cells

The above table shows the proteins from the clone 1G3 vs SH-SY5Y^{Untr} proteomics experiments that were not shown in **Table 4.3** but were still defined as differentially expressed (see **Table 4.3** legend for criteria). For each protein, the mean expression ratio from the two biological replicates was calculated and converted to fold change (FC).

Uniprot ID	Protein	FC	Uniprot ID	Protein	FC
Q9P2K5	Myelin expression factor 2	+1.57	P35610	Sterol O-acyltransferase 1	+1.45
O15240	Neurosecretory protein VGF	+1.56	Q9H1E3	Nuclear ubiquitous casein and cyclin-dependent kinase substrate 1	+1.44
Q92522	Histone H1x	+1.52	Q8N766	ER membrane protein complex subunit 1	+1.44
Q9Y5Q9	General transcription factor 3C polypeptide 3	+1.46	Q12849	G-rich sequence factor 1	+1.43
P13674	Prolyl 4-hydroxylase subunit alpha-1	+1.46	Q969Z0	Protein TBRG4	+1.42
Q9BQ69	O-acetyl-ADP-ribose deacetylase MACROD1	+1.42	Q9Y4F1	FERM, RhoGEF and pleckstrin domain-containing protein 1	+1.32
Q5BKZ1	DBIRD complex subunit ZNF326	+1.42	P21127	Cyclin-dependent kinase 11B	+1.32
Q5URX0	Beta-hexosaminidase subunit beta	+1.40	P49756	RNA-binding protein 25	+1.31
O43719	HIV Tat-specific factor 1	+1.39	P30040	Endoplasmic reticulum resident protein 29	+1.31
H3BND8	Ubiquitin carboxyl-terminal hydrolase	+1.36	P48307	Tissue factor pathway inhibitor 2	+1.31
Q9Y2H6	Fibronectin type-III domain-containing protein 3A	+1.36	P27824	Calnexin	+1.30
P18754	Regulator of chromosome condensation	+1.34	K7ENG2	Splicing factor U2AF 65 kDa subunit	+1.30
O75367	Core histone macro-H2A.1	+1.34	O00116	Alkyldihydroxyacetonephosphate synthase, peroxisomal	+1.30
O14979	Heterogeneous nuclear ribonucleoprotein D-like	+1.33	Q8IZL8	Proline-, glutamic acid- and leucine-rich protein 1	+1.30
Q14011	Cold-inducible RNA-binding protein	+1.32	Q9Y2Q3	Glutathione S-transferase kappa 1	+1.30
H0YLZ1	Eukaryotic translation initiation factor 5	-1.64	P23588	Eukaryotic translation initiation factor 4B	-1.61
A0A024QZX5	Serpin B6	-1.64	P43490	Nicotinamide phosphoribosyltransferase	-1.61
C4P0D6	Disrupted in schizophrenia 1 isoform 49	-1.64	Q5H9R7	Serine/threonine-protein phosphatase 6 regulatory subunit 3	-1.61
Q9UGI8	Testin	-1.61	Q92823	Neuronal cell adhesion molecule	-1.59
P48739	Phosphatidylinositol transfer protein beta isoform	-1.61	Q9HC38	Glyoxalase domain-containing protein 4	-1.59

Supplementary table 3 – List of proteins differentially expressed in untransfected SH-SY5Y cells following staurosporine treatment

Table continues on the following pages – legend displayed on the final page of the table.

Uniprot ID	Protein	FC	Uniprot ID	Protein	FC
Q5T123	SH3 domain-binding glutamic acid-rich-like protein 3	-1.59	Q9HB71	Calcyclin-binding protein	-1.47
O75131	Copine-3	-1.56	Q13642	Four and a half LIM domains protein 1	-1.47
O75368	SH3 domain-binding glutamic acid-rich-like protein	-1.56	P07942	Laminin subunit beta-1	-1.47
P00390	Glutathione reductase, mitochondrial	-1.56	O95394	Phosphoacetylglucosamine mutase	-1.47
P43034	Platelet-activating factor acetylhydrolase IB subunit alpha	-1.54	P35527	Keratin, type I cytoskeletal 9	-1.47
P43487	Ran-specific GTPase-activating protein	-1.54	P10768	S-formylglutathione hydrolase	-1.47
P09417	Dihydropteridine reductase	-1.54	P30086	Phosphatidylethanolamine-binding protein 1	-1.45
Q01581	Hydroxymethylglutaryl-CoA synthase, cytoplasmic	-1.54	P23921	Ribonucleoside-diphosphate reductase large subunit	-1.45
Q5QPQ0	Acyl-protein thioesterase 2	-1.52	Q53GG5	PDZ and LIM domain protein 3	-1.45
P15121	Aldose reductase	-1.52	Q9Y617	Phosphoserine aminotransferase	-1.45
K7EQA1	Programmed cell death protein 5	-1.52	Q92734	Protein TFG	-1.45
Q9UBB4	Ataxin-10	-1.52	A0A087X020	Ribosome maturation protein SBDS	-1.45
Q9UKY7	Protein CDV3 homolog	-1.52	P85037	Forkhead box protein K1	-1.45
Q9HA64	Ketosamine-3-kinase	-1.52	P62937	Peptidyl-prolyl cis-trans isomerase A	-1.43
P36871	Phosphoglucomutase-1	-1.49	P16152	Carbonyl reductase [NADPH] 1	-1.43
P62140	Serine/threonine-protein phosphatase PP1-beta catalytic subunit	-1.49	E7ES10	Calpastatin	-1.43
Q8WVC2	40S ribosomal protein S21	-1.49	P60981	Destrin	-1.43
Q8IYD1	Eukaryotic peptide chain release factor GTP-binding subunit ERF3B	-1.49	B1AH49	Sulfurtransferase	-1.43
Q9NPD8	Ubiquitin-conjugating enzyme E2 T	-1.49	O00161	Synaptosomal-associated protein 23	-1.43
Q96FC7	Phytanoyl-CoA hydroxylase-interacting protein-like	-1.49	O14745	Na(+)/H(+) exchange regulatory cofactor NHE-RF1	-1.43
Q8WZA0	Protein LZIC	-1.49	Q15555	Microtubule-associated protein RP/EB family member 2	-1.43

Supplementary table 3 – List of proteins differentially expressed in untransfected SH-SY5Y cells following staurosporine treatment

Table continues on the following pages – legend displayed on the final page of the table.

Uniprot ID	Protein	FC	Uniprot ID	Protein	FC
P49588	Alanine--tRNA ligase, cytoplasmic	-1.41	Q7L1Q6	Basic leucine zipper and W2 domain-containing protein 1	-1.39
P62495	Eukaryotic peptide chain release factor subunit 1	-1.41	Q08752	Peptidyl-prolyl cis-trans isomerase D	-1.39
Q99536	Synaptic vesicle membrane protein VAT-1 homolog	-1.41	O43264	Centromere/kinetochore protein zw10 homolog	-1.39
Q96HC4	PDZ and LIM domain protein 5	-1.41	O00299	Chloride intracellular channel protein 1	-1.37
P46109	Crk-like protein	-1.41	Q14166	Tubulin--tyrosine ligase-like protein 12	-1.37
P17655	Calpain-2 catalytic subunit	-1.41	Q9UHV9	Prefoldin subunit 2	-1.37
Q9NZZ3	Charged multivesicular body protein 5	-1.41	O94855	Protein transport protein Sec24D	-1.37
Q9Y281	Cofilin-2	-1.41	K7ES11	E2/E3 hybrid ubiquitin-protein ligase UBE2O	-1.37
F5H365	Protein transport protein Sec23A	-1.41	K7EM73	Calpain small subunit 1	-1.37
Q9BRA2	Thioredoxin domain-containing protein 17	-1.41	F8WBF9	Protein NDRG3	-1.37
P08133	Annexin A6	-1.39	P19174	1-phosphatidylinositol 4,5-bisphosphate phosphodiesterase gamma-1	-1.37
Q15056	Eukaryotic translation initiation factor 4H	-1.39	P20339	Ras-related protein Rab-5A	-1.37
Q6YP21	Kynurenine--oxoglutarate transaminase 3	-1.39	P63151	Serine/threonine-protein phosphatase 2A 55 kDa regulatory subunit B alpha isoform	-1.37
P04818	Thymidylate synthase	-1.39	Q99717	Mothers against decapentaplegic homolog 5	-1.37
P63000	Ras-related C3 botulinum toxin substrate 1	-1.39	P07355	Annexin A2	-1.35
P13797	Plastin-3	-1.39	P13489	Ribonuclease inhibitor	-1.35
Q6P2E9	Enhancer of mRNA-decapping protein 4	-1.39	Q01813	ATP-dependent 6-phosphofructokinase, platelet type	-1.35
Q92626	Peroxidasin homolog	-1.39	B8ZZU8	Transcription elongation factor B (SIII), polypeptide 2 (18kDa, elongin B), isoform CRA_b	-1.35
Q9H2J4	Phosducin-like protein 3	-1.39	Q13404	Ubiquitin-conjugating enzyme E2 variant 1	-1.35
P29762	Cellular retinoic acid-binding protein 1	-1.39	P61970	Nuclear transport factor 2	-1.35
A6NKB8	Aminopeptidase B	-1.39	C9J0K6	Sorcin	-1.35

Supplementary table 3 – List of proteins differentially expressed in untransfected SH-SY5Y cells following staurosporine treatment

See following page for legend…

Uniprot ID	Protein	FC	Uniprot ID	Protein	FC
P61586	Transforming protein RhoA	-1.35	Q5T6V5	UPF0553 protein C9orf64	-1.33
P14550	Alcohol dehydrogenase [NADP(+)]	-1.35	Q92556	Engulfment and cell motility protein 1	-1.33
E7EWP2	Triple functional domain protein	-1.35	P30566	Adenylosuccinate lyase	-1.33
P53004	Biliverdin reductase A	-1.35	Q96ME1	F-box/LRR-repeat protein 18	-1.33
C9J470	Condensin complex subunit 2	-1.35	P31150	Rab GDP dissociation inhibitor alpha	-1.32
C9JP16	Cartilage-associated protein	-1.35	P48147	Prolyl endopeptidase	-1.32
P50395	Rab GDP dissociation inhibitor beta	-1.33	O75874	Isocitrate dehydrogenase [NADP] cytoplasmic	-1.32
P37802	Transgelin-2	-1.33	Q9NY33	Dipeptidyl peptidase 3	-1.32
Q01518	Adenylyl cyclase-associated protein 1	-1.33	P60953	Cell division control protein 42 homolog	-1.32
P16949	Stathmin	-1.33	P20290	Transcription factor BTF3	-1.32
Q15181	Inorganic pyrophosphatase	-1.33	P11137	Microtubule-associated protein 2	-1.32
Q96G03	Phosphoglucomutase-2	-1.33	P30405	Peptidyl-prolyl cis-trans isomerase F, mitochondrial	-1.32
B1AK87	Capping protein (Actin filament) muscle Z-line, beta, isoform CRA_a	-1.33	Q96T51	RUN and FYVE domain-containing protein 1	-1.32
P08758	Annexin A5	-1.33	H3BU16	Hematological and neurological-expressed 1-like protein	-1.32
Q9UJU6	Drebrin-like protein	-1.33	Q9BR76	Coronin-1B	-1.32
O95865	N(G),N(G)-dimethylarginine dimethylaminohydrolase 2	-1.33	P11177	Pyruvate dehydrogenase E1 component subunit beta, mitochondrial	-1.32
Q99615	DnaJ homolog subfamily C member 7	-1.33	P49773	Histidine triad nucleotide-binding protein 1	-1.32
Q9GZP4	PITH domain-containing protein 1	-1.33	Q9BTW9	Tubulin-specific chaperone D	-1.32
Q14232	Translation initiation factor eIF-2B subunit alpha	-1.33	Q9UI15	Transgelin-3	-1.32
H0Y2Y8	Zyxin	-1.33			

Supplementary table 3 – List of proteins differentially expressed in untransfected SH-SY5Y cells following staurosporine treatment

The above table shows the proteins that underwent an expression change in SH-SY5Y^{Untr} upon exposure to STS but that are not listed in **Table 4.6** (see **Table 4.6** legend for details of criteria defining differential expression). FC = fold change

Uniprot ID	Protein	FC	Uniprot ID	Protein	FC
O96008	Mitochondrial import receptor subunit TOM40 homolog	+1.40	Q58FF6	Putative heat shock protein HSP 90-beta 4	+1.32
Q9Y4F1	FERM, RhoGEF and pleckstrin domain-containing protein 1	+1.39	Q6I9Y2	THO complex subunit 7 homolog	+1.32
Q86XI2	Condensin-2 complex subunit G2	+1.38	P50454	Serpin H1	+1.31
Q10570	Cleavage and polyadenylation specificity factor subunit 1	+1.37	E7EPB3	60S ribosomal protein L14	+1.31
Q8NFQ8	Torsin-1A-interacting protein 2	+1.36	Q13620	Cullin-4B	+1.31
Q9H6T3	RNA polymerase II-associated protein 3	+1.36	Q9Y6K1	DNA (cytosine-5)-methyltransferase 3A	+1.31
Q9NV70	Exocyst complex component 1	+1.35	Q9Y696	Chloride intracellular channel protein 4	+1.31
O75494	Serine/arginine-rich splicing factor 10	+1.35	P24534	Elongation factor 1-beta	+1.30
Q9BQ69	O-acetyl-ADP-ribose deacetylase MACROD1	+1.34	P07858	Cathepsin B	+1.30
Q9H1E3	Nuclear ubiquitous casein and cyclin-dependent kinase substrate 1	+1.33	B4DE93	NADH dehydrogenase [ubiquinone] flavoprotein 1, mitochondrial	+1.30
Q13724	Mannosyl-oligosaccharide glucosidase	+1.33	O60828	Polyglutamine-binding protein 1	+1.30
P61604	10 kDa heat shock protein, mitochondrial	+1.32	J3KTJ8	60S ribosomal protein L26	+1.30
A0A087WUK2	Heterogeneous nuclear ribonucleoprotein D-like	+1.32	Q6YN16	Hydroxysteroid dehydrogenase-like protein 2	+1.30
Q96FC7	Phytanoyl-CoA hydroxylase-interacting protein-like	-1.54	Q9NTJ3	Structural maintenance of chromosomes protein 4	-1.49
D6RDM7	Ubiquitin-conjugating enzyme E2 K	-1.54	P49006	MARCKS-related protein	-1.49
Q8WXD2	Secretogranin-3	-1.54	Q9NPD8	Ubiquitin-conjugating enzyme E2 T	-1.49
P23381	Tryptophan--tRNA ligase, cytoplasmic	-1.52	P22061	Protein-L-isoaspartate(D-aspartate) O-methyltransferase	-1.49
P48307	Tissue factor pathway inhibitor 2	-1.52	P53004	Biliverdin reductase A	-1.45
C4P0D6	Disrupted in schizophrenia 1 isoform 49	-1.52	Q7Z2K8	G protein-regulated inducer of neurite outgrowth 1	-1.45
Q92626	Peroxidasin homolog	-1.52	F8VQE1	LIM domain and actin-binding protein 1	-1.43

Supplementary table 4 – List of proteins differentially expressed in clone 2E3 following staurosporine treatment

Table continues on the following pages – legend displayed on the final page of the table.

Uniprot ID	Protein	FC	Uniprot ID	Protein	FC
G3V529	ATP-dependent RNA helicase DDX24	-1.43	Q5VTR2	E3 ubiquitin-protein ligase BRE1A	-1.35
P26373	60S ribosomal protein L13	-1.41	Q9BV57	1,2-dihydroxy-3-keto-5-methylthiopentene dioxygenase	-1.35
P11766	Alcohol dehydrogenase class-3	-1.41	P63000	Ras-related C3 botulinum toxin substrate 1	-1.33
P48739	Phosphatidylinositol transfer protein beta isoform	-1.41	P63208	S-phase kinase-associated protein 1	-1.33
P07108	Acyl-CoA-binding protein	-1.41	Q9Y6H1	Coiled-coil-helix-coiled-coil-helix domain-containing protein 2	-1.33
E9PMI6	Methylosome subunit pICln	-1.41	Q07960	Rho GTPase-activating protein 1	-1.33
Q9HC38	Glyoxalase domain-containing protein 4	-1.39	E5RGX5	Stathmin	-1.33
Q96A49	Synapse-associated protein 1	-1.39	K7EQA1	Programmed cell death protein 5	-1.33
P23921	Ribonucleoside-diphosphate reductase large subunit	-1.37	Q92905	COP9 signalosome complex subunit 5	-1.33
K7ES11	E2/E3 hybrid ubiquitin-protein ligase UBE2O	-1.37	A0A096LNN4	Thioredoxin reductase 2, mitochondrial	-1.33
Q9UBG0	C-type mannose receptor 2	-1.37	P14550	Alcohol dehydrogenase [NADP(+)]	-1.33
Q9BRX5	DNA replication complex GINS protein PSF3	-1.37	P49773	Histidine triad nucleotide-binding protein 1	-1.33
Q9H4L7	SWI/SNF-related matrix-associated actin-dependent regulator of chromatin subfamily A containing DEAD/H box 1	-1.37	Q9Y570	Protein phosphatase methylesterase 1	-1.33
P37837	Transaldolase	-1.35	Q9Y3P9	Rab GTPase-activating protein 1	-1.33
P0CW22	40S ribosomal protein S17-like	-1.35	O14745	Na(+)/H(+) exchange regulatory cofactor NHE-RF1	-1.33
P28289	Tropomodulin-1	-1.35	Q9Y237	Peptidyl-prolyl cis-trans isomerase NIMA-interacting 4	-1.33
P30085	UMP-CMP kinase	-1.35	O00161	Synaptosomal-associated protein 23	-1.33
P47813	Eukaryotic translation initiation factor 1A, X-chromosomal	-1.35	P07355	Annexin A2	-1.32
P17655	Calpain-2 catalytic subunit	-1.35	O60271	C-Jun-amino-terminal kinase-interacting protein 4	-1.32
P60983	Glia maturation factor beta	-1.35	Q15056	Eukaryotic translation initiation factor 4H	-1.32

Supplementary table 4 – List of proteins differentially expressed in clone 2E3 following staurosporine treatment

See following page for legend…

Uniprot ID	Protein	FC	Uniprot ID	Protein	FC
P19174	1-phosphatidylinositol 4,5-bisphosphate phosphodiesterase gamma-1	-1.32	Q15819	Ubiquitin-conjugating enzyme E2 variant 2	-1.32
Q9Y4C2	TRPM8 channel-associated factor 1	-1.32	H0Y630	Serine/threonine-protein kinase 24	-1.32
P04264	Keratin, type II cytoskeletal 1	-1.32	P19784	Casein kinase II subunit alpha'	-1.32
Q99436	Proteasome subunit beta type-7	-1.32	C9J931	GTP-binding protein Rheb	-1.32
Q08752	Peptidyl-prolyl cis-trans isomerase D	-1.32	Q3KQU3	MAP7 domain-containing protein 1	-1.32

Supplementary table 4 – List of proteins differentially expressed in clone 2E3 following staurosporine treatment

The above table shows the proteins that underwent an expression change in clone 2E3 upon exposure to STS but that are not listed in **Table 4.7** (see **Table 4.7** legend for details of criteria defining differential expression). FC = fold change

Uniprot ID	Protein	FC	Uniprot ID	Protein	FC
Q9BRR6	ADP-dependent glucokinase	+1.33	A0AVT1	Ubiquitin-like modifier-activating enzyme 6	+1.32
P31937	3-hydroxyisobutyrate dehydrogenase, mitochondrial	+1.32	O75340	Programmed cell death protein 6	+1.31
P48307	Tissue factor pathway inhibitor 2	-1.49	P36507	Dual specificity mitogen-activated protein kinasPe kinase 2	-1.37
E5RJR5	S-phase kinase-associated protein 1	-1.47	Q14738	Serine/threonine-protein phosphatase 2A 56 kDa regulatory subunit delta isoform	-1.37
K7EN45	Peptidyl-prolyl cis-trans isomerase NIMA-interacting 1	-1.47	C9J712	Profilin-2	-1.35
Q99436	Proteasome subunit beta type-7	-1.45	Q13617	Cullin-2	-1.35
Q14789	Golgin subfamily B member 1	-1.45	Q8NBX0	Saccharopine dehydrogenase-like oxidoreductase	-1.35
P10599	Thioredoxin	-1.43	P56381	ATP synthase subunit epsilon, mitochondrial	-1.35
Q99439	Calponin-2	-1.41	Q16658	Fascin	-1.33
F6WQW2	Ran-specific GTPase-activating protein	-1.41	A6NKB8	Aminopeptidase B	-1.33
P31689	DnaJ homolog subfamily A member 1	-1.41	P48739	Phosphatidylinositol transfer protein beta isoform	-1.33
Q9NUQ9	Protein FAM49B	-1.41	O15511	Actin-related protein 2/3 complex subunit 5	-1.33
15104	Glutamine synthetase	-1.41	P25787	Proteasome subunit alpha type-2	-1.33
P49006	MARCKS-related protein	-1.39	R4GMT0	Alpha-centractin	-1.33
P62942	Peptidyl-prolyl cis-trans isomerase FKBP1A	-1.39	B3KQ25	Proteasome activator complex subunit 3	-1.33
P53004	Biliverdin reductase A	-1.39	P31350	Ribonucleoside-diphosphate reductase subunit M2	-1.33
Q9BV57	1,2-dihydroxy-3-keto-5-methylthiopentene dioxygenase	-1.39	P30533	Alpha-2-macroglobulin receptor-associated protein	-1.33
A1X283	SH3 and PX domain-containing protein 2B	-1.37	Q9UBG0	C-type mannose receptor 2	-1.32
Q07954	Prolow-density lipoprotein receptor-related protein 1	-1.37	Q8NBY1	Serine/threonine-protein kinase 26	-1.32
Q9NZU5	LIM and cysteine-rich domains protein 1	-1.37	Q92626	Peroxidasin homolog	-1.32

Supplementary table 5 – List of proteins differentially expressed in clone 1G3 following staurosporine treatment

See following page for legend…

Uniprot ID	Protein	FC	Uniprot ID	Protein	FC
P61019	Ras-related protein Rab-2A	-1.32	Q13564	NEDD8-activating enzyme E1 regulatory subunit	-1.32
P14550	Alcohol dehydrogenase [NADP(+)]	-1.32	Q9Y617	Phosphoserine aminotransferase	-1.32
P60983	Glia maturation factor beta	-1.32			

Supplementary table 5 – List of proteins differentially expressed in clone 1G3 following staurosporine treatment

The above table shows the proteins that underwent an expression change in clone 1G3 upon exposure to STS but that are not listed in **Table 4.8** (see **Table 4.8** legend for details of criteria defining differential expression). FC = fold change

Appendix III: Datasets from coexpression analyses

NCBI ID	Gene symbol	Correlation	NCBI ID	Gene symbol	Correlation	NCBI ID	Gene symbol	Correlation
19122	*prnp*	1.000	72480	*tspyl4*	0.858	218038	*amph*	0.840
224938	*pja2*	0.928	66104	*tceal6*	0.857	66158	*fam127c*	0.838
12876	*cpe*	0.905	26422	*nbea*	0.857	234593	*ndrg4*	0.838
56442	*serinc1*	0.902	18195	*nsf*	0.856	50884	*nckap1*	0.837
219181	*akap11*	0.897	56409	*nudt3*	0.856	14670	*gnl1*	0.837
56736	*rnf14*	0.891	13807	*eno2*	0.856	331532	*tceal5*	0.837
72320	*kif1bp*	0.886	66855	*tcf25*	0.855	59049	*slc22a17*	0.836
22129	*ttc3*	0.884	16579	*kifap3*	0.854	76965	*slitrk1*	0.835
67826	*snap47*	0.878	20616	*snap91*	0.854	26950	*vsnl1*	0.834
19339	*rab3a*	0.875	107767	*scamp1*	0.854	57776	*ttyh1*	0.833
14567	*gdi1*	0.874	104001	*rtn1*	0.853	319504	*nrcam*	0.830
76252	*atp6v0e2*	0.874	70834	*spag9*	0.852	12805	*cntn1*	0.829
18189	*nrxn1*	0.872	14660	*gls*	0.850	108013	*celf4*	0.829
108123	*napg*	0.871	20614	*snap25*	0.846	56462	*mtch1*	0.829
52696	*zwint*	0.870	68095	*ociad1*	0.845	17257	*mecp2*	0.828
18645	*pfn2*	0.870	72661	*serp2*	0.845	11803	*aplp1*	0.828
72685	*dnajc6*	0.869	236794	*slc9a6*	0.844	13429	*dnm1*	0.827
17263	*meg3*	0.867	107528	*magee1*	0.844	226518	*nmnat2*	0.827
20168	*rtn3*	0.861	20910	*stxbp1*	0.843	14758	*gpm6b*	0.827
109169	*igip*	0.861	12315	*calm1*	0.842	224020	*pi4ka*	0.826
77574	*tcaf1*	0.861	234267	*gpm6a*	0.842	18749	*prkacb*	0.825
19084	*prkar1a*	0.859	11820	*app*	0.840	270192	*rab6b*	0.825
26414	*mapk10*	0.858	57436	*gabarapl1*	0.840	11899	*astn1*	0.824

Supplementary table 6 – List of genes highly coexpressed with *Prnp* (mouse data)

Table continues on the following pages – legend displayed on the final page of the table.

NCBI ID	Gene symbol	Correlation	NCBI ID	Gene symbol	Correlation	NCBI ID	Gene symbol	Correlation
59021	*rab2a*	0.824	237052	*tceal1*	0.812	11735	*ank3*	0.800
347740	*2900097c17rik*	0.824	80985	*trim44*	0.812	319604	*fam168a*	0.799
14406	*gabrg2*	0.824	76217	*jakmip2*	0.812	20085	*rps19*	0.799
76884	*cyfip2*	0.823	232975	*atp1a3*	0.811	109205	*sobp*	0.799
72711	*2810037o22rik*	0.823	110911	*cds2*	0.811	19283	*ptprz1*	0.798
68097	*dynll2*	0.823	13602	*sparcl1*	0.811	233878	*sez6l2*	0.798
259302	*srgap3*	0.822	52837	*tmx4*	0.811	230903	*fbxo44*	0.798
207777	*tspoap1*	0.821	225283	*rprd1a*	0.811	320873	*cdh10*	0.798
64294	*itm2c*	0.821	76897	*ralyl*	0.810	18472	*pafah1b1*	0.798
269643	*ppp2r2c*	0.821	72948	*tppp*	0.809	67937	*tmem59l*	0.798
68729	*trim37*	0.819	207212	*arhgef17*	0.808	56541	*habp4*	0.798
17933	*myt1l*	0.818	14402	*gabrb3*	0.808	232333	*slc6a1*	0.797
20024	*sub1*	0.818	20972	*syngr1*	0.807	333605	*frmpd4*	0.797
17762	*mapt*	0.818	75104	*mmd2*	0.807	229521	*syt11*	0.797
380686	*cnrip1*	0.818	52323	*klhl7*	0.807	19647	*rbbp6*	0.796
320365	*fry*	0.817	19291	*purb*	0.806	13829	*dmtn*	0.794
71532	*fam217b*	0.816	68839	*ankrd46*	0.805	19347	*dennd5a*	0.794
11981	*atp9a*	0.816	228356	*c11orf49*	0.805	67287	*parp6*	0.794
66237	*atp6v1g2*	0.815	232232	*hdac11*	0.805	50876	*tmod2*	0.793
19417	*rasgrf1*	0.815	213760	*prepl*	0.804	17751	*mt3*	0.793
29819	*stau2*	0.815	16561	*kif1b*	0.804	14559	*gdf1*	0.792
73447	*wdr13*	0.815	211739	*vstm2a*	0.803	19280	*ptprs*	0.792
18744	*pja1*	0.814	18611	*pea15*	0.803	76980	*ube2ql1*	0.792
104015	*synj1*	0.814	11836	*araf*	0.803	108902	*b4gat1*	0.790
22110	*tspyl1*	0.813	54561	*nap1l3*	0.803	216856	*nlgn2*	0.790
54161	*copg1*	0.813	70661	*sik3*	0.801	11785	*apbb1*	0.790
269700	*hectd4*	0.813	11864	*arnt2*	0.801	17984	*ndn*	0.790
83965	*enpp5*	0.812	16570	*kif3c*	0.800	16795	*large*	0.789

Supplementary table 6 – List of genes highly coexpressed with *Prnp* (mouse data)

Table continues on the following pages – legend displayed on the final page of the table.

NCBI ID	Gene symbol	Correlation	NCBI ID	Gene symbol	Correlation	NCBI ID	Gene symbol	Correlation
81898	*sf3b1*	0.789	100072	*camta1*	0.777	26562	*ncdn*	0.771
72590	*ppme1*	0.789	26875	*pclo*	0.777	56839	*lgi1*	0.770
320150	*zdhhc17*	0.788	14658	*glrb*	0.777	20974	*syngr3*	0.770
96935	*susd4*	0.787	18377	*omg*	0.777	13682	*eif4a2*	0.770
12050	*bcl2l2*	0.787	216831	*arhgap44*	0.777	76898	*b3gat1*	0.770
233812	*c16orf52*	0.786	70082	*lysmd2*	0.776	16531	*kcnma1*	0.769
22318	*vamp2*	0.785	109934	*abr*	0.776	239364	*tspyl5*	0.769
11975	*atp6v0a1*	0.785	210044	*adcy2*	0.776	381820	*smim10l1*	0.769
21912	*tspan7*	0.784	330908	*opcml*	0.776	20983	*syt4*	0.769
65113	*ndfip1*	0.783	18549	*pcsk2*	0.776	268723	*a830039n20rik*	0.769
26420	*mapk9*	0.782	232370	*clstn3*	0.776	212448	*kiaa0408*	0.769
56786	*tmem9b*	0.782	72991	*2900075n08rik*	0.775	26413	*mapk1*	0.769
67602	*necap1*	0.781	77796	*a930009e05rik*	0.775	229709	*ahcyl1*	0.768
101490	*inpp5f*	0.781	104718	*ttc7b*	0.775	73834	*atp6v1d*	0.768
17954	*nap1l2*	0.781	230235	*frrs1l*	0.775	13527	*dtna*	0.768
218793	*ube2e2*	0.780	260299	*cadm4*	0.773	14681	*gnao1*	0.768
20964	*syn1*	0.780	270162	*elmod1*	0.773	56370	*tagln3*	0.768
100223	*9630041g16rik*	0.780	106014	*fam19a5*	0.773	68666	*svop*	0.768
94229	*slc4a10*	0.779	66625	*pnisr*	0.773	74493	*tnks2*	0.768
56295	*higd1a*	0.779	22151	*tubb2a*	0.773	225392	*rell2*	0.767
494448	*cbx6*	0.779	212307	*mapre2*	0.773	64051	*sv2a*	0.767
20250	*scd2*	0.779	70620	*ube2v2*	0.772	19099	*mapk8ip1*	0.767
93699	*pcdhgb1*	0.779	52589	*ncald*	0.772	381338	*lonrf2*	0.766
235380	*dmxl2*	0.779	24012	*rgs7*	0.772	11519	*add2*	0.766
69886	*2610002j23rik*	0.779	80890	*trim2*	0.771	75712	*tmem14a*	0.766
72844	*kctd17*	0.779	12032	*bcan*	0.771	51792	*ppp2r1a*	0.766
12727	*clcn4*	0.778	18163	*ctnnd2*	0.771	12953	*cry2*	0.765
329165	*abi2*	0.777	74525	*fam234b*	0.771	56807	*scamp5*	0.765

Supplementary table 6 – List of genes highly coexpressed with *Prnp* (mouse data)

See following page for legend…

NCBI ID	Gene symbol	Correlation	NCBI ID	Gene symbol	Correlation	NCBI ID	Gene symbol	Correlation
170719	*oxr1*	0.764	77531	*anks1b*	0.758	110876	*scn2a*	0.756
223601	*fam49b*	0.764	11842	*arf3*	0.757	56637	*gsk3b*	0.755
22628	*ywhag*	0.764	224170	*dzip3*	0.757	20404	*sh3gl2*	0.755
270109	*pcnx2*	0.764	19085	*prkar1b*	0.757	226970	*arhgef4*	0.754
27062	*cadps*	0.762	22763	*zfr*	0.756	107065	*lrrtm2*	0.754
14395	*gabra2*	0.762	432450	*nkain2*	0.756	12069	*bex1*	0.754
53623	*gria3*	0.761	108686	*ccdc88a*	0.756	75409	*slitrk5*	0.751
72902	*spock3*	0.760	20979	*syt1*	0.756	215708	*fam73a*	0.751
109676	*ank2*	0.759	20262	*stmn3*	0.756	235180	*fez1*	0.751
14677	*gnai1*	0.759	224019	*tmem191c*	0.756	245446	*slitrk4*	0.751

Supplementary table 6 – List of genes highly coexpressed with *Prnp* (mouse data)

The above table shows the 267 genes that are highly correlated with *Prnp* in terms of their expression in various mouse tissues/cell types (GNF1M transcriptomic dataset accessible through BioGPS; see **section 6.2** for more details). The correlation values are Pearson product-moment correlation coefficients (r) and the correlation tool in BioGPS was used to select only those genes with $r > 0.75$. Since this dataset was analysed by IPA, only those genes considered by the software to be "analysis-ready" are shown (this excludes some unannotated genes and any duplicate entries in the original dataset).

NCBI ID	Gene symbol	Correlation	NCBI ID	Gene symbol	Correlation	NCBI ID	Gene symbol	Correlation
5621	*prnp*	1.000	351	*app*	0.823	56111	*pcdhga4*	0.786
57142	*rtn4*	0.893	23116	*fam179b*	0.822	56110	*pcdhga5*	0.786
5870	*rab6a*	0.883	5110	*pcmt1*	0.814	56109	*pcdhga6*	0.786
84084	*rab6c/wth3di*	0.883	2824	*gpm6b*	0.812	56108	*pcdhga7*	0.786
4675	*nap1l3*	0.867	5573	*prkar1a*	0.810	56104	*pcdhgb1*	0.786
6500	*skp1*	0.859	2181	*acsl3*	0.809	56103	*pcdhgb2*	0.786
5516	*ppp2cb*	0.855	1759	*dnm1*	0.805	56102	*pcdhgb3*	0.786
5217	*pfn2*	0.855	116987	*agap1*	0.801	56098	*pcdhgc4*	0.786
64112	*moap1*	0.848	23208	*syt11*	0.801	11041	*b4gat1*	0.783
3423	*ids*	0.847	6529	*slc6a1*	0.801	10966	*rab40b*	0.783
9581	*prepl*	0.847	10133	*optn*	0.799	23387	*sik3*	0.781
23270	*tspyl4*	0.847	477	*atp1a2*	0.799	27122	*dkk3*	0.781
26994	*rnf11*	0.841	599	*bcl2l2*	0.797	23362	*psd3*	0.780
11165	*nudt3*	0.835	6990	*dynlt3*	0.796	23201	*fam168a*	0.779
100505385	*iqcj-schip1*	0.834	6416	*map2k4*	0.796	23229	*arhgef9*	0.777
29970	*schip1*	0.834	114876	*osbpl1a*	0.795	527	*atp6v0c*	0.776
9732	*dock4*	0.834	7259	*tspyl1*	0.794	10857	*pgrmc1*	0.774
3831	*klc1*	0.833	2823	*gpm6a*	0.794	5101	*pcdh9*	0.773
27020	*nptn*	0.831	5862	*rab2a*	0.792	5901	*ran*	0.773
1363	*cpe*	0.831	1501	*ctnnd2*	0.792	50810	*hdgfrp3*	0.773
801	*calm1*	0.829	51335	*ngrn*	0.792	7143	*tnr*	0.772
9829	*dnajc6*	0.826	6717	*sri*	0.792	54769	*diras2*	0.772
490	*atp2b1*	0.824	23259	*ddhd2*	0.792	7905	*reep5*	0.771
11215	*akap11*	0.824	576	*adgrb2*	0.786	10150	*mbnl2*	0.770
4747	*nefl*	0.824	26025	*pcdhga12*	0.786	10049	*dnajb6*	0.769
22903	*btbd3*	0.823	56113	*pcdhga2*	0.786	65084	*tmem135*	0.769

Supplementary table 7 – List of genes highly coexpressed with *PRNP* (human data)

See following page for legend…

NCBI ID	Gene symbol	Correlation	NCBI ID	Gene symbol	Correlation	NCBI ID	Gene symbol	Correlation
4698	*ndufa5*	0.769	57515	*serinc1*	0.765	9863	*magi2*	0.756
9867	*pja2*	0.769	4697	*ndufa4*	0.765	10313	*rtn3*	0.755
4905	*nsf*	0.769	55884	*wsb2*	0.764	27018	*bex3*	0.755
5128	*cdk17*	0.768	10900	*rundc3a*	0.763	10740	*rfpl1s*	0.755
56271	*bex4*	0.768	5747	*ptk2*	0.763	6857	*syt1*	0.754
2743	*glrb*	0.768	6616	*snap25*	0.759	114088	*trim9*	0.753
10923	*sub1*	0.768	23001	*wdfy3*	0.759	6853	*syn1*	0.752
288	*ank3*	0.767	10971	*ywhaq*	0.759	10079	*atp9a*	0.752
55228	*pnmal1*	0.767	9240	*pnma1*	0.759	11275	*klhl2*	0.751
56947	*mff*	0.767	80213	*tm2d3*	0.758	56106	*pcdhga10*	0.751
64850	*etnppl*	0.766	9892	*snap91*	0.756	377	*arf3*	0.751
5048	*pafah1b1*	0.766	79068	*fto*	0.756			

Supplementary table 7 – List of genes highly coexpressed with *PRNP* (human data)

This table shows the 113 genes that are highly correlated with *PRNP* in terms of their expression in various human tissues/cell types (U133A transcriptomic dataset accessible through BioGPS; see **section 6.2** for more details). The correlation values are Pearson product-moment correlation coefficients (r) and the correlation tool in BioGPS was used to select only those genes with $r > 0.75$. Since this dataset was analysed by IPA, only those genes considered by the software to be "analysis-ready" are shown (this excludes some unannotated genes and any duplicate entries in the original dataset).